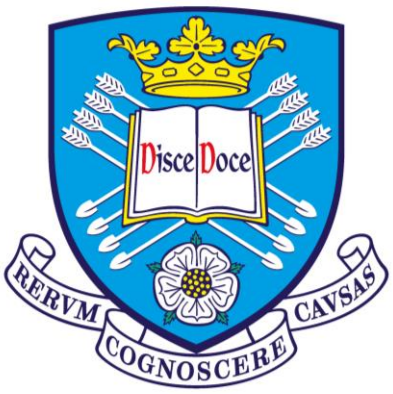

The University Of Sheffield.

Towards defining roles for PIERCE1 and C15ORF65 in multiciliated cells through gene editing

By:

Md Miraj Kobad Chowdhury

A thesis submitted in partial fulfilment of the requirements for the degree of Doctor of Philosophy

September 2022

The University of Sheffield

Faculty of Medicine, Dentistry & Health

Department of Infection, Immunity & Cardiovascular Disease

Supervisors: Professor Dr Colin D Bingle and Dr Lynne Bingle

Dedicated to

My Family, Friends and Teachers who built me up to this stage

Towards defining roles for PIERCE1 and C15ORF65 in multiciliated cells through gene editing

Abstract

Motile cilia, the microtubule-based appendages found on the apical surface of multiciliate cells, develop through the process of ciliogenesis. Defective ciliogenesis underpins many diseases in humans, collectively called primary ciliary dyskinesia (PCD). Systemic approaches have identified many cilia-associated genes and their function in cilia, but the roles of *PIERCE1* and its' paralogue *C15ORF65* in human ciliogenesis has not been studied. Preliminary analysis suggested increased expression of these genes during mucociliary differentiation, and the proteins could localise at the ciliary axoneme. Thus, the functional roles of these genes in ciliated cells were studied using the immortalized human bronchial epithelial cell line, HBEC3-KT. HBEC3-KT cells were shown to able to undergo mucociliary differentiation to generate multiciliated cells and secretory cells in both air-liquid interface (ALI) and under submerged culture conditions. These cells expressed PIERCE1 and C15ORF65 upon mucociliary differentiation conceivably localised in the cilia-like structure of potential progenitors of ciliated cells. Both genes, alone and in combination, were edited in HBEC3-KT cells using CRISPR-CAS9 technology. *FOXJ1*-knockout HBEC3-KT cells were developed as a control. *FOXJ1* is the master regulator of ciliogenesis and loss of FOXJ1 blocked HBEC3-KT differentiation into multiciliated cells at the ALI or under submerged conditions. Individual *PIERCE1*$^{-/-}$ or *C15ORF65*$^{-/-}$ cells were able to differentiate into multiciliated cells, but *PIERCE1*$^{-/-}$ *C15ORF65*$^{-/-}$ HBEC3-KT cells failed to differentiate into multiciliated cells at ALI. Interestingly, these double knockout cells were able to produce multiciliated cells under submerged conditions. This thesis evaluates the similarities between *PIERCE1* and *C15ORF65* as candidate cilia genes, the capacity of HBEC3-KT cell differentiation in submerged conditions in addition to ALI, the potential of CRISPR-CAS9 gene editing in HBEC3-KT cells, and the ciliary axonemal localisation of PIERCE1 and C15ORF65. It is proposed here that loss of both *PIERCE1* and *C15ORF65* could affect cilia function significantly and hence these genes should be included in genetic tests for PCD.

Acknowledgement

First, I would like to declare all praise to Almighty Allah (Alhamdulillah). My heartfelt gratitude and honours go to my supervisor Professor Dr Colin D Bingle and his beloved wife and my co-supervisor Dr Lynne Bingle to choose me as their PhD student, to provide me lots of opportunities to explore the realm of respiratory medicine and secretory biology and helped me to grow up as a prospective researcher. Their kind supervision, guidance, encouragement, and support have led me to this point.

My special gratitude goes to Dr Priyanka Anujan who did excellent work on PIERCE1 prior to me and helped me to get into the biology of PIERCE1 with excellent efforts, kept a constant eye on my progress and supported with late discoveries related to PIERCE1. Thank you for being beside me. I am grateful to Dr Helen Marriott who provided mice whenever I need and Dr Andrew Streets who helped me with microscopy at the last and very important moments. I also thank my PGR tutor Dr Simon Danby, PGR lead Dr Lynne Prince, the technical staff of IICD, Sheffield including Dr Mark Ariaans, Jonathan Kilby, Dr Benjamin S Durham, Kay Hopkinson, Marta M Gallis Ramalho, Peijun Zhang, John Finner and Dr Linda Kay for their constant support and inspiration. I consider myself very lucky to have senior fellows (Dr Esra B Amoura, Dr Vivian Petersen Wagner, Dr Mehul V Makwana, Dr Adrienn Angyal and Dr Natalia Hajdamowicz) around me always guiding me throughout my PhD. I also like to thank my PhD colleagues Abdulaziz SA Alkhoshaiban, Zeyad M Alharbi, Cameron T James and Fawaz Aljuhani from IICD and Lin Zhang (Ireen), Isabel BF Parreira and Fatma Elalawy from the Dental School for their time, support, inspiration, and suggestions. I would also like to specially thank Dr Fahad ES Albalawi for being with me almost all the time during Covid pandemic. Sincere thanks go to Dr Alabdelay Bader, AbdulKhalag Alfaify, Arturo Landeros de la Isla, Dr Fiona Macloed, Dr Stavroula Louka, Faith Tolliday, and Dr Taghreed Shamrani for their time during my PhD life.

I would like to thank Mohammad Robel Hossen Patwary and SM Hasan-ul-Bari for making my Sheffield life very beautiful and enjoyable. Without these two guys my social life in Sheffield would have been very difficult.

My special thanks also go to the Commonwealth Council for funding my research, without such funding it would be impossible for me to study at the University of Sheffield.

I am indebted to my son Ma-arij Bin-Miraj Chowdhury who sacrificed the most during my PhD life alongside my wife Farjana Sharmin. I am grateful to all of my family members for their unconditional love, support, and guidance, specially to my Mother whom I lost 23 years ago, and my Father who left us during the Covid-19 pandemic. My special thanks also go to my best friends Md Muhaimin and Azir Imraul Hasan for being beside me since 1989.

Last of all, I thank the reviewers of all of the research I have done previously and will do in the future, without their work science would not be so beautiful today.

List of Publications

1. Research articles:

- Apoorva Mulay, Md Miraj Kobad Chowdhury, Cameron T James, Lynne Bingle, and Colin D Bingle. **2021**. The transcriptional landscape of the cultured murine middle ear epithelium *in vitro*. **Biology Open. 10(4): bio056564**.
- Lynne Bingle, Hanna Armes, David J Williams, Olivia Gianfrancesco, Md Miraj Kobad Chowdhury, Ronny Drapkin and Colin D Bingle. **2020**. Expression and function of murine WFDC2 in the respiratory tract. **bioRxiv. 05.05.079293.**

2. Abstract publication:

- Md Miraj Kobad Chowdhury, Priyanka Anujan, Lynne Bingle, and Colin Bingle. **2020**. PIERCEing ciliogenesis: defining a role for PIERCE1 and its' paralog C15ORF65 in multiciliogenesis. **European Respiratory Journal. 56: 1902**.
- Md Miraj Kobad Chowdhury, Priyanka Anujan, Apoorva Mulay, Lynne Bingle, and Colin Bingle. **2020**. Comparative transcriptional analysis of differentiation in murine mucociliary epithelia. **European Respiratory Journal. 56: 916.**
- Zeyad Alharbi, Md Miraj Kobad Chowdhury, Lynne Bingle and Colin Bingle. 2020. Air liquid interface (ALI)-grown immortalized human cell lines: a promising tractable model for human airway. **European Respiratory Journal. 56: 4327.**

3. Conference/Congress Presentation:

- Poster presentation: Defining spatial secretome and ciliome across multiciliated epithelia. European Respiratory Society Congress - 2022, Barcelona, Spain.
- Poster presentation: Defining the functions of PIERCE1 and C15ORF65 during ciliogenesis of HBEC3-KT cells. European Respiratory Society Congress - 2022, Barcelona, Spain.
- Poster presentation: Comparative transcriptional analysis of differentiation in murine mucociliary epithelia. British Association of Lung Research Summer Meeting – 2021 (online).
- Poster presentation: PIERCEing ciliogenesis: defining a role for PIERCE1 and its' paralog C15ORF65 in multiciliogenesis. British Association of Lung Research Summer Meeting – 2021 (online).

- Poster presentation: PIERCEing ciliogenesis: Defining a role for PIERCE1 and its' paralog C15ORF65 in multiciliogenesis. The Medical School Research Meeting of the University of Sheffield - 2020, Sheffield, UK.
- Poster presentation: Deciphering the differential gene expression during ciliogenesis. British Association of Lung Research Summer Meeting - 2019, Cambridge, UK.
- Poster presentation: Deciphering the differential gene expression during ciliogenesis. The Medical School Research Meeting of the University of Sheffield - 2019, Sheffield, UK.

Table of Contents

List of Abbreviations

ALI: Air-liquid interface

BB: Basal body

BLAST: Basic local alignment search tool

BPE: Bovine pituitary extract

BPIFA1: Bactericidal/permeability-increasing protein fold containing family A member 1

BPIFB1: Bactericidal/permeability-increasing protein fold containing family B member 1

BSA: Bovine serum albumin

C15ORF65: Protein encoded by the open reading frame 65 of chromosome 15

CCDC: Coiled-coil domain containing

CDHR3: Cadherin-related family member 3

CDK: Cyclin-dependent kinase

Cdk4: Mouse cyclin-dependent kinase 4

CF: Cystic fibrosis

CFTR: Cystic fibrosis transmembrane conductance regulator

COPD: Chronic obstructive pulmonary disease

CRISPR: Clustered regularly interspaced short palindromic repeats

CT: Computed tomography

DAPT: *N*-[*N*-(3,5-difluorophenacetyl)-L-alanyl]-*S*-phenylglycine *t*-butyl ester

DEUP1: Deuterosome assembly protein 1

DGE: Differential gene expression

DMEM: Dulbecco's modified eagle medium

DUF4490: Domain of unknown function number 4490

EBI: European bioinformatics institute

EGF: Epidermal growth factor

ENaC: Epithelial sodium channel

ESLD: End stage lung disease

FBS: Fetal bovine serum

FHD: Forkhead domain

FOXJ1: Forkhead box protein J1

GEO: Gene expression omnibus

GFP: Green fluorescence protein

GRHL2: Grainyhead-like transcription factor 2

gRNA: Guide RNA

GTEx: Genotype-tissue expression

HBEC: Human bronchial epithelial cell

HPA: Human protein atlas

HRSV: Human respiratory syncytial virus

hTERT: Human telomerase reverse transcriptase

IFT: Intra-flagellar transport

IGV: Integrated genome viewer

IL13: Interleukin 13

IQUB: IQ motif and ubiquitin domain containing

I-TASSER: Iterative threading assembly refinement

KIF24: Kinesin family member protein 24

KSFM: Keratinocyte serum-free media

LIMMA: linear models for microarray data

MCC: Mucociliary clearance

MEGA: Molecular evolutionary genetics analysis

MSA: Multiple sequence alignment

mTEC: Mouse tracheal epithelial cell

MUC5AC: Mucin protein 5AC

MUC5B: Mucin protein 5B

MUSCLE: Multiple sequence comparison by Log-expectation

NCBI: National center for biotechnology information

NHEJ: Non-homologous end-joining

nTPM: Normalized count of transcript per million

OAZ1: Ornithine decarboxylase antizyme 1

ODF2: Outer dense fibre of sperm tails 2 protein

PALI: PneumaCult™ air-liquid interface media

PAM: Protospacer adjacent motif

PCD: Primary ciliary dyskinesia

PCR: Polymerase chain reaction

PE: Pulmonary epithelium

PIERCE1: p53-Induced expression in Rb-null cells 1

PKD: Polycystic kidney disease

PLK4: Polo-like kinase 4

qPCR: Quantitative polymerase chain reaction

qRT-PCR: Quantitative reverse transcriptase polymerase chain reaction

RB: Retinoblastoma

RE: Respiratory epithelium

RFX: Regulatory factor X

RMA: Robust microarray average

SAS6: Spindle assembly abnormal protein 6 homolog

SPAG6: Sperm associated antigen 6

STIL: SCL/TAL1-interrupting locus protein

TAC: Transcriptome analysis console

TEC: Tracheal epithelial cell

TEER: Transepithelial/endothelial electrical resistance

TEKT1: Tektin 1

TERT: Telomerase reverse transcriptase

TreeBeST: Tree building guided by species tree

UVC: Ultraviolet C

List of Figures

List of Tables

Chapter 1: Introduction

1.1 A brief introduction to cilia and ciliogenesis

Cilia are microtubule-based hairlike appendages found on the apical surface of many cells and are highly conserved subcellular organelles in eukaryotes. They can be grouped broadly as primary cilia and motile cilia. In human, 30-300 motile cilia are present on multiciliated cells of the respiratory epithelia, fallopian tube epithelia and brain ventricles, amongst others (middle ear epithelia, nasal cavity epithelia etc.), where they beat in a synchronized fashion to promote directional fluid movement (Legendre, Zaragosi et al. 2021). Though no evidence suggests mitosis of multiciliated cells, such cells in the respiratory epithelium can be regenerated from basal progenitor cells, whereas ependymal multiciliated cells of the brain ventricles cannot be replenished as they are formed only during the embryonic development (Delgehyr, Meunier et al. 2015, Kempeneers and Chilvers 2018). Motile cilia are associated with diverse functions and loss of cilia can cause many human diseases and developmental defects (Hyland and Brody 2021). Structurally a cilium is composed of a basal body and an axoneme attached to the basal body. The axoneme provides the locomotion of a motile cilium by beating at forward-backward direction (Li, Yang et al. 2021). Cilia are formed through a process called ciliogenesis, often called monociliogenesis when only one cilium is formed per cell, or multiciliogenesis as multiple cilia are projected on the apical surface of the same cell. Two pathways involved in the process of multiciliogenesis have been studied namely canonical centriole-dependent and deuterosome-dependent pathways (Mahjoub, Nanjundappa et al. 2022). About 600 genes have been identified associated with either the regulatory or structural side of cilia so far (Al Jord, Spassky et al. 2019). However, the complete signalling pathway underpinning multiciliogenesis has not been completely defined yet and the full structure of cilia remains under investigated, and therefore cilia research is a very active area (Seidl, Da Silva et al. 2023). Such limitations are mostly attributed to the lack a comprehensive set of cilia-associated genes to validate their function in cilia development. To make the matter more complicated, cilia-associated genes vary from animal to animal, such as *C20ORF85* is highly expressed in human multiciliated cells but not in mouse and GSTM5 is highly expressed in mouse multiciliated cells

but not in human (Travaglini, Nabhan et al. 2020). Multiple *in vitro* models have been developed (as for example, air-liquid interface (ALI) culture) to delineate the function of cilia-associated genes like *CCDC40*, *CFAP300*, *DNAH5* etc (Bukowy-Bieryllo, Daca-Roszak et al. 2022). One good model is primary bronchial cell culture that can be differentiated into respiratory epithelium *in vitro* when cultured at ALI and has served for many years to facilitate understanding of the biology and physiology of multiciliated epithelia. This *in vitro* respiratory epithelial model has allowed researchers to explore the processes involved with development, functional regulation, and maintenance of the mammalian cilia (Peters-Hall, Coquelin et al. 2018). However, *in vitro* multiciliated epithelial models for human sinuses, fallopian tube and middle ear are limited, and still unavailable for human testes or brain ventricle (Ando, Kobayashi et al. 2000, Zhu, Iwano et al. 2019, Mather, Verdon et al. 2021, Schilling, Carcella et al. 2021, Paranjapye, Leir et al. 2022), yet murine radial glial cells can be differentiated *in vitro* into multiciliated ependymal cells (Delgehyr, Meunier et al. 2015). Since loss of ciliary functions are associated with many disease conditions, collectively known as ciliopathies, in depth understanding of ciliogenesis and cilia structure is crucial to manage patients suffering from ciliary disorders. In my thesis, strategies have been developed to characterize the functions of two potential cilia candidate genes, namely *PIERCE1* and *C15ORF65*. Research published during my study found i) both PIERCE1 and C15ORF65 in the doublet microtubular zone of the bovine ciliary axoneme, ii) severe ciliopathies in *pierce1*$^{-/-}$*c15orf65*$^{-/-}$ zebrafish which can partly be rescued by knocking-in either *pierce1* or *c15orf65*, and iii) reduced ciliary beat frequency in *Pierce1*$^{-/-}$ mice or in *C15orf65*$^{-/-}$ mice and embryonic lethality in *Pierce1*$^{-/-}$*C15orf65*$^{-/-}$ mice (Gui, Farley et al. 2021). Though the role of these gene products in bovine cilia structure was reported there (Gui, Farley et al. 2021), evidence on their roles in human cilia remained unknown until now.

1.2 Deducing the function of cilia-associated genes

Function of cilia-associated genes have been mostly studied with model organisms *in vivo* as well as *in vitro*. Specialized cell culture techniques have helped to generate *in vitro* models of respiratory epithelia partly mimicking normal human respiratory physiology, and such models have been widely used to study human ciliogenesis and cilia structure (Schmid, Sailland et al. 2017, Lee, Petris et al. 2020, Saint-Criq, Delpiano et al. 2020). However, the structure and function of cilia may

vary across the types of multiciliated epithelia and such structural and functional diversification could complicate the understanding of cilia biology (Narita and Takeda 2021).

In addition to laboratory experiments, computational biology and bioinformatics have accelerated the analysis of genomic, transcriptomic, and proteomic data. These data in association with laboratory validation have helped researcher to discover novel cilia-associated genes and pathways involved with cilia formation and maintenance. Such approaches in the field of cilia research has provided further insights to ciliogenesis (Gui, Farley et al. 2021, Paranjapye, Leir et al. 2022). As for example, single-cell RNA-sequencing data provided novel insights on the molecular cell atlas of human lung to discover deuterosomal (*FOXJ1*$^{+}$, *CDC20B*$^{+}$ cells) and proximal (*FOXJ1*$^{+}$, *MUC12*$^{+}$ cells) ciliated cells as new ciliated cell types based on the expression of unique sets of genes in these cells (Travaglini, Nabhan et al. 2020, Sun, Perl et al. 2022). It is also possible to identify novel cilia genes by analysing the differential gene expression during mucociliogenesis using multiple gene expression datasets and robust algorithms for gene expression data analysis . Then their functions in cilia can be directly explored with the help of laboratory experiments like the development of gene-knock-outs by CRISPR-CAS9 gene editing technology followed by ALI differentiation of the edited cells and immunofluorescence or cryo-electron microscopy, and with the help of advanced bioinformatics tools like ontology, pathway analysis, and identification of interacting partners.

Bioinformatic tools are constantly being updated with the development of new and innovative algorithms. Such tools are proven to help analysing sequences of nucleic acids and proteins in multiple aspects like sequence alignment, motif finding, and to deduce structures (Gauthier, Vincent et al. 2019). Alignment of multiple sequences is widely used to deduce evolutionary origin of genes and proteins as well as to find orthologs and paralogs. Once a gene is identified, such tools can be applied to predict the possible transcripts of the gene and to estimate the secondary structures of the transcripts. Such transcripts can be virtually translated into protein sequences and the determined protein sequences can be used to predict many possible biological features with high confidence *in silico*. Such biological features include but are not limited to estimating protein structure, defining biologically important motifs

within a protein, subcellular localisation of the protein, determining the half-life of a protein, finding interactive partners, and simulating models of biological pathways (Monti, Zilocchi et al. 2019). Prediction tools have been further improved with the help of artificial intelligence and advanced computing (Tunyasuvunakool, Adler et al. 2021). Utilization of these bioinformatic tools can predict the association of a given protein with a biological pathway or process like ciliogenesis and cilia structure (Walentek and Quigley 2017). Here, these tools are used to predict the structure and functional aspects of PIERCE1 and C15ORF65 in cilia.

1.3 *FOXJ1*, *PIERCE1* and *C15ORF65*

Among the cilia-associated genes discovered so far, *FOXJ1* has been considered as the master regulator of ciliogenesis (Yu, Ng et al. 2008). FOXJ1 is a crucial transcription factor expressed in cells committing to ciliogenesis. Ciliogenesis is absent in cells lacking FOXJ1 and ectopic expression of *Foxj1a,* a FOXJ1 homolog in zebrafish, has been shown to induce ectopic motile-cilia like cilia (Yu, Ng et al. 2008). Down-regulation of *FOXJ1* occurs following SARS-CoV2 infection resulting in dedifferentiation of multiciliated cells indicating the importance of FOXJ1 in maintaining the status of a cell as a multiciliated cell in normal physiology (Robinot, Hubert et al. 2021). Interestingly, studies with *FOXJ1* knockout/knockdown human respiratory epithelial cells are very limited and mostly unpublished (Liu, Zhang et al. 2019, Rapiteanu, Karagyozova et al. 2020). Upregulation of *FOXJ1* was observed in some cancer cells and such upregulation induced cell proliferation and migration, and downregulation of *FOXJ1* could reverse such phenotype indicating a possible role of FOXJ1 in the cell cycle (Xian, Shang et al. 2018, Liu, Zhang et al. 2019).

P53-induced expression in RETINOBLASTOMA-null cells protein 1 (*PIERCE1*), also known as *C9ORF116* in human and *RbEST47* or *1700007K13Rik* in mouse, was initially identified in mouse as a novel Retinoblastoma-regulated, cell cycle-associated gene in 2007 (Sung, Kim et al. 2007). The cell cycle consists of four phases namely G0/G1, S, G2 and M phase; and *PIERCE1* plays important roles in S and/or G2 phase. Murine *Pierce1* is induced by p53 and respond to UVC-induced DNA damage. However, human *PIERCE1* is not P53-inducible and is down-regulated in immortalized cells (Sung, Kim et al. 2010, Kim, Lee et al. 2020). Mice deficient in *Pierce1* showed randomization of body *situs* and in heterotaxia-

associated partial embryonic lethality due to randomized expression of asymmetric genes resulting from defective ciliary beating at embryonic stage. Defective beat frequency of nodal cilia has been reported in *Pierce1*-null mice and zebrafish, and an increased expression of *Pierce1* has been reported during ciliogenesis in these animals (Sung, Baek et al. 2016, Gui, Farley et al. 2021).

Chromosome 15 open reading frame 65 (*C15ORF65*), also known as *TIHL, FLJ27352* or *BX648577* in human and *Gm5918* or *Ccpg1os* in mouse was identified as a gene translocated in Hodgkin lymphoma (TIHL) to form a fusion protein with MHC class II transactivator *(*CIITA) in 2011 (Steidl, Shah et al. 2011). C15ORF65 was identified as a distant paralogue of *PIERCE1* by Gui, Farley et al. in 2021 (Gui, Farley et al. 2021). Like PIERCE1, C15ORF65 contains a 'domain of unknown function 4490 (DUF4490)' motif. *C15ORF65* is included in the list of a catalogue of somatic mutations in cancer (COSMIC) genes and mild phenotype (increased prepulse inhibition, a neurological phenomenon where a prestimulus can inhibit an organism's reaction to a subsequent strong stimulus) was observed in *C15orf65*-KO mice (Stein 2019, Gui, Farley et al. 2021).

Studies on PIERCE1 function have been ongoing in our laboratory for last few years. C15ORF65 was only studied during the period of my thesis. Recent structural studies found FAP182 (PIERCE1 homolog of *Chlamydomonas reinhardtii*) and bovine PIERCE1 and C15ORF65 in the doublet microtubular zone of ciliary axonemes as a part of the microtubule inner protein (MIP) complex of dynein-decorated microtubules. Thus C15ORF65 was renamed as PIERCE2 (Ma, Stoyanova et al. 2019, Gui, Farley et al. 2021). Gui, Farley et al. also observed severe ciliopathies in mice or zebrafish lacking both genes (Gui, Farley et al. 2021). For zebrafish, the phenotype could be partially rescued when either one of these genes was reintroduced. Mice lacking both genes were embryonic lethal but mice lacking any one of these genes were not. Interestingly reduced ciliary beat frequency was observed in knockouts of either of these genes (Gui, Farley et al. 2021). Such findings have made both PIERCE1 and C15ORF65 prime candidates for further studies associated with cilia. Nonetheless, the function of both PIERCE1 and C15OR65 in ciliogenesis has not been studied in human cells. Also, a C15ORF65 homolog of *Chlamydomonas reinhardtii* has so far not been identified. These findings

together led to hypothesis that *PIERCE1*, and perhaps *C15ORF65* are associated with ciliogenesis in human and loss of these genes alone or in combination may cause ciliary defects.

1.4 HBEC3-KT cells as model for cilia studies

Human ciliogenesis has been studied extensively with primary bronchial and small airway epithelial cells donated by volunteers (Zhang, Bukreyev et al. 2005, Hosokawa, Betsuyaku et al. 2007, Ross, Dailey et al. 2007). These cells can be differentiated to multiple cell types of respiratory epithelia *in vitro* using a sophisticated cell culture technique. In such technique, the cells supported by a plastic membrane are fed from the bottom and the apical surfaces remain exposed to the air with regular cleaning/wash of the apical surface using a buffered salt solution like Hank's balanced salt solution (HBSS) to clear up the secreted mucus (Hosokawa, Betsuyaku et al. 2007, Kesimer, Kirkham et al. 2009, Pezzulo, Starner et al. 2011). This method is named ALI culture (Yamaya, Finkbeiner et al. 1992), and the monolayer cells developed this way mimic the normal physiology of respiratory epithelium and allows the basal cells to differentiate into secretory cells, ciliated cells, ionocytes and other cell types (Abraham, Zizzadoro et al. 2011, Pezzulo, Starner et al. 2011, Leung, Wadsworth et al. 2020). One limitation of using primary cells is their limited life span, thus gene knockout/knockdown followed by mucociliary differentiation studies with these cells is technically very challenging. Therefore, an immortalized human cell line capable of undergoing mucociliogenesis at ALI is a valuable tool to carry out such studies. A number of primary human bronchial cells stably transfected with exogenous genes have been immortalized (for example NHBE BMI-1, NHBE-CL1548, HBEC3-KT etc.) and these cells can be differentiated at ALI while they still retain their proliferation capability (Rambhatla, Chiu et al. 2002, Delgado, Kaisani et al. 2011, Walters, Gomi et al. 2013). HBEC3-KT cells were immortalized with mouse Cdk4 and human TERT (Ramirez, Sheridan et al. 2004), and were developed as an alternative to primary bronchial epithelial cells. These cells differentiate into ciliated, goblet, club and other cells of respiratory epithelia when cultured at ALI (Delgado, Kaisani et al. 2011, Nakauchi, Nagata et al. 2019, Lodes, Seidensticker et al. 2020). Itis hypothesized here that HBEC3-KT cells can be edited by CRISPR-CAS9 gene editing system to understand the functions of *PIERCE1* and *C15ORF65* in ciliogenesis.

1.5 Concluding remarks

Motile cilia are associated with diverse biological functions and loss of cilia function can lead to several human diseases (Legendre, Zaragosi et al. 2021). With the advent of latest technologies, research focused on cilia is generating much new information (Jiao, Hu et al. 2022, Seidl, Da Silva et al. 2023). Many questions are yet to be answered to fully understand the biology of cilia. The *in vitro* pulmonary epithelium is a good model to understand the process of multiciliogenesis and can allow the exploration of the processes involved with the development, functional regulation, and maintenance of motile cilia. Thus, the functions of novel cilia-associated genes like *PIERCE1* and *C15ORF65* can be explored *in vitro* along with appropriate control (*i.e., FOXJ1*-null) using such models.

Chapter 2: Literature Review

2.1 Introduction

Secreted mucus in the respiratory tract is continuously cleared by the actions of multiciliated cells in the pulmonary epithelium and the loss of function of this epithelium gives rise to variety of diseases (Kempeneers and Chilvers 2018). Hence, studying this epithelium, especially the multiciliated cells, is crucial to understand such disorders. Multiciliated cells possess multiple motile cilia at their apical surfaces that beat continuously in a rhythmic fashion. Despite the fact that significant research has been undertaken, the structure and molecular biology of cilia and ciliogenesis remains to be completely clarified. Here, the current understanding of cilia structure, function, development of cilia, and ciliary diseases are discussed.

2.2 Respiratory epithelium

The respiratory epithelium (RE) is the pseudostratified columnar epithelial cell layer found throughout the respiratory tract, except larynx and pharynx, which are lined with squamous epithelia and covered by non-keratinized stratified squamous epithelium. These epithelia do not have multiciliated cells (Chen, Huang et al. 2017). The mammalian RE is composed of four major types of cells and a number of minor types of cells attached to a thin basement membrane connected to the lamina propria (Whitsett, Kalin et al. 2019) (Figure 2.1A). The RE is classified as pseudostratified columnar epithelium because most of the cells are columnar and the nucleus of these columnar cells are localised in different heights (Whitsett 2018), whilst the basal surface of each cell abuts the basement membrane, an extracellular matrix mostly composed of type IV collagen. The major function of this epithelium is mucociliary clearance of the airway, which protects the airways by providing a barrier against pathogens and keeps the airway and lung clean (Stanke 2015, Whitsett and Alenghat 2015).

2.2.1 Major cell types of the RE

The major cell types of RE include basal cells, goblet cells, ciliated cells, and club cells (Whitsett, Kalin et al. 2019). The basal cells are the progenitor cells for ciliated, goblet, and club cells and are TP63 positive (Tadokoro, Wang et al. 2014). When

NOTCH signalling is downregulated, the basal cells differentiate into ciliated cells. However, these cells differentiate into goblet cells when high levels of NOTCH signalling are present, and to club cells when the NOTCH signalling is moderate during the early developmental period (Siebel and Lendahl 2017). Goblet cells produce and secrete mucus to absorb allergens, pathogens, dirt, other foreign particles, and inhaled xenobiotics, and this mucus functions as a major protective barrier (Whitsett 2018). Hence, these columnar cells are enriched with secretory vesicles and often MUC5B-positive (Roy, Livraghi-Butrico et al. 2014). On the other hand, ciliated cells possess multiple cilia protruding from the apical surfaces of the cells toward the airway. These beat back-and-forth in a co-ordinated rhythmic fashion to effect mucociliary clearance (MCC) essential for continuous sweeping of excreted mucus (Bustamante-Marin and Ostrowski 2017, Spassky and Meunier 2017) (Figure 2.1B). Ciliated cells are FOXJ1-positive, and can differentiate from both basal cells and club cells (Marshall, Mays et al. 2016). Recently three subsets of ciliated cells namely early (*DNHD1*$^{+}$), mature (*PAMR1*$^{+}$) and immune regulatory (*ETHE1*$^{+}$) ciliated cells have been clustered after single-cell RNA-sequencing analysis of RE (Carraro, Langerman et al. 2021). Like mature goblet cells, ciliated cells are also terminally differentiated. Ciliated cells outnumber goblet cells throughout the RE and are mostly present in trachea followed by bronchioles and terminal bronchioles. It is estimated that the half-life of a typical murine ciliated cell is six to eighteen months (Rawlins and Hogan 2008). Club cells are SCGB1A1 positive versatile columnar secretory cells that are differentiated from basal cells during canalicular period of development. These cells contain small periodic acid-Schiff (PAS)-positive secretory granules and can differentiate into goblet cells or ciliated cells (Hogan, Barkauskas et al. 2014). Club cells are predominant in the RE close to the bronchioles where the number of goblet cells is decreased compared to the upper respiratory tract and they function as the major secretory cells in this location. These cells show high expression of cytochrome P450 detoxifying enzyme CYP2F and many defence proteins (like SCGB1A1, SFTPA1 and SFTPD), indicating that they function in response to pathogen, injury, or other environmental stress (Mayer, Bartz et al. 2008, Miller, Dye et al. 2019).

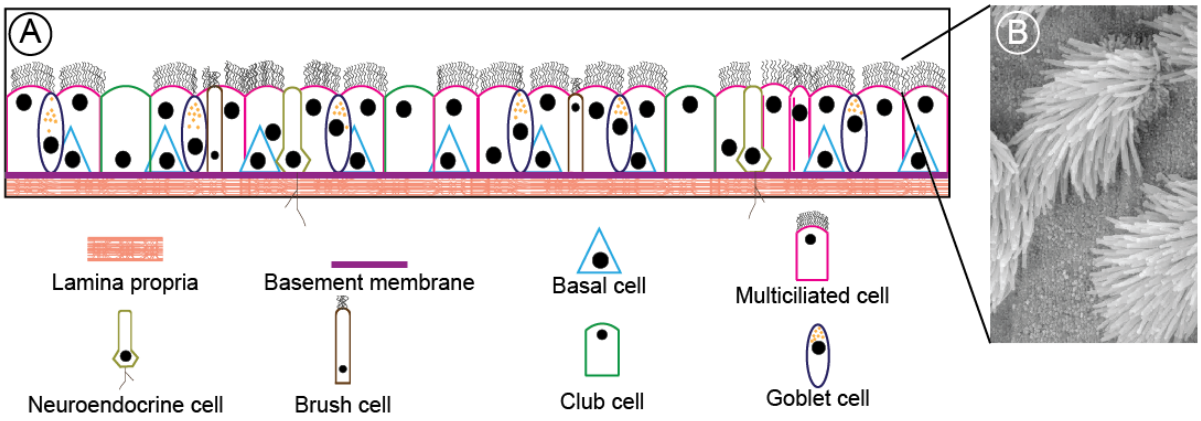

Figure 2.1 Cell types of respiratory epithelia. The RE consist of lamina propria, a basement membrane and six types of cells including multiciliated cells (A). An electron microscopy image showing multiple cilia potruding from a multiciliated cell in RE (B) (with permission; license number : 4521870971281, (Ishikawa and Marshall 2011, Zaragosi, Deprez et al. 2020, Davis and Wypych 2021)).

2.2.2 Minor cell types of the RE

In addition to these major cell types, minor cell types in RE include brush cells and neuroendocrine cells (Whitsett, Kalin et al. 2019) (Figure 2.1A). Brush cells, also known as tuft cells, are columnar cells containing filamentous 'brush-like' microvilli extended toward the airway surface connected with a dense, apical microtubular network (Reid, Meyrick et al. 2005). Despite these cells being found in intestinal and nasal epithelia, their function in RE is yet to be clarified (Gerbe and Jay 2016). It is hypothesized that these cells express chemoreceptors for sensing microorganism and parasites, or to provide some sort of innate immunity to the RE (Gerbe, Sidot et al. 2016). Recent report suggests that the function of tuft cells could be tuned in a tissue-specific manner and plays vital roles as chemosensory epithelial cells to detect toxic substances and ligands produced by pathogenic bacteria, protists, or helminths (Billipp, Nadjsombati et al. 2021). The neuroendocrine cells, also known as Kulchitsky cells or small granule cells, are the smallest cell population of the RE and can be recognized by the presence of dense-core secretory granules in their cytoplasm, however the origin of these cells is not known yet (Miller, Dye et al. 2019). These cells function as sensors for air oxygen and carbon dioxide levels as supported by the presence of oxygen-sensitive potassium channel which is coupled to oxygen sensory protein hypoxia induced factor (HIF), as well as for other environmental stimuli and in the generation of an innate immunity inflammatory response (Kuo and Krasnow 2015, Kapsimali 2017). Recent scRNAseq studies have

identified a novel rare cell type called the ionocyte originating from the basal cells in the RE. These cells those express FOXI1 and CFTR, account for <1% of epithelia cells and appear to regulate epithelial surface physiology including fluid accumulation and mucus viscosity (Montoro, Haber et al. 2018, Plasschaert, Zilionis et al. 2018). This new finding highlights the importance of understanding the RE and the relationship between diseases and different cell types.

2.3 Cilia: a bird's eye view

Cilia (in singular: cilium; meaning eyelash; derived from Latin; coined by Otto Muller in 1786) are microtubule-based subcellular organelles protruding from the plasma membrane of eukaryotic cells (Margulis 1980). They were discovered first by Antonie Philips van Leeuwenhoek, the discoverer of the microscope, in protozoa in 1675 (Beales and Jackson 2012). Cilia are suggested to have evolved from the proto-eukaryotic cell that existed before the last eukaryotic common ancestor, and have originated from the centriole, another subcellular organelle (Carvalho-Santos, Azimzadeh et al. 2011). A cell can possess one to thousands of cilia on its apical surface. The average length of a typical mature cilium is about 5 μm and the average width is about 0.5 μm; with the smallest cilia found in vascular endothelial cells (1-5 μm in length) and the longest in sperm (also known as flagella, > 15 μm in length, could be up to 5 cm in sperm of *Drosophila bifurca*) (Dummer, Poelma et al. 2016). Cilia are highly conserved in eukaryotes and are regarded as nanomolecular machines composed of over 600 proteins (Bustamante-Marin and Ostrowski 2017). Each cilium is composed of unique structural proteins that form the body of the cilium, and motor proteins in the axoneme that drive the co-ordinated wavelike ciliary motion. Cilia function in cell motility, as sensory appendages, and in signalling to play vital roles in different biological processes such as respiration, fertility, memory development, and left-right asymmetry (Satir and Christensen 2008).

2.3.1 Types of cilia

Cilia are broadly classified into two categories based on their structure and function: i) primary cilia, which are considered as nonmotile and perform sensory and signalling roles, and ii) motile cilia present in the multiciliated cells and that perform ciliary movements (Satir and Christensen 2008). Primary cilia are shorter in length

and found in almost all terminally differentiated cells where they play important roles in development and tissue homeostasis (Venkatesh 2017). Cells responds to external stimuli such as flow of fluids in kidney tubules or light in photoreceptors, by transferring specific cargo proteins from the cytoplasm to the tip of a cilium and vice versa through the intra-flagellar transport (IFT) system. Primary cilia also carry some receptor molecules, *i.e.,* somatostatin receptor 3, that are activated upon binding to its ligand somatostatin and convey signalling cascades through ciliary G-protein coupled receptor pathway (Satir, Pedersen et al. 2010). In addition, primary cilia also play vital roles in Sonic, Indian, and Desert Hedgehog signalling pathways in mammals as they carry Hedgehog receptors Patched-1 and Smoothened receptors within or at the base of the axoneme (Fitzsimons, Brewer et al. 2022). Motile cilia are present in the epithelia of the respiratory tract, sinuses, middle ear, fallopian tube, epididymal duct of testes, and ependymal cells of brain ventricle (Satir and Christensen 2008). In healthy human RE, cilia of the multiciliated cells beat about 12-15 times per second in a co-ordinated metachronal rhythm to transfer the mucus toward the ciliary tips at about 65-260 µm per second (Fahy and Dickey 2010). When performing a forward stroke, cilia tips penetrate the mucus and move the fluid forward. During the backward stroke, the tips slope backward from the fluid and the cilia tips pass underneath the mucus. In this way, motile cilia in multiciliated cells perform sweeping of the mucus from the RE, move the egg through the oviduct, and conduct movement of cerebrospinal fluid in brain (Tilley, Walters et al. 2015). Motile cilia in human RE can also be chemosensory as isoforms of T2R receptor (that mediate bitter taste) and T1R receptor (that mediate sweet taste) have been found in bronchial and sinonasal ciliated cells (Shah, Ben-Shahar et al. 2009).

2.3.2 Structure of cilia

The fine structure of cilia has been explored with the electron microscopy (Mizuno, Taschner et al. 2012). The basic structure of all cilia consists of a basal body (BB) and an axoneme bridged by a transition zone (Figure 2.2A). The axoneme protrudes outside of the cell towards the apical surface and the BB anchors the axoneme onto the cell (Fisch and Dupuis-Williams 2011).

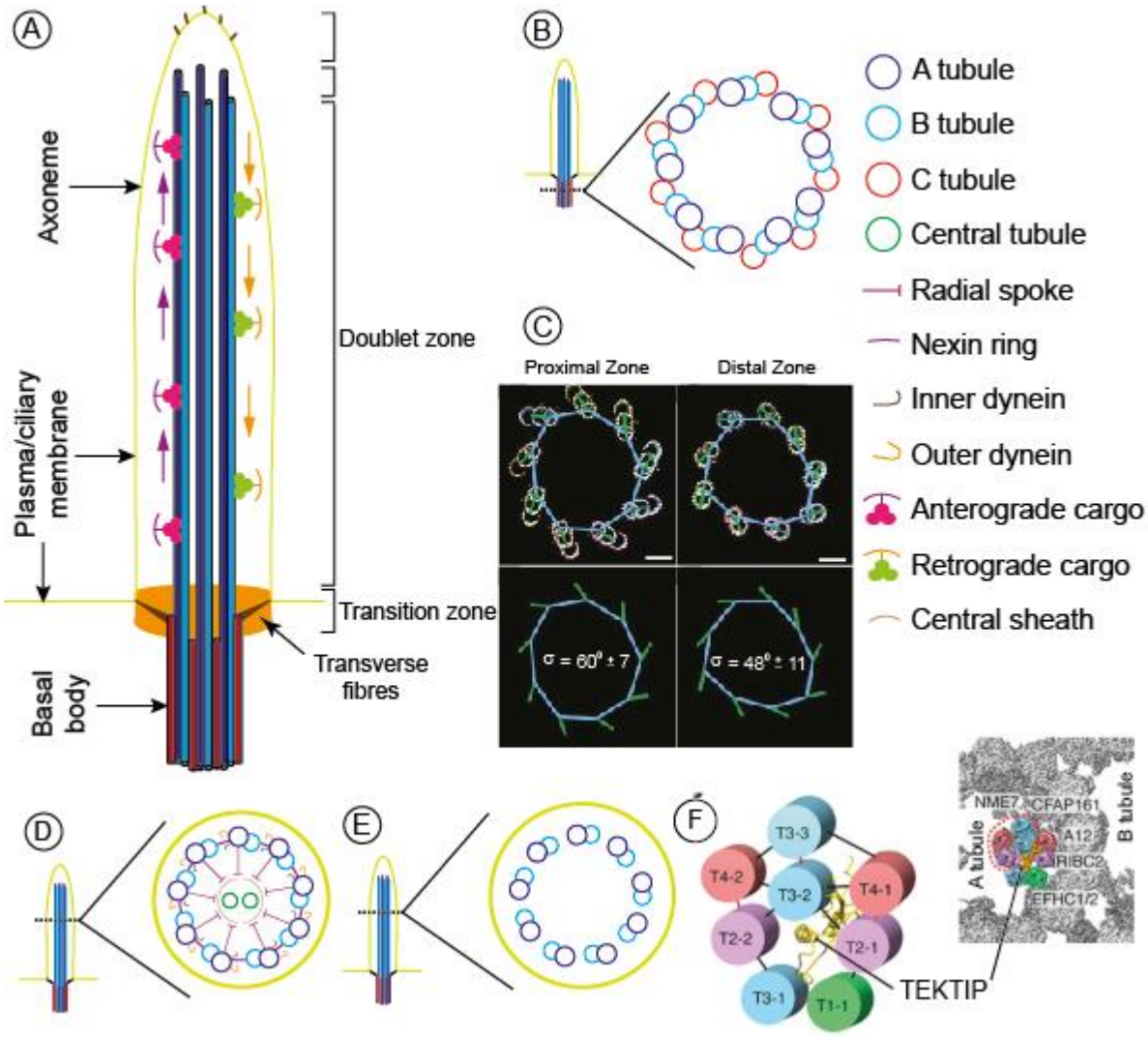

Figure 2.2 Structure of cilium. A cilium consists of a basal body and an axoneme, and the axoneme has four distinct regions namely the transition zone, the doublet zone, the singlet zone and the ciliary tip, purple arrows show the anterograde cargo and yellow arrows show the retrograde cargo movement (A). The basal body has a cartwheel-like 9-fold structure consisting of A, B and C tubules (B). Cross-sectional studies of proximal and distal end of transition zone show a decrease of microtubular angle towards the distal end of the transition zone (C) (image from (Greenan, Vale et al. 2020) licensed under CC BY-NC-SA 4.0). A cross-section of the doublet zone of a primary cilium shows a 9+0 arrangement of microtubules without dynein arms in the primary cilium (D). In a motile cilium, the doublet zone is accompanied with the central pair and shows a 9+2 microtubular arrangement with dynein arms (E). Pentagonal bundle of tektin filaments are found within the common wall of A tubule and B tubule in the doublet zone, and this bundle is stabilized by TEKTINIP (F) (image from (Gui, Farley et al. 2021) licensed under CC BY 4.0).

2.3.2.1 Basal body

The BB originates from the centriole and serves as a template for the axoneme (Figure 2.2B). The BB is barrel-shaped 9-fold symmetric cartwheel-like structure. The length and the width of the BB is about 0.5 µm and 0.25 µm respectively, and

the 9-fold structure is formed by nine triplet microtubules (Marshall 2008). Each triplet microtubule contains A, B, and C tubules. Tubule A consists of 13 complete protofilaments, whereas protofilaments of B and C are incomplete (Lattao, Kovacs et al. 2017). There is no central tubule in the BB, but the lumen of the BB is filled with some unknown amorphous electron-dense material. Tubules A and B continue into the axonemal structure, but tubule C stops in the transition zone, the region between the proximal end of axoneme and distal end of the BB (Lattao, Kovacs et al. 2017). A recent study using electron cryotomography with bovine cilia explained how BB could template the axoneme (Greenan, Vale et al. 2020). This suggested that i) the tubule C gradually disappears, and such process occurs throughout the BB zone, ii) the tubule C completely disappears at the beginning of transition zone, and iii) the microtubule angle begins to reduce at the end of basal body and such changes continue along the early ciliary axoneme.

2.3.2.2 Axoneme

The axoneme is the hair-like appendage of a cilium. The length of axoneme varies from a few micrometres in multiciliated cells to two millimetres in sperm, could be even up to 5 cm (in flagella of *Drosophila bifurca* sperm) (Dummer, Poelma et al. 2016). The whole axoneme is enveloped with a lipid bilayer membrane which is continuous with the plasma membrane of the cell (Ishikawa 2017). The axoneme is divided into three distinct regions: the transition zone, the doublet zone, and the singlet zone (Satir and Christensen 2007).

2.3.2.2.1 Transition zone

The transition zone is a complex region consisting of transition fibres (also called alar sheets), base plate, and Y-linkers and terminals. These structures are conserved but their appearances vary across species (Goncalves and Pelletier 2017). A terminal plate separates the lumen of the BB and the lumen of the transition zone. The transition fibres are localised at the proximal end of the transition zone. These pin-wheel like structures radiate from the B tubules just before the end of C tubules in the BB and at least two proteins in the transition fibres, CEP164 and ODF2, anchor the BB to the plasma membrane (Reiter, Blacque et al. 2012). The IFT52 protein in the transition fibres facilitates the IFT system that targets proteins to the axoneme (Deane, Cole et al. 2001, Webb, Mukhopadhyay et al. 2020). The base plate is

located at the distal end of the transition zone and serves as the nucleation or stabilization point (the minus end) of microtubules of the central tubules in the axoneme of motile cilia. It also restricts the central tubule extension from the axoneme to the basal body and serves as the site for axoneme breakdown during stress-induced autotomy (Quarmby 2004). Formation of the central tubules is controlled by SPAG6, where SPAG6 possibly acts as a chaperone and mediate interaction with other proteins like SNAPIN, COPS5, SPINK2, TAC1 and MSN (Teves, Sears et al. 2014, Liu, Zhang et al. 2019). The Y-linkers and terminals are structural proteins that connect the doublet microtubule to the membrane of the axoneme and are found at the distal end of the transition zone (Goncalves and Pelletier 2017). Such linkers contact between seventh protofilaments of both tubule A and tubule B though sixth protofilament of tubule B also contribute to make such contact (Greenan, Vale et al. 2020). The same study also showed that the microtubular angle is further reduced at the distal end of the transition zone to set the axonemal geometry followed by the addition of axonemal components such as dyneins and radial spokes (Greenan, Vale et al. 2020) (Figure 2.2C).

2.3.2.2.2 Doublet zone

The doublet zone lies between the transition zone and the singlet zone of the axoneme. The microtubular pattern in the doublet zone is the hallmark of structural definition for primary and motile cilia (Fisch and Dupuis-Williams 2011). The primary cilium consists of a 9+0 microtubular pattern, meaning a ring of nine doublets consisting of A and B tubules, each doublet is separated by approximately 0.05 µm, and without the central microtubule pair (Figure 2.2D). Motile cilia typically have a 9+2 configuration of dynein-decorated doublet microtubules (DMTs), as they have a central pair of microtubules separated from each other by a space of about 35 nm (Ishikawa 2017) (Figure 2.2E). However, some motile cilia have 9+0 arrangement, such as in the motile cilia of the murine embryonic node (Nonaka, Tanaka et al. 1998), and some primary cilia have 9+2 arrangement, *i.e.,* in the fish inner ear kinocilia (Flock and Duvall 1965). In motile cilia, the A tubule of each doublet is connected to the central microtubule pair by radial spoke fibres, and the outer dynein arms and inner dynein arms are extended from the A tubules of one doublet towards the B tubules of an adjacent doublets (King 2016). The A tubule of one doublet is also connected to the B tubules of adjacent doublet spaced every 85 nm by a nexin-

dynein regulatory complex (Alford, Stoddard et al. 2016). These features are completely absent in primary cilia. For both primary and motile cilia, the A tubule consists of 13 microtubules and the B tubules consists of 10 microtubules, and their connections are supported by tektins (Steffen and Linck 1988). Here, each single microtubule is a hollow rigid shaft of about 25 nm in diameter. The cargo proteins of IFT system travel in the space between the B tubule and the cilia membrane (Taschner and Lorentzen 2016). The central microtubules are in a central sheath, whereas the A tubules and B tubules possess a common wall (Figure 2.2D and F).

Fine structure of DMTs of the *Chlamydomonas reinhardtii* ciliary axonemal doublet zone has been explored recently using single-particle cryo-electron microscopy (Ma, Stoyanova et al. 2019). This study identified at least 33 microtubule inner proteins (MIPs) in the ciliary axoneme and 5 other MIP-associated proteins forming a 48 nm repeating network at the luminal surface of doublet zone. This study also showed that MIPs maintain a coherent periodicities to along the axoneme to provide the ciliary axoneme a unique architecture (Ma, Stoyanova et al. 2019). A very similar structure was found in bovine ciliary axonemal doublet zone along with a 24 nm periodic repeat (Gui, Farley et al. 2021). The study also identified 29 MIPs, among which 22 were conserved between bovine and *C. reinhardtii*, and also described the mechanism that bridges the 48 nm network with 24 nm network across the microtubular wall of tubule A lumen. Cross-sectional studies within the doublet zone also identified pentagonal bundle of tektin filaments formed by tektin homologs and stabilized by tektin bundle interacting protein 1 (TEKIP1) (Figure 2.2F) (Gui, Farley et al. 2021).

2.3.2.2.3 Singlet zone

In most cilia, their B tubules terminate at the distal end, leaving a singlet A tubule, and in case of motile cilia, the central tubule too. This is the singlet region and most signalling receptors localise here (Fisch and Dupuis-Williams 2011). In mammalian ciliated cells of the RE, this singlet zone supports the propulsion of the mucus in the trachea. Immunogold analysis revealed that the protein SENTAN, which is conserved in vertebrates, is localised in this region as a cilia apical structural protein but the function of this protein in the singlet zone is yet to be discovered (Ghossoub, Lindbaek et al. 2016). At the end of each cilium, a ciliary tip provides a site for

axonemal growth and resorption of primary cilia (Peabody, Shei et al. 2018). Limited studies have focused on this region since it is difficult to section this region for electron microscopic analysis. A cluster of negatively-charged bristles protrude from the ciliary tip is defined as ciliary claws or ciliary crown. It has been suggested that these bristles facilitate mucosal propulsion and cilia-mediated movement of ovum (Raidt, Werner et al. 2015). Also, A tubule and central pair tubules are bound to the ciliary crown through a central cap in tracheal cilia, and A tubules polymerizes and depolymerizes to change the length of the ciliary tips in response to different stimuli like osmotic stress, level of cAMP, presence of pathogens etc. (Soares, Carmona et al. 2019).

2.4 Ciliogenesis

Ciliogenesis is the complex multistage process for the biogenesis of cilia that is coupled to the cell cycle (Ishikawa and Marshall 2011). Since a cell contains either a single cilium (primary cilium) or multiple cilia, the process of ciliogenesis differs in these two scenarios, especially in centriolar division and in expression of a subset of genes (Choksi, Lauter et al. 2014). However, ciliogenesis is tightly regulated with cell division in both cases and the process occurs in the quiescent cell (the cell in G_0/G_1 phase). The basic principles of ciliogenesis include formation of BBs and development of the axoneme from the BB anchored to the plasma membrane (Avasthi and Marshall 2012). Thereby, a cell must exit cell division to free the centrioles from the centrosome for BB formation. Once the mature centriole docs at the plasma membrane, IFT occurs for axonemal assembly and disassembly to regulate the length the cilia (Luo, Cao et al. 2011).

2.4.1 Monociliogenesis

In monociliogenesis, only one primary cilium is generated in the cell. In a cycling mammalian cell, centriole duplication occurs during S phase. The process is tightly regulated by at least 5 centriole duplication factors namely PLK4, CEP192, CENPJ, STIL, and SAS6 (Gonczy 2012, Nigg and Holland 2018). When a dividing cell enters S phase, CEP63 and CEP152 binds at the proximal ends of the mother centriole and form a ring like structure to recruit CEP192 (Varadarajan and Rusan 2018). This complex subsequently recruits PLK4, CENPJ, STIL, and SAS6 to form a cartwheel for microtubule assembly (Arquint and Nigg 2016, Moyer and Holland 2019). PLK4

marks the initiation of centriolar duplication and eventually auto-phosphorylate and is degraded by ubiquitin-dependent pathway (Cunha-Ferreira, Bento et al. 2013, Moyer and Holland 2019). Such a process ensures only one round of centriolar duplication during the cell cycle. When the two centriole pairs are separated at the end of mitosis, the mother centriole serves as the BB of primary cilium (Figure 2.3A). Monociliogenesis follows one of the two pathways depending on how the mother centriole docks on the plasma membrane (Molla-Herman, Ghossoub et al. 2010, Smith, Lake et al. 2020). In the intracellular pathway, the mother centriole is absorbed on the membrane of a primary ciliary vesicle, and the ciliary axoneme grows within this vesicle. Later the developing primary cilium is fused with the plasma membrane (Lo, Lin et al. 2019). In the extracellular pathway, the mother centriole directly docs on the plasma membrane and the axoneme of the primary cilium develops from the mother centriole towards the extracellular territory. When the cilium is formed, P27 is overexpressed leading to inhibition of cyclin-dependent kinase (CDK) activity and cell cycle arrest (Lu and Hunter 2010, Breslow and Holland 2019). Most cells re-entering the cell cycle retract their primary cilia. Such deciliation process involves a first wave deciliation by aurora kinase A- and PLK1-mediated signalling pathways and a second wave of deciliation mediated by NEK2- and KIF24-dependent pathways (Lens, Voest et al. 2010, Kim, Lee et al. 2015, Breslow and Holland 2019).

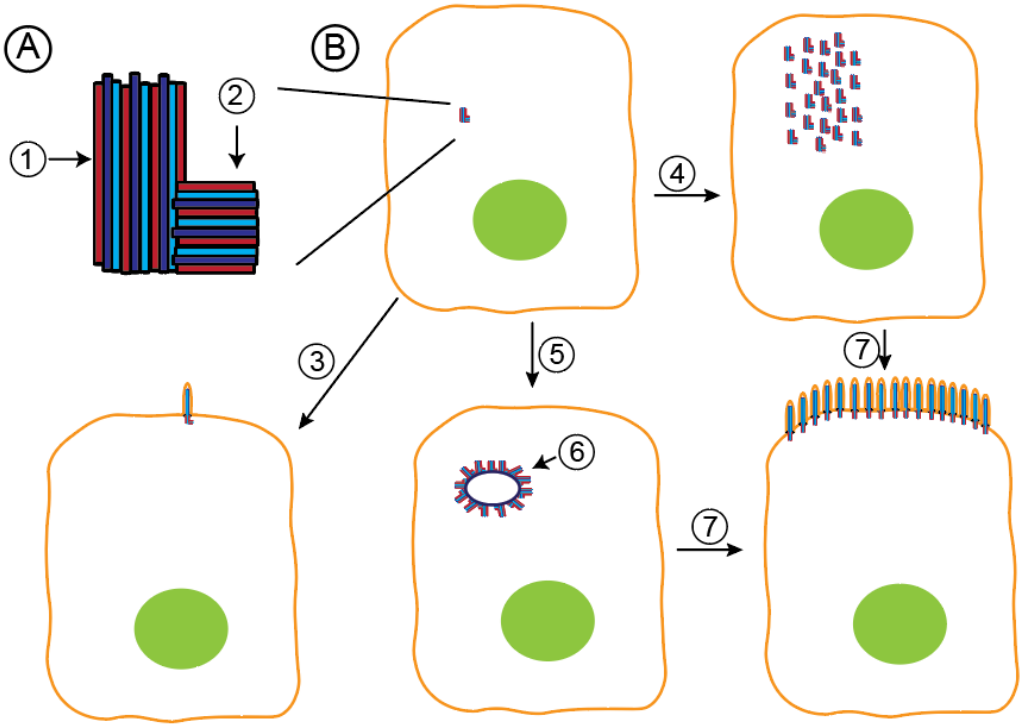

Figure 2.3 Overview of ciliogenesis. The structure of a dividing centriole (A), showing the mother centriole (1) and the daughter centriole (2). Ciliogenesis requires the docking of the centriole (B). During monociliogenesis, the mother centriole docks at the plasma membrane to generate a single cilium (3). Multiple centrioles are synthesized either by the canonical centriole-dependent pathway (4), or by the deuterosome-dependent pathway (5) in multiciliogenesis. A deuterosome is a complex of multiple proteins (6). In both cases, the deuterosome or individual centriole is trafficked to the plasma membrane and multiple cilia are generated at the apical surface of a cell (7).

2.4.2 Multiciliogenesis

Multiciliogenesis is much more complex than monociliogenesis and is associated with multi-step signalling pathways (Whitsett, Kalin et al. 2019). In multiciliogenesis, multiple cilia are formed in a terminally differentiated cell, and this requires mass production of centrioles in the progenitor cells. These multiple centrioles are synthesized either by i) a canonical centriole-dependent pathway, where more than one centriole is assembled at a time using the existing centriole as a platform, or ii) a deuterosome-dependent pathway, where *de novo* assembly of multiple centrioles takes place on an electron-opaque globular structure of proteins named deuterosome (Levine and Holland 2017) (Figure 2.3B). Despite both pathways sharing many components *i.e.,* CEP152, PLK4 etc., the deuterosome-dependent pathway has been suggested as the major pathway for multiciliogenesis (Shahid and Singh 2018). Studies revealed that CEP63 is required for the centriole-dependent

pathway, and DEUP1, a CEP63 paralogue, enables the deuterosome-mediated pathway in cells destined for multiciliogenesis (Arbi, Pefani et al. 2018). Multiciliogenesis begins with inhibition of NOTCH1/2 signalling and the process has been studied mostly during ciliogenesis of multiciliated cells in the RE. NOTCH1/2 is inhibited by GRHL2 or microRNA miR-449, the latter inhibiting NOTCH1 and its Delta-like 1 ligand. Inhibition of NOTCH1/2 promotes degradation of GEMININ and activation of MCIDAS, and such process allows formation of GMNC-E2F4/5-DEUP1 and MCIDAS-E2F4/5-DEUP1 complexes (Balestra and Gonczy 2014, Arbi, Pefani et al. 2016). GRHL2 also promotes MCIDAS-E2F4/5-DEUP1 complexes for deuterosome-dependent biogenesis of centrioles by recruiting PLK4 required for centriolar divisions (Arbi, Pefani et al. 2018). Also, these complexes suppress the expression of genes associated with cell cycle and induce the expression of both structural and regulatory cilia genes. Among these genes, TP73 and MYB are induced, which in turn induce the expression of the master regulator of ciliogenesis, FOXJ1 (Nemajerova, Amelio et al. 2018). TP73 also induces the expression of RFX factors (more specifically RFX2 and RFX3) required for stabilization of FOXJ1 binding at chromatin loops to mediate the expression of FOXJ1-dependent genes including *RFXs* (Jackson and Attardi 2016). As a result, expression of MCIDAS arrests the cell in a quiescent phase (*i.e.,* conversion of TP63-positive basal cell to TP63-TP73-KRT positive progenitor cell in the RE). Then the formation of MCIDAS-E2F4/5-DEUP1 complex upregulates MYB leading to centriolar biogenesis, and finally expression of FOXJ1 allows centriolar docking at the plasma membrane through Rho-GTPase and permits axonemal extension from each centriole by inducing the expression of structural cilia genes (Whitsett, Kalin et al. 2019) (Figure 2.4).

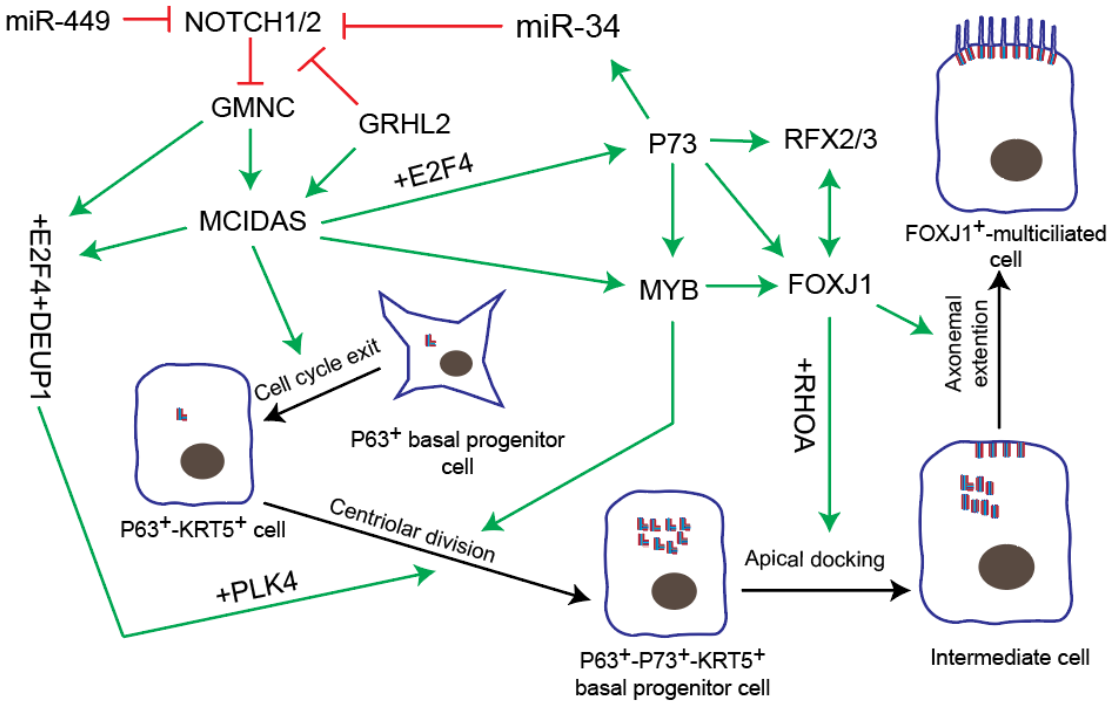

Figure 2.4 The multiciliogenesis signaling pathway. Ciliogenesis requires inhibition of NOTCH signaling by miR-449 or GRHL2, and activation of transcription factors MCIDAS-P73-FOXJ1 signaling cascades resulting in centriolar division, apical docking, and axonemal extension for converting TP63-positive basal progenitor cells to a multiciliated cell. Red arrows indicate inhibitory signals and green arrows indicate activator signaling processes of ciliogenesis. Black arrows indicate the steps in conversion of basal progenitor cells to multiciliated cells.

2.5 Genes involved in ciliogenesis

Over 600 genes have been found associated with ciliogenesis and more remain to be discovered (Bustamante-Marin and Ostrowski 2017). These genes can be classified broadly into three groups: i) structural genes those encode proteins required for formation of ciliary body, ii) regulatory genes, those encode gene products necessary for regulation of cilia formation and resorption, and iii) putative cilia genes, those encode for proteins found associated with cilia, but whose functions have not yet been established. Here, some structural, regulatory, and putative genes associated with multiciliogenesis are highlighted to outline the current understanding of motile cilia.

2.5.1 Structural genes

Structural genes encode necessary proteins to form the structure of the BB and ciliary axoneme. In one study, at least 55 genes were found to be driven by FOXJ1

(the master regulator of ciliogenesis) and among them, 24 encode cytoskeleton-associated motor proteins which form the ciliary body (Jacquet, Salinas-Mondragon et al. 2009). Three examples of these structural genes mostly abundant in cilia are briefly described here.

2.5.1.1 Dyneins

Dynein genes encode for proteins that are part of the microtubule-associated motor protein complex and they decorate the doublet microtubule of ciliary axoneme known as DMTs (Canty, Tan et al. 2021). Dynein proteins are known to regulate ciliary beat frequency and beat pattern in different directions (King 2018). These proteins hydrolyse ATP for their mechanical work during ciliary beating and classified as heavy, intermediate, and light chains based on their molecular weight. At least 19 dynein genes have been identified in humans associated with the ciliary axoneme. Among these, 14 are heavy chain genes (named *DNAH1*, *DNAH2*, *DNAH3*, *DNAH5*, *DNAH6*, *DNAH7*, *DNAH8*, *DNAH9*, *DNAH10*, *DNAH11*, *DNAH12*, *DNAH13*, *DNAH14*, *DNAH17*), two are intermediate chain genes (*DNAI1* and *DNAI2*) and light chain genes (*DNAL1* and *DNAL2*), and one is light intermediate chain gene (*DNALI1*) (Carter, Diamant et al. 2016). Dynein gene products are found within either inner or outer dynein arms (*i.e.,* DNAH2), and also provide structural support between the radial spokes and outer dynein arm (*i.e.,* DNAH1) (Chapelin, Duriez et al. 1997, Sha, Yang et al. 2017). Human patients with biallelic variants in dynein genes are very rare and mostly absent possibly due to the embryonic lethality effect of the mutation. Monoallelic mutation in five different dynein genes including *DNAL1*, *DHANH9*, *DNAH11*, *DNAI1* and *DNAI2* has been reported in primary ciliary dyskinesia (PCD) (Antony, Brunner et al. 2021). Also, absence or mis-localisation of DNAH5 is associated with ciliary abnormalities in nasal polyps and 53% of PCD with outer dynein arm defects (Hornef, Olbrich et al. 2006, Qiu, Peng et al. 2018).

2.5.1.2 Tektins

TEKTIN genes encode for proteins associated with ciliary microtubules. 5 human genes have been identified namely *TEKT1*, *TEKT2*, *TEKT3*, *TEKT4*, and *TEKT5*. Structurally all of them have 4 conserved helices namely Helix 1A, Helix 1B, Helix 2A and Helix 2B, where Helix 1B and Helix 2A are separated by a linker region, and consensus ‘RPNVELCRD’ amino acids are found between Helix 2A and Helix 2B

(Bastin and Schneider 2019). The *TEKTIN*-encoded proteins are required for the structural integrity of ciliary axoneme (Budamagunta, Guo et al. 2018). A recent study showed that these TEKTINs, except TEKT5 which is possibly sperm specific, form a pentagonal bundle in the lumen of tubule A of bovine ciliary axoneme and such bundle is stabilized by TEKIP1. Such TEKTIN bundles repeat across the DMTs by spacing at 8 nm, 16 nm, 24 nm, 48 nm, and even 96 nm (Gui, Farley et al. 2021). Thus, TEKTINs are an integral part of ciliary axoneme and loss of any TEKTIN affects ciliary motility (Bastin and Schneider 2019). It has been assumed that mutations in *TEKTIN* genes would be embryonic lethal in human though mutation in *TEKT2* has been reported with idiopathic asthenozoospermia (Zhang, Zhang et al. 2016).

2.5.1.3 Coiled-coil domain containing genes

Coiled-coil domain containing (CCDC) genes encode diverse proteins, all having a structure typically formed with 2-7 alpha-helices coiled together like a rope (Priyanka and Yenugu 2021). Some of these proteins function in the formation of nexin-dynein regulatory complexes *i.e.,* CCDC65 and CCDC164. Others function in centriolar assembly *i.e.,* CCDC120 and CCDC68 (Huang, Xia et al. 2017). At least 14 CCDC proteins have been found associated with ciliary motility and mutation in six of them including CCDC32, CCDC123, CCDC138, CCDC147, CCDC149, and CCDC164 could cause different ciliopathies. Interestingly expression of some CCDC proteins could be enriched in certain tissue, such as 11 CCDC proteins (CCDC9, CCDC33, CCDC38, CCDC42, CCDC62, CCDC63, CCDC87, CCDC136, CCDC172, CCDC181 and CCDC189) were enriched in male sperm (Priyanka and Yenugu 2021). Their mechanisms of action remain to be resolved. Mutations in *CCDC39* and *CCDC40* causes inner dynein arm defects as well as microtubular disorganization (Antony, Becker-Heck et al. 2013). Mutation in *CCDC39* is found in 4%-9% of PCD cases and mutation in *CCDC40* is found in 3%-4% of PCD cases. Also, mutations in *CCDC103* and *CCDC151* causes defect in outer dynein arm and found in <4% of PCD cases (Panizzi, Becker-Heck et al. 2012, Hjeij, Onoufriadis et al. 2014). Other defective CCDC genes rarely found in PCD are *CCDC65* and *CCDC114* (Horani, Brody et al. 2013, Li, He et al. 2019).

2.5.2 Regulatory genes

The regulatory genes not only control the expression of structural genes, but also decisions on when to form cilia in a cell. FOXJ1 has been considered as the master regulator of ciliogenesis. Other regulators maintain the length of cilia and control ciliary functions. Here, three mostly studied genes commonly known to regulate ciliogenesis are briefly described as examples.

2.5.2.1 Forkhead box gene J1 (*FOXJ1*)

Forkhead box (FOX) genes encode proteins that are transcription factors. These transcription factors contain forkhead/winged helices to bind at the regulatory sequence of genes to switch their expression on or off (Zaiss and Coffer 2018). Among the FOX genes, *FOXJ1* is one of the most studied genes in ciliogenesis and is required for the differentiation of multiciliated cells (Yu, Ng et al. 2008), hence expression of FOXJ1 in the airway epithelium is an indicative of multiciliated cells. FOXJ1 drives the expression of structural cilia genes and maintain the multiciliated stage of a cell, and total loss of ciliogenesis is observed when FOXJ1 expression is absent (Maiti, Bartoloni et al. 2000, Zhang, Huang et al. 2007, Jackson and Attardi 2016). FOXJ1 binds the DNA consensus sequences 5'-HWDTGTTTGTTTA-3' or 5'-KTTTGTTGTTKTW-3' (where H is not G, W is A or T, D is not C, and K is G or T) at the promoter/enhancer region of the target genes to facilitate their transcription. Mice lacking *Foxj1* are perinatal lethal and conditional *Foxj1*-knockout mice showed severe ciliopathies (Maiti, Bartoloni et al. 2000, Zhang, Huang et al. 2007). Though embryonic lethal phenotype is expected for biallelic mutation in *FOXJ1*, *FOXJ1* polymorphisms are associated with systemic lupus erythematosus and allergic rhinitis. Haploinsufficiency of *FOXJ1* has been reported in PCD as well as *de novo* mutation in *FOXJ1* could cause severe ciliopathy with hydrocephalus and left/right body asymmetry known as *situs inversus* (Wallmeier, Frank et al. 2019, Shapiro, Kaspy et al. 2021). FOXJ1 is also known to promote the growth of certain cancer cells and knockdown of FOXJ1 has been reported to inhibit proliferation, migration and invasion of laryngeal squamous cell carcinoma cells (Xian, Shang et al. 2018, Liu, Zhang et al. 2019), and could reduce growth of bladder cancer cells (Xian, Shang et al. 2018). Interestingly, *FOXJ1* knockout/knockdown studies with human cells are very limited and one report suggested knockdown of *FOXJ1* could reduce ciliation of nasal epithelial cells (Zahid, Feinstein et al. 2020), and highly efficient

FOXJ1 editing in primary HBEC could significantly reduce the number of ciliated cells (Rapiteanu, Karagyozova et al. 2020).

2.5.2.2 Geminin family genes

GMNN, *GMNC*, and *MCIDAS* are three genes constituting the geminin family and the proteins encoded by them function in cell proliferation and differentiation (Luo, Yang et al. 2004, Arbi, Pefani et al. 2018). GMNN induces cell cycle progression, but GMNC and MCIDAS is required for cellular differentiation toward ciliogenesis. MCIDAS forms a complex with E2F4/5 and DEUP1 to activate the expression of FOXJ1 and to regulate centriolar division (Hoque, Kim et al. 2022). However, GMNC can sufficiently promote multiciliogenesis, and hence is considered as another master regulator for ciliogenesis, through inducing overexpression of *FOXJ1* and *MCIDAS* (Arbi, Pefani et al. 2018). A recent study suggested that MCIDAS acts upstream of CCNO, is required for multiple BB production during multiciliogenesis through deuterosomal pathway, and is induced by GMNC (Lu, Anujan et al. 2019, Ma, Wu et al. 2021). *Gmnn* knockout mice show embryonic lethality, but *Gmnc* or *Mcidas* knockout mice are normal with impaired spermatogenesis and hence these mice are sterile (Terre, Lewis et al. 2019). Heterozygous mutation in *MCIDAS* can cause PCD in humans (Boon, Wallmeier et al. 2014).

2.5.2.3 Regulatory factor X genes

Regulatory factor X (RFX) genes are well studied in ciliogenesis, and they encode transcription factors containing conserved winged helix DNA binding domain called X-box (Sugiaman-Trapman, Vitezic et al. 2018). Among the 7 known RFXs, RFX1, RFX2, RFX3 and RFX7 are known to be associated with ciliogenesis (Manojlovic, Earwood et al. 2014, Lemeille, Paschaki et al. 2020). RFX1 is known to interact with RFX3 to regulate the expression of target genes. RFX2 stabilizes the FOXJ1 in the promoter region of FOXJ1-dependent genes and is directly associated with ciliogenesis (Quigley and Kintner 2017). Also, RFX3 directs nodal cilia formation and RFX7 is required for the formation of cilia in neural tube (Didon, Zwick et al. 2013, Choksi, Lauter et al. 2014). Mice lacking *Rfx1* and *Rfx3*, or *Rfx2* alone show embryonic lethality. Diseases associated with *RFX1* includes systemic lupus erythematosus, with *RFX3* includes visceral heterotaxy and *situs inversus*, and with

RFX7 includes deafness. Possibly, mutation in *RFX2* could be lethal in human (Lemeille, Paschaki et al. 2020).

2.5.3 Putative cilia-associated genes

With recent advances in technologies, multiple genes (*i.e., TEKTIP1*, *ENKUR*, *CDHR3* etc.) have been identified that have a temporal and spatial association with ciliogenesis (Everman, Sajuthi et al. 2019, Gui, Farley et al. 2021). Genetic and mutagenetic studies involved with some of these genes revealed that defective gene products exhibit phenotypic alterations associated with cilia function. However, their exact role in cilia structure or function is yet to be discovered (Lai, Gupta et al. 2011). This review describes four (out of many) putative cilia-associated genes where *PIERCE1* and *C15ORF65* are used as examples of genes with ongoing research in the lab, and *CDHR3* and *IQUB* are used as two differentially expressed genes during mucociliogenesis (Ross, Dailey et al. 2007, Ruiz Garcia, Deprez et al. 2019).

2.5.3.1 *PIERCE1* and *C15ORF65*

PIERCE1 (also known as C9ORF116) was initially identified as a p53 target gene in ultraviolet-induced DNA damage response (Sung, Kim et al. 2010). *Pierce1*$^{-/-}$ mice showed left-right asymmetry and expression of PIERCE1 was observed in both nucleus and cytoplasm of ciliated cells suggesting it might have a role in ciliogenesis (Sung, Baek et al. 2016). Previous study in our group has shown that *pierce1*-knockout zebrafish fail to show synchronous ciliary movement in Kupffer's vesicle. Recent studies suggested human *PIERCE1* is not a tumour protein 53 (TP53) target whereas murine *Pierce1* is a TP53 target (Kim, Lee et al. 2020). PIERCE1 seems to promote the proliferation of hepatocellular carcinoma cells and KRAS-mutant non-small cell lung carcinoma cells (Roh, Lee et al. 2020). However, loss of *PIERCE1* has no effect on survival of these cells indicating PIERCE1 possibly plays no oncogenic or tumour suppressor role (Park, Kim et al. 2020). *C15ORF65* is a distant paralogue of *PIERCE1* and is ubiquitously expressed in many tissues. C15ORF65 was initially discovered in malignant haematopoiesis and the functions of this protein remain unknown (Stein 2019). There exists no clear evidence on whether *PIERCE1* or *C15ORF65* is a target of FOXJ1 or not, but expression of *pierce1* in zebrafish was increased by 5.2-fold in *foxj1a*-overexressing cells (Choksi, Babu et al. 2014). Both PIERCE1 and C15ORF65 contain the domain of unknown function 4490 (DUF4490)

motif and two isoforms of human *PIERCE1* exists in databases. A recent report suggests that PIERCE1 and C15ORF65 are MIPs in the outer dynein arms-docking complex (ODA-DC), they span the microtubule wall to link the external ODA-DC to CFAP53 in DMT of bovine ciliary axoneme. PIERCE1 and C15ORF65 alternate every 24 nm within this structure although the structure of these proteins were found similar (Gui, Farley et al. 2021). The same study also revealed that maternal zygotic *pierce1*$^{-/-}$*c15orf65*$^{-/-}$ zebrafish: (i) showed increased situs anomalies which could be rescued by the presence of any one of these genes; (ii) missed outer dynein arms of Kupffer's vesicle cilia; (iii) showed no change in cilia number and size. The research also showed (i) embryonic lethality in *Pierce1*$^{-/-}$*C15orf65*$^{-/-}$ mice; (ii) reduced beat frequency of nodal and tracheal cilia of *Pierce1*$^{-/-}$ mice; and (iii) a reduction only in nodal ciliary beat frequency of *C15orf65*$^{-/-}$ mice; and (iv) disrupted beat pattern or absence of outer dynein arm of tracheal cilia in individual *Pierce1*$^{-/-}$ or *C15orf65*$^{-/-}$ mice (Gui, Farley et al. 2021). However, the regulatory role for these proteins in ciliogenesis in mice or their role in human ciliogenesis is still unknown. Also, no mutations have been reported in these genes in humans to date.

2.5.3.2 *CDHR3*

Cadherins are calcium-dependent cell-adhesion molecules required for cell-cell junctions and to regulate cytoskeletal complexes. They also play critical roles in cell proliferation and differentiation by mediating diverse signalling pathways (Yulis, Kusters et al. 2018). Among the known cadherins, Cadherin-related family member 3 (*CDHR3*) is expressed during mucociliary differentiation (Ross, Dailey et al. 2007) and expressed only in multiciliated cells (Ruiz Garcia, Deprez et al. 2019) suggesting that *CDHR3* a putative cilia-associated gene. Mutations in *CDHR3* have been associated with childhood asthma, chronic obstructive pulmonary disease (COPD), and chronic rhinosinusitis (Bonnelykke, Sleiman et al. 2014, Chang, Willis et al. 2017). CDHR3 plays important roles in rhinoviral C entry in the RE and could be involved in ciliogenesis (Palmenberg 2017, Everman, Sajuthi et al. 2019). Recent reports suggests that CDHR3 plays a critical role in otitis media susceptibility in patients and is downregulated within 3 hours after viral infection of mouse middle ear (Hirsch, Elling et al. 2021).

2.5.3.3 *IQUB*

IQ motif and ubiquitin domain containing (IQUB) shows biased expression towards multiciliated cells (Lai, Gupta et al. 2011). *IQUB* produces three different proteins in human and no association of this gene with disease has been reported. IQUB interacts with the cilia gene ZMYND10, which plays important role in formation of axonemal structure organization and motility (Cho, Noh et al. 2018). IQUB has been found in the human ciliome (Sigg, Menchen et al. 2017), however the function of IQUB in ciliogenesis has yet to be explored. Upregulation of *IQUB* could promote the cell proliferation and migration of breast cancer cell line (Li, Ma et al. 2018).

2.6 Diseases associated with ciliary defects

Developmental abnormality or functional alteration of cilia due to genetic defects, or pathogenic infection and environmental challenges cause multiple diseases in humans (Figure 2.5) (Joachimiak, Wloga et al. 2018, Wallmeier, Nielsen et al. 2020, Modarage, Malik et al. 2022). These diseases include PCD and COPD affecting the lung (Tilley, Walters et al. 2015); polycystic kidney disease (PKD) and nephronophthisis affecting the kidney (Dell 2015); Joubert syndrome and autism spectrum disorder affecting the brain (Youn and Han 2018); cone-rod dystrophy and Senior-Loken syndrome affecting the eye (Bujakowska, Liu et al. 2017, May-Simera, Nagel-Wolfrum et al. 2017); situs anomalies/ambiguous and asphyxiating thoracic dysplasia affecting the thorax (Mayer, Campbell et al. 2016), Bardet-Biedl syndrome and Meckel-Gruber syndrome affecting multiple organs; and many more (Bergmann 2012). Ciliary defects from genetic abnormalities are termed as ciliopathies and more than 50 cilia-associated genes have been identified to cause severe pulmonary diseases (Tilley, Walters et al. 2015, Spassky and Meunier 2017, Niziolek, Bicka et al. 2022). Since ciliopathies are considered as complex multisystem disorders, they are now classified into two broad groups: motile ciliopathies and sensory ciliopathies (Kempeneers and Chilvers 2018). Although the incidence of each ciliopathy is rare, collectively ciliopathies affect 1 in 2000 people around the globe (Vos, Abajobir et al. 2017, Kempeneers and Chilvers 2018). The RE is mostly affected in ciliopathies as the epithelium constantly encounters pathogens, dust, and allergens from the inhaling air, and these agents put an extra pressure on MCC activities resulting in reduction of the number of active cilia and disruption of the normal ciliary movement (Mayer, Bartz et al. 2008, Boon, Wallmeier et al. 2014). Here, some common

pulmonary diseases arising from direct ciliary defects, or indirectly associated with ciliary function are discussed.

2.6.1 Direct ciliary defects: primary ciliary dyskinesia

Pulmonary disease would be expected to arise from defective ciliary function or defective ciliogenesis as cilia play the critical role in mucus clearance and without such function, could cause mucus accumulation throughout the trachea and bronchia blocking the airways. Such blockage makes breathing difficult enough to eventually lower the blood oxygen level, can reduce the forced expiratory volume in 1 second (FEV_1) and also the forced vital capacity (FVC). Thus, artificial ventilation can become ineffective for these patients and thus ultimately could lead to death. Most of the mutations associated with direct ciliary defects are considered as embryonic lethal, fetuses with mild defect in cilia can be still born and show severe respiratory distress (Cortellino, Wang et al. 2009, Shamseldin, Tulbah et al. 2015). Pulmonary diseases associated with ciliary defects are termed as PCD.

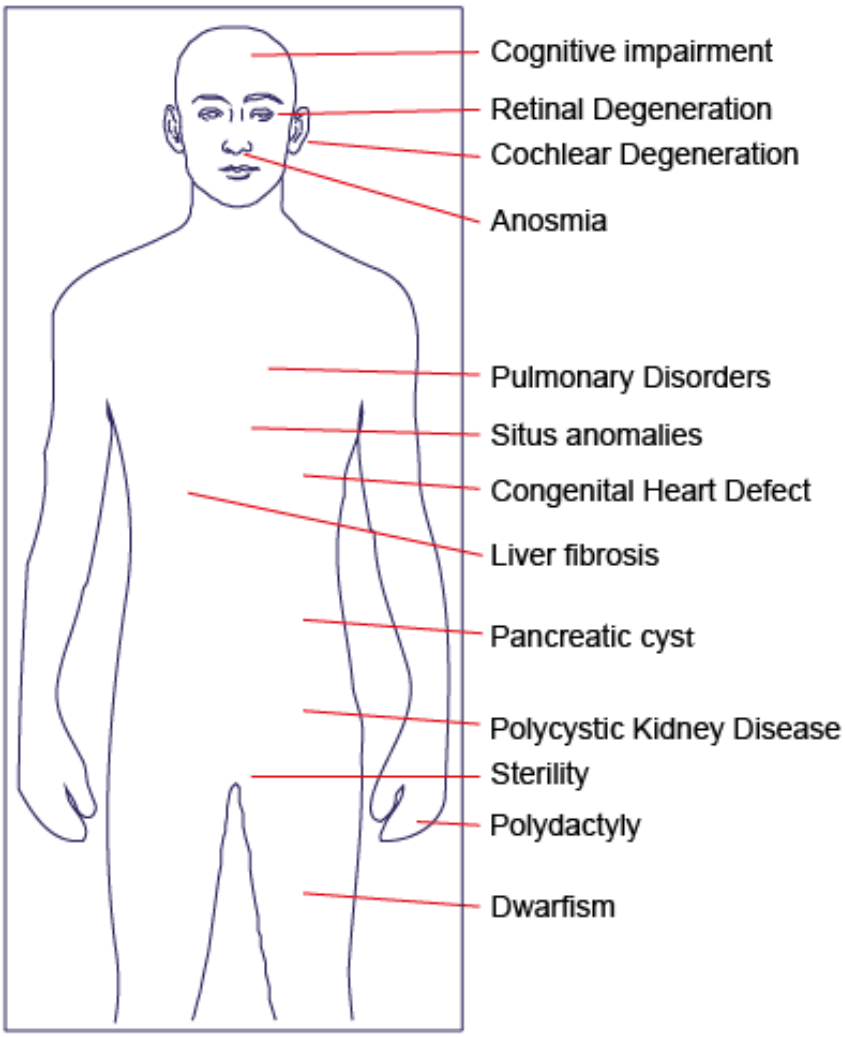

Figure 2.5 Spectrum of ciliary defects in humans. Loss of cilia structure or function can give rise to several disorders in humans. The locations of these disorders are illustrated in this figure.

PCD is a group of predominantly autosomal recessive disorders affecting cilia structure, function, and biogenesis (Knowles, Zariwala et al. 2016). The disease is associated with variable clinical features such as, but not limited to, chronic otosinopulmonary disease, situs abnormalities, and male subfertility (Lobo, Zariwala et al. 2014). Abnormal ciliary structure and function in PCD causes retention of mucus in the RE resulting in respiratory distress and eventually bronchiectasis; and accumulation of fluid leads to recurrent otitis media and hydrocephalus (Butterfield 2017). Diagnosis of PCD is based on clinical findings, laboratory tests including digital high-speed video microscopy with ciliary beat pattern analysis (HSVM), nasal nitric oxide level, cell culture and ultrastructural abnormalities of the cilia, and genetic tests using a multigene panel (Shapiro, Davis et al. 2018, Wang, Chen et al. 2018).

Though more than 50 genes could be mutated in PCD (Niziolek, Bicka et al. 2022), mutation in at least 32 genes have been identified in about 66% patients with PCD, of which 17 are common and 15 are rare. And, 57% of these patients from Europe or North America have mutation in either *DNAH5*, *DNAH11*, *CCDC39*, or *DNAI1* (Rumman, Jackson et al. 2017). Most of the structural defects are observed in dynein arms and central apparatus (Wang, Chen et al. 2018). About 30% of PCD patients with clinical symptoms show no noticeable structural abnormalities in cilia as examined by transmission electron microscopy (Papon, Coste et al. 2010, Shoemark, Boon et al. 2020). Differential diagnosis of PCD includes chronic sinopulmonary disease and bronchiectasis, and situs abnormalities (Shapiro, Davis et al. 2018, Wallmeier, Nielsen et al. 2020). Complications of PCD include severe respiratory distress and recurrent infections in the respiratory tract in early childhood (bronchiectasis), later developing into severe lung disease. Other complications includes loss of hearing and central nervous system, genitourinary, and skeletal malformations (Goutaki, Meier et al. 2016). At present, there is no specific treatment for PCD. Patients are routinely immunized to provide protection from respiratory pathogens and approaches are taken to enhance mucus clearance from the respiratory tract. Despite such efforts, PCD patients of all ages suffer from significant disease burden with decreased quality of life (Rubbo and Lucas 2017).

2.6.2 Pulmonary diseases indirectly associated with ciliary defects

Some pulmonary diseases are associated with function ciliary defects that make the disease condition worse. Excess mucus secretion could be considered as the main culprit for such conditions putting too much stress on cilia to clear the mucus. Thus, such diseases could be indirectly associated with ciliary defects, mostly with abnormal ciliary beat and reducing the half-life of ciliary axoneme resulting in axonemal shedding. Alternatively, viral infection specific to multiciliated cells (such as rhinovirus C) could reduce the number of ciliated cells across RE causing accumulation of excess mucus. COPD (Thomas, Koh et al. 2021), cystic fibrosis and bronchiolitis are common and well-studied examples of such pulmonary diseases. Other diseases include bronchiectasis and asthma (Thomas, Rutman et al. 2010).

2.6.2.1 Chronic obstructive pulmonary disease (COPD)

COPD is a progressive, complex, multifactorial, and common pulmonary disorder which is associated with a significant morbidity and mortality of people throughout the world (Boudewijns, Babu et al. 2018). Mostly affecting adults, COPD causes the death of more than 3 million people annually with about 180 million people suffering around the globe (Vos, Abajobir et al. 2017). The typical symptoms of COPD include accelerating, irreversible obstruction of airflow through respiratory tract resulting in shortness of breath, chronic bronchitis, persistent cough with phlegm, and emphysema (Sarkar, Bhardwaz et al. 2019). End stage lung disease (ESLD), jugular venous distention, peripheral edema, and ischemic heart disease occurs at the advanced stages of COPD (Boudewijns, Babu et al. 2018). Most common causes of COPD are environmental such as air pollution including smoking, exposure to heavy metals and coal, and dust from silica, fibreglass, and cotton industries, comprising 95% of cases. These airborne irritants increase mucus secretion, which turn put excessive pressure on ciliated cells for MCC (Thomas, Koh et al. 2021). Also, these irritants induce inflammation and apoptosis in RE cells including ciliated cells (Rai, Adab et al. 2018). The remaining 5% cases of COPD are considered hereditary and 13 candidate genes have been proposed, of which autosomal co-dominant inheritance of *A1AT* was confirmed (Patrucco, Venezia et al. 2018). Diagnosis of COPD is based on symptoms, spirometry measurements, and chest X-ray showing expanded lungs with flattened diaphragm (Mirza, Clay et al. 2018). The differential diagnosis of COPD includes asthma, congestive heart disease, and pneumonia. There is no curative treatment for COPD, however, preventive measures to improve air quality are suggested and bronchodilators, corticosteroids, and antibiotics are recommended to reduce respiratory distress and to improve prognosis (Oba, Keeney et al. 2018).

2.6.2.2 Cystic fibrosis (CF)

CF is an autosomal recessive, early-childhood onset, multisystem disease affecting the respiratory epithelia, intestine, hepatobiliary system, exocrine pancreas and sweat glands through building up of thick mucus (Ong, Marshall et al. 1993). Clinical features of CF include chronic sinopulmonary disease, meconium ileus, obstructive azoospermia, acute salt depletion, digital clubbing, and elevated immunoreactive trypsinogen (Guo, Liu et al. 2018). CF is diagnosed by clinical presentation, sweat

test, and genetic screening. Biallelic mutations in cystic fibrosis transmembrane conductance regulator (CFTR) gene disrupting the function of the CFTR protein causes CF and hence the genetic test involves sequence analysis of this gene (Rodrigues, Gabetta et al. 2008). Eight different mutations in *CFTR* are commonly found in patients with CF and the incidence of CF is 1:3200 live births with 1:25 as a carrier (Foil, Powers et al. 2018). Other mutations in *CFTR* are rarer. The frequencies of these mutations vary among the races, however the Phe508del is considered as the common mutation in severe CF (Jackson and Goss 2018). CF is differentially diagnosed from PCD, asthma, primary dysphagia and gastrointestinal reflux, pediatric aspergillosis, congenital airway anomalies, and bronchiectasis (Villanueva, Marceniuk et al. 2017). Although CFTR is not abundant in ciliated cells of the RE and is predominantly present in ionocytes, ciliated cells possess epithelial sodium channel (ENaC) interacting with the CFTR (Rossi, Morelli et al. 2019). When the CFTR function is disrupted, ENaC activity is upregulated and increases the cellular reabsorption of sodium and water from the mucus (Sharma, Hanukoglu et al. 2018). Thick mucus generated in this way disrupts the MCC function of cilia and cause loss of cilia function (Blue, Louie et al. 2018). CF is incurable and the patients are managed with pulmonary rehabilitation, antibiotics, and aerosolized hypertonic saline. Triple therapy composed of ivacaftor (a chloride channel potentiator), elexacaftor and tezacaftor (which repairs and corrects CFTR F508del) has been approved recently (in 2021) for the treatment of CF patients aged six years or older has made a very significant effect on CF disease, and it is no longer considered to be a paediatric condition (Barry and Taylor-Cousar 2021). The average life expectancy of patients with CF is about 50 years (Savant and McColley 2018).

2.6.2.3 Bronchiolitis

Bronchiolitis is caused by human respiratory syncytial virus (HSRV) or rhinovirus that infect ciliated cells in the RE and leads to blockage of the small airways (Kusak, Grzesik et al. 2018). Loss of MCC occurs due to the death of ciliated cell from viral infection and causes accumulation of mucus in bronchiolitis (Wong, Rutman et al. 2005). Bronchiolitis is the most common cause of breathing problem in children under two years of age and mostly requires supportive care to recover, like supplemental oxygen therapy and nebulizing hypertonic saline. Diagnosis of bronchiolitis is based on clinical examination of coughing, wheezing, shortness of

breath, and rhonchi (low-pitched wheezing and snoring sounds from the lungs. Chest X-rays are sometimes done to rule out pneumonia (Gold, Hametz et al. 2019).

2.6.2.4 Bronchiectasis

Bronchiectasis is the permanent enlargement of airways of the lungs resulting in excess mucus deposition that can plug up the lungs, causing obstruction in breathing and make the lung vulnerable to infection (Chalmers, Chang et al. 2018). Common symptoms of bronchiectasis include breathlessness and persistent cough with phlegm associated with chest pain (O'Donnell 2018). Cilia impairment occurs in bronchiectasis causing aberrant RE remodelling. Congenital disorders affecting cilia motility as well as recurrent bacterial infection causes bronchiectasis in most affected people (Chen, Li et al. 2018). Hence, bronchiectasis can develop in people with PCD or CF (Firth 2019). Diagnosis of bronchiectasis is done by computed tomography (CT) analysis (Hill, Sullivan et al. 2018). Currently there is no treatment available for bronchiectasis and disease progression is controlled with antibiotics and postural drainage of mucus (O'Donnell 2018, Grimwood and Chang 2019).

2.6.2.5 Asthma

Asthma is a complex reversible obstructive lung disease where pulmonary airways are inflamed (Fireman 2003). Clinical symptoms of asthma include bronchospasm, bronchial hyperresponsiveness, and wheezing resulting in breathlessness, chest tightness, shortness in breath and coughing (Khatri and Erzurum 2019). Bronchoconstriction also usually occurs in asthma leading to death in some cases. Asthma occurs throughout life and affects 350 million people around world and causes about 4 million deaths every year (Vos, Abajobir et al. 2017). The major causes of asthma are allergens and inheritance of asthma-associated genes. Hundreds of genes have been associated with asthma (Kim and Ober 2019). Ciliary dysfunction and ultrastructural abnormalities of cilia are observed in severe asthma in children resulting in significant reduction of MCC activity (Thomas, Rutman et al. 2010). Exposure to allergens causes loss of cilia in ciliated cells and loss of the cohesive beating of cilia across the RE (Cokugras, Akcakaya et al. 2001). Diagnosis of asthma is based on clinical presentation and spirometry test (Khatri and Erzurum 2019). There is no cure for asthma; prognosis with managements like preventing allergen exposure, and treatments like the use of antihistamines and bronchodilators

is generally good, and these are indicated for patients (Haktanir Abul and Phipatanakul 2019).

2.7 The importance of studying cilia

Cilia are cellular antenna performing motility, sensory, and signalling role in cells. Multiciliated cells are essential for normal respiratory function, memory development, and fertility. Impairment of cilia structure and/or function in the RE causes respiratory disorders and restoration of normal ciliary function is a target to reduce the pathogenesis of such diseases. Moreover, ciliogenesis is linked with cell cycle, and genes involved with ciliogenesis have been implicated in cancer development and metastasis (*i.e.*, *FOXJ1*, *PRK1* and *PRK2*, *IFT88* etc.) as well as in neurological disorders (Shpak, Goldberg et al. 2014, Yamamoto and Mizushima 2021). Hence, more research is needed to fully elucidate both the structural and functional regulation of cilia. Such research could identify potential therapeutic or diagnostic targets and in the broad sense, possible therapeutics to block defective ciliary functions and to promote intrinsic ciliogenesis. Since the complete set of genes involved in ciliogenesis is yet to be identified, it is of the utmost priority to study multiciliated cells in the RE to define novel genes and their functions associated with ciliogenesis.

2.8 Approaches to identify novel cilia genes

Most structural and functional studies involving cilia were done with light and electron microscopies and these techniques are still in use. With the use of electron microscopy, ultrastructure of cilia was determined to define the ciliary function more precisely (Cokugras, Akcakaya et al. 2001). Early studies on genes involved with ciliogenesis was undertaken with genetic linkage studies in patients with defective ciliary (van Dorp, Wright et al. 1992, Ho, Williams et al. 1998, Pennarun, Escudier et al. 1999, Blouin, Meeks et al. 2000). Later, genome-wide association studies identified several genes associated with cilia structure and function (Corvol, Blackman et al. 2015). Also, mutational studies in ciliated protozoa, or in other animal models like mouse, zebrafish, and *Xenopus* led to the discovery of multiple cilia genes and their functions (Brooks and Wallingford 2015, Leventea, Hazime et al. 2016, Lodh, Yano et al. 2016, Siller, Sharma et al. 2017, Baehr, Hanke-Gogokhia et al. 2018, Jiang, Maier et al. 2019). Technologies such as differential gene

expression studies or more recently RNA-Sequencing and single cell RNA-Sequencing analysis can now be used to define the set of cilia genes in broader studies (Ross, Dailey et al. 2007, Miao, Leng et al. 2017, Stauber, Weidemann et al. 2017, Wesolowska-Andersen, Everman et al. 2017, Ruiz Garcia, Deprez et al. 2019, Patir, Fraser et al. 2020, Zaragosi, Deprez et al. 2020, Jiao, Hu et al. 2022). Proteomic analysis on cell fragments collected by laser capture microdissection revealed the list of proteins found in the basal body and axoneme of cilia (Blackburn, Bustamante-Marin et al. 2017) and similar studies have also been done using ciliary axonemes (Muhlhans, Brandstatter et al. 2011, Ma, Stoyanova et al. 2019, Sahabandu, Kong et al. 2019, Gui, Farley et al. 2021). Currently most of the studies are done with cells cultured in an air-liquid interface (ALI) culture (Ross, Dailey et al. 2007, Mulay, Akram et al. 2016, Jiang, Schaefer et al. 2018, Leung, Wadsworth et al. 2020, Ziegler, Allon et al. 2020). In ALI experiments, cells are cultured in conditions that mimic the normal physiological condition. The epithelial cells of the RE get nutrients from the lamina propria which lies below them, and the apical surface is covered with mucus (Figure 2.1A). In ALI culture, cultured cells are fed from the bottom of a semi-permeable transwell and the apical surface of the cells is exposed to air mimicking normal physiologic condition, with occasional washing the surface with buffered salt solution *i.e.,* Hank's balanced salt solution to clear the deposited mucus (Chandrasekaran, Kouthouridis et al. 2019). Hence, ALI culture is considered as an *in vitro* model a physiologic epithelium that mimics the process of ciliogenesis and mucus secretion. A combinatorial strategy involving ALI culture, differential gene expression studies, and CRISPR-CAS9 gene editing system to define cilia-associated genes is depicted in Figure 2.6. Beside this, latest strategies include electron cryotomography and single-particle cryo-electron microscopy have discovered the basal body to axoneme transition in cilia and detailed structures of *Chlamydomonas reinhardtii* and bovine ciliary axonemal doublet zone (Ma, Stoyanova et al. 2019, Greenan, Vale et al. 2020, Gui, Farley et al. 2021). Such studies, along with other, have revealed a clearer picture of cilia structure as well as have identified several cilia-associated genes and novel proteins associated with cilia structure (Zaragosi, Deprez et al. 2020).

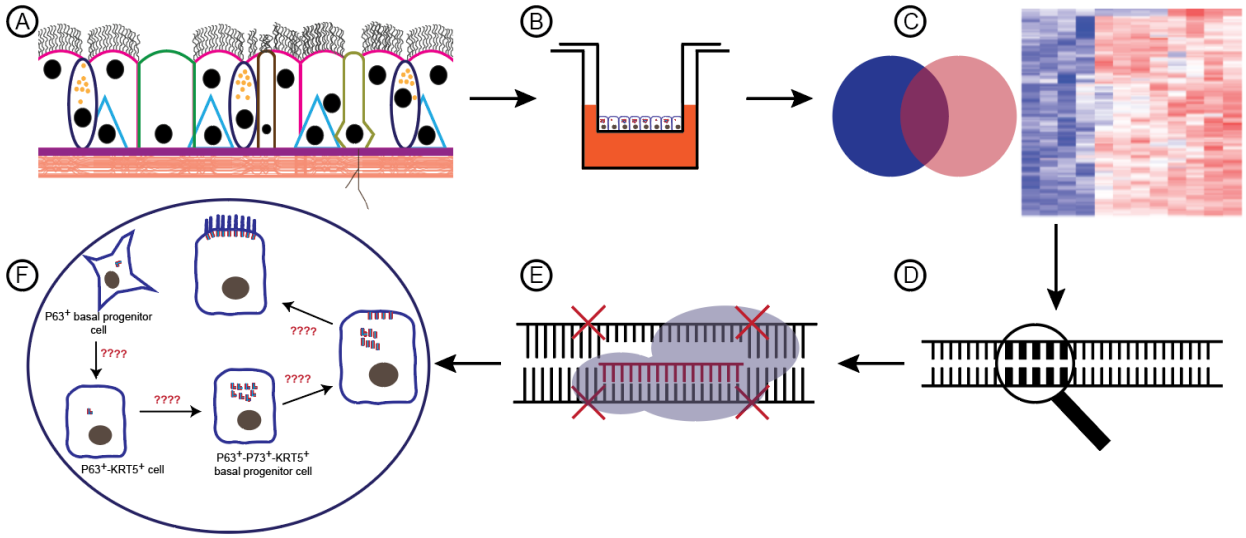

Figure 2.6 A combinatorial strategy to define cilia-associated genes. RNA isolated from multiciliated epithelial cells (A) cultured in ALI (B) can be subjected to DGE analysis (C) to identify candidate genes (D). CRISPR-CAS9 gene editing (E) will allow the functional characterization of these candidate genes in ciliogenesis or cilia structure (F).

2.9 Concluding remarks

Cilia in multiciliated cells perform diverse functions and any disruption in ciliary activity underpins many human diseases. Many aspects of cilia structure and function have been resolved yet and research is continuing in the area of biology to unravel the fine structure and other functions of cilia. With the discovery of putative cilia-associated genes, strategies can be taken to elucidate their functions in cilia. Better understanding of cilia could lead to the discovery of novel therapeutics to treat primary ciliary dyskinesia. Thus, further research is needed in this area of biology to comprehend cilia biology more. Since research with PIERCE1 function is ongoing in my current laboratory and C15ORF65 is a distant paralogue of PIERCE1, it would be interesting to elucidate their role in cilia.

2.10 Hypothesis and objectives

Here, it is hypothesized that ALI culture can be used to define the unknown functions of putative cilia genes like *PIERCE1* and *C15ORF65*. The objective of the study is to undertake functional characterization of the cilia-associated gene *PIERCE1* and its' distant paralog *C15ORF65*. The objectives of this thesis are:

1. To perform a thorough bioinformatic analysis on *PIERCE1* and *C15ORF65*.
2. To validate the mucociliary differentiation of HBEC3-KT cells in ALI and submerged culture.
3. To perform CRISR-CAS9 based knockout of *FOXJ1*, *PIERCE1*, *C15ORF65* and dual *PIERCE1-C15ORF65* and single clone proliferation.
4. To investigate the differentiation of knockout and wildtype HBEC3-KT cells to define PIERCE1 and C15ORF65 functions associated with cilia.

Chapter 3: Materials and Methods

3.1 Preface

All the experimental protocols performed during this study are described in this chapter. It also includes all information about the bioinformatic tools and software (including the version number) used to analyse data. Information about specific commercial kits and reagents are mentioned in respective protocols. All mouse work was done in collaboration with Professor Dominic Norris (MRC Harwell Institute).

3.2 Cell culture

Human bronchial epithelial cells immortalized with mouse cyclin-dependent kinase 4 (*Cdk4*) and human telomerase reverse transcriptase (*hTERT*), commonly known as HBEC3-KT cells (Nakauchi, Nagata et al. 2019), were used a model for ciliary differentiation studies. The cells were provided by Dr Frank McCaughan, Cambridge University. These cells were routinely cultured in keratinocyte serum-free media (KSFM) supplemented with 50 mg/L bovine pituitary extract (BPE) and 5 μg/L prequalified recombinant human epidermal growth factor 1-53 (EGF 1-53) (all were supplied by ThermoFisher Scientific, Cat# 17005042) and were maintained in a cell culture incubator at 37 ºC with 5% CO_2 and humidified environment. Confluent cells in T25 flasks were trypsinized for 3 minutes at 37 ºC followed by neutralization of trypsin using soybean trypsin inhibitor (both were supplied as Detach kit, PromoCell, Cat# 41220). Detached cells were briefly spun at 500 g for 5 minutes and the supernatant was discarded. Cells were seeded at 1×10^6 cells for a T25 flask, 6×10^4 cell in each well of a 24 well plate, or 3×10^4 cells in each transwell (0.4 μm, Falcon, Cat# 353095) for air-liquid interface (ALI) culture in BPE/ EGF 1-53 supplemented KSFM media. For ALI culture, cells were fed from the bottom of each transwell with 700 μl PneumaCult™-ALI (PALI) complete media (STEMCELL Technologies, Cat# 05001) with changing the media and washing the cells surface with 200 μl Hank's Balanced Salt Solution (HBSS) (Gibco, Cat# 14175095) every two days for up to 21 days. For submerged culture with PALI media, 500 μl of complete PALI media was added in each well of a 24-well plate and the media was changed every two days for up to 21 days. Cells were also grown on complete PneumaCult™-Ex Plus (Ex+) media (STEMCELL Technologies, Cat# 05040) with or

without 0.2 μM hydrocortisone (STEMCELL Technologies, Cat# 07925). For treatment, HBEC3-KT cells were treated with either 10 μM DAPT ((2*S*)-*N*-[(3,5-difluorophenyl)acetyl]-L-alanyl-2-phenyl]glycine 1,1-dimethylethyl ester, TOCRIS, Cat# 2634) or 1 ng/ml recombinant human interleukin-13 (IL13) (NOVUS BIOLOGICALS, Cat# 213-ILB) was added to each well of a 24-well plate.

3.3 Culture of murine nasal cavity epithelial, middle ear epithelial and tracheal epithelial cells

C57BL6 mice were dissected to collect the multiciliated epithelia from middle ear, nasal cavity, and trachea in sterile condition. Cells were isolated from these tissues and were cultured using previously published protocol (Mulay, Akram et al. 2019). Briefly, tissues were treated with Dulbecco's Modified Eagle Medium (DMEM)/F-12 (Sigma, Cat# D6421) containing 0.15% (w/v) pronase isolated from *Streptomyces griseus* (Roche, Cat# 10165913103) and incubated overnight at 4 ºC keeping the tube upright. After inverting the tube five times, the tissue fragments were removed using sterile Pasteur pipette and cells were collected by centrifugation at 500 g for 10 minutes. Then the cells were suspended in DMEM media containing 10% heat-inactivated fetal bovine serum (FBS) (Gibco, Cat# 10082147), 0.5 mg/ml bovine pancreatic DNase I (Sigma, Cat# 4716728001) and 1 mg/ml bovine serum albumin (BSA) (Sigma, Cat# A9418). After incubation for 5 minutes on ice, cells were collected by centrifugation at 500 g for 5 minutes. Cells were suspended again on DMEM containing 10% FBS, 2 mM L-glutamine (Gibco, Cat# 25030081) and 200 units/ml penicillin – 200 μg/ml streptomycin (Gibco, Cat# 15140122) and incubated for 4 hours at 37 ºC with 5% CO_2 and humidified environment in a cell culture dish to facilitate the adherence of fibroblasts. After that, the supernatant was collected and was centrifuged at 500 g for 5 minutes to collect the epithelial cells. Then the cells were suspended with PneumaCult™-Ex Plus media (STEMCELL Technologies, Cat# 05040) and 3×10^4 cells were seeded in each transwells of a 24-well plate. After the cells became confluent, they were subjected to ALI culture using PneumaCult™-ALI complete media (STEMCELL Technologies, Cat# 05001) for up to 21 days with changing media and washing the cell surface with HBSS every two days. This culture work was previously undertaken by Dr Apoorva Mulay (middle

ear), Priyanka Anujan (nasal cavity), and Renata Caikauskaite (trachea). I repeated two replicates of nasal cavity and tracheal epithelial cell culture and differentiation.

3.4 Isolation of genomic DNA, RNA, and preparation of cDNA

For isolation of genomic DNA, cells were treated with tissue lysis solution (50 mM Tris–HCl, 100 mM NaCl, 0.1 mM EDTA, 1% SDS, 20 μg/ml proteinase K (Invitrogen, Cat# 25530031, pH 7.4) overnight and then the protein was precipitated using equal volume of 5M NaCl. Supernatant was collected after centrifuging at 10,000 g for 10 minutes. DNA was precipitated from the supernatant with equal volume of isopropanol and then washed three times with 70% ethanol. Genomic DNA was suspended in TE (10 mM Tris, 1mM EDTA, pH 8.0) buffer after removal of all ethanol. Alternatively, DNA was extracted using DNArealesy advanced (NIPPON Genetics EUROPE GmbH, Cat# LS06). Briefly, cell pellet was suspended with 20 μl TE buffer and then 5 μl of DNAreleasy Advance was added. Then the solution was incubated at 65 ºC for 30 minutes followed by 96 ºC for 5 minutes. Then the lysate was cooled at 20 ºC for 5 minutes followed by centrifuging at 10,000 g for 5 minutes. The supernatant was collected and 1 μl of such supernatant was used as a template for PCR. Prepared DNA samples was stored at 4 °C for one week or at -20 °C for longer periods.

RNA was isolated from cultured cells using Direct-zol RNA microprep (ZYMO RESEARCH, Cat# R2062) with the manufacturer's protocol. Briefly, cells in each well of a 24-well plate or in a transwell were treated with 300 μl TRI-reagent (Sigma, Cat# T9424) and the lysates were transferred to Zymo-Spin™ IC column and in-column DNase I digestion was followed. After washing with buffers, the RNA was eluted from the column using DNase-RNase free water. RNA concentration was measured by NanoDrop™ 2000 spectrophotometer, and 200 ng of RNA was converted to cDNA in all cases of reverse transcription. RNA samples were stored at -80 °C until the samples were used to prepare cDNA.

cDNAs were prepared from the RNA using Avian Myeloblastosis Virus (Amv) reverse transcriptase enzyme system (Promega, Cat# M5101) following manufacturer's protocol. Briefly, 200 ng of RNA was digested with 1 unit of RQ1 RNase free DNase

(Promega, Cat# M6101) for 30 minutes at 37 °C to ensure complete removal of trace amount of genomic DNA contaminant if present, followed by inactivating the DNase with 1 μl of RQ1 DNase stop solution at 65 °C for 10 minutes. 20 μg oligo(dT) (Promega, Cat# C1101) and 20 μg random hexamer (Promega, Cat# C1181) was added to this solution and the solution was incubated at 37 °C for 5 minutes. After cooling on ice, 1 mM dNTP mix (Prepared from 100 mM dNTP set provided by Promega, Cat# U1240, U1330, U1410 and U1420), 20 units of RNasin® RNase inhibitor (Promega Cat# N2511), and 2.5 units of AMV RT were added to this processed RNA sample and was incubated at 42 °C for 60 minutes, followed by 95 °C for 5 minutes. Prepared cDNA was stored at -20 °C.

3.5 Microarray data analysis

Mouse Clariom™ S microarray analysis (ThermoFisher Scientific, Cat# 902930) was performed using RNA isolated from mouse cells by Dr Paul Heath at SITRAN, University of Sheffield, UK. The Clariom™ S data on the expression of >20,000 well-annotated genes in murine model system were converted to spreadsheet using Transcriptome Analysis Console (TAC) tool version 4.02. Then the data was analysed in TAC tool or in Microsoft™ Excel for difference in intensity, fold change, and p-value ($p<0.05$ was considered significant). All the calculations and statistical analyses such as average, standard deviation, p-value calculation ($p<0.05$ was considered significant) and differential analyses were performed using TAC tool or Microsoft™ Excel. Log2(Intensity) < 5 was considered as negative for expression and Log2(Intensity) ≥ 5 was considered as positive for expression of individual genes (Miller, Menon et al. 2014). The microarray data were normalized and background-corrected using robust multi-array average-linear models for microarray data (RMA-LIMMA) algorithm integrated in TAC tool (Ritchie, Phipson et al. 2015). Data are uploaded at Gene Expression Omnibus (GEO) database (https://www.ncbi.nlm.nih.gov/geo) and the obtained accession numbers are GSE150764 (middle ear epithelium), GSE162259 (nasal cavity epithelium) and GSE 162257 (tracheal epithelium).

Gene Expression Omnibus (GEO) dataset GSE32036 (Byers, Diao et al. 2013, Hight, Mootz et al. 2020) was used for HBE3-KT cell gene expression analysis,

GSE5264 (Ross, Dailey et al. 2007) was used for gene expression studies during human bronchial epithelial cell differentiation at ALI, and GSE75717 (Nemajerova, Kramer et al. 2016) was used for gene expression studies during murine tracheal epithelial cell differentiation at ALI. For analysing GEO data, GEO2R (Barrett, Wilhite et al. 2013) (provided by National Center for Biotechnology Information (NCBI, www.ncbi.nlm.nih.gov)) was used. P-values were adjusted with Benjamini & Hochberg method (non-parametric), and LIMMA was applied for normalization, and Log(Fold change) more than 1.5 or less than -1.5 was considered as differentially expressed genes. For all cases, P-value < 0.05 was considered significant.

3.6 Basic bioinformatic analyses

Human *FOXJ1* (Gene ID: 2302), *PIERCE1* (Gene ID: 138162) and *C15ORF65* (Gene ID: 145788) sequences for protein, RNA, and genomic DNA were retrieved from NCBI website. For mouse Pierce1 transcript analysis, Gene ID: ENSMUSG00000026831 was used at Ensembl (www.ensembl.org). Multiple sequence alignment with multiple sequence comparison by Log-expectation (MUSCLE) and maximum-likelihood phylogenetic tree construction was performed using Molecular Evolutionary Genetics Analysis (MEGA) version X using Jones-Taylor-Thornton model and maximum parsimony model as initial tree on which 1000 Bootstrap replicates were applied (Edgar 2004). Sequences of PIERCE1 and C15ORF65 used in for these purposes are given in Table 3.1. Mutational analysis in HEK293 genomes were analysed with integrated genome viewer (IGV) linked to HEK293genomes version 2 (http://hek293genome.org/v2) (Lin, Boone et al. 2014). Gene trees built with Tree building guided by species tree (TreeBeST) were collected from Ensembl (www.ensembl.org) with Gene IDs: ENSG00000160345 and ENSG00000261652 respectively for PIERCE1 and C15ORF65. The cryo-electron microscopic structure of bovine ciliary axoneme (PDB ID: 7RRO) (Gui, Farley et al. 2021) was downloaded from Protein Data Bank (PDB) and was analysed using PyMol for extraction of bovine PIERCE1 and C15ORF65 structures to serve as a template to deduce human PIERCE1 and C15ORF65 structures. Protein structures were also predicted using I-TASSER or collected from AlphaFold database (https://alphafold.com). Later these structures were aligned using PyMol. PIERCE1 (NP_001041730.1) and C15OF65 (NP_001185713.1) sequences were analysed to find any known motif using Motif Scan available at Swiss Institute of Bioinformatics

(SIB) (myhits.sib.swiss/cgi-bin/motif_scan). All data associated with Human Protein Atlas (HPA) were collected from HPA database (proteinatlas.org). Single-cell RNA-sequencing based analysis of gene expression in HBEC and mouse tracheal epithelial cells (mTEC) were collected from Harvard Medical School (kleintools.hms.harvard.edu/tools/springViewer_ 1_6_dev.html?datasets/reference_HBECs, and kleintools.hms.harvard.edu/tools/ springViewer_1_6_dev.html?datasets/uninjured_MTECs). Gene annotations were done using BioGPS (Wu, Jin et al. 2016). *in silico* translation was performed using Expasy translate tool. Protein subcellular localisation was predicted using DeepLoc version 1.0 and 2.0 available at the Technical University of Denmark (services.healthtech.dtu.dk/service.php?DeepLoc).

Table 3.1 NCBI accession numbers of PIERCE1 and C15ORF65 sequences. These sequences were collected from NCBI database and were used for MSA and phylogenetic tree development using MUSCLE.

Organism	PIERCE1	C15ORF65
Human	NP_001041730.1	NP_001185713.1
Bovine	NP_001032568.1	A0A3Q1LFK7.1
Mouse	NP_081316.1	NP_001185718.1
Rat	NP_001100034.1	NP_001185725.1
Zebrafish	NP_001116715.1	XP_021323402.1

3.7 Polymerase chain reaction (PCR)

PCR was carried out using the genomic DNA or cDNA prepared earlier. PCR primers were designed using Primer-BLAST at NCBI (Ye, Coulouris et al. 2012). List of primers are given in Table 3.2. Simply, 1 μl of diluted cDNA sample or 50 ng of genomic DNA was added to 10 μl of 2x PCR mastermix (Maxima^{TM} Hot Start Green, ThermoFisher Scientific, Cat# EP0602; or, FastGene 2X ReadyMix, NIPPON Genetics EUROPE GmbH, Cat# LS27), 1 μl of 10 μM forward primer, 1 μl of 10 μM reverse primer and 7 μl of water. PCR was carried out in thermocycler with initial denaturation at 95 ^{0}C, followed by 35 cycles of denaturation at 95 ^{0}C for 30 seconds, annealing at 60 ^{0}C for 30 seconds, and extension at 72 ^{0}C for 1 minute, followed by a final extension at 72 ^{0}C for 7 minutes. PCR products were resolved in 1.5% agarose gel containing ethidium bromide and then the gel was imaged using BioRad gel documentation system. Water was used as a negative control when genomic DNA was used for template, and crude RNA was used as a negative control when

cDNA was used as a template. To confirm an amplicon, PCR product was purified from the agarose gel using Monarch® DNA Gel Extraction kit (New England Biolabs Inc., Cat# T1020S) using manufacturer's protocol and cloned in pCRII-TOPO cloning system with manufacturer's protocol (ThermoFisher Scientific, Cat# K461020) followed by transformation in competent *E. coli* and sequencing using SP6 primer (forward) or T7 primer (reverse) as described later.

Table 3.2 List of primers used for PCR. gDNA = Genomic DNA.

Name	**Sequence (5'→3')**	**Amplicon**
hFOXJ1FA	TCGCAGGCACCACATACTTA	846 bp on gDNA
hFOXJ1RA	AAGTCAAAGGAGGGGCAGTT	
hPIERCE1CrispF1	GCAGTGCTTAAACCCCGTCA	757 bp on gDNA
hPIERCE1CrispR1	GAGAGGAGACTCACCCGACA	
hC15ORF65CrispF1	GCAGCGGTGAAGAGAAGAAC	565 bp on gDNA
hC15ORF65CrispR1	CACCTTCAGAGGCTATTCGGA	
hOAZ1F2	AAACGCATTAACTGGCGAAC	164 bp on cDNA
hOAZ1R2	CGGTTCTTGTGGAAGCAAAT	
hBPIFA1 Forward	ATGCCCTCAGCAATGGCCTGC	466 bp on cDNA
hBPIFA1 Reverse	GAGAGGCTGTCCAGAAGACC	
hTEKT1 Forward	TGGAGCTGTGTCGTCATGTC	198 bp on cDNA
hTEKT1 Reverse	GCATACACAGCACTTCGTCG	
hPIERCE1F	AGGACCAGCGACTACTACCG	258 bp on cDNA
hPIERCE1R	CACGATGCTTTTCTCCAGGT	
hC15ORF65F	CGCAACCGGGATAAGAAAAGT	320 bp on cDNA
hC15ORF65R	CTGGTTCTGTCAGGTGCAGT	

3.8 Designing and cloning of guide RNAs

Guide RNAs (gRNAs) for gene-editing of *PIERCE1* (Gene ID: 138162) and *C15ORF65* (Gene ID: 145788) using CRISPR-CAS9 technology were designed using the online Zhang Lab E-CRISPR tool available at http://www.e-crisp.org/E-CRISP/designcrispr.html. Five gRNAs were selected for each gene based on the off-target value < 1 (Table 3.3). *FOXJ1* gRNAs to delete defined part of FOXJ1-forkhead domain were previously designed, cloned into PX458 plasmid, midi-prepared and optimized by Ahmad Hassan (Hassan 2018). Locations of the gRNAs are given in

Figure 3.1. Reverse complementary sequences for each gRNA were designed to facilitate cloning. Each of double stranded gRNAs was cloned in PX458 plasmid for green fluorescence protein (GFP) selection. Plasmids were linearized with *Bbs*I digestion and purified from the gel after agarose gel electrophoresis using Monarch® DNA Gel Extraction kit (New England Biolabs Inc., Cat# T1020S) with manufacturer's protocol. Guide RNAs were annealed with respective complementary sequences by thermal renaturation and ligated into the linearized plasmid using T4-DNA ligase (New England Biolabs Inc., UK, Cat# M0202S) using manufacturer's protocol.

Table 3.3 List of gRNAs to edit *FOXJ1*, *PIERCE1*, and *C15ORF65* using CRISPR-CAS9. PAM: Protospacer adjacent motif. OTS: Off-target score.

Gene	Score	Sequence (5'→3')	PAM	Maximum OTS	gRNA No.
FOXJ1	93	GTCCACTTGTAGATGGCCGAC	AGG	0.3	F1
	88	GCGGGCAGGTTCAACAACCCG	TGG	0.6	F5
PIERCE1	98	GCTCACGCGGTAGTAGTCGC	TGG	0.3	P1
	94	GCACGTGACCTGGCCGTCGCT	TGG	0.6	P3
	93	GCGGGCAGGTTCAACAACCCG	GGG	0.8	P4
	92	GGTTGTTGAACCTGCCCGGC	AGG	0.6	P5
	91	GCCTGTTGCCAAGCGACGGCC	AGG	0.8	P7
C15ORF65	93	GAGAAAGCCGGTGAACGCCTA	GGG	0.8	C2
	92	GCGAAAATGACAGACCGCAAC	CGG	0.5	C3
	91	GAAAATGACAGACCGCAACC	GGG	0.3	C5
	91	GCGAAAATGACAGACCGCAAC	TGG	0.6	C6
	88	GAAGAAAGCCGGTGAACGCCT	AGG	0.6	C7

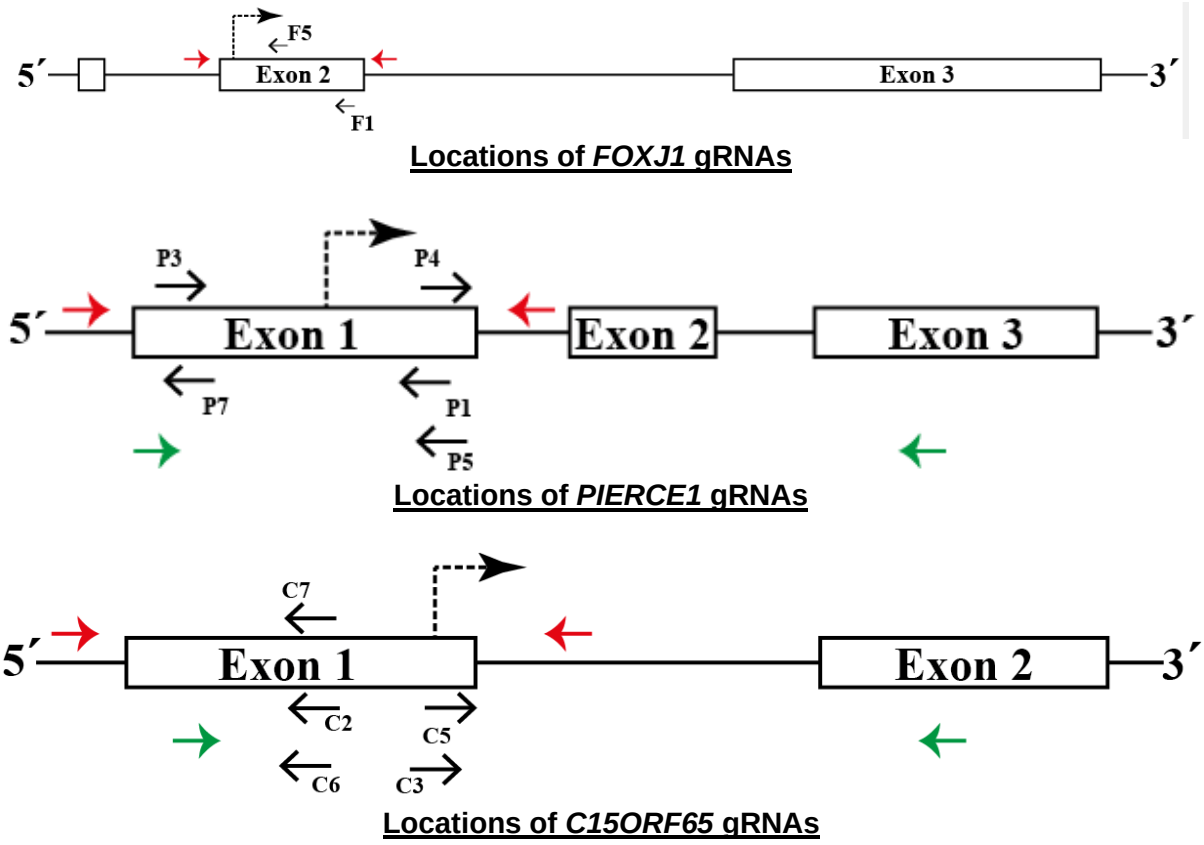

Figure 3.1 Locations of gRNAs used for CRISPR-CAS9 gene editing of *FOXJ1*, *PIERCE1* and *C15ORF65* in HBEC3-KT cells. Arrow beside individual gRNA indicates the direction of gRNA sequence. Broken arrow indicates the transcription start site. Red arrows indicate the locations of primers used for genotyping PCR. Green arrows indicate the locations of primers used for RT-PCR.

3.9 Transformation, minipreparation of plasmids and sequencing

After ligation with T4 DNA ligase (for gRNAs) or with pCRII-TOPO plasmid (for PCR product), plasmids were introduced into competent *Escherichia coli* strain TOP10 through heat shock for 45 seconds followed by incubation in ice. Transformed bacteria were selected on LB-agar plates containing 50 μg/ml ampicillin. Selected colonies were cultured in LB broth containing 50 μg/ml ampicillin followed by mini-preparation of plasmid using Monarch® Plasmid miniprep kit (New England Biolabs Inc., UK, Cat# T1010S) with manufacturer's protocol. Finally, the plasmids were sequenced by Sanger's di-deoxy method using U6 primer (5'-GAGGGCCTATTTCCCATGATTCC-3') for confirmation of gRNA insertion into PX458 plasmid, or with Sp6 primer (5'-ATTTAGGTGACACTATAG-3') and T7 primer (5'-TAATACGACTCACTATAGG G-3') for PCR product sequencing. Sequence reads were analysed using FinchTV version 1.5.0 (digitalworldbiology.com/FinchTV) or Sequencher demo version (genecodes.com). For genotyping, retrieved sequences

was aligned using Basic Local Alignment Search Tool (BLAST) at NCBI (www.ncbi.nlm.nih.gov), mRNA was predicted by editing the wildtype mRNA accordingly, and the predicted mRNA was translated into protein sequence with ExPASy translate tool (web.expasy.org/translate). The predicted protein sequence was aligned with corresponding wildtype proteins sequence (see Table 3.1, for FOXJ1 accession no. NP_001445.2 was used) using Clustal Omega (Sievers and Higgins 2018). Also, the predicted protein sequence was used to predict the structure of protein with I-TASSER (see section 3.6 for details) using corresponding bovine protein structure, if available, as a template.

3.10 Transfection and cell sorting

For transfection, HBEC3-KT cells (at mid passage) were seeded in a 24-well plate before the day of transfection. 500 ng of single plasmid or 250 ng of each of the randomly selected two PX458 plasmids containing gRNAs were used to transfect HBEC3-KT cells using FuGENE® HD transfection reagent (Fugent LLC, Cat# HD-5000) at 1 to 4 ratio (μl of transfection reagent per μg of DNA). An empty PX458 vector expressing GFP was used as a control transfection. Transfected cells were sorted for GFP expression after 72 hours with BD FACSMelody™ (service provided by the flow cytometry core facility at the University of Sheffield, UK) after imaging through Leica DMI4000B wide-field fluorescence microscopy or ZOE™ Fluorescent Cell Imager to confirm the transfection.

3.11 Western blotting

Western blotting was performed with modification from the protocol as described before (Fam, Chowdhury et al. 2013). Briefly, cells were lysed using 2X SDS-sample buffer (63 mM Tris HCl, 10% glycerol, 2% SDS, 0.0025% bromophenol blue, pH 6.8) followed by denaturation through boiling for 5 minutes. Then 20 μg of each sample was separated in a 10% polyacrylamide gel, transferred to a polyvinylidene fluoride (PVDF) membrane, blocked for an hour at room temperature with blocking buffer (5% skimmed milk in TBS with 0.1% Tween 20). Primary antibody against GFP (Mouse monoclonal GF28R, Invitrogen Cat# MA5-15256) was diluted in blocking buffer (1:1000) and incubated overnight at 4 ^{0}C. The membrane was washed with Tris-buffered saline for 5 minutes three times each and horse-radish peroxidase

(HRP)-conjugated secondary antibody (goat anti-mouse IgG, DAKO, Agilent Technologies, USA, Cat# P0447) diluted in blocking buffer (1:2000) was applied for an hour at room temperature. After washing with TBS, the membrane was developed with enhanced chemiluminescence (ECL) solution (Biological Industries, Israel, Cat# 20-500-120) and image was taken using BioRad Gel documentation system.

3.12 Immunofluorescence microscopy

Immunofluorescence microscopy was done according to previous method (Mulay, Akram et al. 2016). Briefly, undifferentiated or differentiated cells in transwell membranes (for ALI culture) or on round glass coverslips (12 mm in diameter, for submerged culture) were fixed with 10% (v/v) phosphate-buffered formalin at 37°C for 30 min followed by washing with PBS for 5 minutes. The cells were then permeabilised with 0.5% Triton X-100 in PBS followed by blocking with block solution (10% goat serum in PBS) at room temperature for 1 hour at 80 rpm on an orbital shaker. Primary antibodies (Table 3.4) were diluted in block solution and the permeabilised cells were incubated with 200 μl of diluted primary antibodies overnight at 4°C at 80 rpm on the shaker. The next day, the antibody solution was discarded, and the cells were washed three times with PBS for 5 min at 150 rpm. Alexa Flour secondary antibodies (Table 3.5) were diluted with block solution and the cells were incubated with 200 μl of diluted secondary antibodies at room temperature in the dark for 1 hour. From this point, the transwell or the coverslips were kept in the dark as much as possible to minimize light exposure to avoid photobleaching. After incubation with secondary antibody, the cells were washed again with PBS for three times 5 minutes each at 150 rpm shaker. For transwell membrane, the membrane was detached carefully from their transwell support with a fine scalpel and was placed on a glass microscope slide with the cells facing upwards. Nuclei were counterstained using Vectashield DAPI mounting medium (Vector Laboratories, Cat# H-1200-10) followed by sealing the membrane with a rectangular glass coverslip with nail polish. For cells on cover slips, a drop of Vectashield DAPI mounting medium (Vector Laboratories, Cat# H-1200-10) was placed on a clean glass slide with cells facing the glass slide followed by sealing with nail polish. The slides were observed using Imaging Systems inverted IX71 microscope (Olympus, Tokyo, Japan) at 10X and 40X magnification and images were acquired using SimplePCI imaging software

(Compix, Hamamatsu, Sewickley, PA) and analysed with ImageJ version 1.52a (imagej.nih.gov/ij).

Table 3.4 List of primary antibodies used in immunofluorescence staining.

Name	Company/Clone	Dilution
Mouse anti-acetylated α-TUBULIN	Monoclonal 6-11B-1, Sigma T7451	1:400
Rabbit anti-acetylated α-TUBULIN	Monoclonal K40 (D2063) XP®, Cell signalling 5335S	1:400
Mouse anti-FOXJ1	Monoclonal 2A5, Invitrogen 14-9965-82	1:200
Rabbit anti-C9ORF116	Polyclonal, Invitrogen PA5-72760	1:100
Rabbit anti-C15ORF65	Polyclonal, Invitrogen PA5-64314	1:100
Rabbit anti-BPIFB1	Generated by the Lab	1:80

Table 3.5 List of secondary antibodies used in immunofluorescence staining.

Name	Company/Clone	Dilution
Alexa-568 Goat Antimouse IgG (H+L)	Polyclonal, Abcam ab175473	1:200
Alexa-555 Goat Antirabbit IgG (H+L)	Polyclonal, Invitrogen A21428	1:200
Alexa-488 Goat Antimouse IgG (H+L)	Polyclonal, Life technologies A11001	1:200
Alexa-488 Goat Antirabbit IgG (H+L)	Polyclonal, Invitrogen A11008	1:200

3.13 Figure preparation and statistical analyses

Figures were prepared using Adobe Illustrator version 2020 (24.0). Data are expressed as means ± standard error of mean (SE). Student's unpaired *t*-test was applied for statistical comparison with GraphPad Prism software version 9. P- value of < 0.05 was considered as statistical significance in cases where the observation numbers are more than 2.

Chapter 4: Bioinformatic analyses of PIERCE1 and C15ORF65

4.1 Preface

p53-Induced expression in Rb-null cells 1 (PIERCE1), recently renamed as piercer of microtubule wall 1, (and also known as C9ORF116), is directly regulated by p53 and was suggested to be a crucial component of ultraviolet C (UVC)-induced DNA damage response in mouse embryonic fibroblasts (Sung, Kim et al. 2010). *Pierce1*$^{-/-}$ mice exhibit *situs solitus* similar to the *situs* anomalies observed in different ciliopathies (Sung, Baek et al. 2016), leading to the hypothesis that the protein might function in ciliogenesis. Moreover, functional loss of *Pierce1* resulted in defective nodal ciliogenesis and/or ciliary movement similar to that seen in dynein axonemal heavy chain 11-knockout (*Dnahc11*$^{-/-}$) mice (Sung, Baek et al. 2016). Also, recent work from our group showed that the ciliary beat frequencies of tracheal and nodal cilia were significantly reduced in *Pierce1*$^{-/-}$ mice though *pierce1*$^{-/-}$ zebrafish showed no obvious phenotype (Gui, Farley et al. 2021). However, the role of PIERCE1 in ciliogenesis has not been characterized in human cells and the pathways it is involved in remain unresolved. PIERCE1 is a distant paralog to another uncharacterized protein C15ORF65 (recently renamed as piercer of microtubule wall 2 (PIERCE2), however, the name C15ORF65 is used in this thesis) in man. To date, there has been limited information on the function of *C15ORF65* including a possible growth promoting role in acute myeloid leukaemia cell lines NB4 and KG1a (Okoye-Okafor, Bartholdy et al. 2012). Gene expression omnibus (GEO) reports suggested absence of *C15ORF65* transcript in teratozoospermia and increased expression of *C15ORF65* during mucociliary differentiation of ALI-cultured human airway epithelial cells (Goodale, Rayack et al. 2017, Zhang, Wu et al. 2018). Studies reported during my thesis identified both PIERCE1 and C15ORF65 to be MIPs, integral elements of bovine cilia, and hence they were named PIERCE1 and PIERCE2 respectively (Gui, Farley et al. 2021). Thereby, I hypothesised that these proteins would likely be involved with human cilia function. Structural and functional analyses for these two proteins were undertaken here using various bioinformatic tools and exploiting existing datasets, to build a better understanding of these proteins.

4.2 Phylogenetic and structural analysis

Since PIERCE1 and C15ORF65 were recently identified as distant paralogs in bovine cilia (Gui, Farley et al. 2021), the sequence of these two proteins would be expected to show sequence similarity and regions of such similarity could likely be functionally important. The structure and phylogeny of these two proteins would likely be comparable.

4.2.1 Transcript variants *of PIERCE1* and *C15ORF65*

Two transcript variants of *PIERCE1* are found in the NCBI database, one (NM_001048265.2) is considered to be the major transcript and the other (NM_144654.3) can be considered to be the minor transcript. For *C15ORF65*, only one transcript (NM_001198784.2) was found in the NCBI dataset. These transcripts are shown schematically in Figure 4.1.

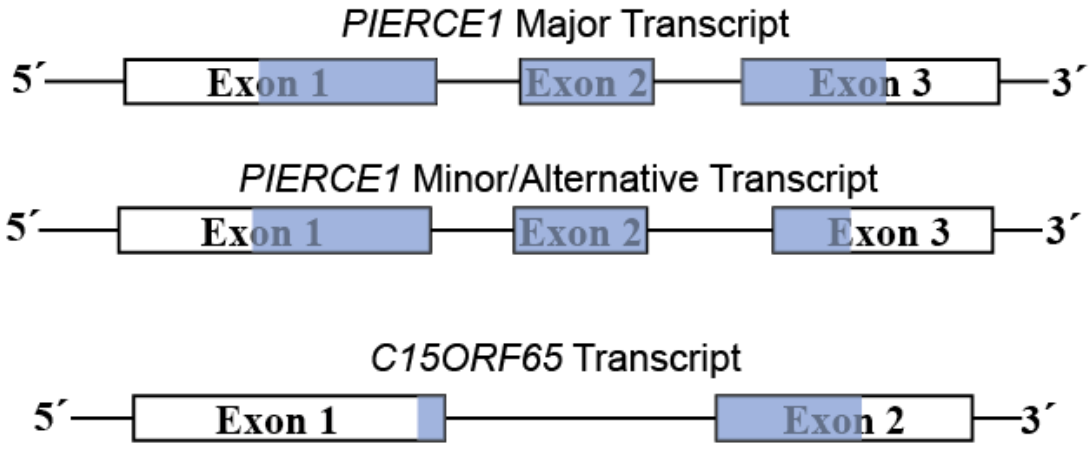

Figure 4.1 Transcript variants of *PIERCE1* and *C15ORF65*. Two transcript variants for *PIERCE1* have been found (top). *C15ORF65* had only one transcript (bottom). Boxes represent the exons and shaded areas of the exons indicate coding region.

Both *PIERCE1* transcripts were detected by RT-PCR in cancer cell lines tested in the lab previously including, MOR, H841, H441 and H358, whereas only the minor transcript variant of *PIERCE1* was expressed in HEK293 cells, and the primary HBECs expressed only the major transcript variant (Appendix A). The minor transcript encodes a protein consisting of 92 amino acids instead of 136 amino acids encoded by the major transcripts, and 74 amino acids from N-terminal are identical between them. The protein encoded by the *PIERCE1* major transcript contains full

length (98 amino acids long region from N-terminal) domain of unknown function 4490 (DUF4490), minor transcript also lacks the full length DUF4490 as this minor transcript variant differs from the major transcript at the exon 3 encoding 34 % of such domain. Thus, the protein encoded by the minor transcript variant of *PIERCE1* could possibly be non-functional. To understand why HEK293 predominantly expressed the *PIERCE1* minor transcript variant, genomic sequence of *PIERCE1* was analysed for different HEK293 cell derived sequences (Figure 4.2). The analysis suggested that all the 8 different HEK293 samples (Lin, Boone et al. 2014) contained the same 8 SNPs within the intron flanking exon 2 and exon 3, as well as 7 different HEK293 cell types contained an insertion in the same intron. Thereby, it could be possible that the minor transcript of *PIERCE1* could be a result of alternative splicing due to these mutations and such transcript would not be present in the wildtype cells. Moreover, the alternatively spliced *Pierce1* in mouse were not common and these alternatively transcripts of *Pierce1* were designated with Transcript Support Level – 3 at Ensembl (www.ensembl.org), as these transcripts were supported by only one expressed sequence tag (Figure 4.3). Hence, it can be concluded that the wildtype cells produced only the major transcript variant of *PIERCE1*, and this transcript is expected to encode for the functional isoform of PIERCE1. This major transcript variant of *PIERCE1* and the 136-amino acid protein encoded by this transcript was used for further studies.

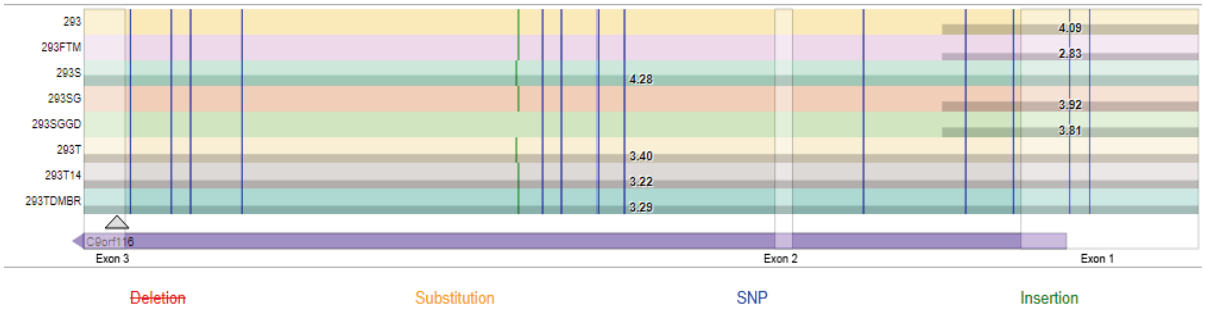

Figure 4.2 *PIERCE1* mutations in HEK293 cells. Sequence analysis of eight different HEK293 cell line samples as indicated above ((Lin, Boone et al. 2014)) showing locations of SNPs and insertional mutations. Copy number of each cell line is visualized as numbers. Arrow indicates the location of sequence showed below.

Transcript ID	Name	bp	Protein	Biotype	CCDS	UniProt Match	Flags
ENSMUST00000086370.11	1700007K13Rik-201	812	167aa	Protein coding	CCDS15837	Q5BN45	Ensembl Canonical GENCODE basic APPRIS P1 TSL:1
ENSMUST00000127683.2	1700007K13Rik-203	445	132aa	Protein coding		B0R017	TSL:3 CDS 3' incomplete
ENSMUST00000126242.2	1700007K13Rik-202	666	No protein	Processed transcript		-	TSL:3

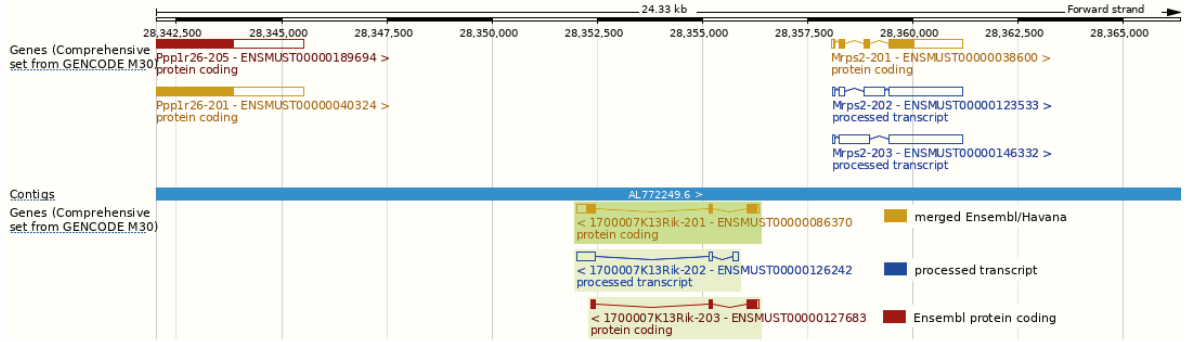

Figure 4.3 Transcript variants of *Pierce1* in mice. Data was retrieved from Ensembl (www.ensembl.org). TSL level indicates the transcript quality tags where TSL-1 means the transcript is well annotated and TSL-3 means the transcript is supported by only one expressed sequence tag.

4.2.2 Sequence alignment of PIERCE1 and C15ORF65

To date, PIERCE1 has been identified as an evolutionary conserved protein in Euteleostomi (bony vertebrates) and the Mouse Genome Database (MGD) suggested that C15ORF65 is conserved in Supraprimates (Bult, Blake et al. 2019). However, *Chlamydomonas reinhardtii* FAP182 is a potential homolog of PIERCE1 (Ma, Stoyanova et al. 2019) and presence of C15ORF65 in *Bugula neritina* (a bryozoan) (Rayko, Komissarov et al. 2020) indicates that the evolutionary conservation of these proteins could be much deeper and that they could be present in organisms of lower clades. To understand the evolutionary relatedness and to find common protein motifs in model organisms, the sequences of PIERCE1 and C15ORF65 from human, three model organisms (mouse, rat, and zebrafish) and bovine, for which both PIERCE1 and C15ORF65 structures has been resolved, were aligned using multiple sequence comparison by Log-expectation (MUSCLE) (Edgar 2004). Multiple sequence alignment (MSA) of PIERCE1 sequences showed that these proteins share the signature motif of domain of unknown function 4490 (DUF4490) (Figure 4.4A). The conserved amino acids found for such domain were S, T, YG, P, F and D as reported before (Sung, Kim et al. 2007, El-Gebali, Mistry et al. 2019). A maximum-likelihood (ML) phylogenetic tree as expected suggested that human PIERCE1 is more closely related to bovine PIERCE1 than that from rodents or fish (Figure 4.4B). Similar to PIERCE1, a MSA of C15ORF65 showed that 33 amino acids are conserved in the tested organisms, and all the tested protein

sequences contained the DUF4490 motif (Figure 4.5A). Again, a ML phylogenetic tree suggested that human C15ORF65 is more closely related to bovine C15ORF65 than to that from rodents or fish (Figure 4.5B). For both cases, a new conserved sequence motif was identified (Figure 4.4A and Figure 4.5A). The new PIERCE1 motif contained conserved 'RFNNP' amino acids and the new C15ORF65 motif included 'CVNPGNPVFSCML' amino acids. Beside these, a polyproline motif (Qi, Motz et al. 2018) is also identified near the N-terminal of PIERCE1. Thereby, these genes should have expectedly similar functions in the model organisms and in human. The ML phylogenetic tree for all known PIERCE1 and C15ORF65 sequences displayed on Ensembl (www.ensembl.org) are given in Appendix B and in Appendix C, respectively. When the protein sequences of both PIERCE1 and C15ORF65 were aligned together using MUSCLE, the alignment showed more diversity between PIERCE1 and C15ORF65 with eight amino acids found to be conserved within the DUF4490 motif (Figure 4.6). Such findings suggest that both PIERCE1 and C15ORF65 evolved differently after a duplication event of their ancestor gene. All these findings suggested that eight paralogous conserved amino acids were found in PIERCE1 and C15ORF65, both proteins are similar across the tested organisms, and bovine PIERCE1 or C15ORF65 are more closely related to the human homologues indicating there could be structural and functional similarities for both proteins between bovine and human.

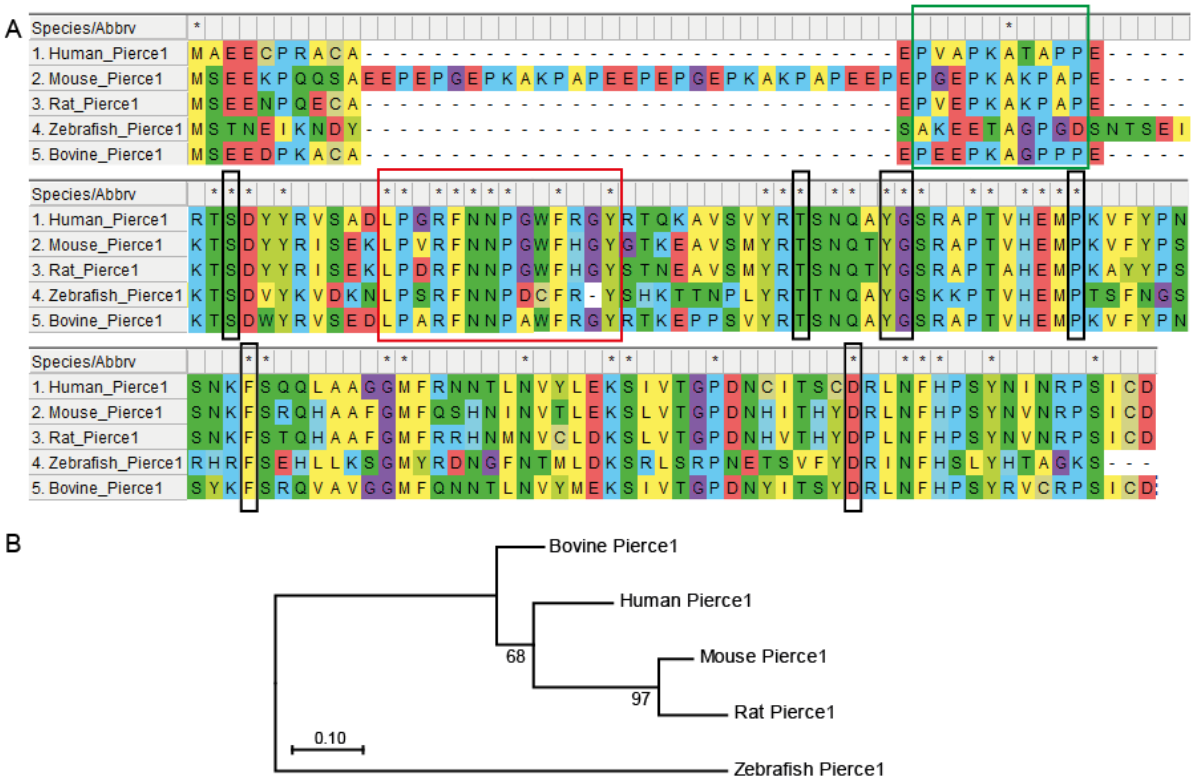

Figure 4.4 PIERCE1 multiple sequence alignment and phylogenetic tree. Sequences of PIERCE1 from the indicated organisms were aligned using MUSCLE. '*' indicates identical amino acid residue. Colour code indicates yellow: hydrophobic amino acids; green: polar amino acids; blue: positively-charged amino acids and proline; and pink: negatively-charged amino acids. Cysteine, glycine, and tyrosine are individually coloured. The black box indicates conserved amino acids commonly found in domain of unknown function 4490 (DUF4490) motif, the red box indicates the newly identified conserved motif, and the green box indicates the polyproline motif (A). Maximum-likelihood tree based on multiple sequence alignment of PIERCE1 from indicated organisms. The value on branch node indicates the percentage of clustering (values > 50% are indicated). Scale bar indicates genetic distance (number of substitutions per site) (B).

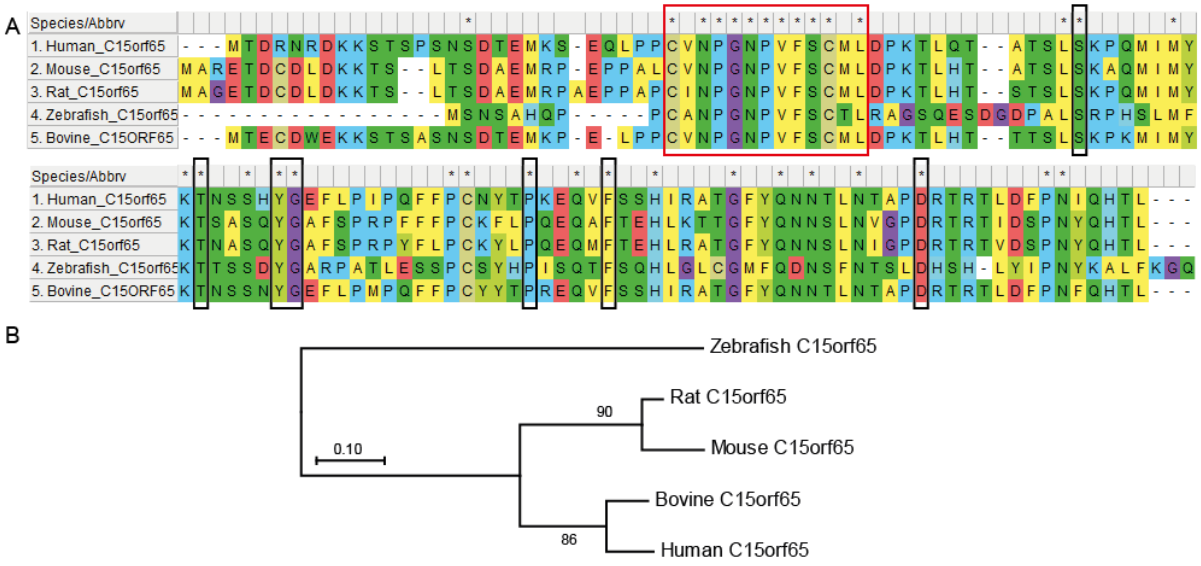

Figure 4.5 C15ORF65 multiple sequence alignment and phylogenetic tree. Sequences of C15ORF65 from the indicated organisms were aligned using MUSCLE. '*' indicates identical amino acid residue. Colour code indicates yellow: hydrophobic amino acids; green: polar amino acids; blue: positively-charged amino acids and proline; and pink: negatively-charged amino acids. Cysteine, glycine, and tyrosine are individually coloured. The black box indicates conserved amino acids commonly found in domain of unknown function 4490 (DUF4490) motif and the red box indicate the newly identified conserved motif (A). Maximum-likelihood tree based on multiple sequence alignment of C15ORF65 from indicated organisms. The value on branch node indicates the percentage of clustering (values > 50% are indicated). Scale bar indicates genetic distance (number of substitutions per site) (B).

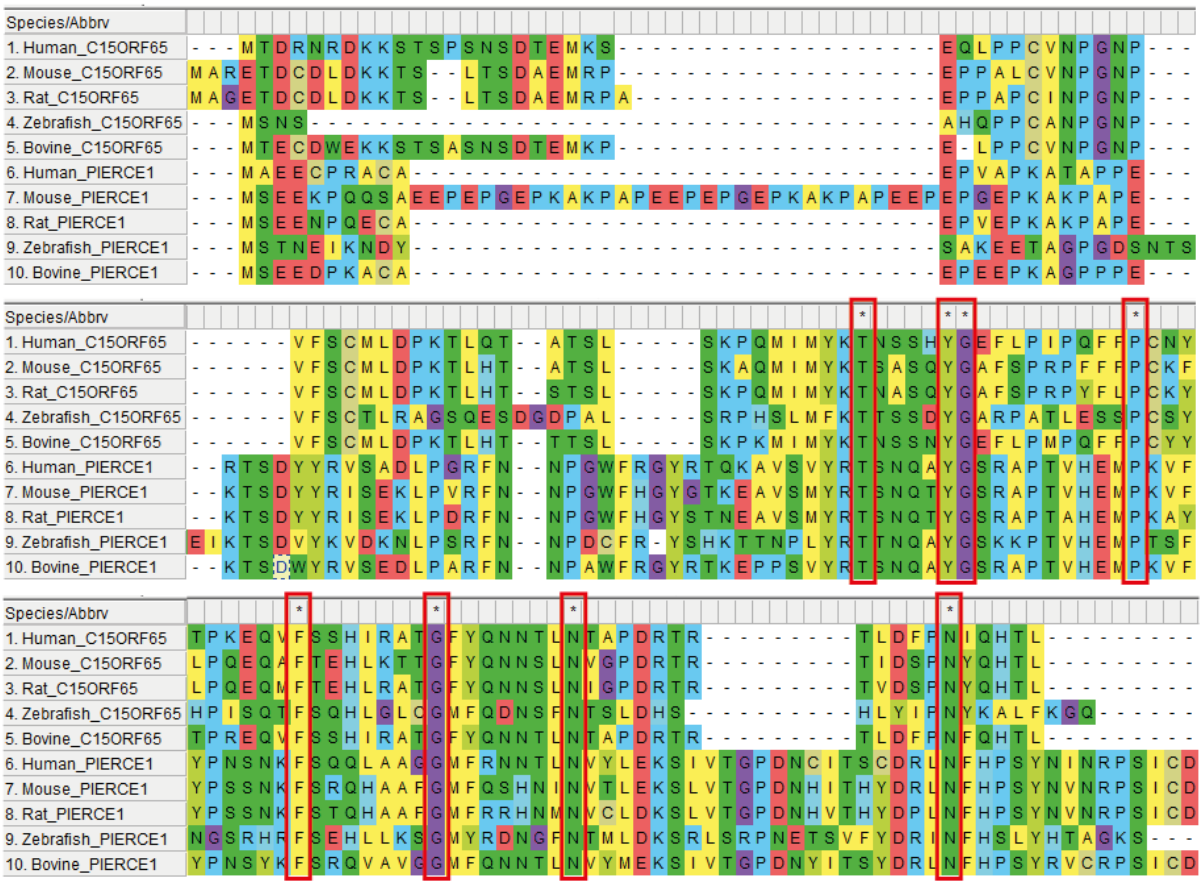

Figure 4.6 Multiple sequence alignment of PIERCE1 and C15ORF65 protein sequences from selected organisms. Sequences are aligned using MUSCLE. '*' indicates identical amino acid residue. Colour code indicates yellow: hydrophobic amino acids; green: polar amino acids; blue: positively-charged amino acids and proline; and pink: negatively-charged amino acids. Cysteine, glycine, and tyrosine are individually coloured. The red box indicates conserved amino acids.

4.2.3 Predicting the structures of PIERCE1 and C15ORF65

The structures of human PIERCE1 and C15ORF65 were modelled using I-TASSER (Yang, Yan et al. 2015) using the recently resolved bovine ciliary axonemal doublet microtubule structure (PDBID: 7RRO) (Gui, Farley et al. 2021) as a template. Both PIERCE1 and C15ORF65 are component parts of the MIP complex where both interact with CFAP53 (data not shown) in the structure. The confidence level for all these structures (confidence (C) score was -1.47 for PIERCE1 and -1.71 for C15ORF65) (Figure 4.7). Also, the template modelling (TM) score for PIERCE1 and C15ORF65 structures were 0.53±0.15 and 0.44±0.15 respectively indicating that these structures fall in an acceptable range (acceptable TM score is ≥ 0.5). When these structures were aligned using PyMOL, a limited alignment at the middle region and at the C-terminal was observed (Figure 4.7). In addition to these, Motif Scan

analyses revealed that none of them possess any known functional motif other than some weak post-translational modification sites like glycosylation, phosphorylation and myristylation sites (Figure 4.8). DUF4490 (typically 90-220 amino acid in length) was not included here as the function of this motif is still unknown and questionable. Overall, these structural findings indicate that both proteins could have their own structural significance and their function could be similar but may not be identical if the modelled structures are a true representation.

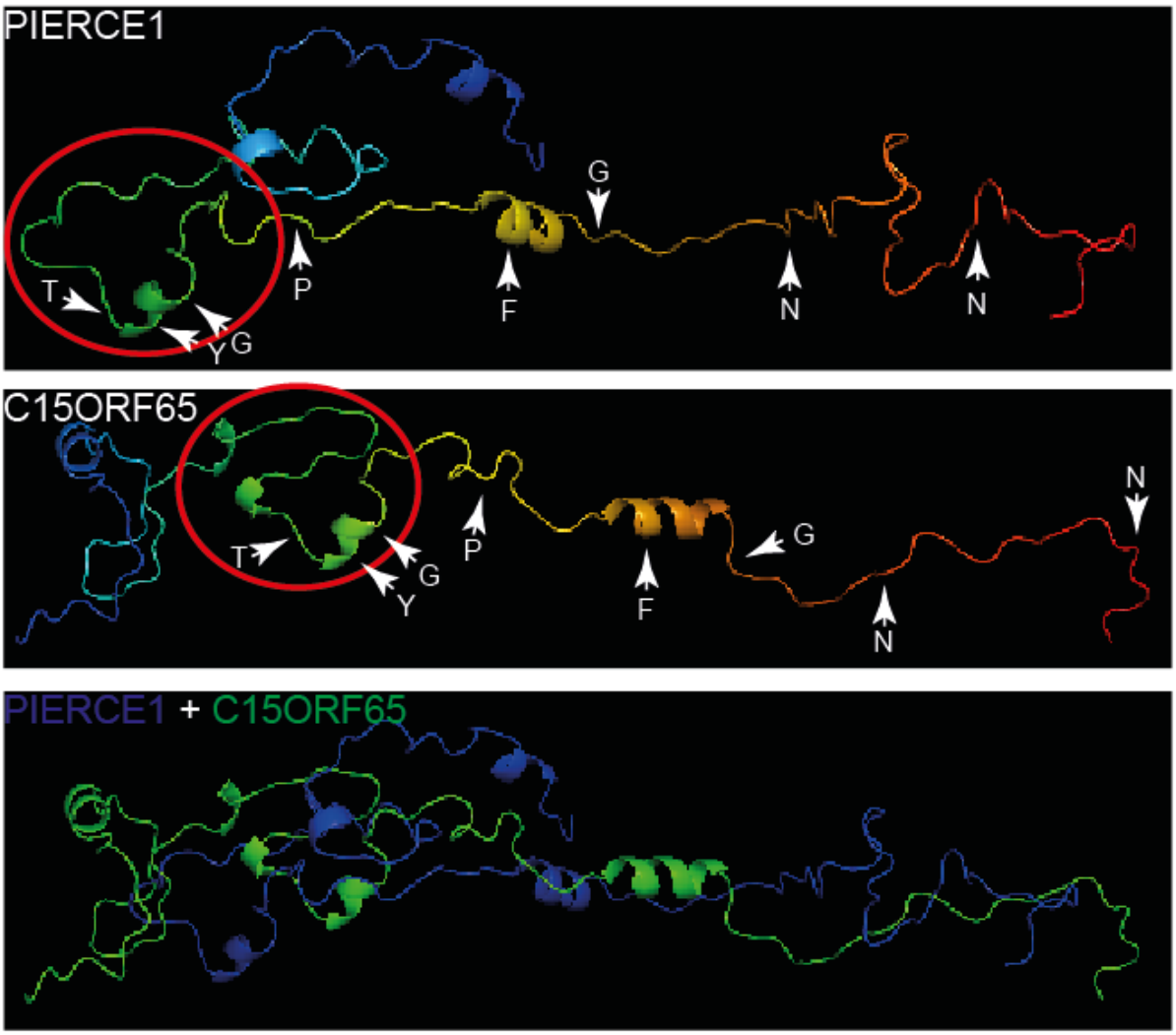

Figure 4.7 Predicted structures of PIERCE1 and C15ORF65. High-confidence I-TASSER structures in rainbow colour scheme (N-terminal to C-terminal) of PIERCE1 (top) and C15ORF65 (middle) generated by using bovine ciliary doublet microtubule structure (PDBID:7RRO) (Gui, Farley et al. 2021) as a template. These structures were aligned together using PyMOL (bottom) where PIERCE1 is coloured as blue and C15ORF65 was coloured as green. Red circle indicates the structural regions covered by the newly identified conserved amino acids (See Figure 4.4A and Figure 4.5A for details). White arrows with amino acids in single letter code indicate the locations of conserved amino acids within the structure of PIERCE1 and C15ORF65 (see Figure 4.6 for details).

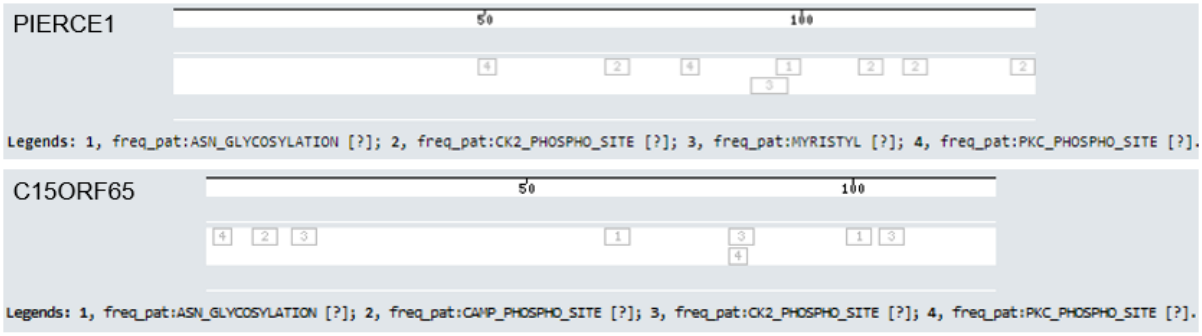

Figure 4.8 Motif Scan analysis of PIERCE1 and C15ORF65. PIERCE1 (top) and C15ORF65 (bottom) sequences were analysed for presence of any known motifs. [?] indicates questionable or weak matches for a given site.

4.3 Functional analyses of PIERCE1 and C15ORF65

The basic bioinformatic analyses done above suggested that both PIERCE1 and C15ORF65 is conserved in vertebrates and their structures are also similar with no known functional motifs. Such findings indicated that the proteins might have similar cellular function. To explore their potential function, expression of *PIERCE1* and *C15ORF65* in BioGPS, Human Protein Atlas (HPA) and Gene Expression Omnibus (GEO) databases were further studied here.

4.3.1 Expression of *PIERCE1* and *C15ORF65*

Expression of *PIERCE1 and C15ORF65* was evaluated across multiple datasets. BioGPS data suggested that both *PIERCE1* and *C15ORF65* were highly expressed in respiratory epithelial cells, testes, and fallopian tube in human (Appendix D), and both were highly expressed in murine testes, though only *Pierce1* was highly expressed in lung and embryonic stem cells (Appendix E). The HPA tissue RNA expression dataset also suggested that both PIERCE1 and C15ORF65 were highly expressed in testes and fallopian tube as compared to other tissues, whereas higher expression of C15ORF65 was also detected in kidney, pancreas, pituitary gland, salivary gland, skeletal muscle, and stomach (Figure 4.9). Thus, both BioGPS and HPA datasets of tissue RNA expression suggested that both *PIERCE1* and *C15ORF65* is highly expressed in testes and fallopian tube. Combining respiratory epithelia with these tissues, suggests possible expression of these genes in the multiciliated epithelia commonly found in these three tissues.

Figure 4.9 Expression of *PIERCE1* and *C1ORF65* in Human Protein Atlas (HPA) tissue RNA expression dataset. This consensus normalized data was generated by combining HPA and genotype-tissue expression (GTEx) transcriptomic datasets using the internal normalized pipeline. Colour code indicates tissue groups in a functional system. X-axis indicates normalized count of transcript per million (nTPM).

Next, the cellular localisation of these genes was investigated using datasets in HPA and single-cell RNA-seq data. HPA tissue immunohistochemistry datasets, expression clustering and correlation suggested that both *PIERCE1* and *C15ORF65* transcripts were localised in ciliated cells and their expression was correlated with expression of other known cilia-associated genes in human (Figure 4.10). Also, examination of the published single-cell RNA-seq data (Plasschaert, Zilionis et al. 2018) suggested that both *PIERCE1* and *C15ORF65* transcripts were expressed mostly in ciliated cells of human bronchial and mouse tracheal epithelia, except for *C15ORF65* in differentiated mTECs (Figure 4.11). These data in combination, as well as other single cell RNA-sequencing datasets (not shown) strongly suggested multiciliated cell localisation of both *PIERCE1* and *C15ORF65* transcripts in the multiciliated epithelia and provided strong support to consideration of *PIERCE1* and *C15ORF65* as signature genes of multiciliated cells.

Neighbour	Description	Correlation
LRTOMT	Leucine rich transmembrane and O-methyltransferase domain containing	0.9825
FAM187A	Family with sequence similarity 187 member A	0.9807
CFAP251	Cilia and flagella associated protein 251	0.9684
DNALI1	Dynein axonemal light intermediate chain 1	0.9614
RSPH1	Radial spoke head component 1	0.9596
CFAP94	Cilia and flagella associated protein 94	0.9579
DLEC1	DLEC1 cilia and flagella associated protein	0.9561
IQCG	IQ motif containing G	0.9561
CFAP57	Cilia and flagella associated protein 57	0.9526
PPIL6	Peptidylprolyl isomerase like 6	0.9526
LRRC23	Leucine rich repeat containing 23	0.9491
CATIP	Ciliogenesis associated TTC17 interacting protein	0.9491
WDR93	WD repeat domain 93	0.9491
RIBC1	RIB43A domain with coiled-coils 1	0.9474
CNGA4	Cyclic nucleotide gated channel subunit alpha 4	0.9474

Neighbour	Description	Correlation
IFT22	Intraflagellar transport 22	0.7596
CFAP44	Cilia and flagella associated protein 44	0.7386
TTC30A	Tetratricopeptide repeat domain 30A	0.7368
KIAA1549	KIAA1549	0.7333
CLBA1	Clathrin binding box of aftiphilin containing 1	0.7246
CFAP36	Cilia and flagella associated protein 36	0.7228
LMLN	Leishmanolysin like peptidase	0.7211
FSCN2	Fascin actin-bundling protein 2, retinal	0.7158
CCNO	Cyclin O	0.7158
SCGB1C2	Secretoglobin family 1C member 2	0.7123
IQCC	IQ motif containing C	0.7123
G6PC2	Glucose-6-phosphatase catalytic subunit 2	0.7088
SLC2A11	Solute carrier family 2 member 11	0.7070
FZD3	Frizzled class receptor 3	0.7018
KATNIP	Katanin interacting protein	0.7000

Figure 4.10 Localisation of *PIERCE1* and *C15ORF65* transcripts in HPA datasets. Cluster in yellow colour indicated ciliated cells. Table on the right for respective transcript indicates the correlation coefficient of co-expressed (Neighbour) genes.

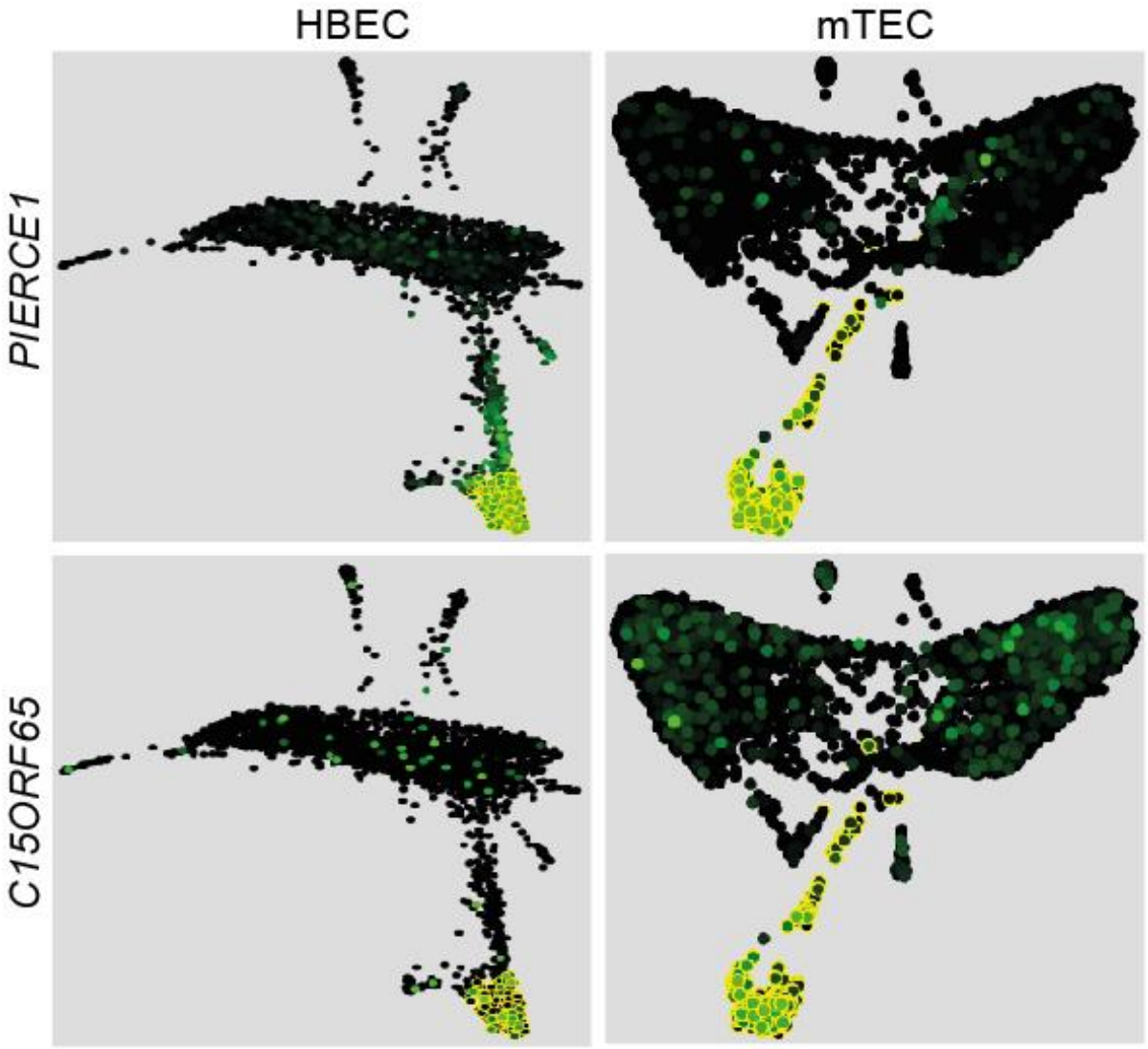

Figure 4.11 Localisation of *PIERCE1* and *C15ORF65* transcripts from single-cell RNA-seq data. Single-cell RNA-seq data were generated from freshly isolated human bronchial epithelial cells (HBEC) or murine tracheal epithelial cells (mTEC). The figure was generated using SPRINGviewer with the dataset GSE102580 (Plasschaert, Zilionis et al. 2018). Yellow circles indicate multiciliated cells. Green indicates the presence of the transcript.

4.3.2 Subcellular localisation of PIERCE1 and C15ORF65

Next, further bioinformatic analyses were conducted to predict the localisation of PIERCE1 and C15ORF65. The protein subcellular localisation prediction software DeepLoc (version 1.0 and 2.0) using deep learning algorithm (Bregeat 1986, Almagro Armenteros, Sonderby et al. 2017) predicted that both human and murine PIERCE1 and C15ORF65 could be localised in the cytoplasm as soluble proteins or can be present in the nucleus (likelihood value > 0.95 for all cases) indicating these proteins are not part of mitochondria, Golgi bodies, lysosome, endoplasmic reticulum, or plasma membrane (Figure 4.12). The likelihood values (ranging 0 to 1)

for cytoplasmic localisation of PIERCE1 were 0.552 for human and 0.596 for mouse. Similar values for C15ORF65 were 0.39 for human and 0.366 for mouse. A weak nuclear localisation signal sequence was detected at the C-terminal in all sequences, except in mouse PIERCE1 (Appendix F). To evaluate the localisation of both PIERCE1 and C15ORF65 further, I examined the HPA immunohistological data for their localisation in multiciliated epithelia in tissues of the bronchus and fallopian tube. A strong immunohistochemical signal for both PIERCE1 and C15ORF65 was detected in the ciliary axoneme (according to the histological analysis in the HPA) in the bronchial epithelia or fallopian tube epithelia (Figure 4.13). In addition to these, previous work from the lab showed that murine nasal cavity and murine tracheal epithelial cells could be differentiated into multiciliated cells at ALI, and these multiciliated cells showed PIERCE1 staining in their cytoplasm. Perhaps the cytoplasmic PIERCE1 could co-localise with ciliary axoneme of these multiciliated cells (Appendix G). These findings indicated that both PIERCE1 and C15ORF65 could be localised in the ciliary axoneme present at the multiciliated epithelia.

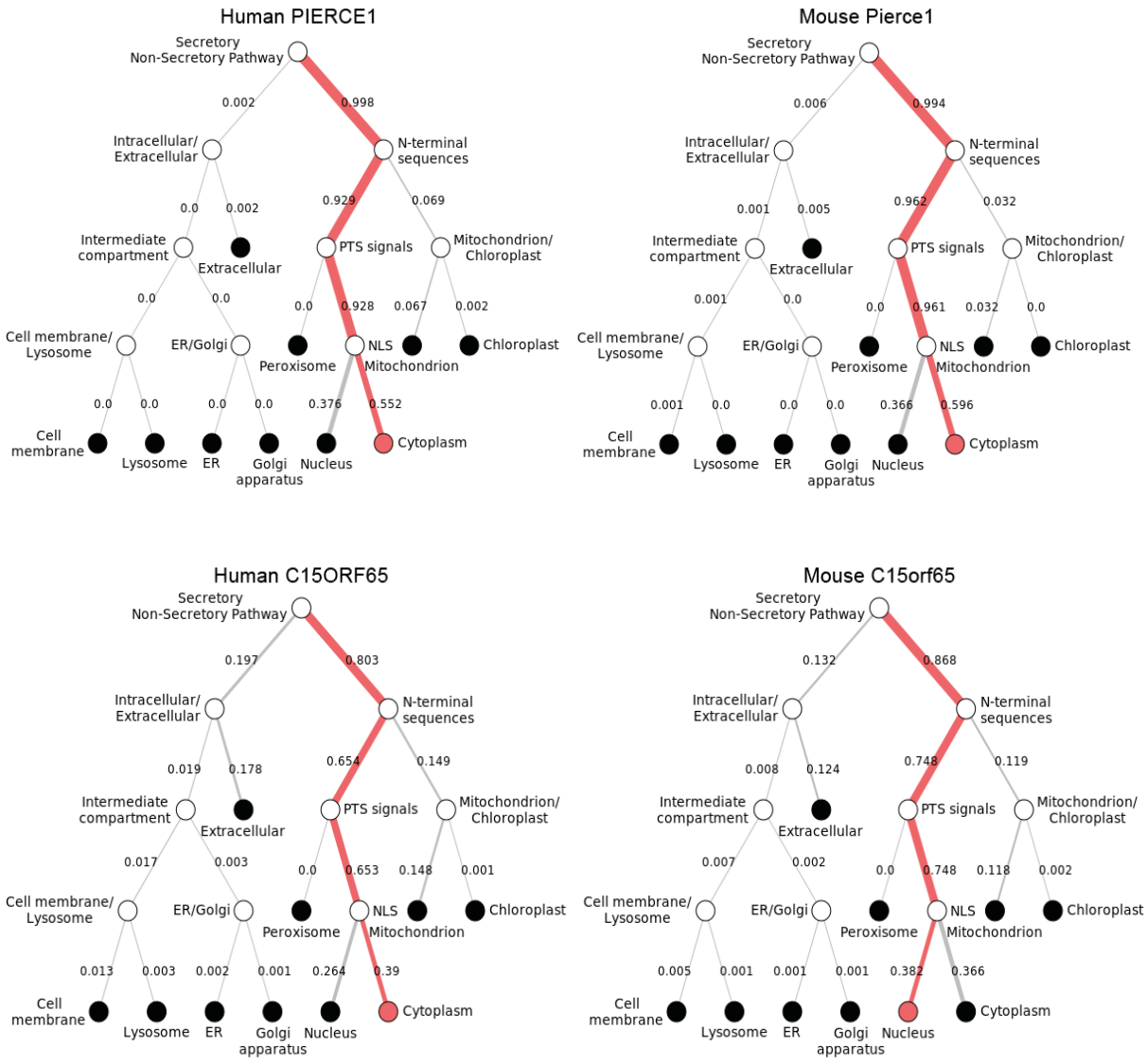

Figure 4.12 Predicting subcellular localisation of human and mouse PIERCE1 and C15ORF65. Subcellular localisation was predicted with DeepLoc (version 1.0). Pathway in pink indicates the possible subcellular localisation. Black circles indicate unacceptable localisation. Values given in each branch indicates the likelihood value of subcellular localisation.

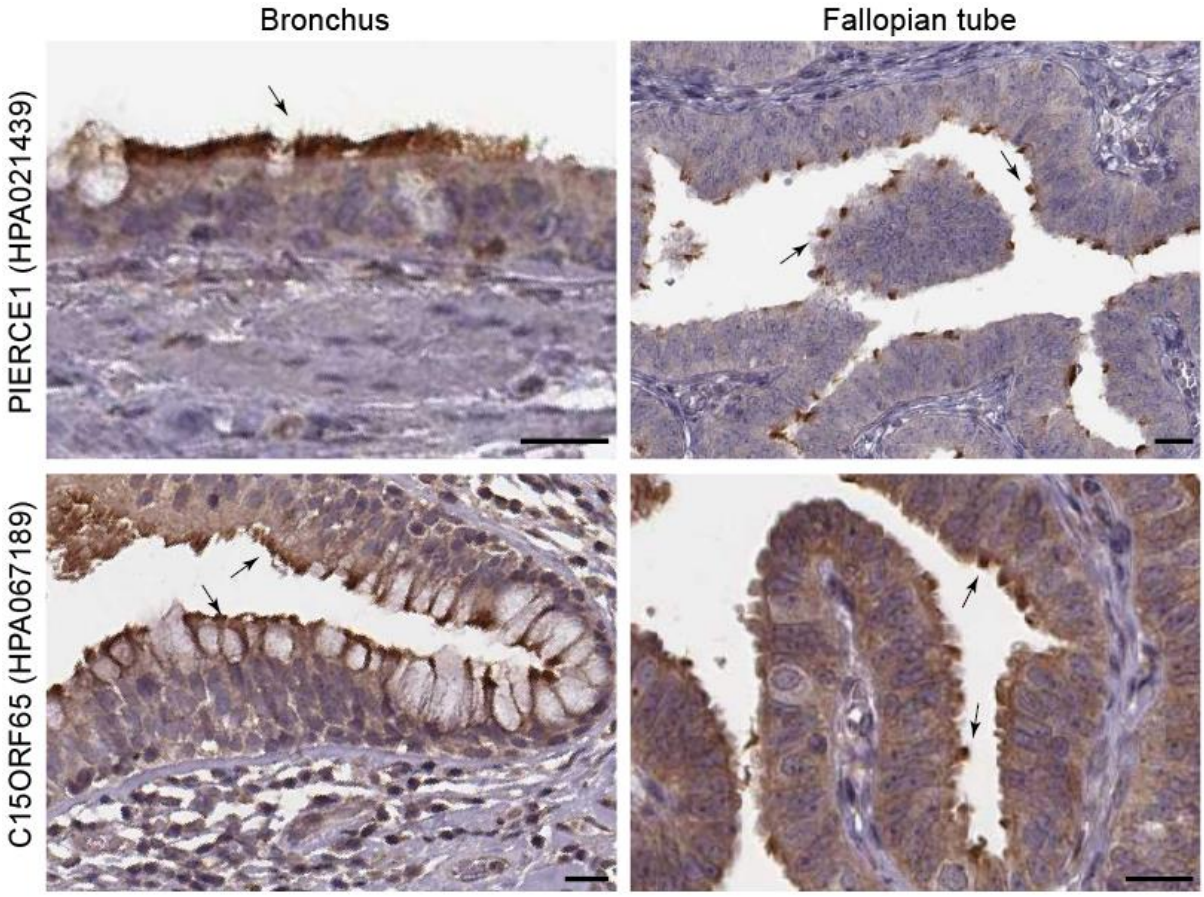

Figure 4.13 Expression of PIERCE1 and C15ORF65 in human bronchus and fallopian tube. All the images were collected from Human Protein Atlas (www.proteinatlas.org). The code of antibody used for immunostaining is given in a bracket beside the protein name. Black arrows indicate the multiciliated epithelia. Images are licensed under CC BY-SA 3.0. Scale bar = 20 μm.

4.3.3 Expression of *PIERCE1* and *C15ORF65* during mucociliogenesis

To support the functional association of *PIERCE1* and *C15ORF65* with cilia, expression of these genes was evaluated during mucociliary differentiation in Clariom^{TM} S data sets from three murine multiciliated epithelia (middle ear, nasal cavity, and tracheal) recently generated in our laboratory, and in HBEC and mTECs data available in the GEO. Expression of both *Pierce1* and *C15orf65* was increased significantly during mucociliary differentiation of all the three murine multiciliated epithelial cells tested here, except for the expression of *C15orf65* in middle ear epithelial cells (Figure 4.14). Also, only the expression of *Pierce1* was significantly higher in middle ear and tracheal epithelia (from which the basal epithelial cells were collected as undifferentiated cells (day 0 at ALI) for mucociliary differentiation), as compared to undifferentiated cells (Figure 4.14). Differentiated middle ear, nasal cavity and tracheal epithelial cells expressed *Pierce1,* 17, 11, and 44 times higher

respectively than their corresponding undifferentiated cells. Also, differentiated nasal cavity and tracheal epithelial cells expressed *C15orf65* 6 and 10 times higher respectively than their corresponding undifferentiated cells. Such findings indicated that expression of both *Pierce1* and *C15orf65* was lowest in undifferentiated cells and was induced during the mucociliary differentiation.

Expression of both *PIERCE1* and *C15ORF65* was gradually increased from day 0 to day 28 of ALI-cultured HBECs and mTECs (Figure 4.15). In HBECs, the expression of these genes became significantly increased ($p < 0.05$ for all cases) from day 8 of ALI culture as compared to day 0, and higher expression was maintained following longer culture times. Expression of both genes were significantly increased from day 4 of ALI-cultured mTECs. In combination with the mouse data, these findings suggested that expression of both genes were minimal at the beginning of ALI followed by an increase of expression of these genes as the cells started to follow ciliogenesis. Since PIERCE1 and C15ORF65 are located in the ciliary axoneme and their expression is increased during mucociliogenesis, it supports the conclusion that they may have some functional role in cilia.

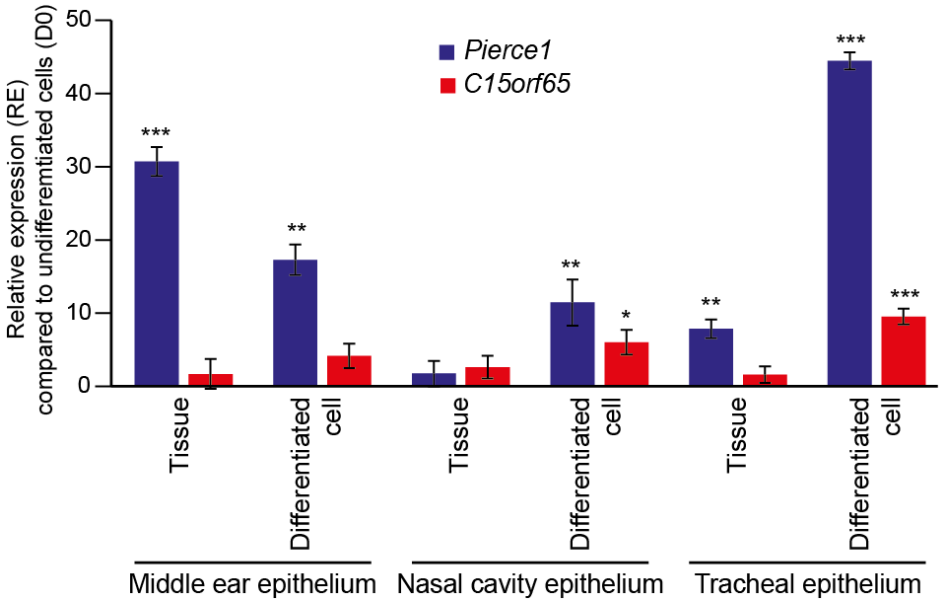

Figure 4.14 Expression of *Pierce1* and *C15orf65* across multiple murine multiciliated epithelial cell differentiation. Epithelial cells collected from middle ear, nasal cavity and trachea were differentiated at ALI following Clariom^{TM} S assay with extracted RNA. The graph shows relative expression of *Pierce1* and *C15orf65* in source cells (Tissue) and ALI-differentiated cells (Differentiated cell) relative to undifferentiated cells (day 0 at ALI) (n = 3). * = $p<0.05$, ** = $p<0.01$, *** = $p<0.001$.

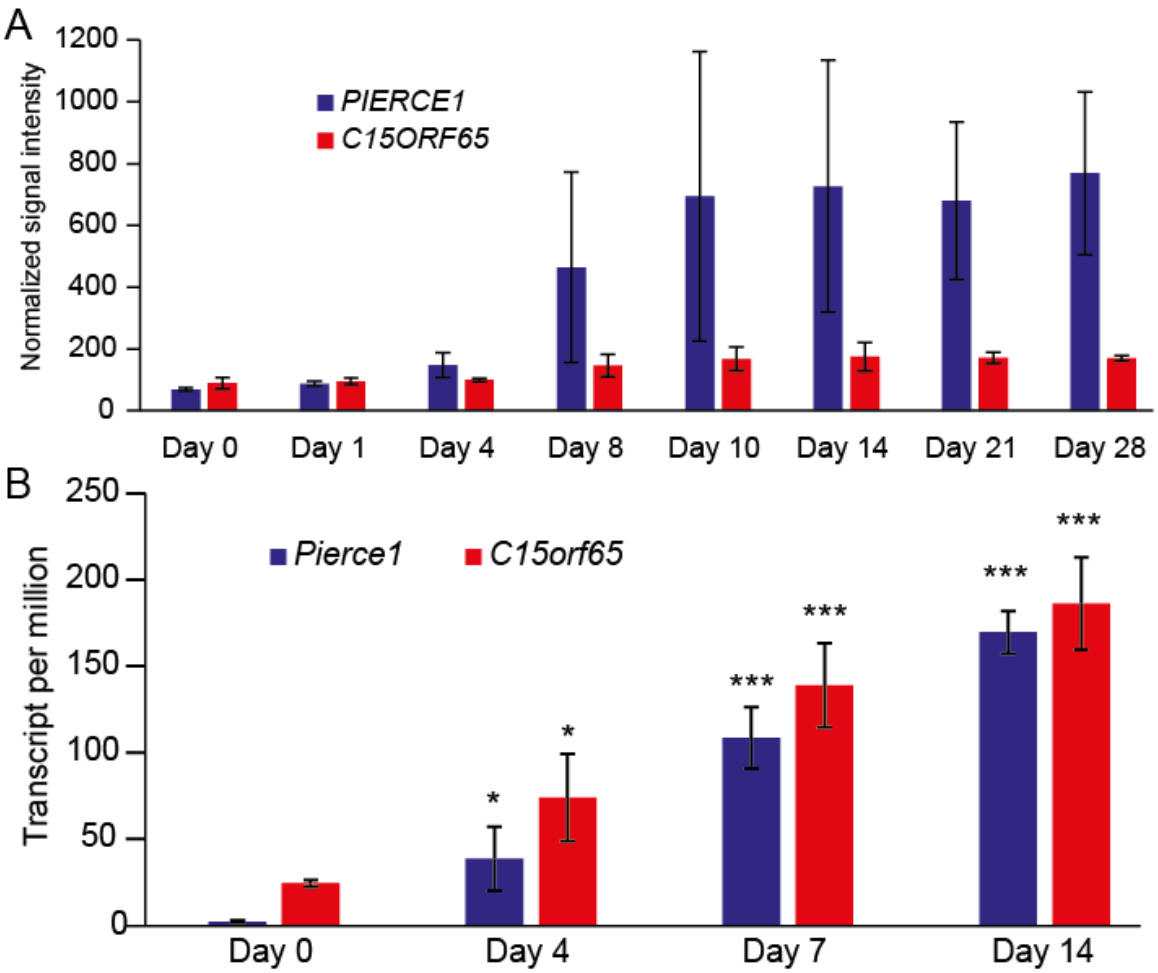

Figure 4.15 Expression of *PIERCE1* and *C15ORF65* during mucociliary differentiation of respiratory epithelial cells. This graph was generated from GEO accession GSE5264 data (Ross, Dailey et al. 2007) representing gene expression data sets of HBECs collected from three different donors followed by cultured at ALI up to 28 days (A). Probe signal intensity was normalized using robust multi-array avarage (RMA). *Pierce1* and *C15orf65* expression during ALI-differentiation of mTECs, data were collected from GEO accession GSE75717 (Nemajerova, Kramer et al. 2016) (B). Detailed methods and statistics used for data analysis is given in section 3.5, page 38.

4.4 Chapter discussion

PIERCE1 became of interest in the field of ciliogenesis when studies showed that mice lacking the protein develop altered let-right laterality, commonly a result of a ciliary defect (Sung, Baek et al. 2016). Recently C15ORF65 was shown to be a paralogue of PIERCE1. During the course of my studies both were identified as MIPs in a structural study (Gui, Farley et al. 2021). Despite research work with PIERCE1 and/or C15ORF65 in ciliogenesis having been studied in zebrafish, mouse and bovine, there exists no direct research on human PIERCE1 and C15ORF65 in cilia. Generally, it is considered that orthologues function in the same manner across

species, but a recent report suggests that several genes are highly expressed in murine ciliated cells and are absent in human ciliated cells *vice versa* (Travaglini, Nabhan et al. 2020). At the beginning of my PhD studies, information regarding the association of PIERCE1 in ciliogenesis included i) mice and zebrafish lacking PIERCE1 show laterality defects, and ii) zebrafish lacking PIERCE1 show abnormal ciliary beating; however, no information was available on C15ORF65. Therefore, I was interested to study the function of these genes in human cilia.

MSA can provide some information regarding the functional relationship among the orthologs. Thus, MSA of both PIERCE1 and C15ORF65 identified the DUF4490 in these proteins across human, mouse, rat, zebrafish, and bovine. The protein encoded by the major transcript variant of *PIERCE1* was considered here as the other transcript variants either do not encode a viable protein or are found to contain intronic mutations. MUSCLE was used to align the protein sequences as this software can deal with protein sequence alignment more accurately than TCOFFEE, COBALT, MAFET or Clustal Omega by using a Log of expectation value (Edgar 2004). Given that DUF4490 is a conserved domain with no known function in both PIERCE1 and C15ORF65, the question remains whether this domain is associated with a cilia function or not. This could be tested by deleting a portion of the gene encoding this domain using CRISPR-CAS9 gene editing or by using the power of site directed mutagenesis to introduce multiple missense mutations in that domain in cells capable of undergoing mucociliary differentiation. Subsequent mucociliary differentiation of these mutant cells along with wildtype cells could be used to compare cilia formation, cilia length or ciliary beat frequency. Interestingly, the MUSCLE alignment identified a previously unknown conserved polyproline motif near the N-terminus of PIERCE1 indicating a possible translational regulatory role of these prolines (Huter, Arenz et al. 2017, Meneguello, Barbosa et al. 2019). In addition, another conserved motif found within the DUF4490 of PIERCE1 produces a loop within the secondary structure of the protein. A similar loop was also formed by the C15ORF65 conserved motif (Figure 4.7) indicating that they might have similar functional significance. Protein loops are known to play important roles in protein-protein interaction, providing binding sites, and to contribute signal transduction pathways (Gavrilov, Dagan et al. 2015). Thus, the newly identified loops in PIERCE1 and C15ORF65 could have diverse function, particularly in protein-protein interaction

within the MIP complex. To test this, portion of the gene encoding the amino acids of this loops could be deleted or replaced in cells followed by mucociliary differentiation or a yeast two-hybrid system or some other form of protein-protein interaction assay could be employed to deduce the interaction between one of these proteins and other proteins (CFAP53 as an example) (Gui, Farley et al. 2021). In addition to these motifs, the two cysteine residues present in both PIERCE1 (position 5 and 9) and C15ORF65 (position 28 and 38) could form disulphide bonds as their thiol groups are in close proximity within each structure. It is reported that such disulphide bonds could form spontaneously and can cleave during mechanical force (Beedle, Mora et al. 2018). Thus, it can be hypothesized here that these disulphide bonds could play a role in ciliary beating indicating that these proteins might have a structural role in ciliary axoneme. One way to test this would be replacing one or both cysteine residues with serine or glycine through site-directed mutagenesis and compare the cryo-EM structures with the wildtype counterpart.

Phylogenetic trees show the evolutionary relationship of a proteins across multiple genus and species (Hall 2013). Commonly used phylogenetic tree includes ML, neighbour-joining, minimum-evolution trees and among these ML tree is considered as more accurate though it is relatively difficult to build such trees due to the algorithms involving complex calculations (Truszkowski and Goldman 2016). The constructed ML trees for PIERCE1 and C15ORF65 imply the functional importance of other PIERCE1 and C15ORF65 conserved motifs as such conserved motif could have mammal-specific function.

The structures of PIERCE1 and C15ORF65 have recently been resolved by cryo-electron microscopy in bovine cilia and were found as a part of microtubule inner protein complex (Gui, Farley et al. 2021). Thereby, I-TASSER (Iterative Threading ASSEmbly Refinement) program was used to predict the structure of human PIERCE1 and C15ORF65 using the bovine structure as a template. I-TASSER uses a deep learning algorithm coupled with hierarchical template-based modelling approach to predict structure and structure-based functional prediction more accurately than other programs available such as AlphaFold (Zheng, Zhang et al. 2021). The predicted I-TASSER structures of human PIERCE1 and C15ORF65 were more similar to those of bovine as compared to the AlphaFold structures (Appendix

H and Appendix I) and suggested that human PIERCE1 and C15ORF65 were structurally similar to each other except 10-12 amino acids from the N-terminal region. Since the TM values and C-scores were within the acceptable range, the predicted structures were considered accurate. Moreover, MotifScan was not able identify any known motif in PIERCE1 and C15ORF65, indicating any motif present in these proteins would be unique. Based on these findings, it can be concluded that PIERCE1 and C15ORF65 may contain structurally unique conserved motifs and these motifs might have critical functional role.

To assess the functional association of human PIERCE1 and C15ORF65 with cilia, their expressions in established datasets like HPA (Colwill, Renewable Protein Binder Working et al. 2011, Uhlen, Fagerberg et al. 2015, Karlsson, Zhang et al. 2021) were evaluated and the findings suggested that both of them are mostly expressed in tissues containing multiciliated epithelial cells like fallopian tube, testes and respiratory epithelium. Consistent with HPA dataset, single-cell RNA-seq data sets from human and mouse respiratory epithelia showed localisation of both *PIERCE1* and *C15ORF65* transcripts mostly in multiciliated cells. This further supports the association of these genes with cilia. Interestingly, DeepLoc analysis suggested that these proteins are possibly absent in cellular organelle and the HPA immunohistochemical data consistently showed the localisation of these proteins in ciliary axoneme, though the validation of used antibody remained questionable. However, unpublished data from our lab shows that murine PIERCE1 is localised to ciliated cells but not specifically with in the axonemes (Appendix G). Localising PIERCE1 and C15ORF65 in cilia could be challenging if these proteins are localised as MIPs, the antibody may fail to access the epitope even after a harsh permeabilization steps. Such limitations could be overcome with immunohistochemistry using immunogold staining followed by transmission electron microscopy, as the ciliary axonemes can be cut through during the processing steps revealing the MIPs in ciliary axoneme. This could be a possible reason for detecting PIERCE1 in immunohistochemistry of tissue but not with immunofluorescence microscopy of cells. However, it can be concluded that both PIERCE1 and C15ORF65 could be localised in human cilia. To confirm this, specific antibodies can be generated for immunohistochemical analysis on bronchial sections and/or immunofluorescence microscopy can be done with ALI-differentiated HBECs along

with ciliated cell markers like FOXJ1 or acetylated α-TUBULIN or ARL13B (axonemal markers).

It can be expected that if human PIERCE1 and C15ORF65 are truly associated with cilia, then the expression of these genes should be increased during the process of ciliogenesis and knockout (by CRISPR-CAS9 gene editing technology) or knockdown (by RNAi) of either or both genes should impair the process of ciliary axonemal development. My analysis shows that expression of both genes was increased during mucociliary differentiation across three murine multiciliated epithelial cell types. A similar observation was found following examination of gene expression in another mTEC data set where the expression of both genes started to increase from day 4 (Nemajerova, Kramer et al. 2016). Furthermore, a linear increase of the expression of both genes was observed in primary HBECs undergoing ALI differentiation, stabilizing after day 14 of ALI culture. Nonetheless, primary HBEC starts to produce beating cilia at this point (day 14 of ALI) (Ross, Dailey et al. 2007).

In summary, the expression of the conserved genes *PIERCE1* and *C15ORF65* was increased during the process of mucociliogenesis, and the corresponding transcripts were localised in the ciliated cells. To further confirm their function in cilia, a suitable *in vitro* knockout model for these genes is required. In the next chapter, I'll evaluate an *in vitro* human cell line model where these genes can be knocked-out by CRISPR-CAS9 gene editing system to validate the functional association of PIERCE1 and C15ORF65 in human cilia.

Chapter 5: Validating HBEC3-KT cells as a model to study mucociliogenesis

5.1 Preface

An immortalized cell line model is preferred over primary HBECs to elucidate the functions of PIERCE1 and C15ORF65 as primary cells have a limited lifespan meaning that it is difficult to generate monoclonal knockout cell lines. An ideal immortalized cell line for molecular studies involved with mucociliary differentiation should: (i) undergo mucociliogenesis upon differentiation analogous to that seen in primary HBECs, (ii) be suitable for transfection by CRISPR-CAS9 gene editing using dual guide RNAs and selection of knockout cells, (iii) fail to produce ciliated cells upon knockout of *FOXJ1*, the master regulator of ciliogenesis, and (iv) be suitable for generating multiple knockouts and stable knock-ins. HBEC3-KT cells were immortalised by over-expressing mouse *Cdk4* and human *TERT* (Ramirez, Sheridan et al. 2004). However, several efforts of immortalization resulted in diminishing differentiation potentials of basal bronchial epithelial cells to generated multiple bronchial epithelial cell types (Delgado, Kaisani et al. 2011, Walters, Gomi et al. 2013, Lodes, Seidensticker et al. 2020, Orr and Hynds 2021). In this chapter, HBEC3-KT cells were validated for their differentiation potential and their fitness for use to investigate *PIERCE1* and *C15ORF65* functions in ciliogenesis. Findings of this chapter suggested that these cells expressed markers for ciliated cells and secretory cells, and *PIERCE1* and *C15ORF65* after mucociliary differentiation both at ALI and under submerged culture.

5.2 Differentiation of HBEC3-KT cells at the ALI and *PIERCE1 and C15ORF65* expression

HBEC3-KT cells were evaluated for their differentiation potential by culturing them at the ALI for up to 14 days as a validation step. In addition to this, the effect of initial expansion in different media on HBEC3-KT differentiation was also evaluated as it was considered that cells may behave differently during the expansion phase (under submerged conditions) which in turn could affect the downstream (mucociliogenesis at the ALI) process.

5.2.1 Differentiation of HBEC3-KT cells at the ALI

HBEC3-KT cells were grown at the ALI for 14 days using PALI media. Cells were observed at day 0 (undifferentiated), day 7, and day 14 during the differentiation process and samples were collected for further analysis. Brightfield microscopic observation suggested that the morphology of these cells changed over the time when cultured at the ALI using PALI media (Figure 5.1 A). A typical cobblestone appearance of these cells was observed prior to further culture at the ALI, however such morphology disappeared over time and the cells looked tightly packed. At day 0, the gap between the cells were visible but eventually such gaps disappeared as these cells underwent differentiation (Figure 5.1 B). These observations indicated that at the ALI, the cells formed tighter cell-cell junctions required for the barrier properties of airway lining (Figure 5.1) (Wan, Winton et al. 2000).

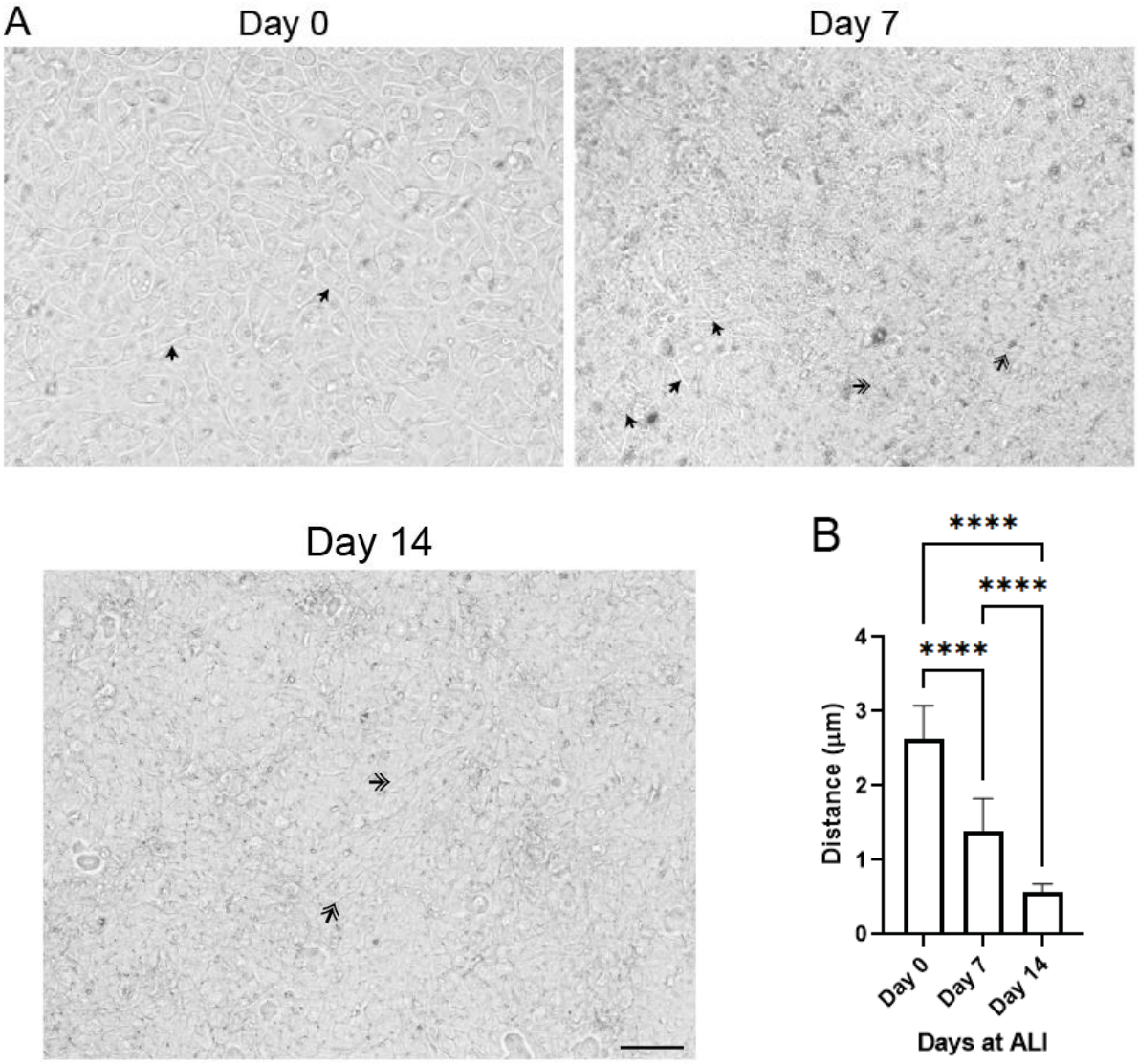

Figure 5.1 Morphology of HBEC3-KT cells cultured at the ALI using PALI media. Representative images (n=3) of HBEC3-KT cells were cultured at the ALI using PALI media for up to 14 days and their morphology was observed under a light microscope (A). Cell-cell attachment was evaluated on light microscopy images based on measured distance between cells after they were grown confluently (n = 50) (B). Single arrow indicates loosely packed cells and double arrow indicates tightly attached cells. Scale bar = 50 µm. **** = $p<0.0001$ based on unpaired t-test.

HBEC3-KT cells were grown at the ALI media changes undertaken every two days to induce differentiation in primary airway cells. When grown in this manner, HBEC3-KT cells started to express markers for secretory (*BPIFA1*) and ciliated cells (*TEKT1*) after 7 days and the expression appeared to increase over time. The cells also expressed *PIERCE1* and *C15ORF65* starting at day 7 of their mucociliary differentiation and their expression also seemed to increase over time (Figure 5.2). Immunofluorescence microscopy further confirmed that these cells differentiated into

secretory (BPIFB1 positive) cells and potentially progenitor ciliated (acetylated α-TUBULIN and FOXJ1 positive) cells (Figure 5.3). FOXJ1 was distinctly localised in the nucleus of acetylated α-TUBULIN positive potentially progenitors of multiciliated cells and BPIFB1 was detected in the cytoplasm of the secretory cells. All three proteins were absent in undifferentiated cells at day 0. When stained for PIERCE1 and C15ORF65, strong cytoplasmic expression was detected for both proteins at day 14 in few cells whereas relatively weak nuclear staining was apparent for both proteins at day 0 and day 14. Interestingly, the cytoplasmic staining was partly co-localised with acetylated α-TUBULIN, a component of cilia, for both proteins in the differentiated cells (Figure 5.4). These findings indicated that HBEC3-KT cells possessed some potential to differentiate into multiple respiratory epithelial cells, expressed cilia-localised PIERCE1 and C15ORF65 upon differentiation at the ALI, and could be a useful model to study the functions of *PIERCE1* and *C15ORF65* in ciliogenesis.

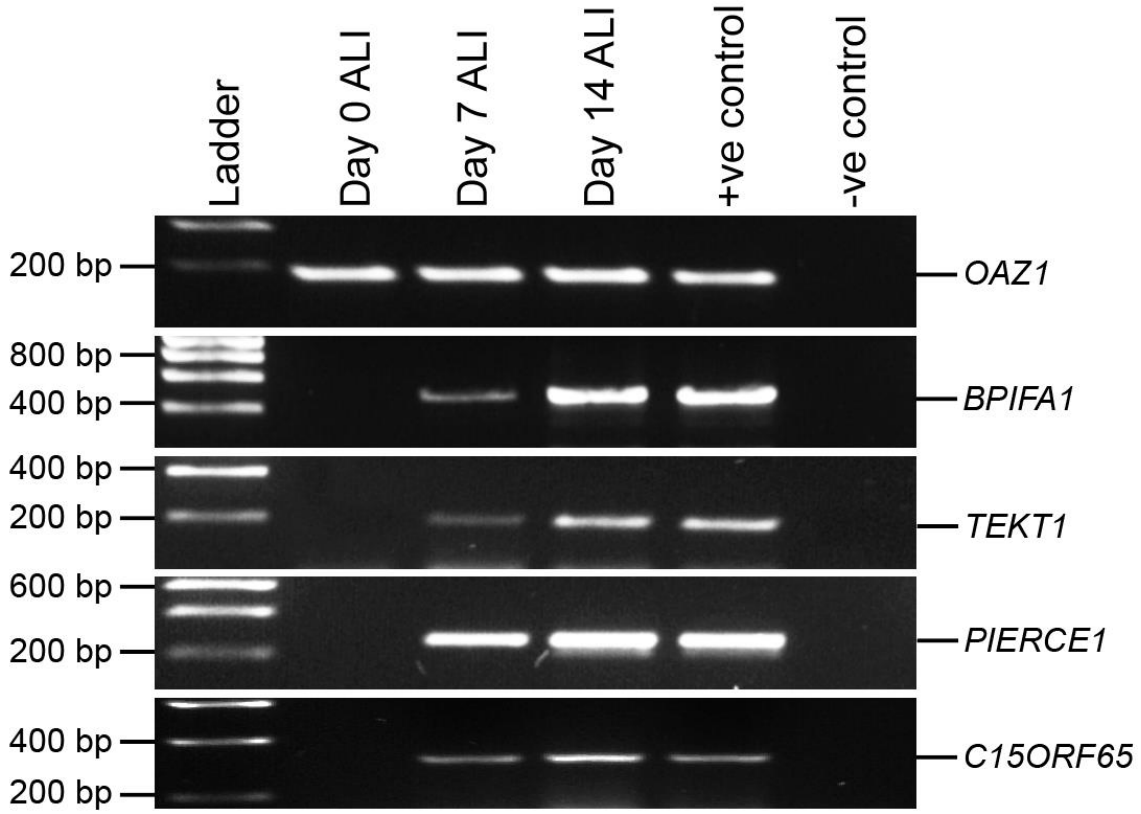

Figure 5.2 Expression of marker genes in the ALI-differentiated HBEC3-KT cells. End-point PCR was performed using cDNA generated from RNA collected from the ALI cultured HBEC3-KT cells on the indicated days to assess the expression of indicated genes. The gel is representative of an n = 3.

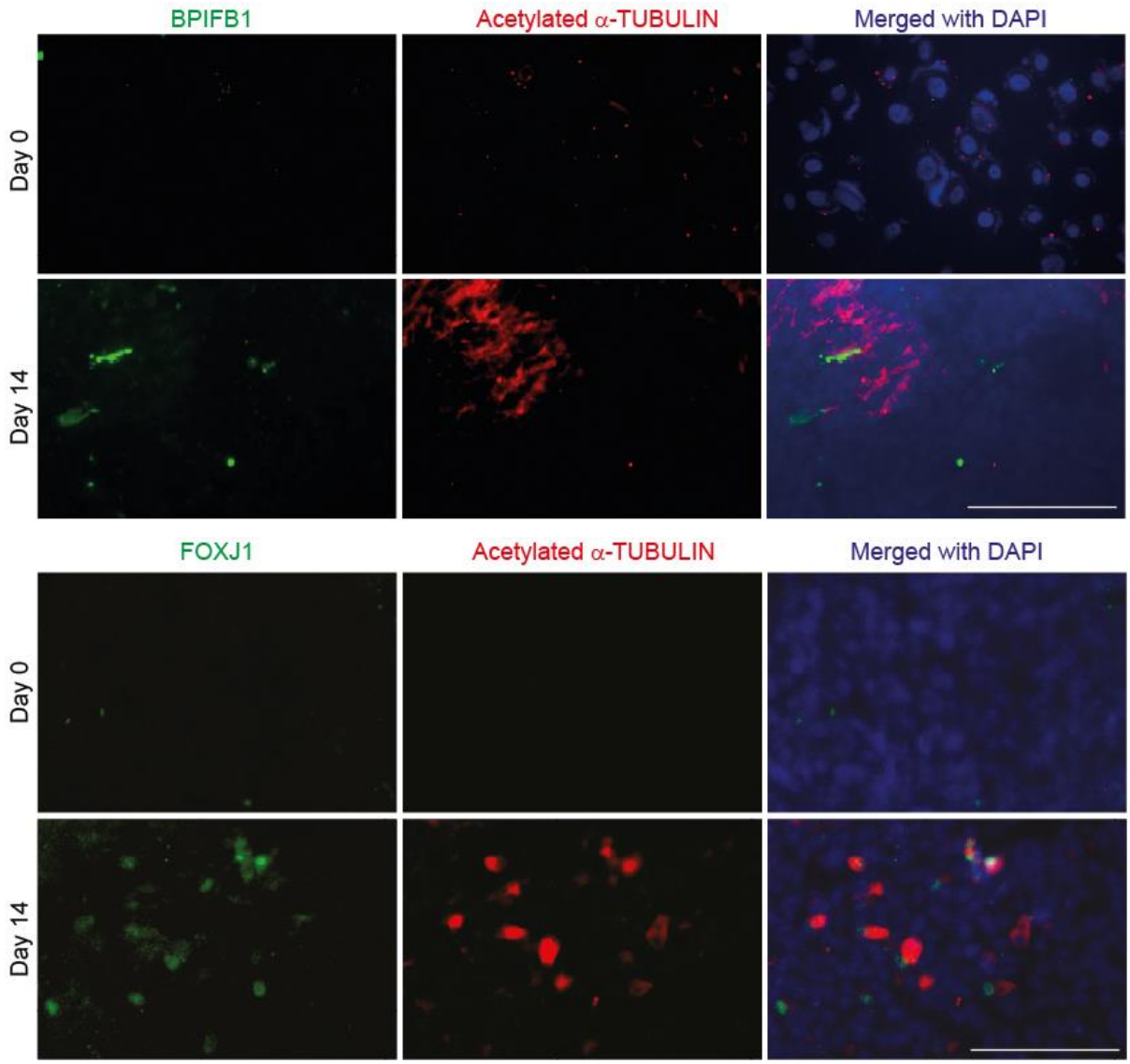

Figure 5.3 Immunofluorescence microscopy of undifferentiated (day 0) and the ALI-differentiated (day 14) HBEC3-KT cells. BPIFB1 was used as a marker for secretory cell and both FOXJ1 and acetylated α-TUBULIN were used as markers of ciliated cells. Scale bar = 100 μm. Images are representative of n = 3 experiments.

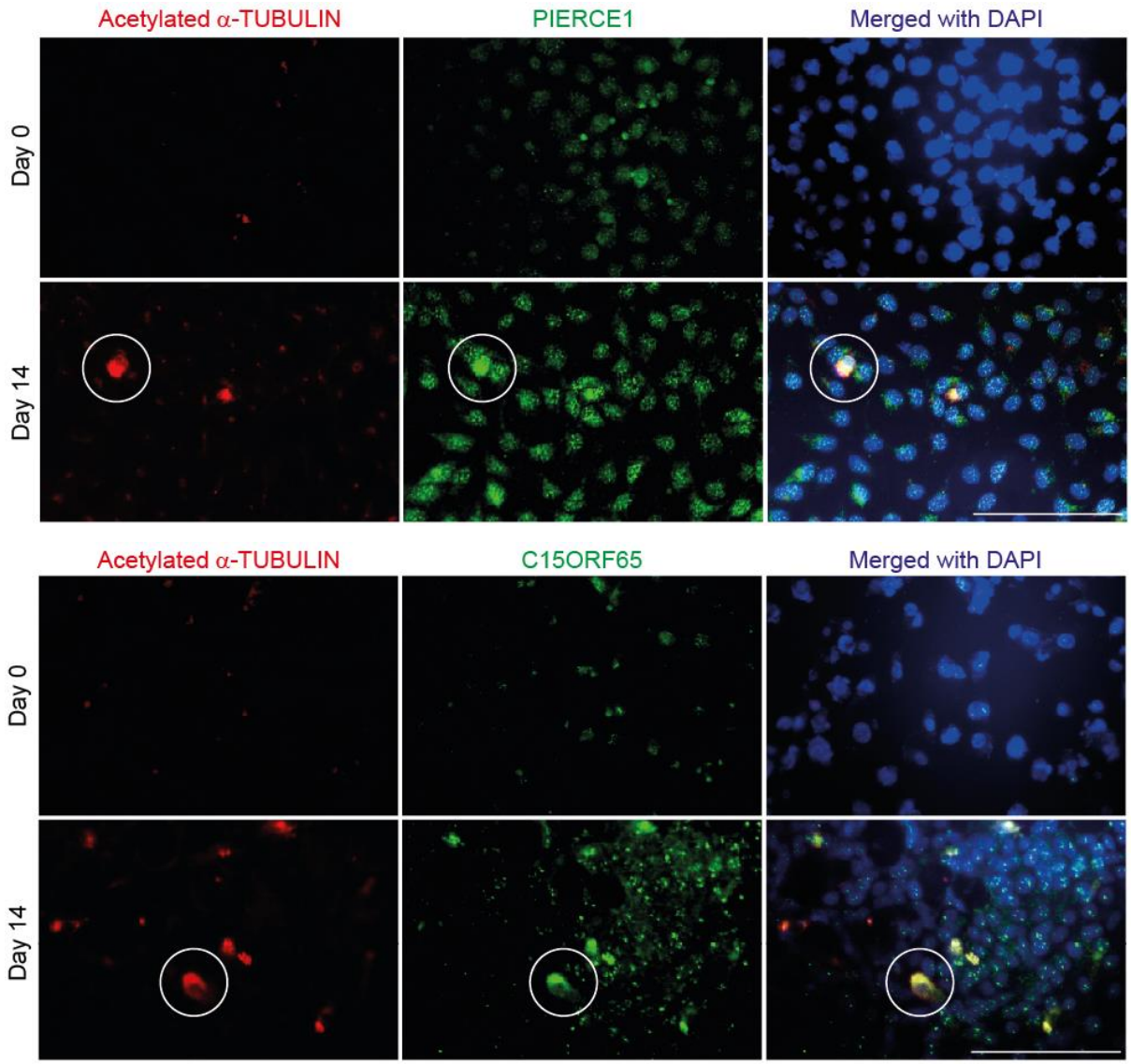

Figure 5.4 PIERCE1 and C15ORF65 expression in HBEC3-KT cells grown at the ALI. HBEC3-KT cells were stained for PIERCE1 (top panel) or C15ORF65 (bottom panel) during ALI differentiation along with acetylated α-TUBULIN. Scale bar = 100 μm. White circles indicate potential co-localization of PIERCE1 or C15ORF65 with acetylated α-TUBULIN. Images are representative of n = 3 experiments.

To investigate why HBEC3-KT cells could retain their differentiation potential, basal gene expression data from HBEC3-KT was compared to that of 29 other HBEC-KT cells and some selected lung cancer cell lines (A549, Calu-3, H226, H322, H358, H441, H522, H647 and H841) using GEO dataset GSE32036, Platform GPL6884 (Byers, Diao et al. 2013, Hight, Mootz et al. 2020). The analysis was undertaken using GEO2R (see section 3.5 under materials and methods). These nine cell lines were chosen as they previously failed to produce multiciliated cells when assessed in the lab following the ALI differentiation. 16 genes were found upregulated in

HBEC3-KT compared to the lung cancer cell lines. Among differentially expressed genes, 8 were associated with cell-cell adhesion (Table 5.1). However, expression of these genes was comparable between HBEC3-KT and the other *Cdk4-TERT* induced immortalized HBEC-KTs HBECs. Non-canonical WNT-signalling pathway promotes cell differentiation (Raslan and Yoon 2020) and two genes associated with this pathway (*PRICKLE1* and *FZD4* respectively) were differentially expressed between HBEC3-KT cells and other HBEC-KT lines (Table 5.1). These findings suggest that the immortalised HBEC3-KT cells may increase cell-cell adhesion prior to differentiation by inducing several cell-cell adhesion-associated genes and/or by downregulating the canonical WNT-signalling pathway to promote differentiation.

Table 5.1 Differential gene expression between HBEC3-KT cell and other lung cell lines. FC (log2) = log2 value of fold change ($p<0.05$ in all cases). GEO2R was used to analyse differential gene expression between HBEC3-KT cells and previously studied cancer cell lines or other KT-immortalized HBECs (see 3.5 under Materials and Methods for details) (Byers, Diao et al. 2013, Hight, Mootz et al. 2020).

Gene	Gene name	FC (log2)	Function
HBEC3-KT vs Lung cancer cell lines			
KRT5	Keratin 5	8.99	Mediate adhesion to basal membrane, part of hemidesmosome (Walko, Castanon et al. 2015).
KRT14	Keratin 14	8.69	
COL17A1	Collagen type XVII alpha 1 chain	6.75	
DSG3	Desmoglein 3	5.65	Cell-cell junction between epithelial cells (Fuchs, Foresti et al. 2019).
PKP1	Plakophilin 1	5.39	Stabilizes desmosome formation for cell-cell junction between epithelial cells (Fuchs, Foresti et al. 2019).
KRT6A	Keratin 6A	4.77	Required for cell-cell adhesion (Wang, Chen et al. 2018).
CDH13	Cadherin 13	4.59	Calcium-dependent cell-cell adhesion (Roman-Gomez, Castillejo et al. 2003).
ITGA6	Integrin subunit alpha 6	4.57	Required for cell-cell adhesion and hemidesmosome formation (De Arcangelis, Hamade et al. 2017).
HBEC3-KT vs Other HBEC-KTs			
PRICKLE1	prickle planar cell polarity protein 1	5.367	Negative regulator of WNT signalling pathway (Chan, Chan et al. 2006).
FZD4	Frizzled class receptor 4	-1.623	Component of WNT signalling pathway (Zhang, Harada et al. 2011).

5.2.2 Differentiation of HBEC3-KT cells during expansion with different media

Growth media as well as serum may exert effects on growth and differentiation of cells (Lund, Pilgaard et al. 2009). HBECs have been reported to show altered epithelial-mesenchymal transition when expanded with different growth medium and this can affect differentiation potential (Hasan, Harith et al. 2020). To evaluate such effects in HBEC3-KT cells, two different passages of cells (early passage and late passage) were proliferated using complete KSFM media or complete PneumaCult™ Ex+ media prior to the start of the ALI culture. Complete KSFM contains bovine pituitary extracts as an alternative to serum to provide hormones and essential mitosis-promoting growth factors, to maintain normal morphology by avoiding fibroblastic transformation and to reduce oxidative stress (Kent and Bomser 2003, Xu, Li et al. 2013). Complete PneumaCult™ Ex+ media contains a fraction of human plasma, and this may change the morphology and growth of the cultured cells during their growth. Interestingly, HBEC3-KT cells looked tightly packed even at day 0 of the ALI when they were proliferated in PneumaCult™ Ex+ media as compared to KSFM media. This observation was consistent across the two passages evaluated here (Figure 5.5). The cell morphology was grossly similar after differentiation at the ALI using PALI media irrespective of whether they had originally been proliferated using KSFM or PneumaCult™ Ex+ media.

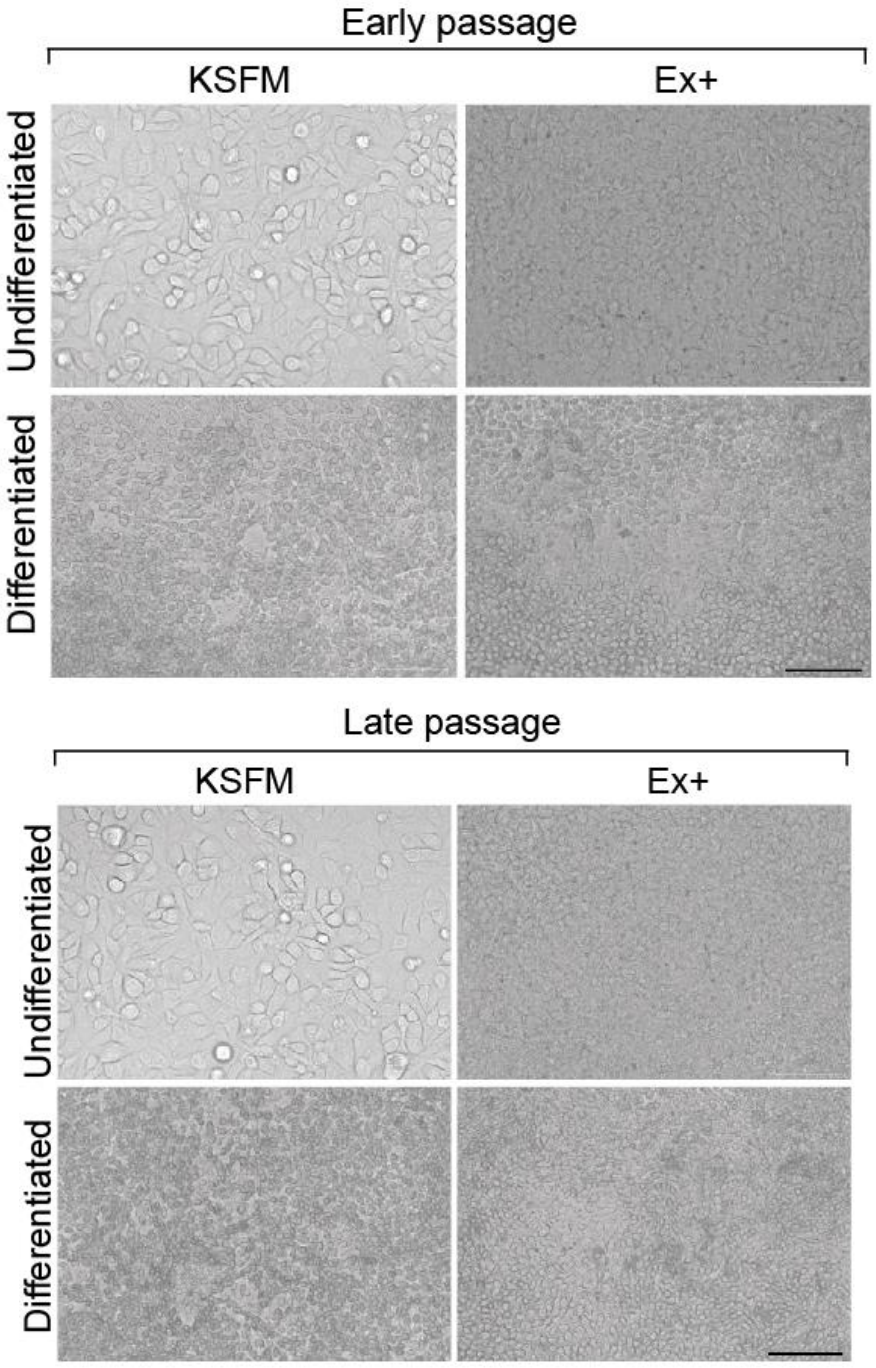

Figure 5.5 Growth and the ALI-differentiation of HBEC3-KT cells proliferated using different media. HBEC3-KT cells of early and late passages were proliferated using either KSFM (top panel) or PneumaCult™ Ex+ media (bottom panel) for a week and later differentiated using PALI media for 14 days. Scale bar = 100 μm. Images are representative of n = 2 experiments.

End-point PCR confirmed that HBEC3-KTs expressed *BPIFA1*, *TEKT1*, *PIERCE1* and *C15ORF65* after differentiation using PALI media irrespective of passage or initial media used for cell proliferation (Figure 5.6). Interestingly, these cells consistently expressed *BPIFA1*, *PIERCE1* and *C15ORF65* when proliferated on

plastic using PneumaCult™ Ex+ media (Figure 5.6) whereas cells grown in KSFM did not. Overall, the findings suggested that HBEC3-KT differentiated into secretory (*BPIFA1* positive) and potentially progenitors of ciliated (*TEKT1* positive) cells and expressed *PIERCE1* and *C15ORF65* irrespective of passage number or proliferation condition. *TEKT1* expression was only seen in the ALI differentiated cells. This data suggests HBEC3-KT cells might be undergoing an initial differentiation when proliferated in PneumaCult™ Ex+ media.

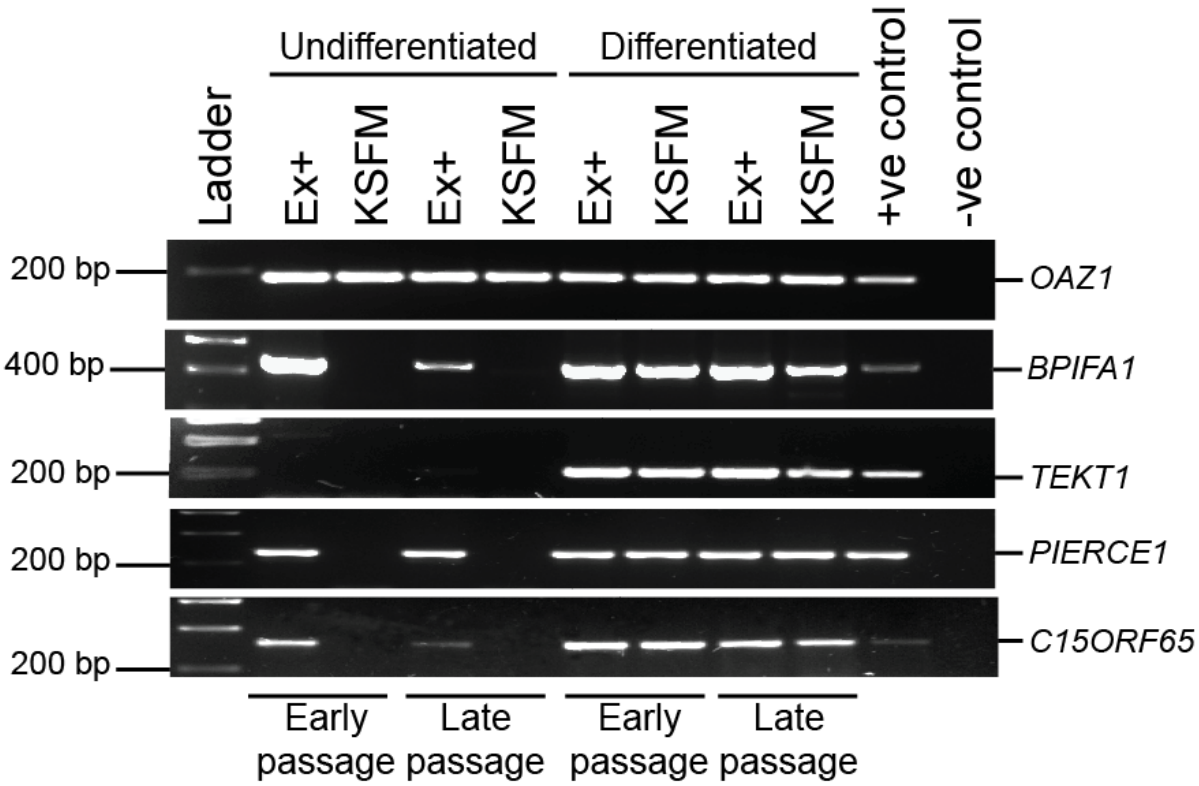

Figure 5.6 Expression of marker genes in the ALI-differentiated HBEC3-KT cells across passage numbers and initial proliferation media. End-point PCR was performed using cDNA generated from RNA collected from HBEC3-KT cells cultured in different media and following the ALI differentiation for 14 days. The gel is representative of n = 2 experiments.

5.2.3 Effect of hydrocortisone on *PIERCE1* and *C15ORF65* expression

Since hydrocortisone may induce monociliogenesis (Khan, Willemarck et al. 2016) in cancer cells, promote mucociliary differentiation by sensitizing the basal progenitor cells to growth factors (Volz, Huber et al. 2017) and could influence the ion transport system located in the cilia of multiciliated cells (Zaidman, Panoskaltsis-Mortari et al. 2016); and since the complete PneumaCult™ Ex+ media contains hydrocortisone,

the effect of adding hydrocortisone in pre-differentiation cultures on *PIERCE1* and *C15ORF65* expression was tested. HBEC3-KT cells were proliferated in KSFM media with or without 0.2 μM of exogenous hydrocortisone and either complete PneumaCult™ Ex+ media or the same media lacking hydrocortisone (where hydrocortisone is normally present at 0.2 μM). The cells were proliferated for a week, brightfield images were taken and cDNA samples were prepared from extracted RNA. Hydrocortisone seemed to have no major effect on cell morphology (Figure 5.7).

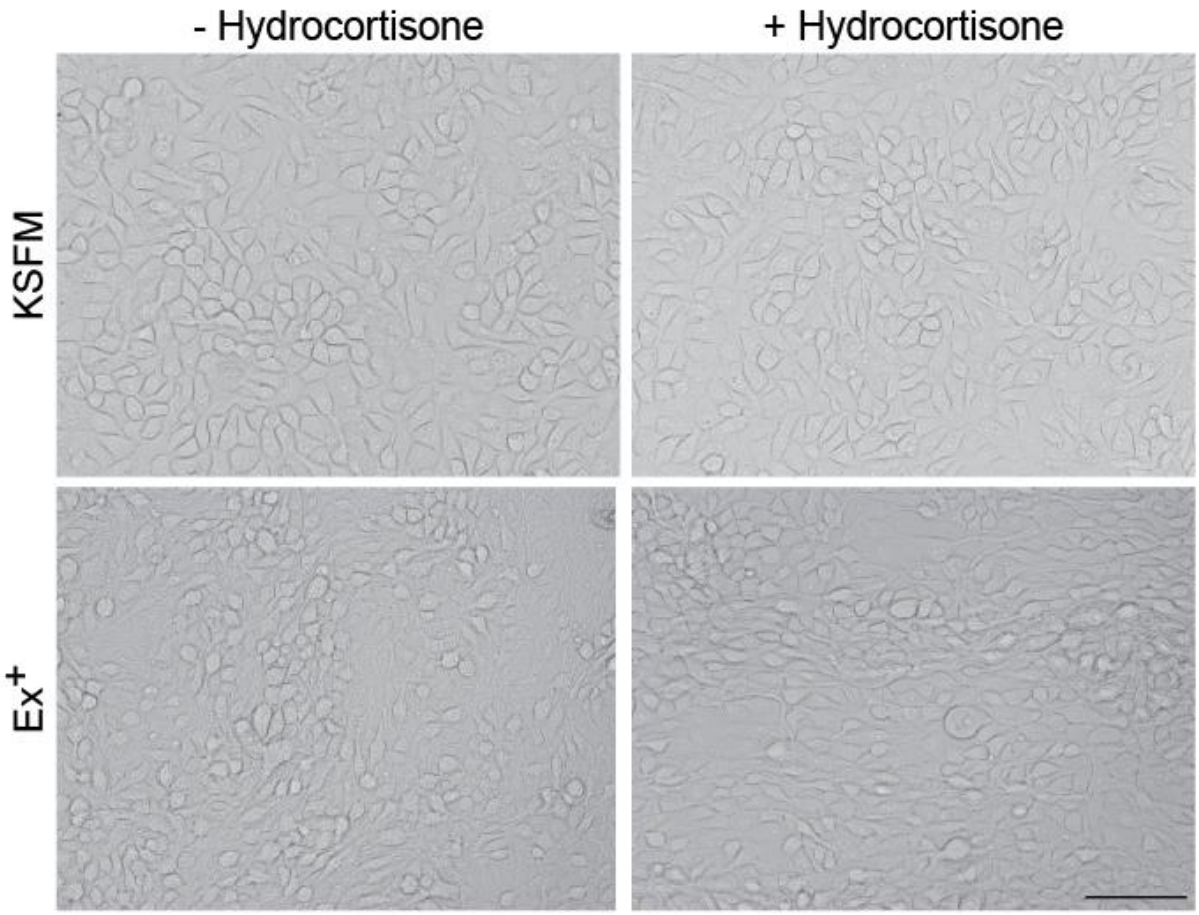

Figure 5.7 Effect of hydrocortisone on HBEC3-KT cell morphology. The cells were grown with indicated media with or without 0.2 μM hydrocortisone under submerged culture for a week. Images are representative of n = 3 experiments. Scale bar = 100 μm.

End-point RT-PCR showed that cells expressed *BPIFA1*, *PIERCE1* and *C15ORF65* when PneumaCult™ Ex+ media was used for cell proliferation irrespective of the addition of hydrocortisone. None of the cells expressed *TEKT1*. Cells expressed *PIERCE1* and *C15ORF65* but not *BPIFA1* or *TEKT1* when they were grown in KSFM

media supplemented with hydrocortisone (Figure 5.8). Expression appeared lower compared to that of the cells grown with PneumaCult™ Ex+ media but was not quantitated using qPCR. The data indicates that hydrocortisone induced some expression of *PIERCE1* and *C15ORF65* but does not play a role in pre-differentiation induced by PneumaCult™ Ex+ media.

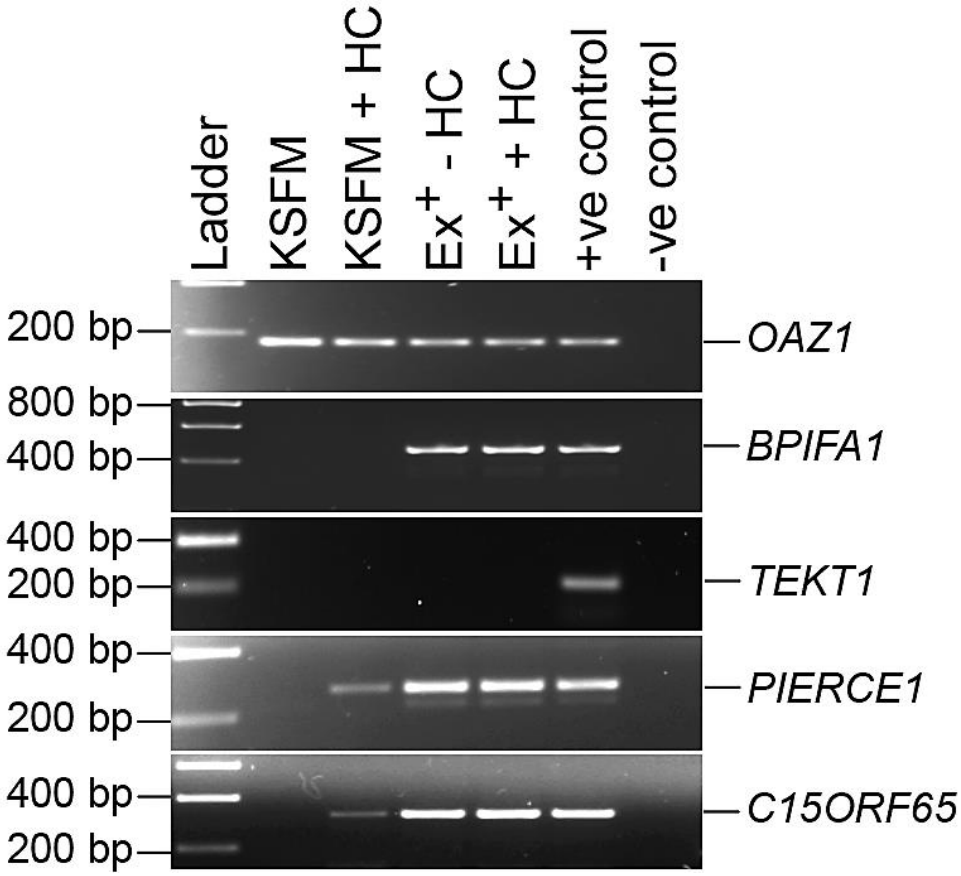

Figure 5.8 Effect of hydrocortisone on *PIERCE1* and *C15ORF65* expression. HBEC3-KT cells were grown in either KSFM media or PneumaCult™ Ex+ media with or without 0.2 μM hydrocortisone for a week. The gel is representative of n = 3 experiments.

5.3 Differentiation of HBEC3-KT cells under submerged condition

A previous report showed that hypoxia induced by submersion with media could induce ciliogenesis in primary HBECs (Gerovac, Valencia et al. 2014). Also, differentiation of primary HBECs could be promoted by increasing the availability of oxygen in the media through submerged culture (Kouthouridis, Goepp et al. 2021). To investigate whether HBEC3-KT cells retained the capacity to be differentiated in submerged culture, cells were grown with either KSFM media or complete PALI media for up to 21 days. Since DAPT and IL13 are considered to induce the

differentiation of ciliated and secretory cells respectively (Laoukili, Perret et al. 2001, Zahid, Feinstein et al. 2020), the effects of DAPT and IL13 were assessed to validate whether these agents could alter the process of differentiation under submerged conditions or not.

5.3.1 Differentiation of HBEC3-KT cells under submerged condition

Cells grown under submerged culture with KSFM, or PALI were imaged, and RNA samples were collected every week starting day 0 of the culture. Cells grown in KSFM maintained their cobblestone morphology after 21 days. The morphology of cells grown in PALI media started to alter from day 7 and this was better visualized after day 14 and at day 21 (Figure 5.9). Cells became tightly packed indicating tighter cell-cell junction when grown with PALI media under submerged culture. These observations indicated that cells might be differentiating beginning from day 14 under submerged culture with PALI media.

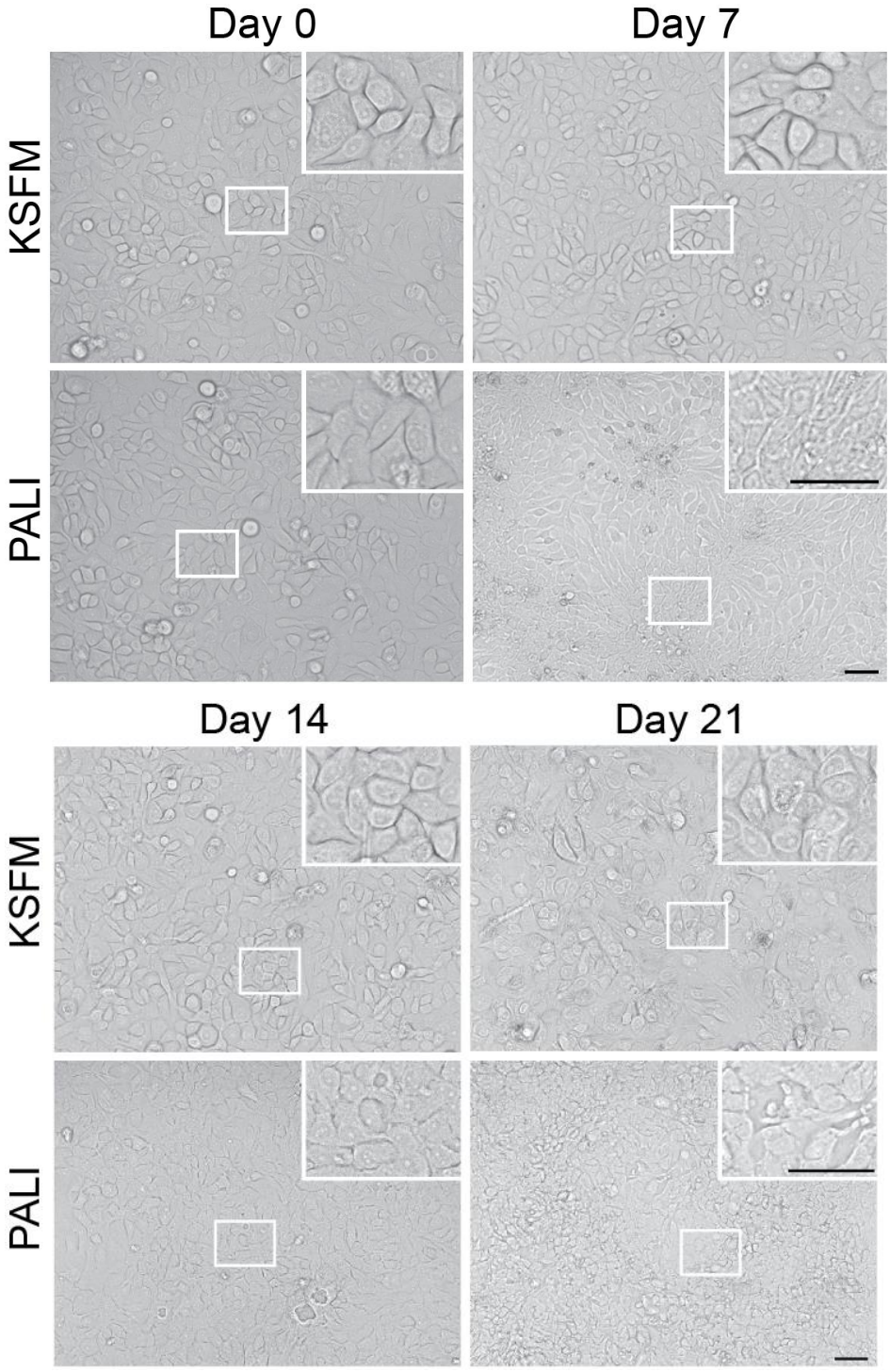

Figure 5.9 Morphology of HBEC3-KT cells under submerged culture with KSFM or PALI media. HBEC3-KT cells were grown with KSFM or PALI media under submerged conditions for up to 21 days. Brightfield mages were taken at the indicated days. Scale bar = 50 μm. Images are representative of n = 3 experiments.

End-point RT-PCR suggested that HBEC3-KT cells expressed *BPIFA1* at day 7, but *TEKT1* as well as *PIERCE1* and *C15ORF65* from day 14 when cultured with PALI media under submerged conditions (Figure 5.10). This is particularly interesting for two reasons: i) *TEKT1* was expressed in the ALI-cultured HBEC3-KT cells from day 7 (Figure 5.2), and ii) *PIERCE1* and *C15ORF65* were expressed in cells expanded with PneumaCult™ Ex+ media on transwells for a week (Figure 5.6), in the ALI-cultured HBEC3-KT cells from day 7, and in HBEC3-KT cells treated with 0.2 μM hydrocortisone for a week (Figure 5.8). Cells grown in KSFM did not express any of these four genes.

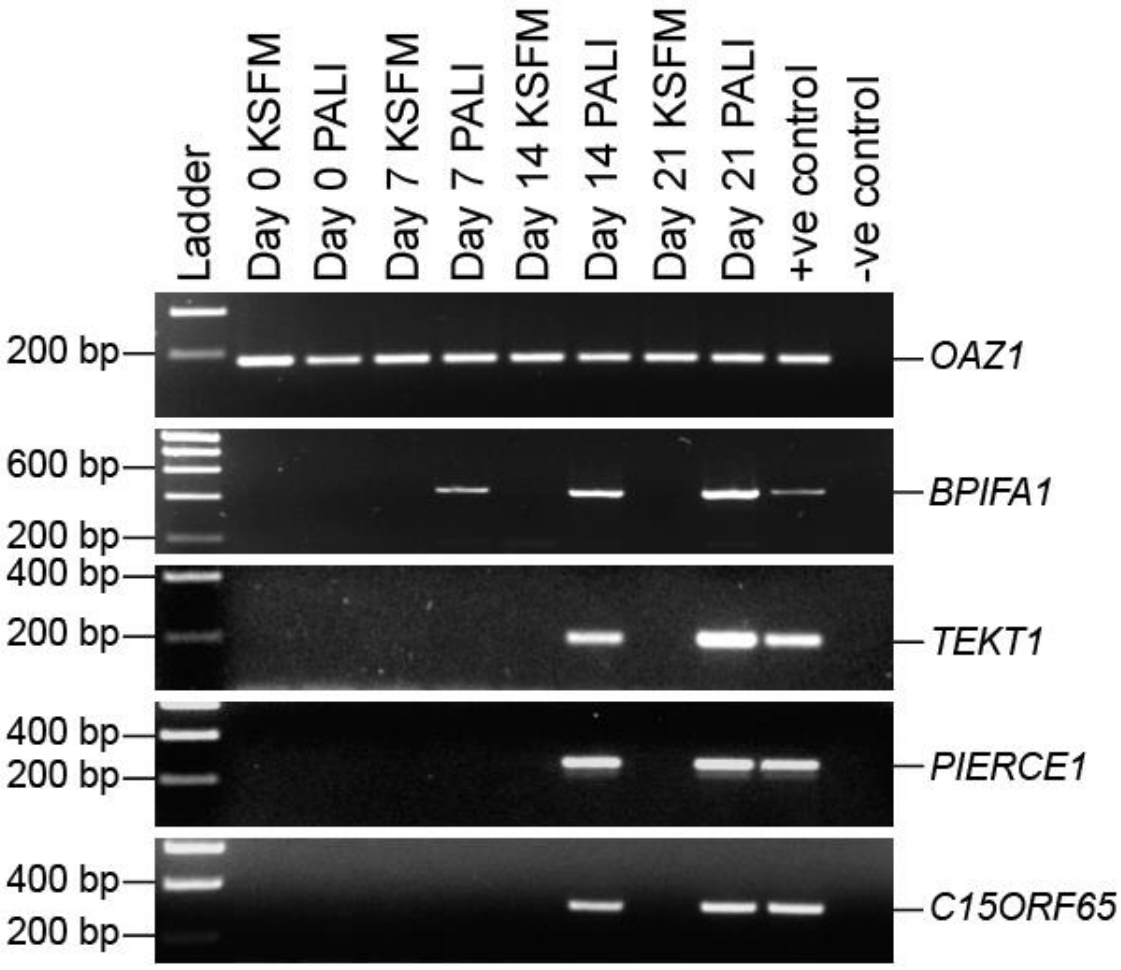

Figure 5.10 Expression of marker genes in HBEC3-KT cells cultured with KSFM or PALI media under submerged conditions. Cells were grown with indicated media for up to 21 days with media changed every two days. End-point PCR was done using the cDNA prepared from these samples. The gel is representative of n = 3 experiments.

Immunofluorescence microscopy of HBEC3-KT cells suggested that they produced both BPIFB1 and acetylated α-TUBULIN when grown with PALI media for 21 days but not when grown in KSFM for the same duration. BPIFB1 was localised in the cytoplasm and the acetylated α-TUBULIN was localised in the membrane forming cilia-like structures (Figure 5.11, top panel). These cells also produced FOXJ1 localised in the nucleus of acetylated α-TUBULIN positive cells when grown with PALI media for 21 days. Cells grown with KSFM media did not stain for these markers. This observation further validates the potential of HBEC3-KT cells to begin the process of ciliogenesis and to produce potential progenitors of multiciliated cells (Figure 5.11, bottom panel).

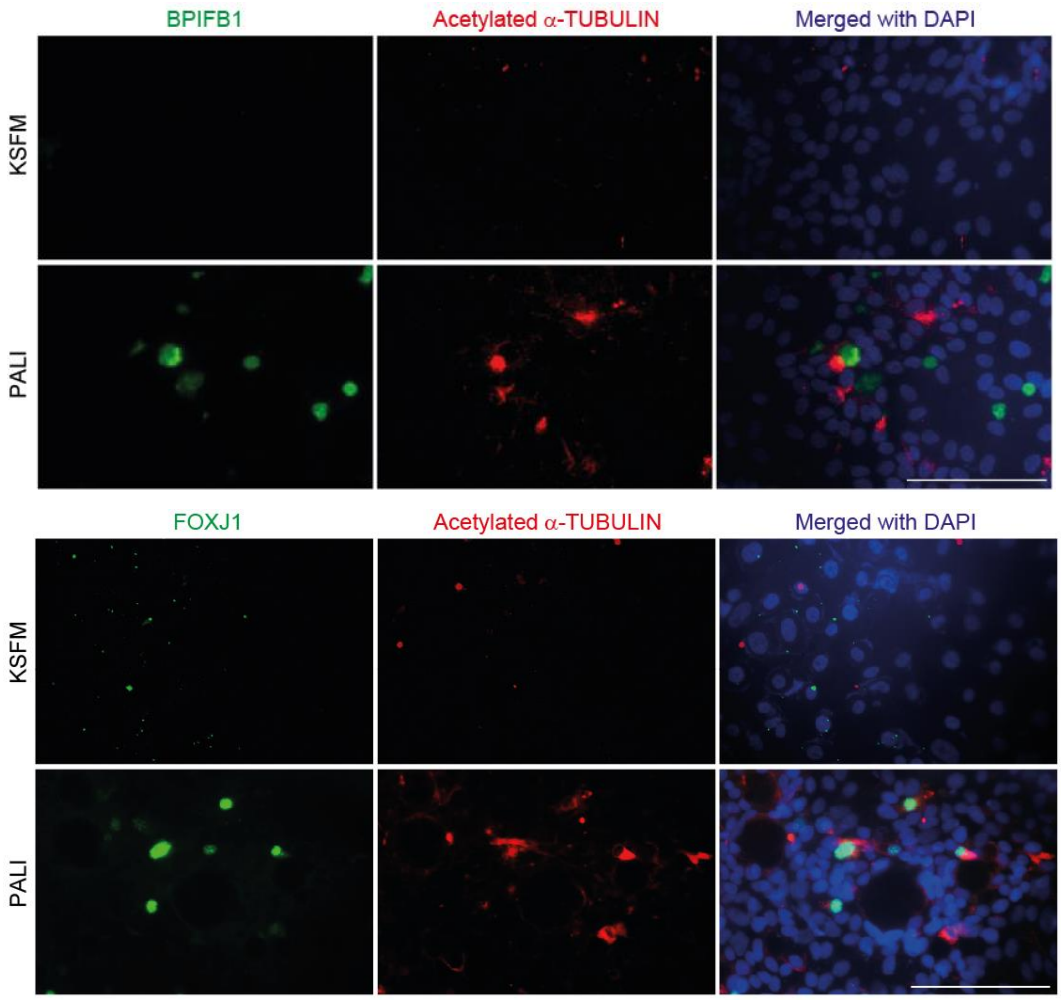

Figure 5.11 Differentiation of HBEC3-KT cells grown in PALI media or KSFM for 21 days. HBEC3-KT cells were grown with KSFM or PALI media under submerged conditions for 21 days and the cells were stained with BPIFB1 and acetylated α-TUBULIN (top panel) or with acetylated α-TUBULIN and FOXJ1 (bottom panel). Scale bar = 100 μm. Images are representative of n = 3 experiments.

When PIERCE1 and C15OF65 was visualized using immunofluorescence microscopy, nuclear staining was detected for both proteins in KSFM-cultured cells. However, a strong staining for both PIERCE1 and C15ORF65 was detected in the cytoplasm of acetylated α-TUBULIN positive PALI media-cultured cells; and a portion of such cytoplasmic staining was co-localised with acetylated α-TUBULIN staining suggesting these proteins were localised in the cilia (Figure 5.12). It is not clear whether the nuclear staining for both PIERCE1 and C15ORF65 were specific or some form of background staining. However, these observations suggested that i) HBEC3-KT cells differentiated into secretory cells possibly, and into potential progenitors of ciliated cells, and ii) expressed PIERCE1 and C15ORF65 partly co-localised with acetylated α-TUBULIN (potentially in cilia), when these cells were cultured under submerged condition with PALI media. Such findings were comparable to what was observed in the ALI differentiated cells before. Thus, HBEC3-KT cells could be a tractable model to study the molecular basis of mucociliogenesis as well as the roles of PIERCE1 and C15ORF65 in ciliogenesis, when cultured at the ALI or under submerged condition using appropriate media for appropriate duration of time (14 to 21 days).

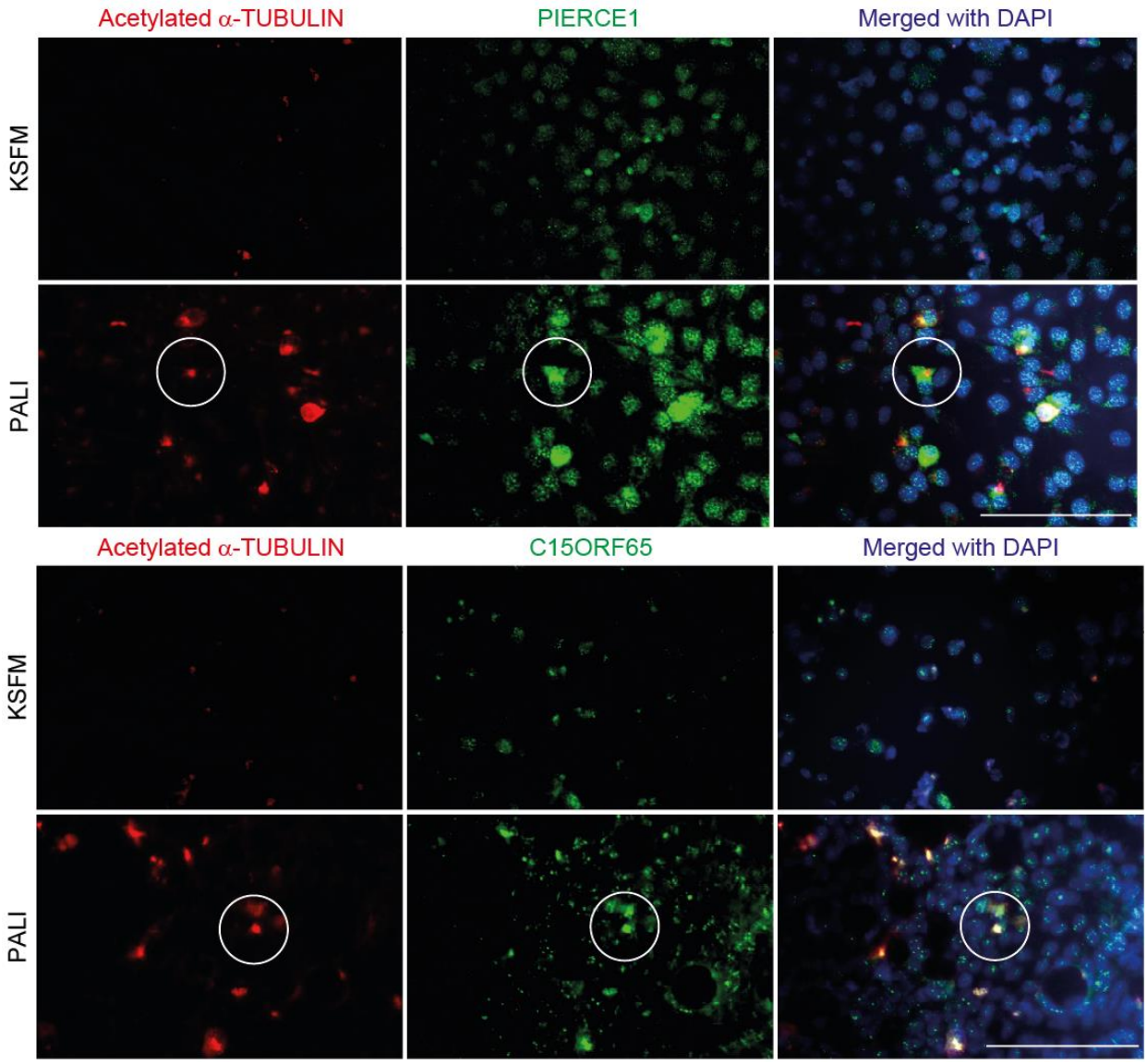

Figure 5.12 Expression of PIERCE1 and C15ORF65 in HBEC3-KT cells under submerged conditions. HBEC3-KT cells were grown with KSFM or PALI for 21 days and were stained for PIERCE1 (top panel) and C15ORF65 (bottom panel). Acetylated α-TUBULIN was used as cilia marker. PIERCE1 and C15ORF65 co-localised with acetylated α-TUBULIN (white circles). Scale bar = 100 μm. Images are representative of n = 3 experiments.

5.3.2 Effects of DAPT and IL13 on HBEC3-KT cell differentiation under submerged condition

DAPT (*N*-[*N*-(3,5-Difluorophenacetyl)-L-alanyl]-*S*-phenylglycine *t*-butyl ester) is a γ-secretase inhibitor (Pongjantarasatian, Nowwarote et al. 2022). γ-secretase cleaves NOTCH to activate the NOTCH signalling pathway (Arumugam, Chan et al. 2006). Previously it was shown that DAPT inhibition of NOTCH1/2 signalling pathway results in increased multiciliogenesis during mucociliary differentiation (Zhu, Iwano et

al. 2019, Zahid, Feinstein et al. 2020). On the other hand, the pleiotropic cytokine IL13 has been reported to increase the proportion of secretory cells during mucociliary differentiation by inhibiting MCIDAS expression as well altering the expression of multiple ciliogenesis-associated genes (Laoukili, Perret et al. 2001, Gerovac and Fregien 2016). This study showed that the number of ciliated cells increased significantly when 10 μM DAPT was added to the media, and the number of ciliated cells was decreased significantly by addition of 1 ng/ml IL13 or greater (Gerovac and Fregien 2016). Also, a recent report showed that IL13 could alter hypoxia-associated genes and increased the basal cell population (Khalil, Bernstein et al. 2020). To study the effects of these agents under submerged culture, HBEC3-KT cells were grown with KSFM and PALI media in presence or absence of 10 μM DAPT or 1 ng/ml IL13 for 21 days (Figure 5.13). Typical cobblestone morphology was observed when the cells were grown with KSFM with or without any of these treatments and the morphology seemed to be altered when cultured with PALI media as observed before. Cell-cell adhesion and stratification could be increased when DAPT was added to PALI media and could be decreased when IL13 was added.

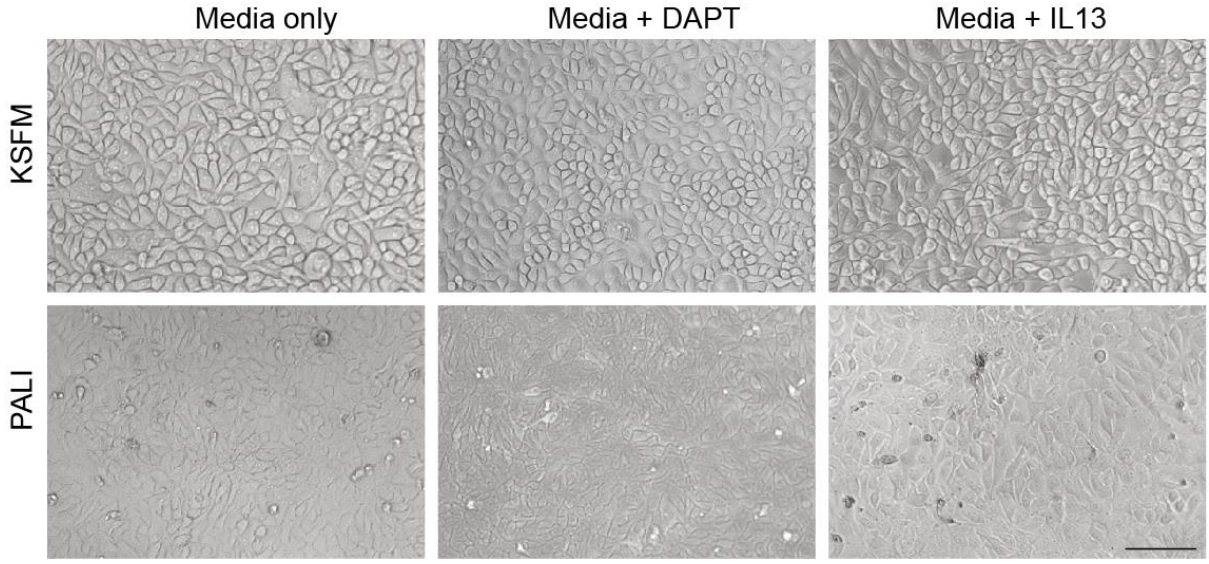

Figure 5.13 Effects of DAPT and IL13 HBEC3-KT cells under submerged culture. Cells were grown with 10 μM DAPT or 1 ng/ml IL13 in either KSFM or PALI media and morphology was observed after 21 days. Scale bar = 100 μm. Images are representative of n = 3 experiments.

cDNA samples were prepared, and end-point PCR was performed to detect the expression of marker genes (Figure 5.14). No markers were expressed with KSFM irrespective of any treatments, other than expression of *C15ORF65* was detected when DAPT was added. Cells cultured with PALI media expressed *BPIFA1, TEKT1*, *PIERCE1* and *C15ORF65*. The expression of these genes in PALI media-cultured cells, whether treated or untreated with either DAPT or IL13, remained essentially unchanged except for lower expression of *BPIFA1* in DAPT-added PALI media relative to PALI media only, and higher expression of *BPIFA1* in IL13-added PALI media relative to untreated PALI media was observed. Further validation by qPCR would be required to confirm the quantitative differences in these findings.

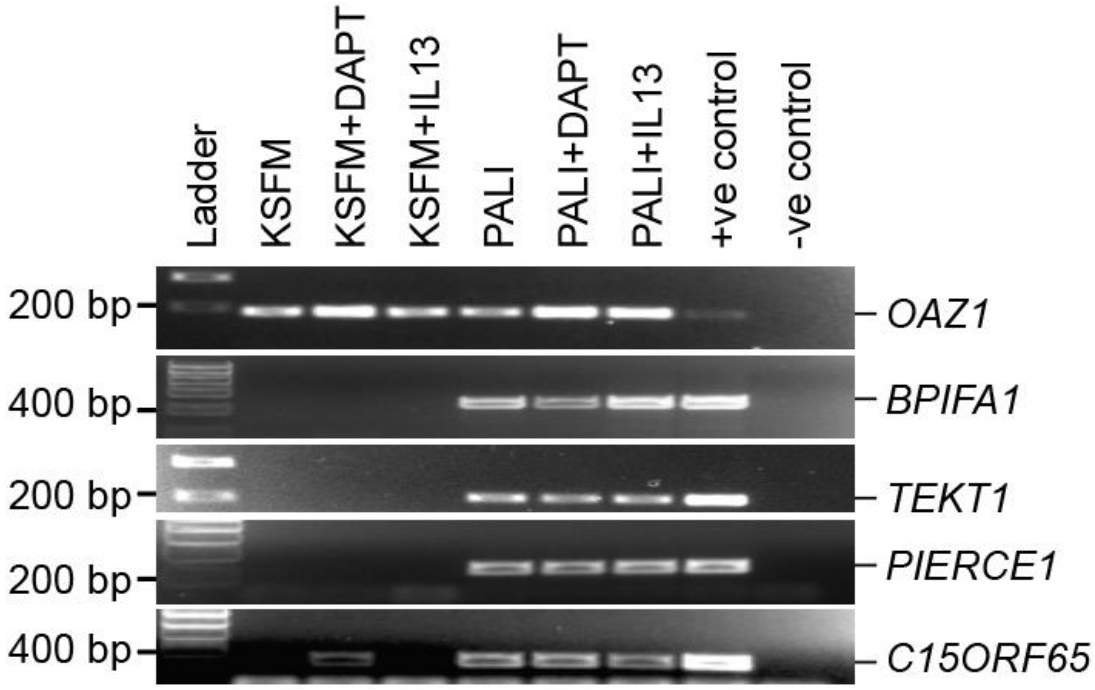

Figure 5.14 Effects of DAPT and IL13 on marker gene expression in submerged cultures of HBEC3-KT cells. Cells grown with KSFM or PALI media with or without 10 μM DAPT or 1 ng/ml IL13 were assessed for secretory or ciliated cell markers as well as *PIERCE1* and *C15ORF65* (gel is representative of n=3).

5.4 Chapter discussion

Validating a suitable human cell line model was a prime requirement to enable me to study the key regulatory process of early mucociliogenesis for my thesis. Human ciliogenesis is mostly studied in airway epithelial cells rather than other epithelial cells like endometrium or fallopian tube, and primary human airway epithelial cells have been shown to differentiate in multiple airway epithelial cell types (Stewart, Torr

et al. 2012, Schamberger, Staab-Weijnitz et al. 2015, Qin, Wu et al. 2019, Leung, Wadsworth et al. 2020). However, the development of gene knockouts in primary human cell lines is still challenging due to the difficulty in achieving clonal selection of gene-edited cells (Everman, Rios et al. 2018, Peters-Hall, Coquelin et al. 2018, Rapiteanu, Karagyozova et al. 2020) and researchers use immortalized or cancer cell lines for the development of gene knockout cell lines. Human bronchial epithelial cells have been immortalized by several research groups to study mucociliary differentiation as an alternative to primary human bronchial epithelial cells. Some notable examples of these immortalized cell lines are papilloma-virus immortalized HBE1 (Yankaskas, Haizlip et al. 1993), immortal 16HBE14o- (Cozens, Yezzi et al. 1994) and IM-HBEpiC (Chen, Huang et al. 2016), SV40-immortalized BEAS-2B (Reddel, Ke et al. 1988), *Bmi-1*/h*TERT* growth-enhanced hBE (Fulcher, Gabriel et al. 2009), polycomb protein complex gene *BMI-1* immortalized NHBE BMI-1 (Munye, Shoemark et al. 2017) and different *Cdk4*/h*TERT* immortalized HBECs (HBEC-KTs) (Ramirez, Sheridan et al. 2004, Orr and Hynds 2021). Here, HBEC3-KT cells were chosen as a model to study the role of PIERCE1 and C15ORF65 in ciliogenesis as i) this cell line was available for this study, ii) this cell line is one of the mostly studied immortalized cell line associated with mucociliogenesis research, iii) they require simple and cheap media compared to the other cell lines, and iv) the differentiation capacity of this cell line has been tested by other researchers (Delgado, Kaisani et al. 2011, Nakauchi, Nagata et al. 2019).

The *in vitro* mucociliary differentiation capacity of HBEC3-KT cells was validated prior to further experiments. The ALI culture remains the gold standard protocol for *in vitro* differentiation of respiratory epithelial cells to produce multiciliated and secretory cells by day 14 to day 28 of the ALI culture (Stewart, Torr et al. 2012). Additionally, it has also been shown that primary airway cells can be differentiated when cultured under submerged condition with differentiation media (Kouthouridis, Goepp et al. 2021), although this technique has been less frequently applied to date. When HBEC3-KT cells were differentiated at the ALI for 14 days or cultured under submerged condition with PALI media for 21 days, the cells were able to express the markers for ciliated cells (*TEKT1*, FOXJ1 or acetylated α-TUBULIN) and secretory cells *(BPIFA1* or BPIFB1) indicating these cells maintained their mucociliary

differentiation potential in my hands similar to that shown in previous studies (Delgado, Kaisani et al. 2011). Maintaining overexpression of 8 cell-adhesion genes and regulation of two WNT signalling pathway genes (as compared to lung cancer cell lines and other HBEC-KT cells) possibly could produce increased cell-cell adhesion and thus could facilitate to maintain their mucociliary differentiation capacity. Unfortunately, no genome wide expression data on differentiated HBEC3-KT cells are available to analyse the expression patterns of these genes in differentiated HBEC3-KT cells to evaluate whether such expression patterns of these genes remain consistent or not.

Although the media used for initial expansion seemed not to affect the early ciliogenesis process in HBEC3-KT cells, induction of *BPIFA1* expression during the expansion phase might be influenced by the fraction of human plasma present in the supplement of the PneumaCult™ Ex+ media. Thus, cells might follow a pre-differentiation stage to produce BPIFA1-positive intermediate secretory cells prior to the ALI when they were expanded with PneumaCult™ Ex+ media. PneumaCult™ Ex+ media differs from PALI media by hydrocortisone content (0.2 μM vs 1 μM), heparin (absent vs present), and media supplements containing human plasma and photosensitive compounds like retinoic acids (according to the manufacturer's declaration). Such variation in media formulation may contribute to the difference in *PIERCE1* and *C15ORF65* expression as expression of these genes was not consistent across these two media, different passage, and length of time in ALI culture. For example, addition of 0.2 μM hydrocortisone in KSFM did appear to induce the expression of *PIERCE1* and *C15ORF65* but not *BPIFA1* (Figure 5.8). Similarly, addition of 10 μM DAPT but not 1 ng/ml IL13 appeared to induce the expression of *C15ORF65* only in KSFM-cultured HBEC3-KT cells indicating NOTCH can inhibit the expression of *C15ORF65* possibly in the same way as *KLF4* (Zheng, Pritchard et al. 2009).

Nonetheless, my studies clearly show that differentiated HBEC3-KT cells expressed PIERCE1 and C15ORF65. Based on these findings it can be concluded that it is possible to differentiate HBEC3-KT cells into potential progenitors of ciliated cells and possibly secretory cells at the ALI or under submerged condition with PALI

media, and the progenitor-ciliated cells generated this way expressed PIERCE1 and C15ORF65. All these findings validate the differentiation capacity of HBEC3-KT cells and justified their use to study the function of PIERCE1 and C15ORF65 in early ciliogenesis. This will be explored in the following sections.

Chapter 6: Development of *FOXJ1*, *PIERCE1*, and *C15ORF65* knockout HBEC3-KT cells

6.1 Preface

The findings of the previous chapter (Chapter 5) suggested that HBEC3-KT cells could be differentiated in both ALI and submerged culture conditions, and that they express *PIERCE1* and *C15ORF65*. Therefore, I confirmed that these cells could be considered as a model to study the molecular basis of mucociliogenesis as well as the roles of PIERCE1 and C15OF65 in cilia. To investigate this, I undertook to generate HBEC3-KT cells cell lines in which the genes for *FOXJ1*, *PIERCE1* and *C15ORF65* were knocked-out. In this chapter, I will describe how HBEC3-KT cells were optimized for transfection and how these three genes were knocked-out using CRISPR-CAS9 gene editing.

6.2 Transfection optimization of HBEC3-KT cells

To optimize the transfection procedure in HBEC3-KT cells, pEGFP-N1, a vector that expresses high levels of enhanced GFP under the direction of a CMV promoter, was initially transfected using $CaPO_4$-based and lipofectamine-based methods. Neither of these methods resulted in any HBEC3-KT cells expressing GFP (data not shown). Next, these cells were transfected with pEGFP-N1 with jetPRIME at 1:3 (μg plasmid:μl reagent) and with FuGENE® HD at 1:2 to 1:4 ratio. The most GFP-positive cells were observed when FuGENE® HD was used at 1:3 and 1:4 ratio and only a few were seen with the 1:2 ratio or with jetPRIME (Figure 6.1). Protein samples were prepared from cells transfected with FuGENE® HD and western blotting was carried with 10 μg of protein per sample to detect GFP. More GFP was detected in 1:4 ratio of FuGENE® HD compared to 1:3 (Figure 6.2). Based in these findings, I decided to use FuGENE® HD at the ratio of 1:4 (μg plasmid:μl reagent) for future transfections.

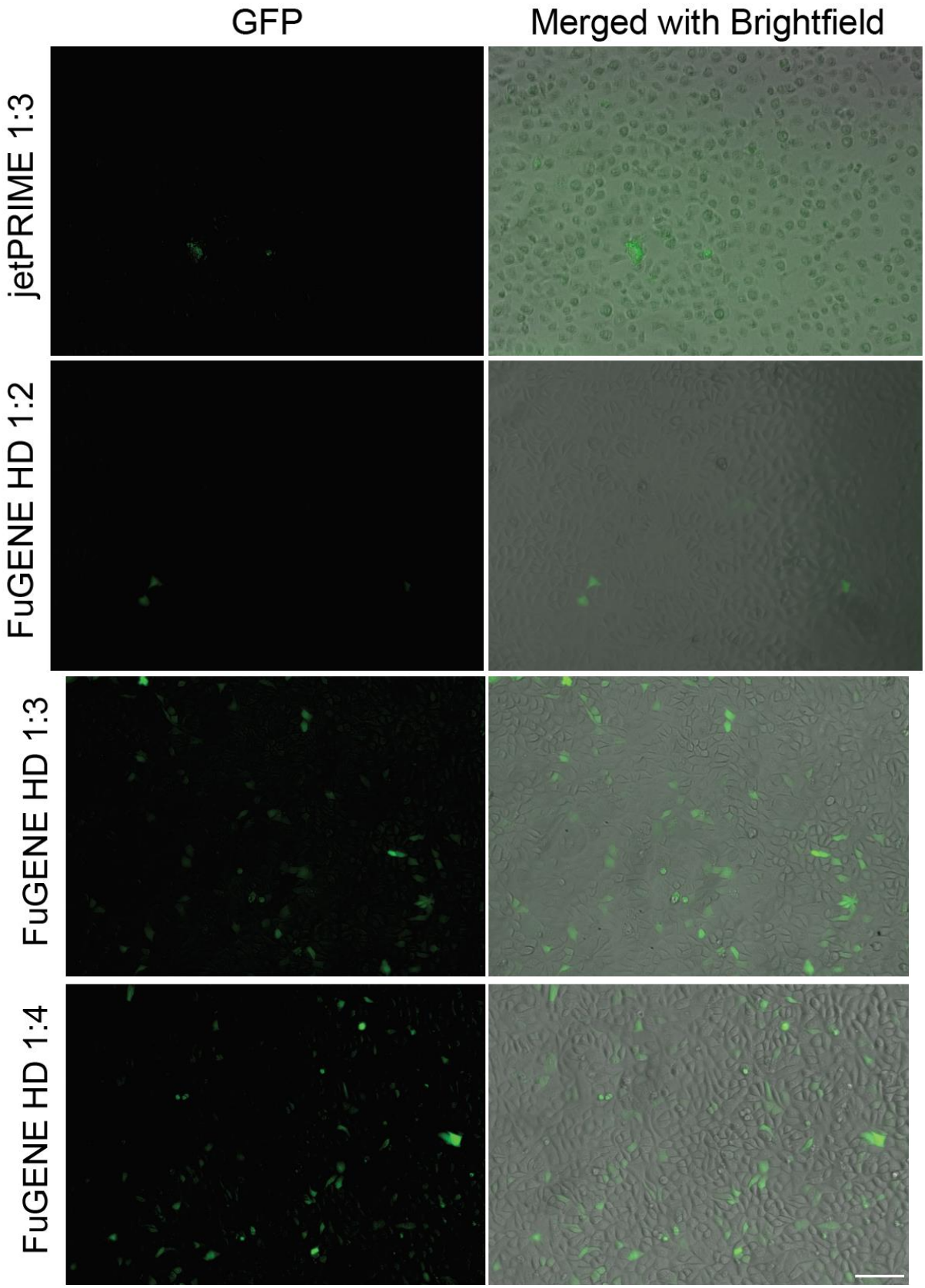

Figure 6.1 Transfection optimization of HBEC3-KT cells. HBEC3-KT cells were transfected with pEGFP-N1 using jetPRIME or FuGENE® HD at different ratios for μg plasmid:μl reagent. Cells were imaged after 72 hours. Scale bar = 100 μm. Image is representative of n = 2 experiments.

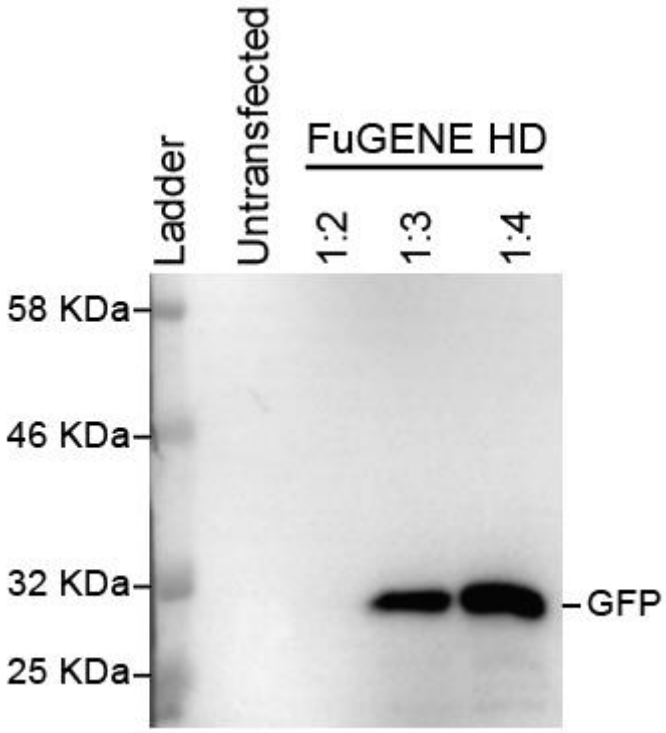

Figure 6.2 Detection of GFP in HBEC3-KT cells transfected with pEGFP-N1 using FuGENE® HD. 10 μg of proteins from untransfected or pEGFP-N1 transfected cells with indicated ratio of FuGENE® HD were probed for GFP. The blot was exposed for 1 minute during imaging. Image is representative of n = 2 experiments.

6.3 Development of *FOXJ1* knockout HBEC3-KT cell lines

FOXJ1 is one of the master regulators of ciliogenesis (Yu, Ng et al. 2008, Choksi, Lauter et al. 2014, Jackson and Attardi 2016, Stauber, Weidemann et al. 2017) and I considered that it would be an important proof of concept study to delete the gene in HBEC3-KT cells. So, to generate *FOXJ1* gene edited cells, HBEC3-KT cells were co-transfected with gRNA F1 and gRNA F5 previously cloned into PX458 (Hassan 2018) (see section 3.8 of materials and methods) or transfected with empty PX458 as a negative control using FuGENE® HD at a 1:4 ratio. These gRNAs flanked most of the forkhead domain (FHD) of FOXJ1 (Figure 3.1). After 72 hours of transfection, cells were visualized using a fluorescence microscopy for GFP positive cells (Figure 6.3). When these GFP-positive cells were sorted using FACS-Melody, 13.67% cells were found GFP-positive in the *FOXJ1* gRNAs co-transfection (Figure 6.4). GFP-positive and GFP-negative cells from empty plasmid transfected cells were also sorted and all these cells were seeded for proliferation. Once cells grew to confluence, DNA was extracted from 50% of the cells and was used for *FOXJ1*-genotyping PCR.

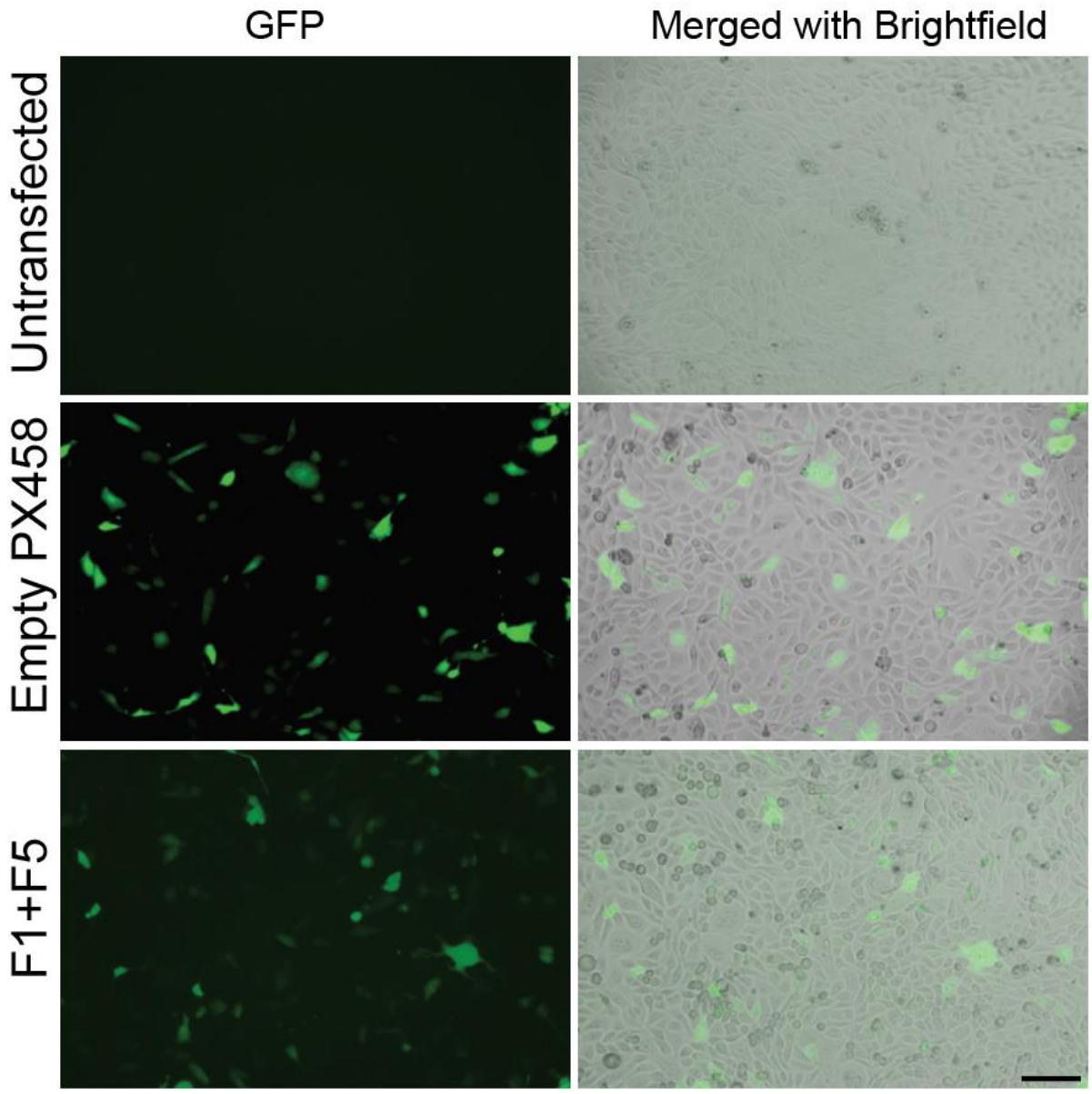

Figure 6.3 Co-transfection of HBEC3-KT for *FOXJ1* knockout. Cells were co-transfected with PX458 plasmid containing *FOXJ1* gRNA F1 and F5 using FuGENE® HD. GFP positive cells were visualized using fluorescence microscope. Empty PX458 was used as a negative control. Scale bar = 100 μm. Image is representative of n = 2 experiments.

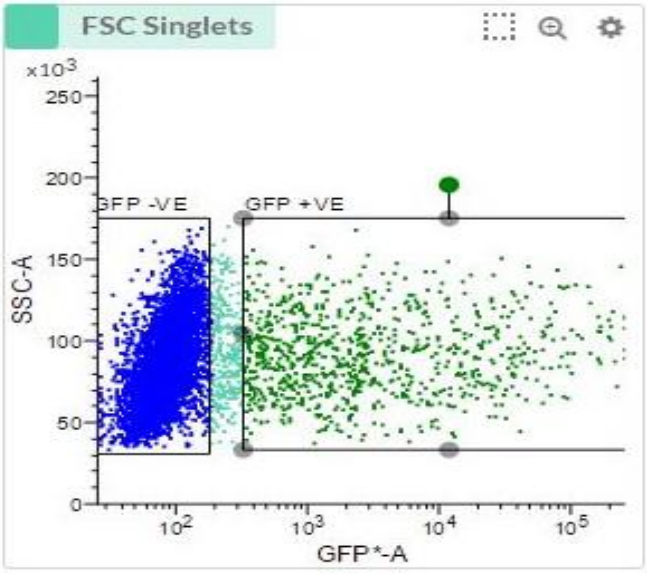

Population	Events	% Parent	% Total
All Events	10,000		100.00 %
Scatter	6,833	68.33 %	68.33 %
SSC Singlets	6,437	94.20 %	64.37 %
FSC Singlets	6,175	95.93 %	61.75 %
GFP -VE	5,053	81.83 %	50.53 %
GFP +VE	844	13.67 %	8.44 %

Figure 6.4 FACS sorting of GFP-positive cells in *FOXJ1* gRNA co-transfected HBEC3-KT cells. This shows an example of FACS sorting of GFP-positive cells. Both GFP-positive and GFP-negative cells were sorted. Figure is representative of n = 2 experiments.

Genotyping PCR of *FOXJ1* suggested that all samples with the exception of the *FOXJ1* gRNA GFP-positive cells showed a single band of the expected size (864 bp) equivalent to wildtype *FOXJ1*. In *FOXJ1* gRNA GFP-positive cells, multiple bands were observed near 600 bp, suggesting multiple deletions had occurred due to the activities of gRNAs (Figure 6.5). These findings indicated that there were a number of cells where a precise deletion of FOXJ1 FHD region occurred due to CRISPR-CAS9 activity inducing different editing by the gRNAs in the cell population. The remaining 50% of the cells were serially diluted to 5 cells/ml of KSFM media and 200 μl of this were seeded in each well of a 96-well plate for clonal selection. These clonally propagated cells were genotyped once they were confluent. The genotyping PCR suggested that clones F2, F3, F10 and F11 were clones as only single band was observed in each case (Figure 6.6). These clones were propagated, re-genotyped and the PCR product was sequenced to confirm the genotype.

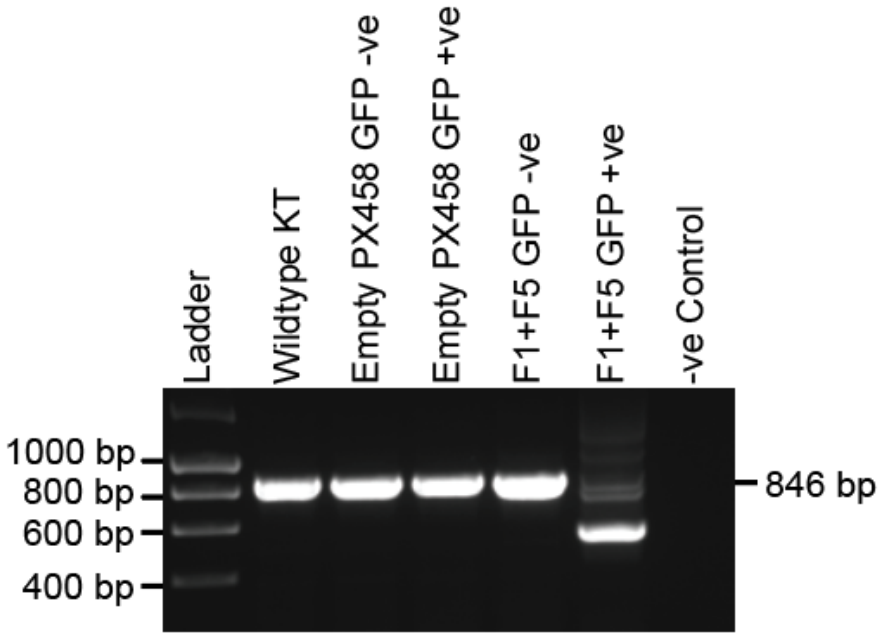

Figure 6.5 *FOXJ1* genotyping of the FACS-sorted HBEC3-KT cells after transfection with gRNAs F1 and F5. *FOXJ1* FHD target region containing gRNA binding sites were amplified using genomic DNA isolated from the respective samples. The PCR products were run on a 1.5% agarose gel. Estimated wildtype amplicon is 864 bp.

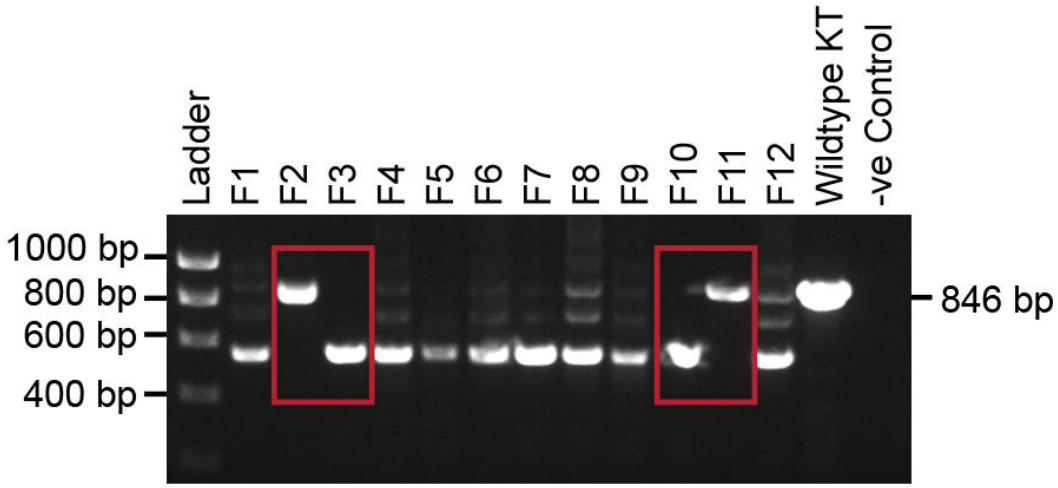

Figure 6.6 Selection of CRISPR-CAS9 *FOXJ1* knockout cells. *FOXJ1* FHD target region was amplified with genomic DNA isolated from clones prepared from dual *FOXJ1* gRNAs-transfected and FACS-sorted GFP-positive cells. Red box indicates clones containing single PCR band.

6.3.1 *FOXJ1*$^{-/-}$ HBEC3-KT cell line

Sequencing of the F2 PCR product revealed a 46 bp nucleotide deletion (c.120-165del) located 119 bp downstream of the *FOXJ1* start codon and the break-point was detected both up-stream and downstream of gRNA F5 within the exon 2 of

FOXJ1 (Figure 6.7). Due to this 46 bp deletion mutation, clone F2 would produce a *FOXJ1* mRNA that would not be able to encode a protein that could have any similarity with wildtype FOXJ1. Thus, the genotype of clone F2 was assigned as *FOXJ1*$^{-/-}$.

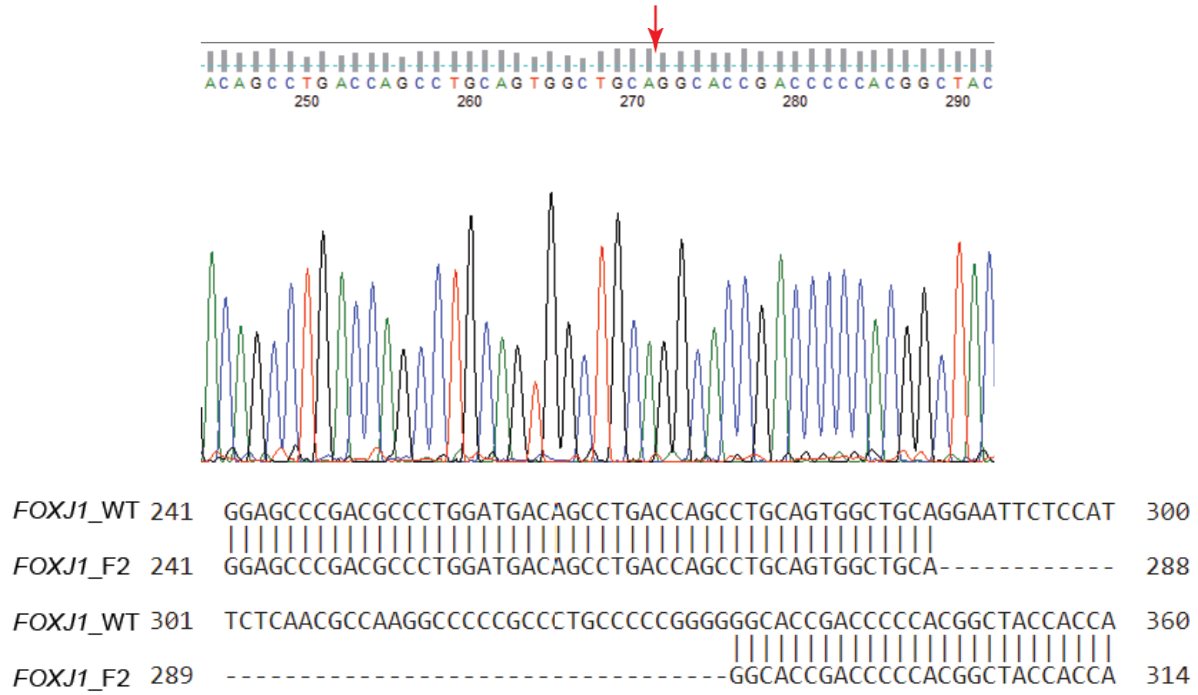

Figure 6.7 Sequencing chromatogram of F2 clone for *FOXJ1* exon 2. Sequencing of *FOXJ1* exon 2 PCR product from F2 clone (top panel), where the red arrow indicates the possible post-dsDNA break joining point. Alignment with wild-type *FOXJ1* exon 2 showing the 46 bp deletion in F2 (bottom panel).

6.3.2 *FOXJ1*$^{\Delta FHD/\Delta FHD}$ HBEC3-KT cell line

When the PCR products of clones F3 and F10 were sequenced, they both showed a 300 bp deletion (c.135-434del) within exon 2 starting from 134 bp downstream of the start codon (Figure 6.8). Both the breakpoints were within the 3'-end of each gRNA binding site. The mRNA was predicted by removing this 300 bp from the wildtype mRNA and the predicted protein showed a missing stretch of 100 amino acids at the N-terminal region resulting in partial loss of the FHD (Figure 6.9A). The nuclear localisation signal sequence was not disrupted. The missing region covers the entire DNA-binding domain of FHD 1 but not FHD 2 (Figure 6.9B). The FHD 1 contains the first helix required to bind DNA at the promoter region during the transcriptional activation of FOXJ1-target genes (Li and Tucker 1993). The structure of F3/10

FOXJ1 was predicted with I-TASSER (C-score = -0.58) and the analysis suggested that the loss of FHD 1 would exert an effect on FHD 2 by disorganizing the helical structure of FHD 2 and disorganising the complete FHD making F3/10 FOXJ1 unable to bind DNA (C-score = 0.15 for F3/10 FOXJ1 and C-score = 0.19 for wildtype FOXJ1) (Figure 6.9C). Based on this analysis, the genotype of clone F3 and F10 was assigned *FOXJ1*$^{\Delta FHD/\Delta FHD}$. For rest of the experiments, clone F3 was used for my experiments.

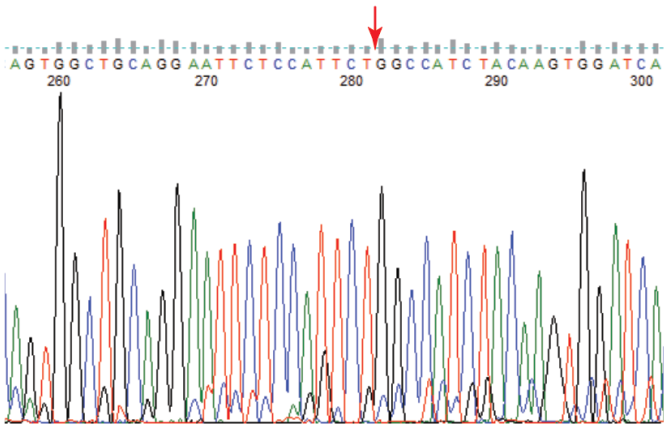


```
FOXJ1_WT    GACCAGCCTGCAGTGGCTGCAGGAATTCTCCATTCTCAACGCCAAGGCCCCCGCCCTGCC 160
FOXJ1_F3/F10 GACCAGCCTGCAGTGGCTGCAGGAATTCTCCATTCT---------------------- 129

FOXJ1_WT    CCCGGGGGGCACCGACCCCCACGGCTACCACCAGGTGCCAGGTTCAGCGGCGCCCGGGTC 220
FOXJ1_F3/F10 ------------------------------------------------------------ 129

FOXJ1_WT    CCCCCTGGCGGCCGACCCCGCCTGCCTGGGGCAGCCACACACGCCGGGCAAGCCCACGTC 280
FOXJ1_F3/F10 ------------------------------------------------------------ 129

FOXJ1_WT    GTCGTGCACGTCGCGGAGCGCGCCCCCGGGGCTGCAGGCCCCACCCCCCGACGACGTGGA 340
FOXJ1_F3/F10 ------------------------------------------------------------ 129

FOXJ1_WT    CTACGCCACCAATCCGCACGTGAAGCCTCCCTACTCGTATGCCACGCTCATCTGCATGGC 400
FOXJ1_F3/F10 ------------------------------------------------------------ 129

FOXJ1_WT    CATGCAGGCCAGCAAGGCCACCAAGATCACCCTGTCGGCCATCTACAAGTGGATCACGGA 460
FOXJ1_F3/F10 ----------------------------------GGCCATCTACAAGTGGATCACGGA 160
```

Figure 6.8 Sequencing chromatogram of clones F3/10for *FOXJ1* genotyping. Sequencing of F3/10 *FOXJ1* PCR product showing the dsDNA joining point (red arrow) after repair of the dsDNA break induced by the action of both gRNA F1 and gRNA F5 (top panel). Chromatogram is representative of clone F3. Alignment with wildtype *FOXJ1* showing the missing 300 bp (bottom panel).

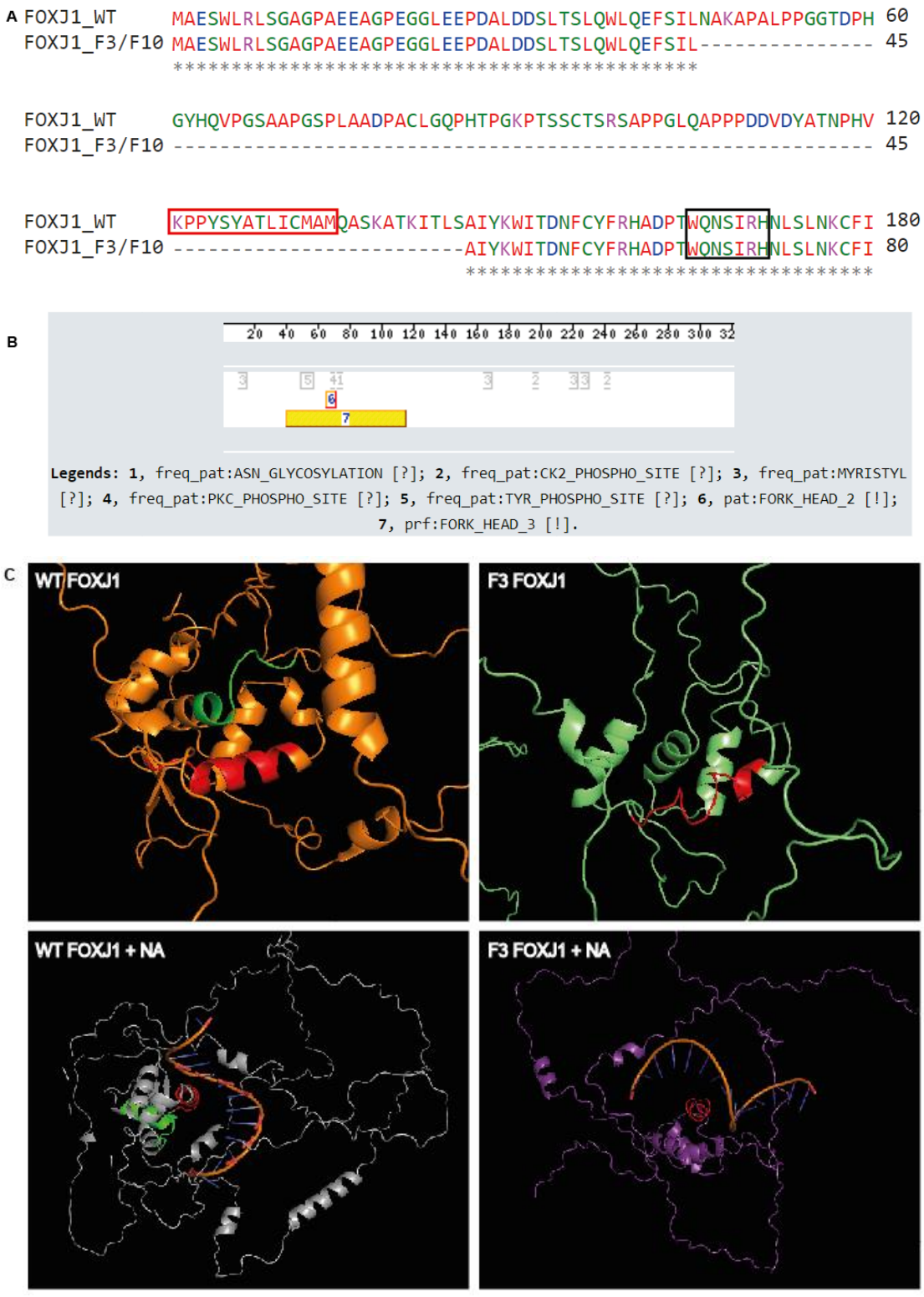

Figure 6.9 Properties of the predicted FOXJ1 protein of clones F3/10. Alignment showing the missing 100 amino acids. The red box indicates the DNA-binding domain containing FHD1 and the black box indicates FHD 2 (A). MotifScan analysis of F3/10 (B). Structural analysis of F3/10 FOXJ1 with I-TASSER showing FHD 1 (green in colour) and FHD 2 (red in colour) and DNA (orange colour) (C). (*) = identical, (!) = strong match, (?) = weak match, NA = nucleic acid. Amino acid colour scheme: blue = acidic; magenta = basic; green = polar; red = nonpolar.

6.3.3 *FOXJ1*$^{\Delta INS+G/\Delta INS+G}$ HBEC3-KT cell line

Next the FOXJ1 exon 2 PCR product of clone F11 was sequenced, and alignment of the retrieved sequences with wildtype showed a single nucleotide (guanyl/G) insertion 133 bp from the start codon (c.133_134insG) within exon 2. This insertional mutation was located within the gRNA F5 binding site close to the PAM site (Figure 6.10). Due to such insertional mutagenesis, the *FOXJ1* mRNA produced from F11 would not be able to produce a protein that could have any similarity with wildtype FOXJ1. Thereby, the genotype of clone F11 was designated as *FOXJ1*$^{\Delta INS+G/\Delta INS+G}$.

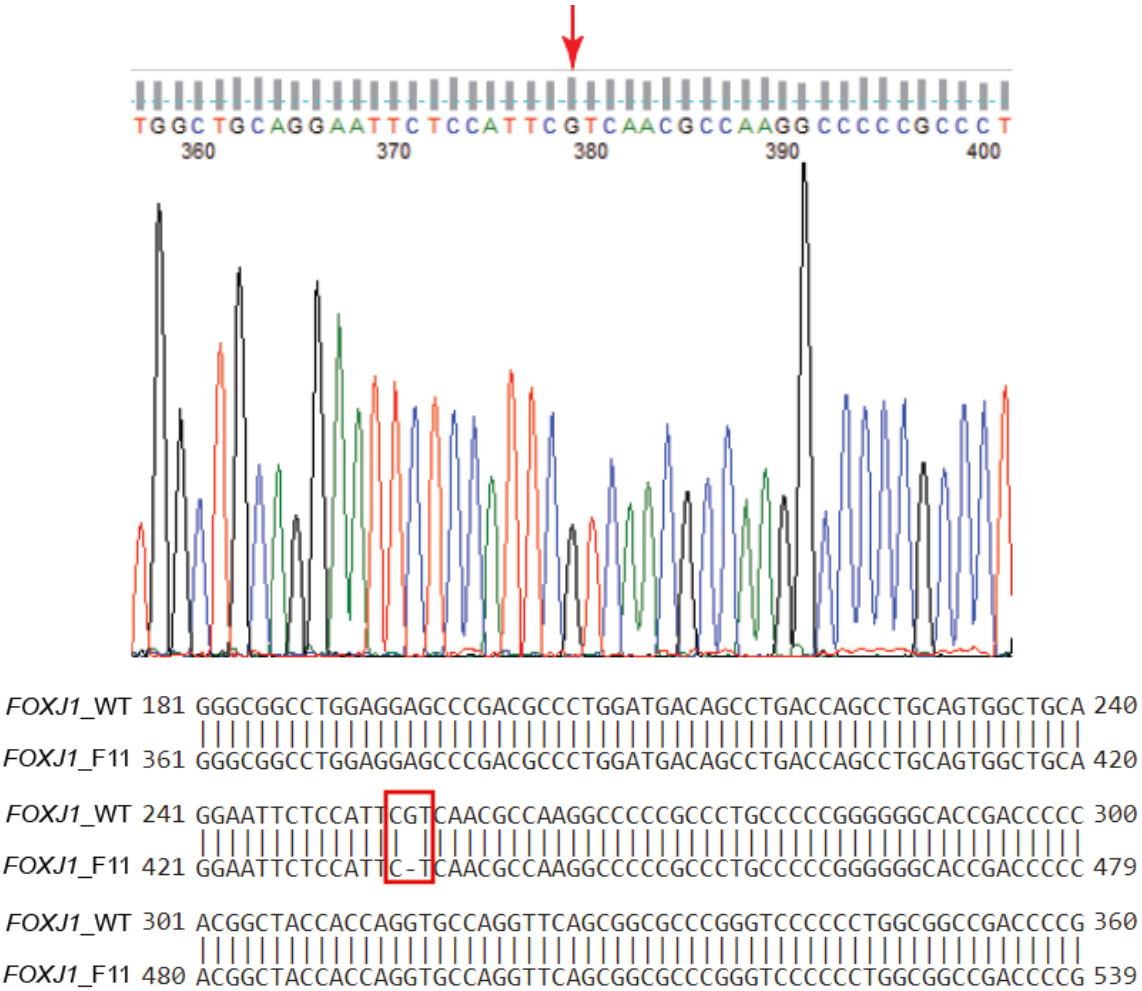

Figure 6.10 Sequencing chromatogram of clone F11 for *FOXJ1* genotyping. Sequencing found an insertional mutagenesis (red arrow) within the gRNA F5 binding site in F11 (top panel). Alignment of the retrieved sequence with wildtype *FOXJ1* showing the insertion (c.133_134insG) within the red box (bottom panel).

6.3.4 Re-genotyping of *FOXJ1*$^{-/-}$, *FOXJ1*$^{\Delta FHD/\Delta FHD}$ and *FOXJ1*$^{\Delta INS+G/\Delta INS+G}$

Finally, all the clones for *FOXJ1* gene editing were re-genotyped along with *PIERCE1* and *C15ORF65* (Figure 6.11). The genotype PCR re-confirmed the loss of 45 bp in *FOXJ1*$^{-/-}$ (clone F2) and a deletion of 300 bp in *FOXJ1*$^{\Delta FHD/\Delta FHD}$ (clone F3) from wildtype, and a PCR band almost close to wildtype or empty PX458-transfected HBEC3-KT cells in *FOXJ1*$^{\Delta INS+G/\Delta INS+G}$ (clone F11). All these *FOXJ1*-edited clones showed PCR bands of equal size to wildtype or empty PX458-transfected HBEC3-KT cells (empty vector control) in case of both *PIERCE1* and *C15ORF65* and confirmed the wildtype identity for these two genes in all the *FOXJ1*-edited clones.

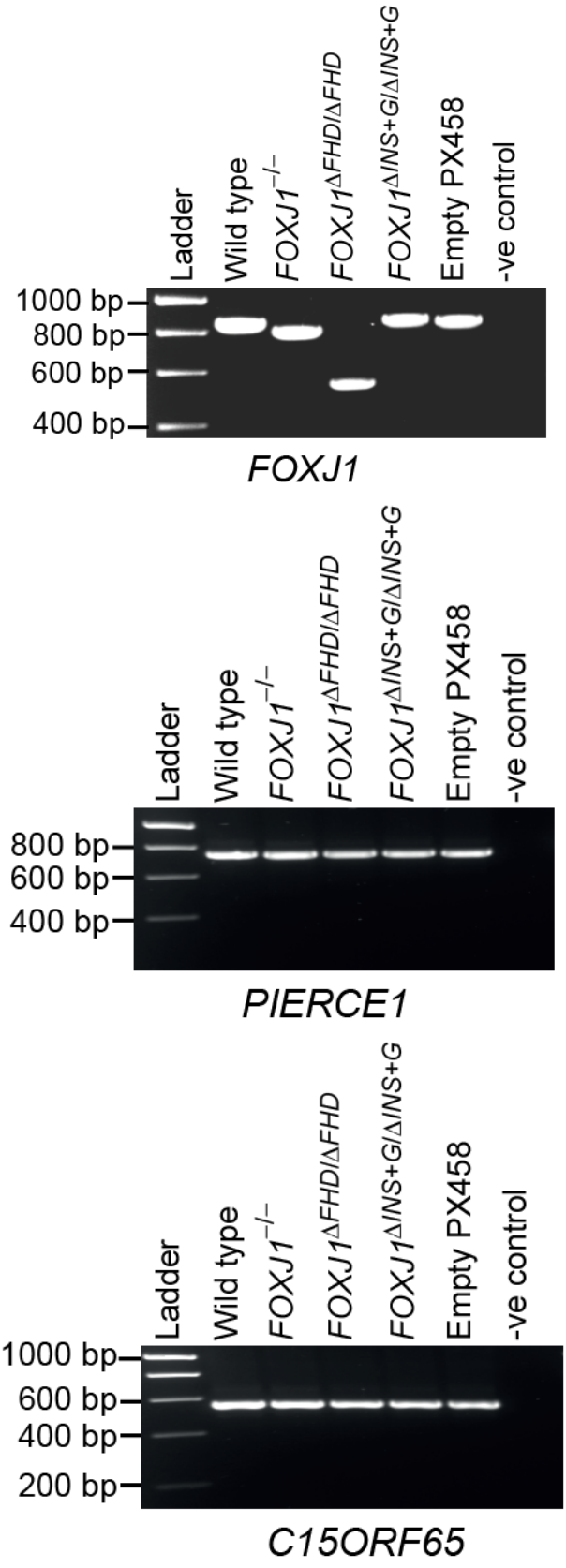

Figure 6.11 Final genotyping of *FOXJ1*-edited clones. All clones were re-genotyped for *FOXJ1* along with *PIERCE1* and *C15ORF65*. Empty PX458-transfected HBEC3-KT cells were used as the mock transfection control. All gel images are representative of n = 3 experiments.

6.4 *PIERCE1* and *C15ORF65* knockout HBEC3-KT cell development

Next HBEC3-KT cell lines knocked-out for either *PIERCE1* or *C15ORF65* or both genes were developed to study their roles in mucociliogenesis. Initially cells deficient of the two individual genes were established and later *PIERCE1* was knocked-out from an established *C15ORF65*$^{-/-}$ HBEC3-KT cell line.

6.4.1 Development of *PIERCE1*$^{-/-}$ HBEC3-KT cell line

To edit *PIERCE1,* individual gRNAs were cloned into PX458 as described in the Materials and Methods section, and clones were sequenced to confirm their identity (Figure 6.12). HBEC3-KT cells were transfected with a combination of the two gRNA-containing plasmids using FuGENE® HD along with an empty PX458 control (Figure 6.13). Combinations of gRNAs were selected based on their locations (Figure 3.1) so that they covered the start codon. GFP-positive cells were observed after 72 hours, and DNA extracted for *PIERCE1* genotyping PCR to estimate the efficiency of gRNAs editing of *PIERCE1*. The PCR suggested the presence of *PIERCE1*-edited cells in samples where gRNAs P3 and P4 or gRNAs P3 and P5 were used in transfections as both the wildtype band (757 bp) and a tentative *PIERCE1*-edited band (lower than 757 bp) was observed (Figure 6.14). The transfection was repeated for these two combinations of gRNAs and cells were sorted for GFP-positive and GFP-negative cells using FACS (Figure 6.15) 72 hours after transfection. Cells were seeded for growth and PCR genotyping was done when they were confluent. Multiple bands were observed in PCR with genomic DNA extracted from GFP-positive cells of dual *PIERCE1* gRNAs co-transfected cells suggesting the presence of *PIERCE1*-edited cells in these cells only (Figure 6.16).

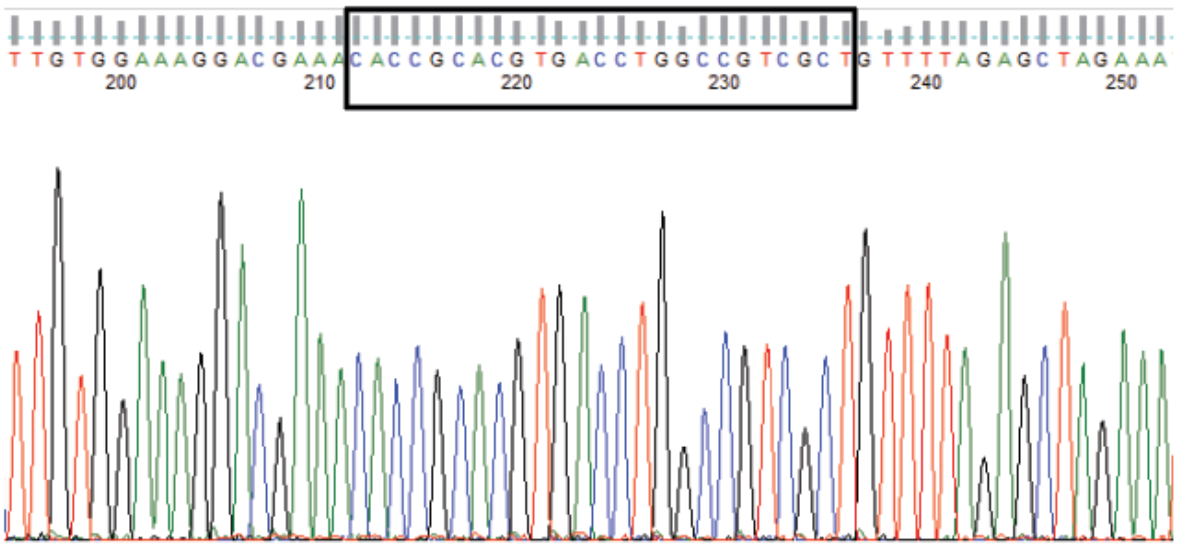

Figure 6.12 Cloning of *PIERCE1* gRNAs in PX458. Representative image of sequencing chromatogram showing the insertion of gRNA P3 (black box) in PX458 (n = 3).

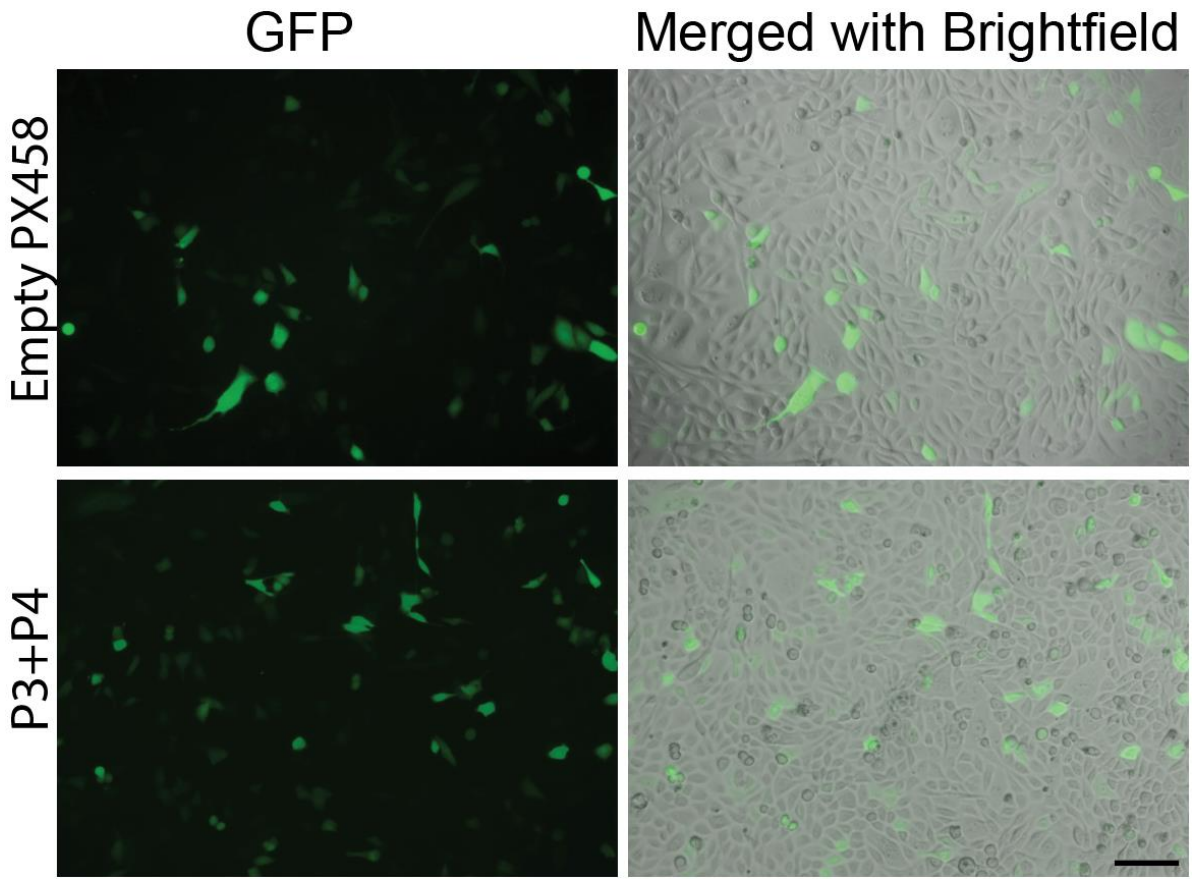

Figure 6.13 Co-transfection of HBEC3-KT cells to develop *PIERCE1* knockout cells. Representative images of GFP-positive cells after transfecting with gRNAs P3 and P4 inserted in PX458 (n = 2). Scale bar = 100 μm.

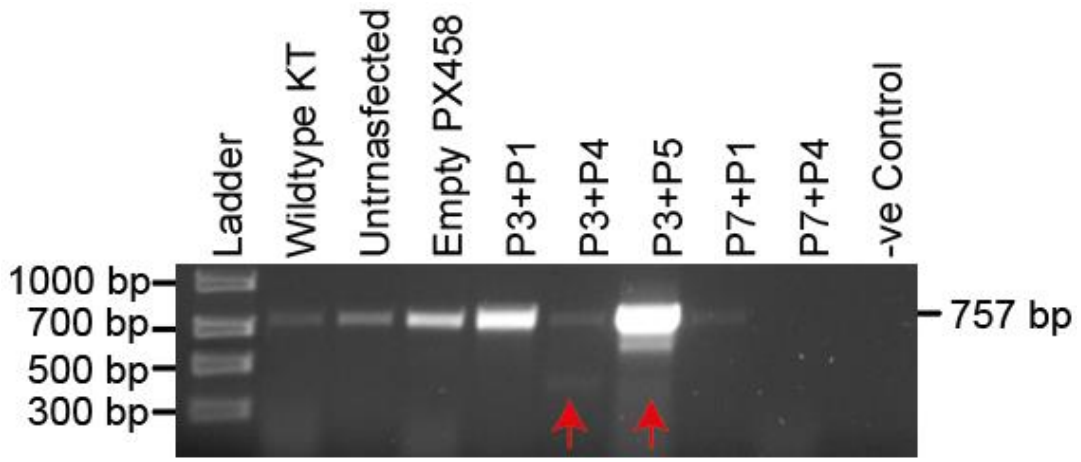

Figure 6.14 Efficiency of gRNAs to edit *PIERCE1*. *PIERCE1* genotyping PCR was done with genomic DNA extracted from HBEC3-KT cells transfected with different combinations of gRNAs. The expected amplicon for wildtype PIERCE1 is 757 bp. Red arrows indicate combinations of gRNAs that produced a PCR band lower than wildtype. The PCR failed in sample P7+P4 due to poor quality and quantity of extracted genomic DNA (n = 1).

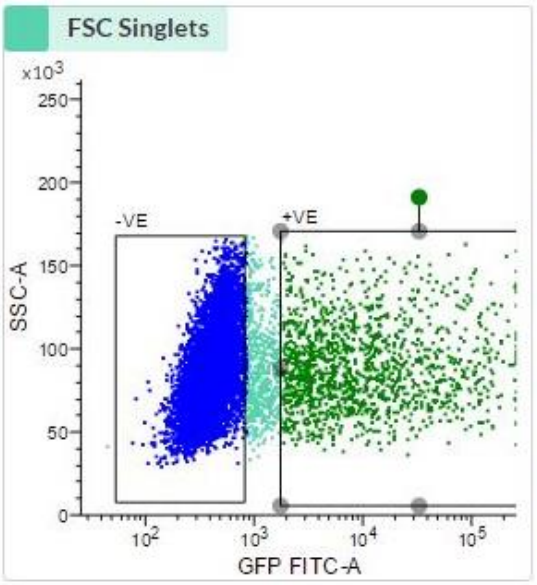

Population	Events	% Parent	% Total
All Events	26,185		100.00 %
Scatter	11,298	43.15 %	43.15 %
SSC Singlets	10,585	93.69 %	40.42 %
FSC Singlets	10,000	94.47 %	38.19 %
-VE	8,060	80.60 %	30.78 %
+VE	1,365	13.65 %	5.21 %

Figure 6.15 FACS sorting of GFP-positive cells during *PIERCE1* knockout. The image represents cells transfected with gRNAs P3 and P4 (n = 2).

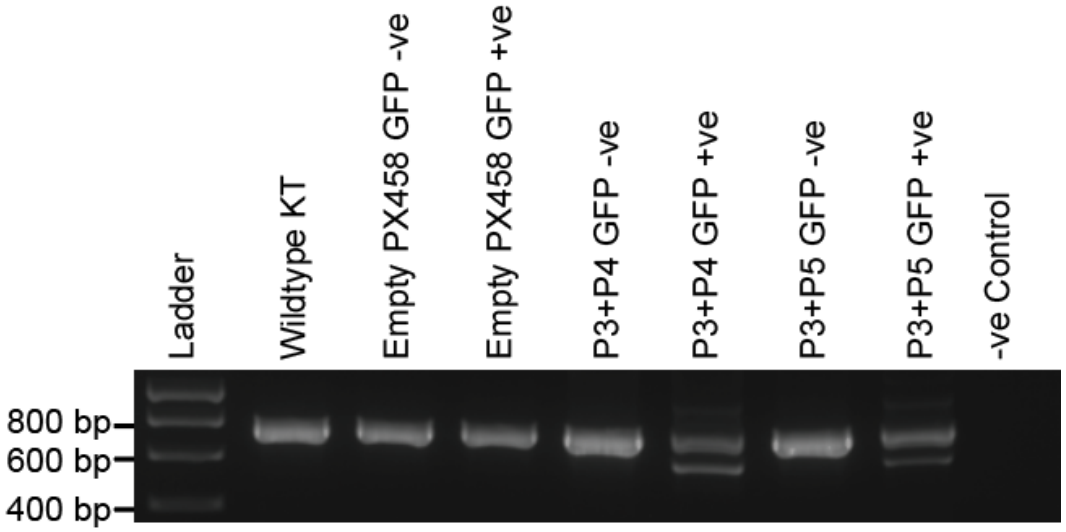

Figure 6.16 *PIERCE1* PCR genotyping of FACS-sorted cells. PCR was done with genomic DNA extracted from indicated FACS sorted cell samples and the PCR products were resolved in a 2% agarose gel.

Cells co-transfected with gRNAs P3 and P4 (P34) were selected for further propagation as they seemed to contain more *PIERCE1*-edited cells than the others. These cells were serially diluted for clonal expansion followed by PCR genotyping. Among the four clones obtained, two of them were wildtype (P343 and P344) and two were comprised of a mixed population (P341 and P342). The wildtype band was dimmer in clone P342 along with some other bands indicating *PIERCE1* deletion (Figure 6.17). This clone was further serially diluted for clonal expansion and genotyping. The genotype suggested that clones P3422 and clone P3423 were homozygous for *PIERCE1* knockout as a single PCR band of a size lower than wildtype was observed (Figure 6.18). These clones along with clone P344 were propagated further and re-genotyped for *PIERCE1*. The PCR bands were sequenced for confirmation of *PIERCE1* knockout. Sequencing showed that clone P343 and P344 remained unedited (Figure 6.19) and thus was considered to be sorted wildtype cells or *PIERCE1*$^{+/+}$ cells. Sequencing of *PIERCE1* genotyping PCR bands obtained from clones P3422 and P3423 revealed that they were both homozygous for a 180 bp deletion (c.-61-119del) located within the first coding exon of *PIERCE1*. The breakpoints lie within the 3'-end of each gRNA binding sites. The first one was at the beginning of the exon and the second one was near the end of

this exon resulting in the loss of almost the entire first coding exon of *PIERCE1* including the Kozak consensus sequence and start codon (Figure 6.20).

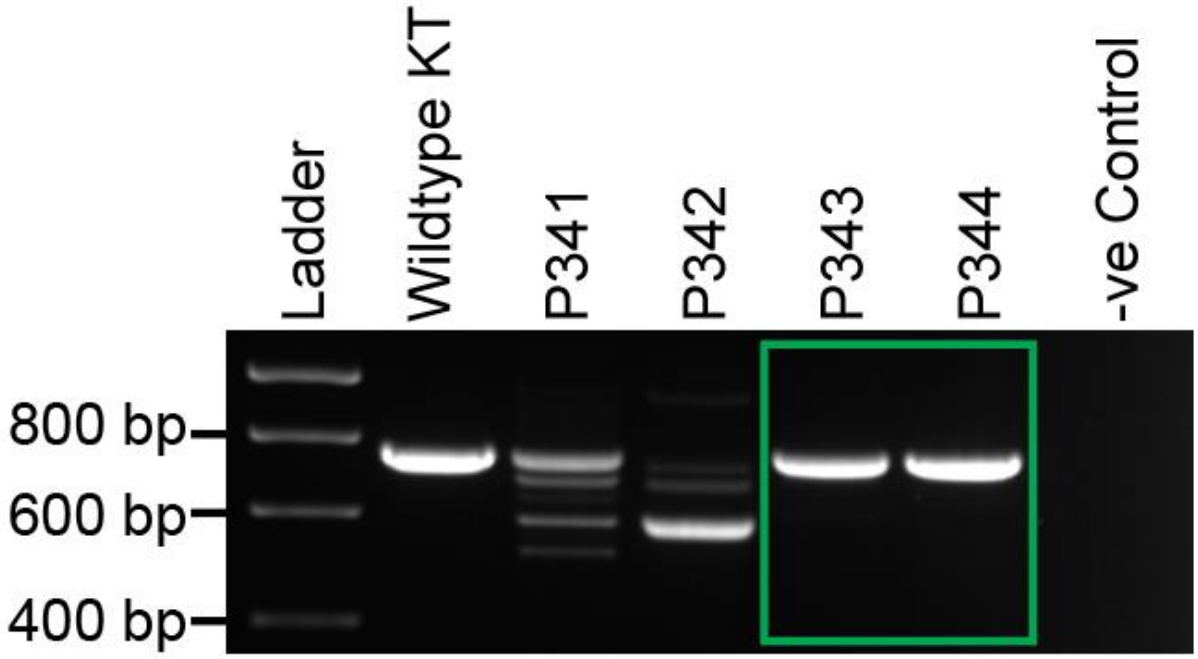

Figure 6.17 Genotyping of clones derived from gRNAs P3 and P4 co-transfected cells. PCR was done with genomic DNA isolated from clones and products were resolved in a 2% agarose gel. PCR bands equivalent to the wildtype were indicated with a green box.

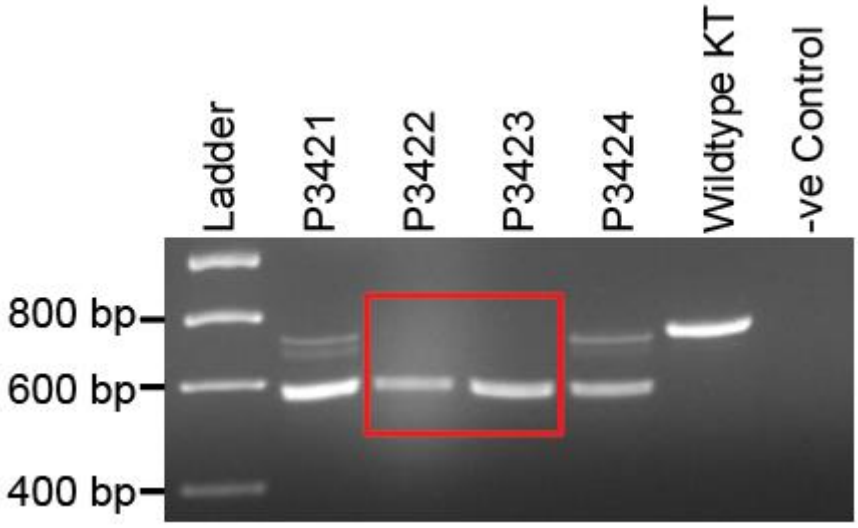

Figure 6.18 Development of *PIERCE1* knockout cell. Further clones derived from P342 were genotyped for *PIERCE1*. Red box indicates clones with single showing *PIERCE1* deletion.

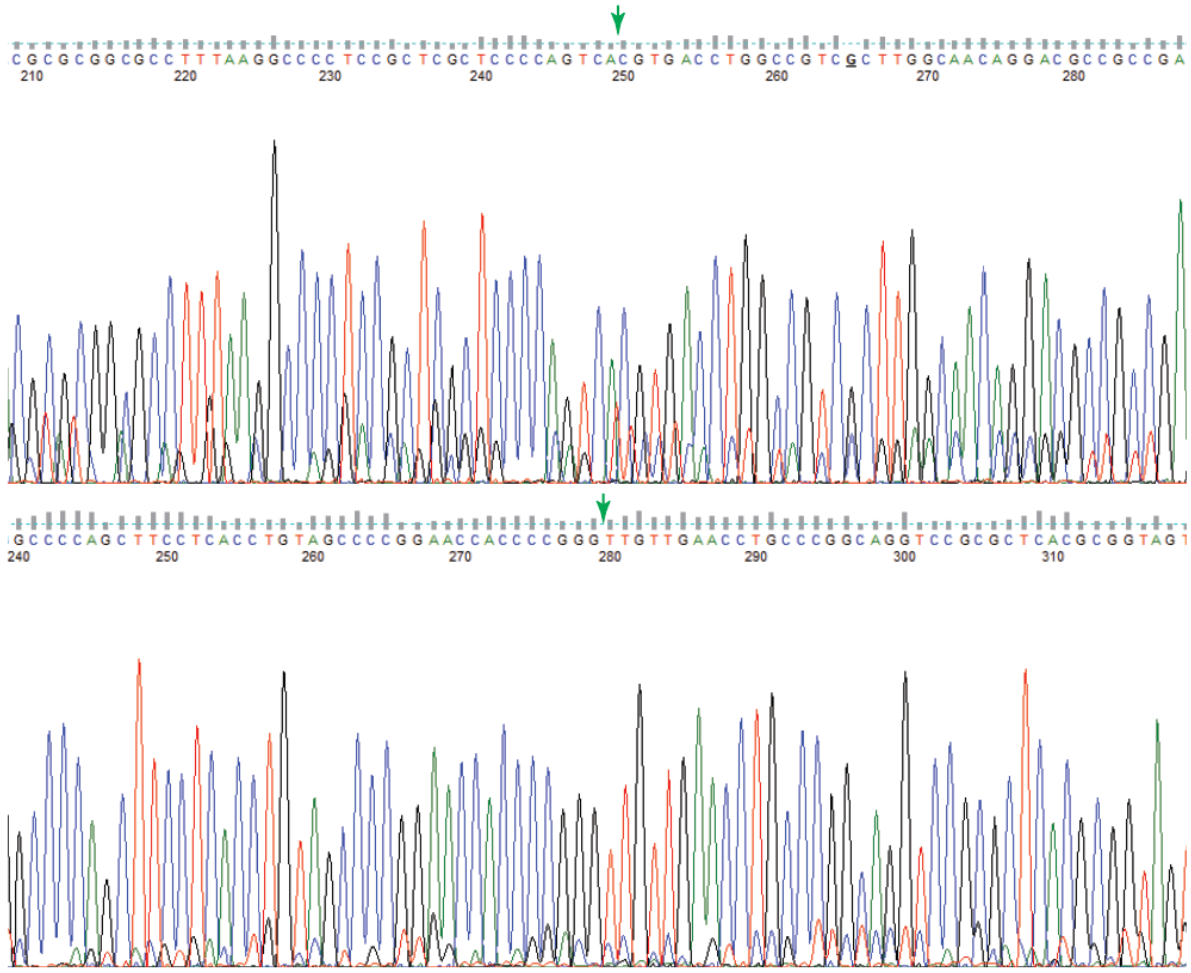

Figure 6.19 *PIERCE1* sequencing chromatogram of clone P343 and P344. Green arrows indicate the possible cleavage sites of the gRNAs P3 (top) and P4 (bottom)

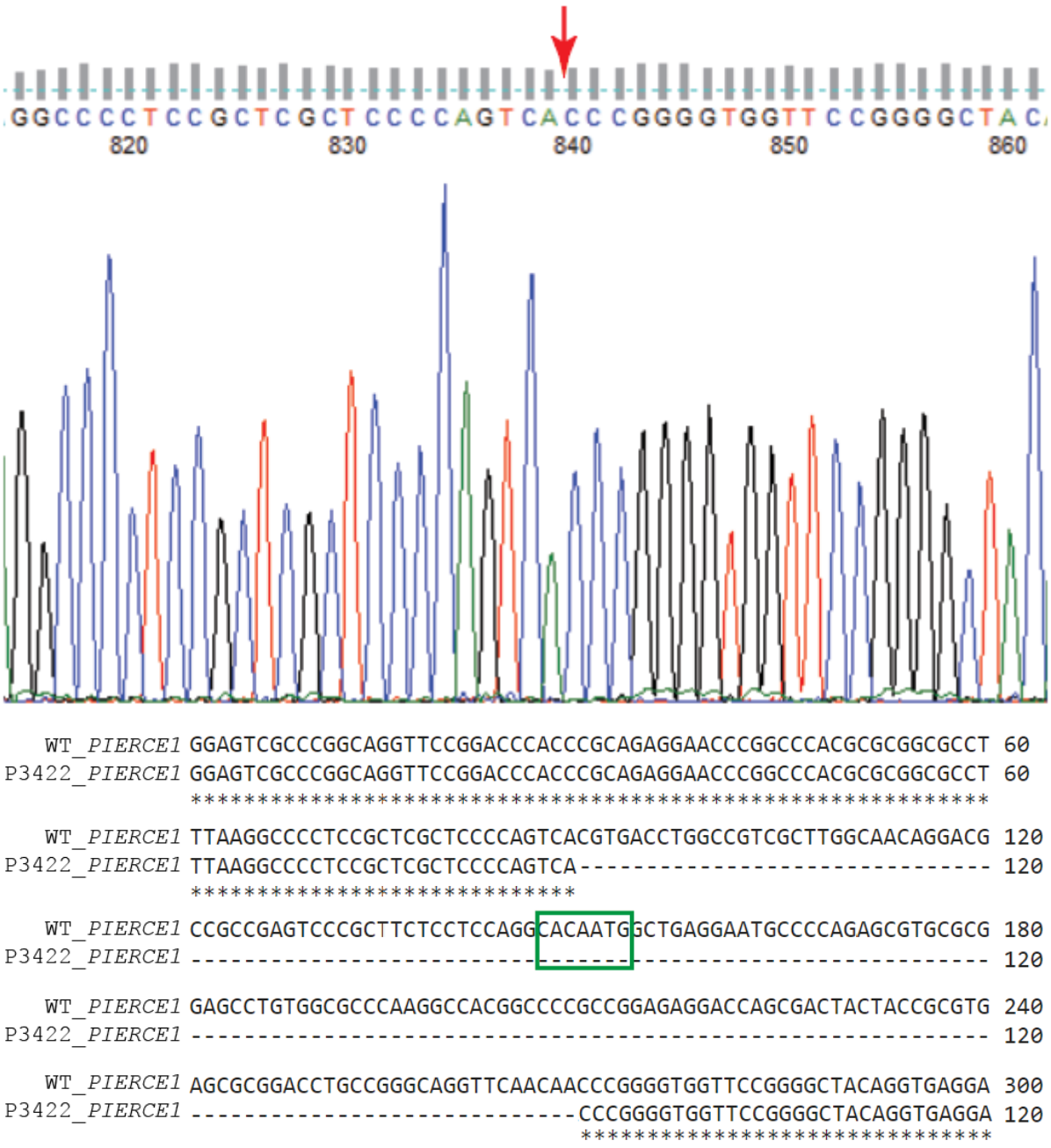

Figure 6.20 Sequencing chromatogram of clone P3422 and P3423 for *PIERCE1* genotyping. Red arrow in the chromatogram indicates the break point (top panel). Alignment of the retrieved sequence with wildtype *PIERCE1* exon 1 showing the deletion (c.-61-119del). Green box indicates the Kozak sequence. (*) = identical.

The mutant *PIERCE1* mRNA was translated to a predicted protein using ExPASy translate tool despite the alternative start codon in the sequence lacking a ribosome entry site. Alignment of this predicted protein with wildtype PIERCE1 confirmed the major portion of PIERCE1 DUF4490 domain (amino acids 9-106) was lost (Figure 6.21). Based on these findings, the genotypes of clones P343 and P344 were assigned as *PIERCE1*$^{+/+}$ and the genotypes of clones P3422 and P3433 were assigned as *PIERCE1*$^{-/-}$. For the rest of the experiments, clone P344 was used as a representative of *PIERCE1*$^{+/+}$ and clone P3422 was used as a representative of *PIERCE1*$^{-/-}$. The genotyping was repeated with *C15ORF65* and *FOXJ1*. The PCR genotyping confirmed the genotype of *PIERCE1*$^{+/+}$ and *PIERCE1*$^{-/-}$ cells as well as the wildtype identity of *C15ORF65* and *FOXJ1* in the selected clone P3422 (Figure 6.22).

```
WT_PIERCE1     MAEECPRACAEPVAPKATAPPERTSDYYRVSADLPGRFNNPGWFRGYRTQKAVSVYRTSN 60
P3422_PIERCE1  ------------------------------------------------------------ 0
WT_PIERCE1     QAYGSRAPTVHEMPKVFYPNSNKFSQQLAAGGMFRNNTLNVYLEKSIVTGPDNCITSCDR 120
P3422_PIERCE1  ------------MPKVFYPNSNKFSQQLAAGGMFRNNTLNVYLEKSIVTGPDNCITSCDR 48
                           ********************************************
WT_PIERCE1     LNFHPSYNINRPSICD     136
P3422_PIERCE1  LNFHPSYNINRPSICD     64
               ****************
```

Figure 6.21 Alignment of wildtype and predicted P3422 PIERCE1. Alignment of predicted P3422 PIERCE1 with wildtype PIERCE1 showing the loss of the first 72 amino acids in P3422 PIERCE1. (*) = identical. Amino acid colour scheme: blue = acidic; magenta = basic; green = polar; red = nonpolar.

Figure 6.22 Final genotyping of *PIERCE1*-edited clones. Clone P3422 was re-genotyped for *PIERCE1* along with *C15ORF65* and *FOXJ1* (n = 3). Empty PX458-transfected HBEC3-KT cells were used as the mock transfection control.

6.4.2 Development of *C15ORF65*$^{-/-}$ HBEC3-KT cell line

Five gRNAs designed to edit *C15ORF65* were cloned in PX458 as before, and sequencing of cloned plasmids confirmed the insertion of gRNAs (Figure 6.23). Two of the cloned plasmids were co-transfected in HBEC3-KT cells using FuGENE® HD and empty PX458 was used as a transfection control. The gRNAs flanked the start codon of *C15ORF65* (Figure 3.1). GFP positive cells were visualized after 72 hours (Figure 6.24) and *C15ORF65* genotyping PCR was performed using DNA extracted from the cells to estimate the gene-editing efficiency. The PCR showed that the combination of gRNAs C2 and C3 was the most efficient combination to edit *C15ORF65* as multiple smaller sized bands were observed as compared to the wildtype (Figure 6.25). Based on the locations of each gRNA (Figure 3.1), co-transfection was repeated with a combination of C2/C3 and C2/C5 plasmids and both GFP-positive and GFP-negative cells were collected following FACS-sorting after 72 hours (Figure 6.26). These cells were seeded and genotyped for *C15ORF65*. The PCR showed the presence of *C15ORF65*-edited cells in both GFP-positive samples. Two bands were observed in these dual *C15ORF65* gRNAs co-transfected cells, with the combination of C2 and C5 showing highest efficiency (Figure 6.27). The cells were serially diluted and seeded for clonal expansion. Two clones (C251 and C252) were obtained. C252 was enriched with more *C15ORF65*-edited cells as the *C15ORF65*-edited PCR band was brighter compared to the wildtype band (Figure 6.28). Clone C252 were further serially diluted and seeded for another round of clonal expansion. Among the three clones obtained, two of them (C2521 and C2523) were homozygous for a *C15ORF65* deletion as only single lower-sized band as compared to the wildtype was observed (Figure 6.29). The PCR products were sequenced to confirm their genotype, and this revealed a deletion of 81 bp (c.-74-3del) in both clones with the breakpoints within the 3'-end of each gRNA binding sites. This deletion was located within the first coding exon of *C15ORF65* and included the start codon (Figure 6.30).

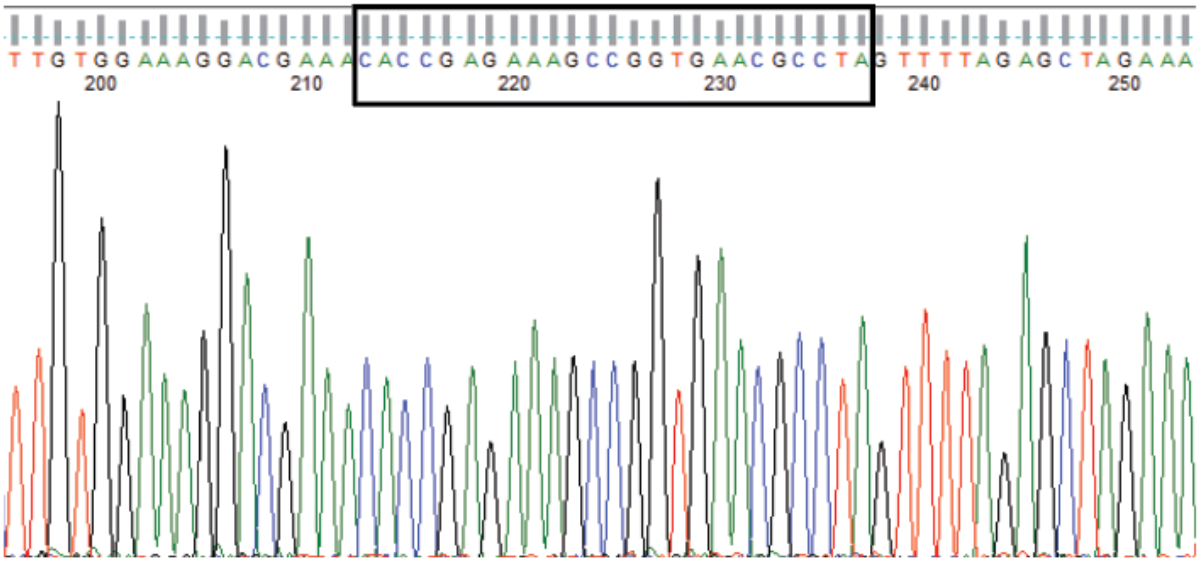

Figure 6.23 Cloning of *C15ORF65* gRNAs in PX458. Representative image of sequencing chromatogram showing the insertion of gRNA C2 (black box) in PX458.

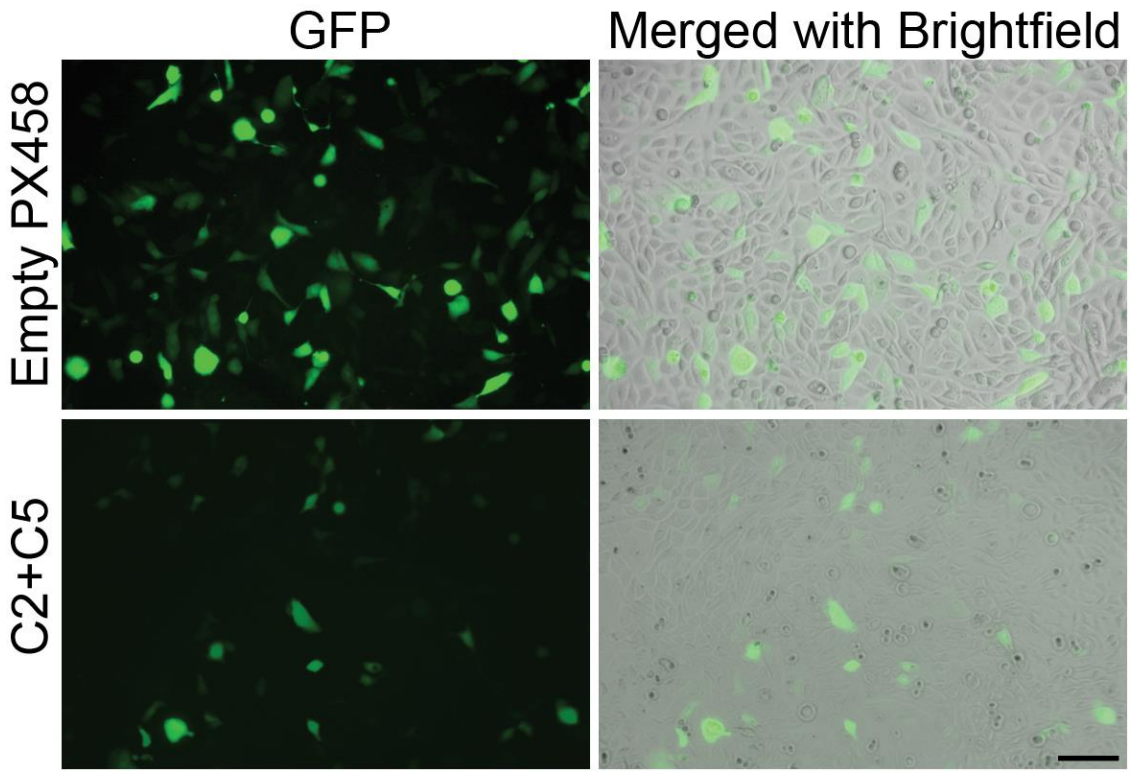

Figure 6.24 Co-transfection of HBEC3-KT cells to develop *C15ORF65* knockout cells. Representative images of GFP-positive cells after transfecting with gRNAs C2 and C5 inserted in PX458 (n = 2). Scale bar = 100 μm.

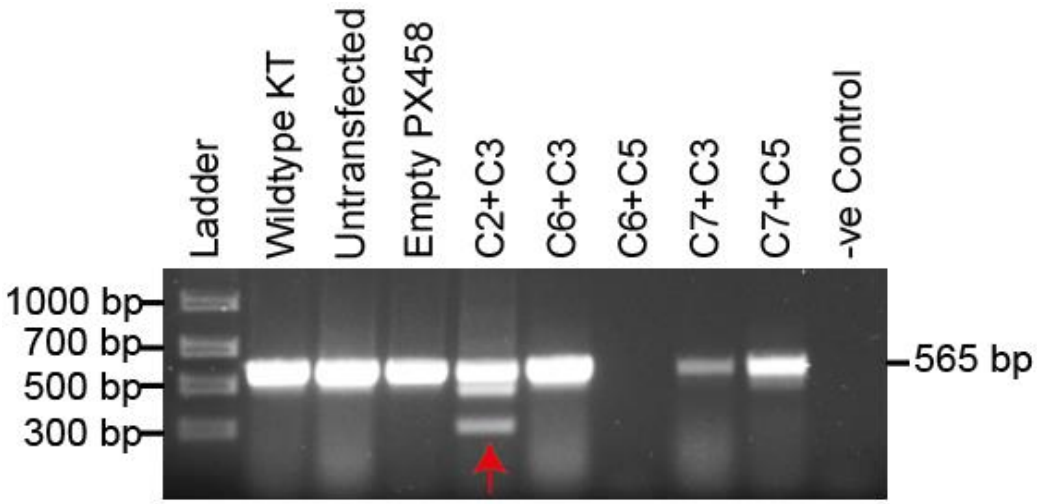

Figure 6.25 Efficiency of gRNAs to edit *C15ORF65*. 72 hours after co-transfection with indicated gRNAs, *C15ORF65* genotyping PCR was carried out. Wildtype amplicon (565 bp) is indicated. Edited band is shown in red arrow. The PCR failed in sample C6+C3 due to poor quality and quantity of extracted genomic DNA.

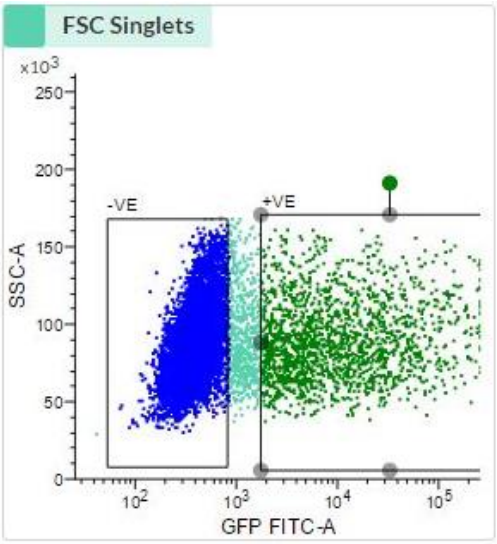

Population	Events	% Parent	% Total
All Events	25,860		100.00 %
Scatter	11,522	44.56 %	44.56 %
SSC Singlets	10,637	92.32 %	41.13 %
FSC Singlets	10,000	94.01 %	38.67 %
-VE	7,574	75.74 %	29.29 %
+VE	1,744	17.44 %	6.74 %

Figure 6.26 FACS sorting of GFP-positive cells during *C15ORF65* knockout. The image is representative of cells transfected with gRNAs C2 and C5 (n = 2).

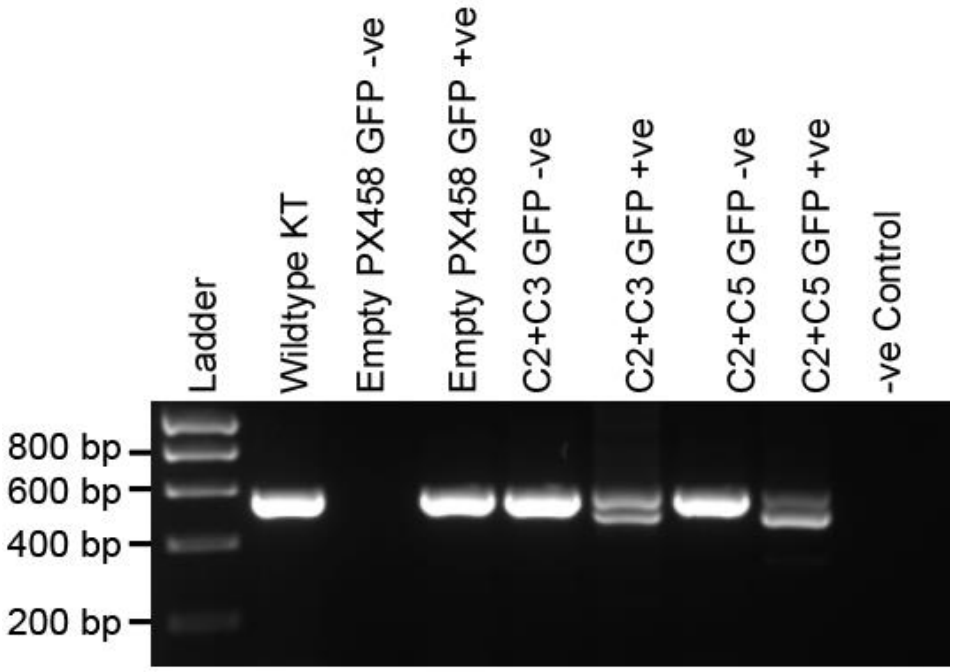

Figure 6.27 *C15ORF65* PCR genotyping of FACS-sorted cells. PCR was carried out with isolated genomic DNA from indicated samples. The PCR products was resolved in a 2% agarose gel. PCR with empty PX458 GFP negative sample failed due to too much dilution of extracted genomic DNA.

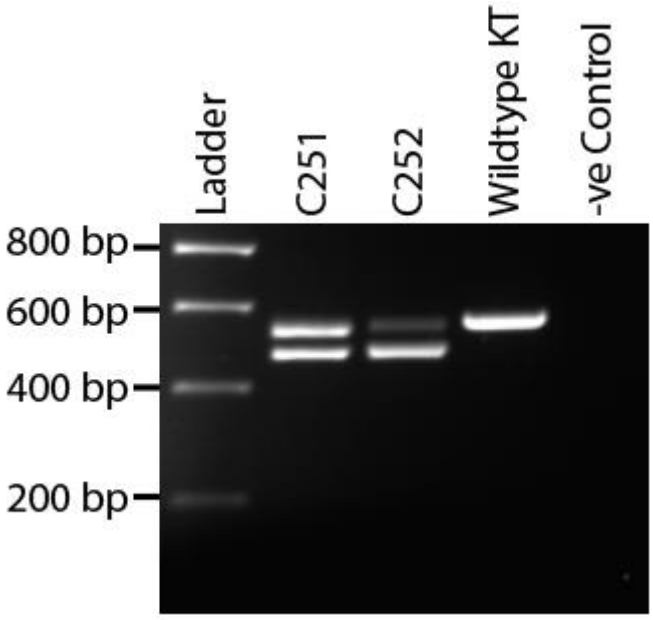

Figure 6.28 Genotyping of clones derived from gRNA C2 and C5 co-transfected cells. Genomic DNA extracted from clone C251 and C252 was used for PCR genotyping. The top band is of wildtype and the bottom band is possibly of *C15ORF65*-edited genomic DNA.

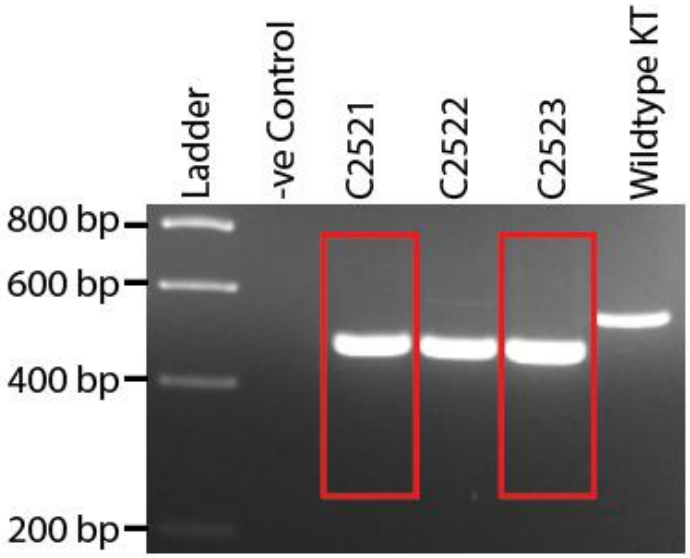

Figure 6.29 Development of *C15ORF65* knockout cell. Agarose gel electrophoresis of *C15ORF65*-genotyping PCR products for indicated samples showed single band in red box. Clone C2522 contained a barely observable wildtype band.

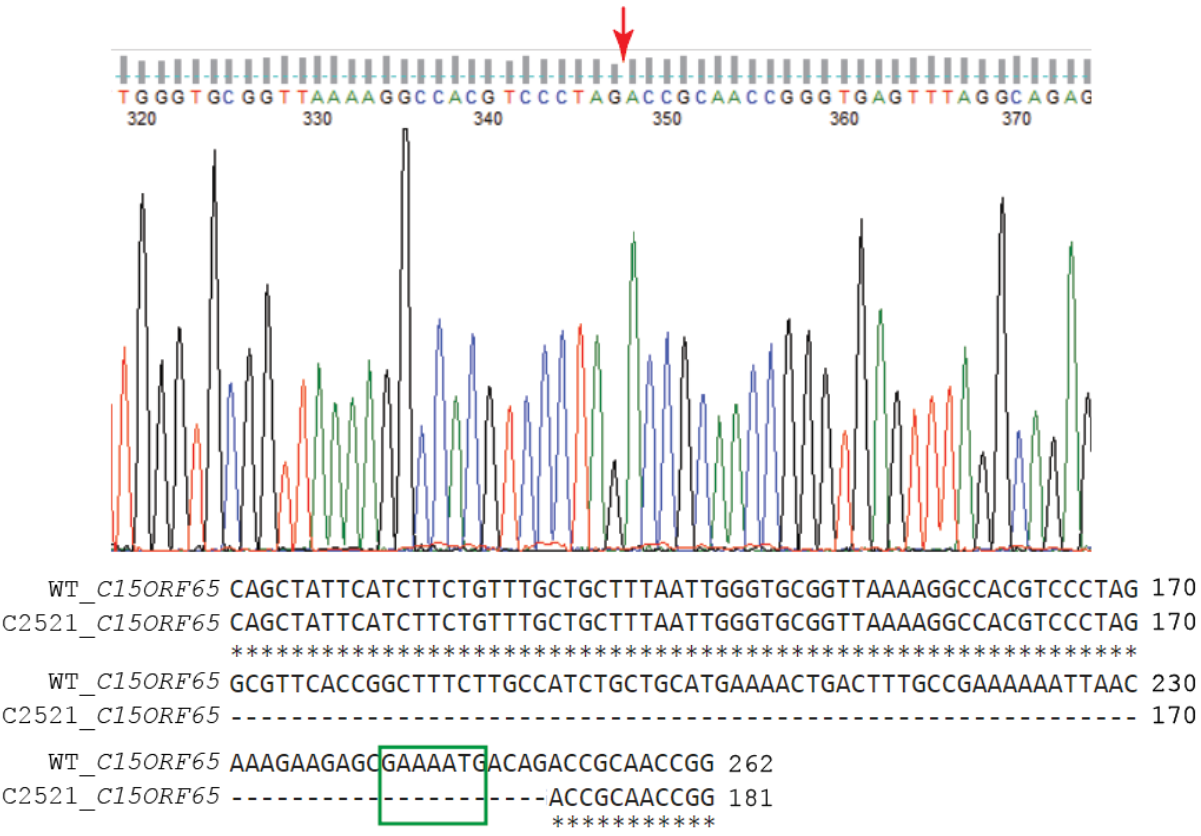

Figure 6.30 Sequence chromatogram of clone C2521 for *C15ORF65* genotyping. Sequencing of *C15ORF65* exon 1 showing the start and end of the deletion (red arrow). Alignment of retrieved sequence with wildtype *C15ORF65* revealing the 81 bp deletion including the Kozak sequence (green box).

Next, the predicted mRNA was converted to a predicted protein using ExPASy translate tool. This predicted protein was aligned with wildtype C15ORF65, and the alignment suggested a loss for 19 amino acids from the N-terminal of the complete ORF (Figure 6.31A). I-TASSER structures showed that the C2521 C15ORF65 would miss the N-terminal region required for interacting with and tethering around CFAP53 within the microtubule inner protein complex (C-score = -2.63) (Figure 6.31B). Based on these findings, the genotype of clone C2521 and C2523 were assigned as *C15ORF65*$^{-/-}$ and clone C2521 was used for further studies. Finally, the clone C2521 was re-genotyped for *C15ORF65*, *PIERCE1* and *FOXJ1* and the PCR confirmed that the clone was wildtype for the latter two genes and possessed the 81 bp deletion in *C15ORF65* (Figure 6.32).

A

```
   WT_C15ORF65 MTDRNRDKKSTSPSNSDTEMKSEQLPPCVNPGNPVFSCMLDPKTLQTATSLSKPQMIMYK  60
C2521_C15ORF65 -------------------MKSEQLPPCVNPGNPVFSCMLDPKTLQTATSLSKPQMIMYK  41
                                  ************************************
   WT_C15ORF65 TNSSHYGEFLPIPQFFPCNYTPKEQVFSSHIRATGFYQNNTLNTAPDRTRTLDFPNIQHTL 121
C2521_C15ORF65 TNSSHYGEFLPIPQFFPCNYTPKEQVFSSHIRATGFYQNNTLNTAPDRTRTLDFPNIQHTL 102
               ************************************************************
```

B

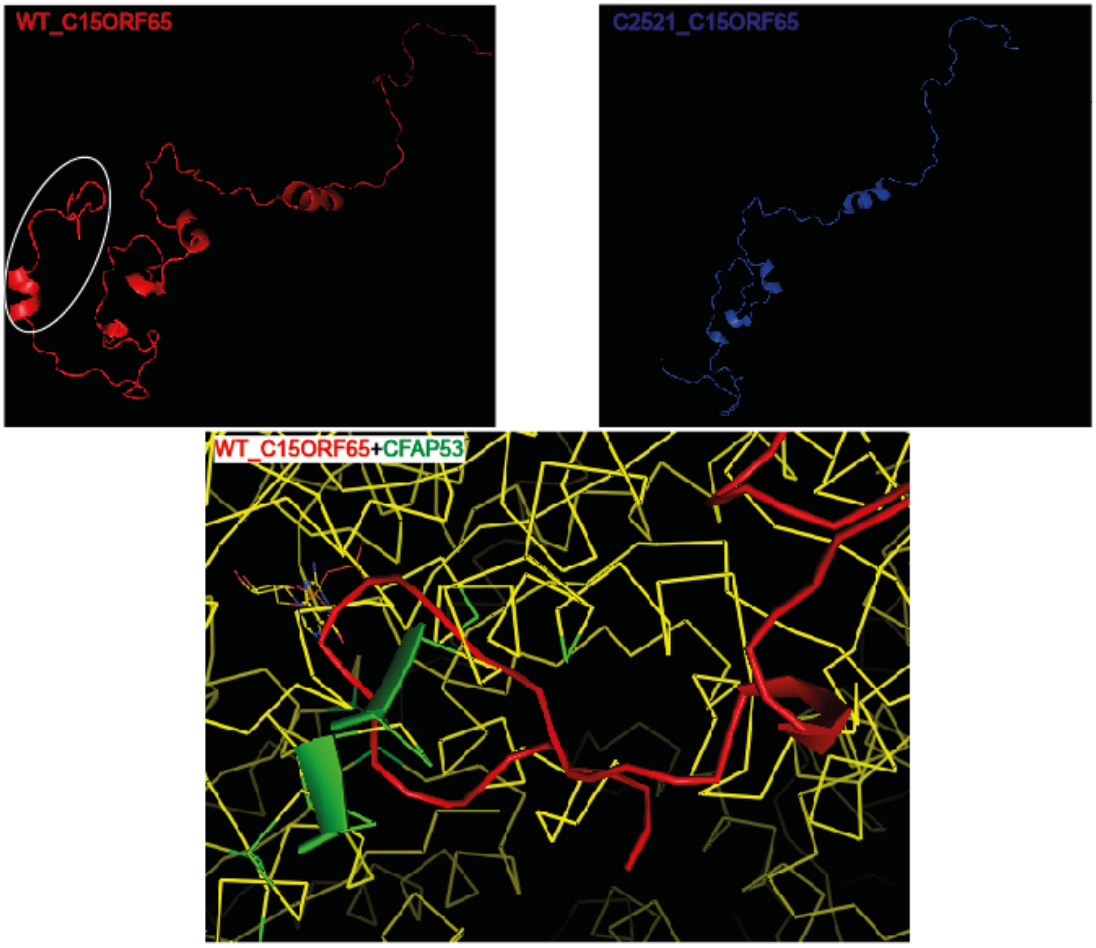

Figure 6.31. Difference between wildtype C15ORF65 and predicted C2521 C15ORF65. The alignment of wildtype C15ORF65 and the predicted C2521 C15ORF65 (A). I-TASSER structures of wildtype C15ORF65, C2521 C15ORF65, and wildtype C15ORF65 tethering around CFAP53 (B). Amino acid colour scheme: blue = acidic; magenta = basic; green = polar; red = nonpolar. PDB ID: 7RRO ((Gui, Farley et al. 2021)) was utilized to deduce the interaction between C15ORF65 and CFAP53. White circle indicates the CFAP53-interacting domain of C15ORF65, which is missing in C2521 C15ORF65.

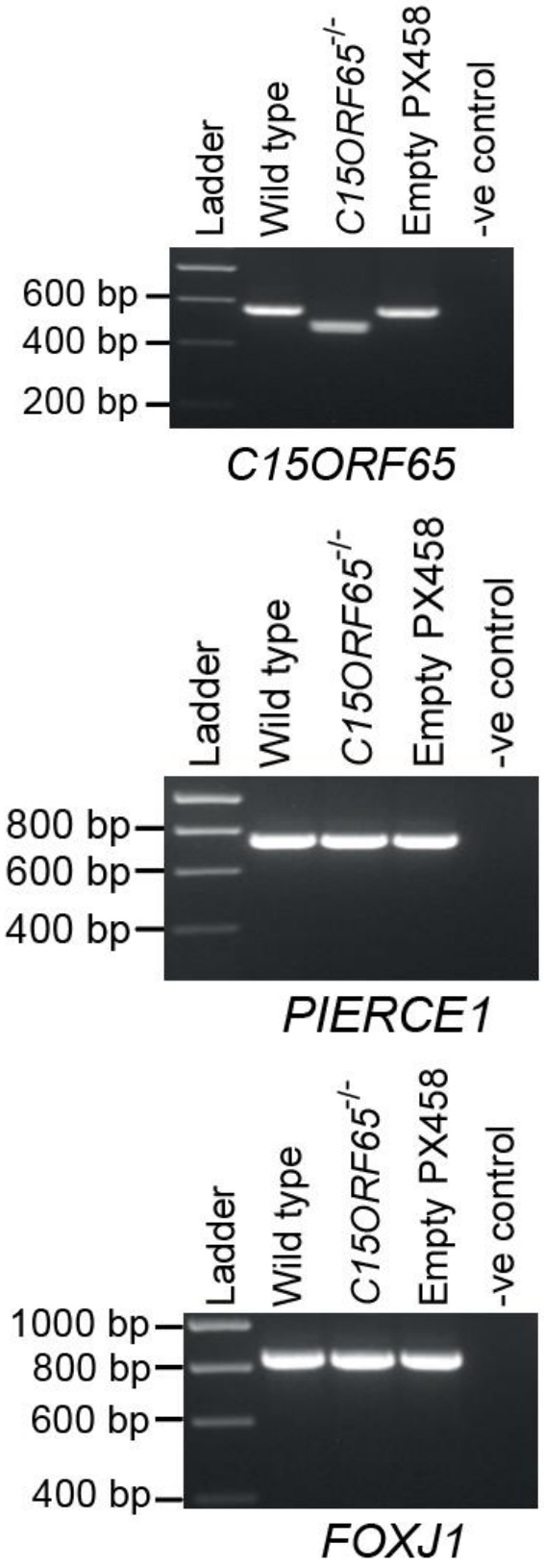

Figure 6.32 Final genotyping of *C15ORF65*-edited clones. Clone C2521 was re-genotyped for *C15ORF65* along with *PIERCE1* and *FOXJ1*. Empty PX458-transfected HBEC3-KT cells were used as the mock transfection control. Images are representative of n = 3 gels.

6.4.3 Development of *PIERCE1*$^{-/-}$*C15ORF65*$^{-/-}$ HBEC3-KT cell line

PIERCE1 C15ORF65 double knockout HBEC3-KT cells were then developed on the *C15ORF65*$^{-/-}$ background. *PIERCE1* gRNAs P3 and P4 were chosen as these gRNAs would be expected to remove a major portion of *PIERCE1* exon 1 and the predicted mRNA would fail to encode functional PIERCE1. *C15ORF65*$^{-/-}$ cells were co-transfected with P3 and P4 gRNAs using FUGENE® HD, and GFP-positive cells observed after 72 hours (Figure 6.33) were sorted using FACS (Figure 6.34) and seeded for growth. The cells were genotyped for *PIERCE1,* and an edited band was observed in GFP-positive cells (Figure 6.35). Then the GFP-positive cells were serially diluted for clonal expansion. After they grew to confluence each well was genotyped and one clone, 3D2, was selected as it showed an edited band for *PIERCE1* along with some unedited band (Figure 6.36). 3D2 cells were further serially diluted and were grown for clonal expansion and cells were again genotyped. Clone 32-3D2, was mostly edited for *PIERCE1* (Figure 6.37) and was again serially diluted. Two clones were obtained this way and one (32-3D21) showed edited bands for both *PIERCE1* and *C15ORF65* (Figure 6.38). The PCR products were sequenced, and the sequencing confirmed the expected breakpoint for *PIERCE1* (as observed in Figure 6.20) and for *C15ORF65* (as observed in Figure 6.30) confirming the loss of both *PIERCE1* and *C15ORF65* (Figure 6.39). The genotype of clone 32-3D21 was assigned as *PIERCE1*$^{-/-}$*C15ORF65*$^{-/-}$, and this double knockout cell line was propagated for further studies. The genotyping PCR was repeated for this clone showing deletions in both *PIERCE1* and *C15ORF65*, but not in *FOXJ1* (Figure 6.40).

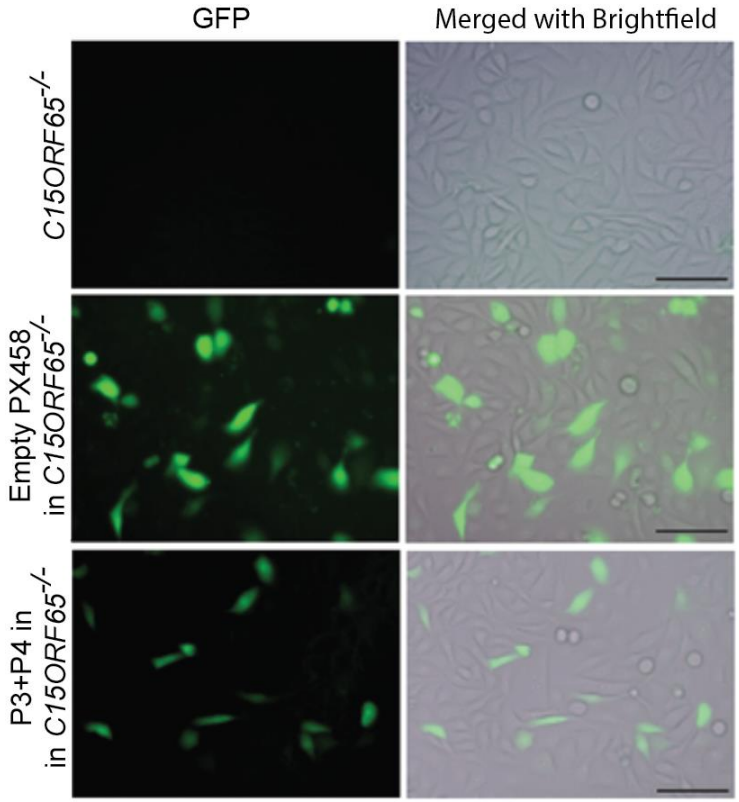

Figure 6.33 Co-transfection of HBEC3-KT cells to develop *PIERCE1 C15ORF65* double knockout cells. Representative images of GFP-positive cells after co-transfecting with gRNAs P3 and P4 for *PIERCE1* knockout in *C15ORF65*$^{-/-}$ cells or with empty PX458 (n = 1). Scale bar = 100 μm.

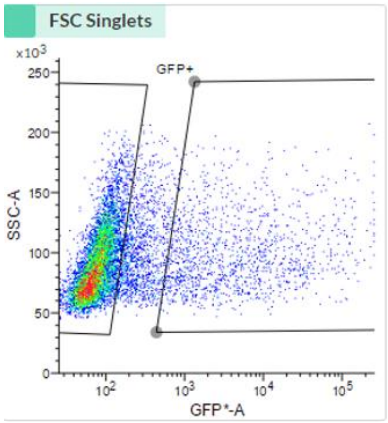

Population	Events	% Parent	% Total
All Events	17,962		100.00 %
Scatter	10,996	61.22 %	61.22 %
SSC Singlets	10,951	99.59 %	60.97 %
FSC Singlets	10,813	98.74 %	60.20 %
GFP-	8,313	76.88 %	46.28 %
GFP+	1,328	12.28 %	7.39 %

Figure 6.34 FACS sorting of GFP-positive cells during generation of *PIERCE1 C15ORF65* double knockout cells. Both GFP-positive and negative cells were collected after sorting.

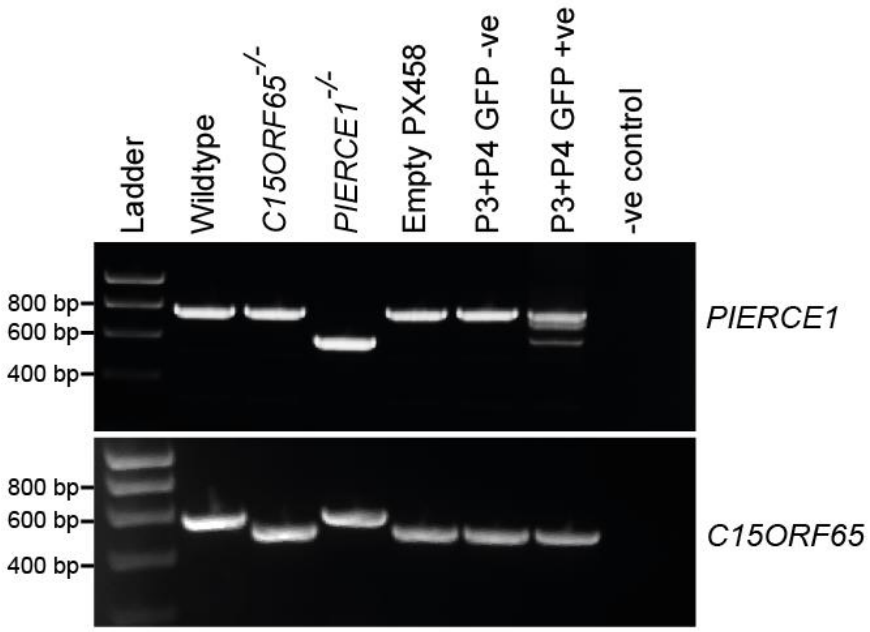

Figure 6.35 *PIERCE1 and C15ORF65* PCR genotyping of FACS-sorted cells. Cells were genotyped after sorting for *PIERCE1* and C15ORF65. All the cells were *C15ORF65*$^{-/-}$ except wildtype or *PIERCE1*$^{-/-}$ cells.

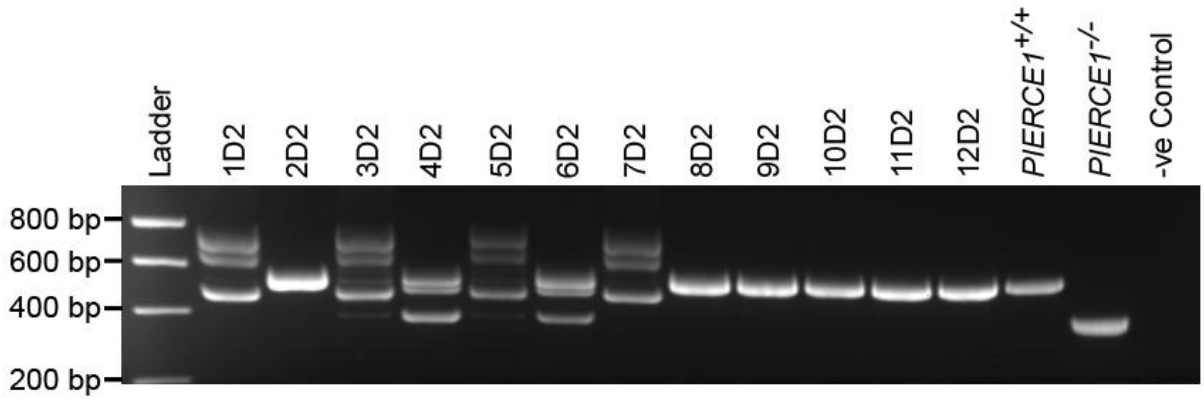

Figure 6.36 Genotyping of clones derived from gRNA P3 and P4 co-transfected cells. Genotyping PCR was done with the genomic DNA extracted from the indicated clones and the products were resolved in a 1.5% agarose gel. *PIERCE1*$^{+/+}$ and *PIERCE1*$^{-/-}$ cells were used as controls.

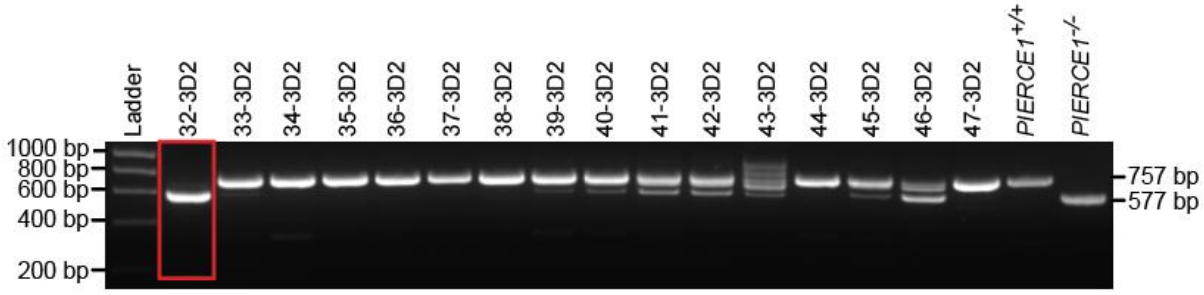

Figure 6.37 Selection of clones derived from clone 3D2. Clones derived from 3D2 were genotyped for *PIERCE1*. Red box indicates the clone with bright *PIERCE1*-edited band.

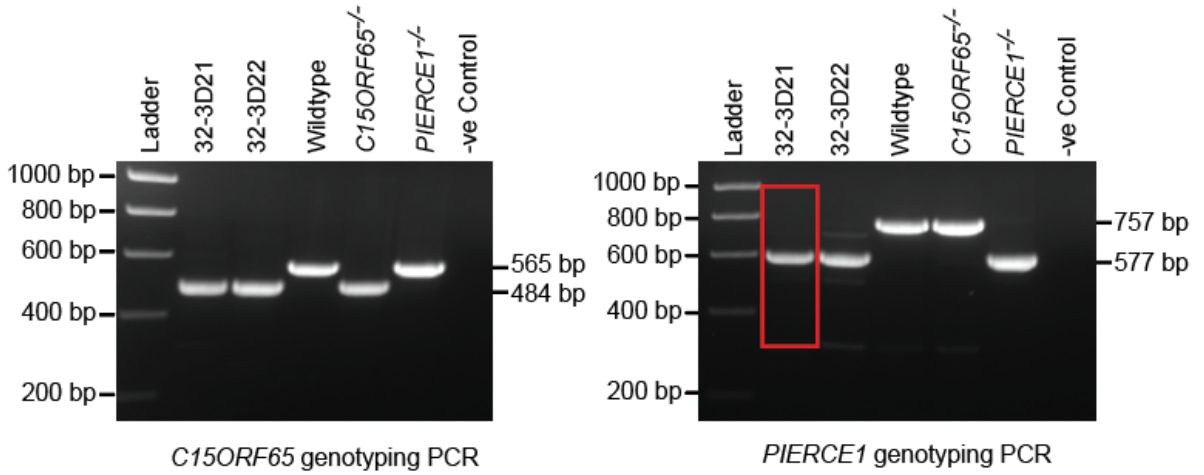

Figure 6.38 Development of *PIERCE1 C15ORF65* double knockout cell. Further clones derived from clone 32-3D2 were genotyped for *PIERCE1*. Red box indicates the clone for which *PIERCE1* was edited.

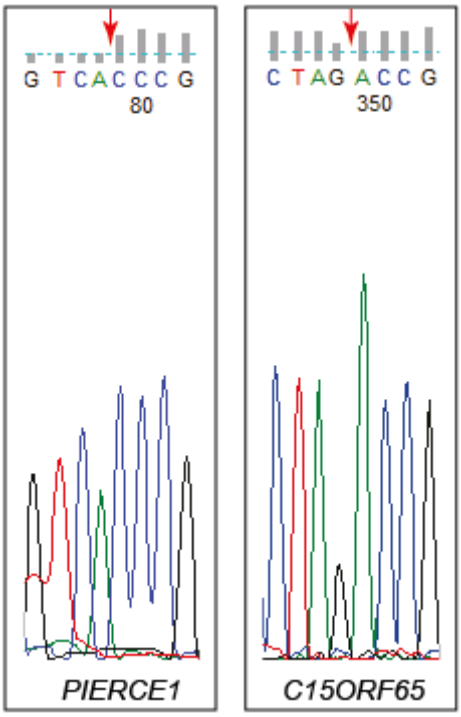

Figure 6.39 Sequence chromatogram of clone 32-3D21 for *PIERCE1 and C15ORF65* genotyping. Red arrows in the chromatograms show the break point for *PIERCE1*-editing as observed in Figure 6.22 as well as the break point for *C15ORF65*-editing as observed in Figure 6.32.

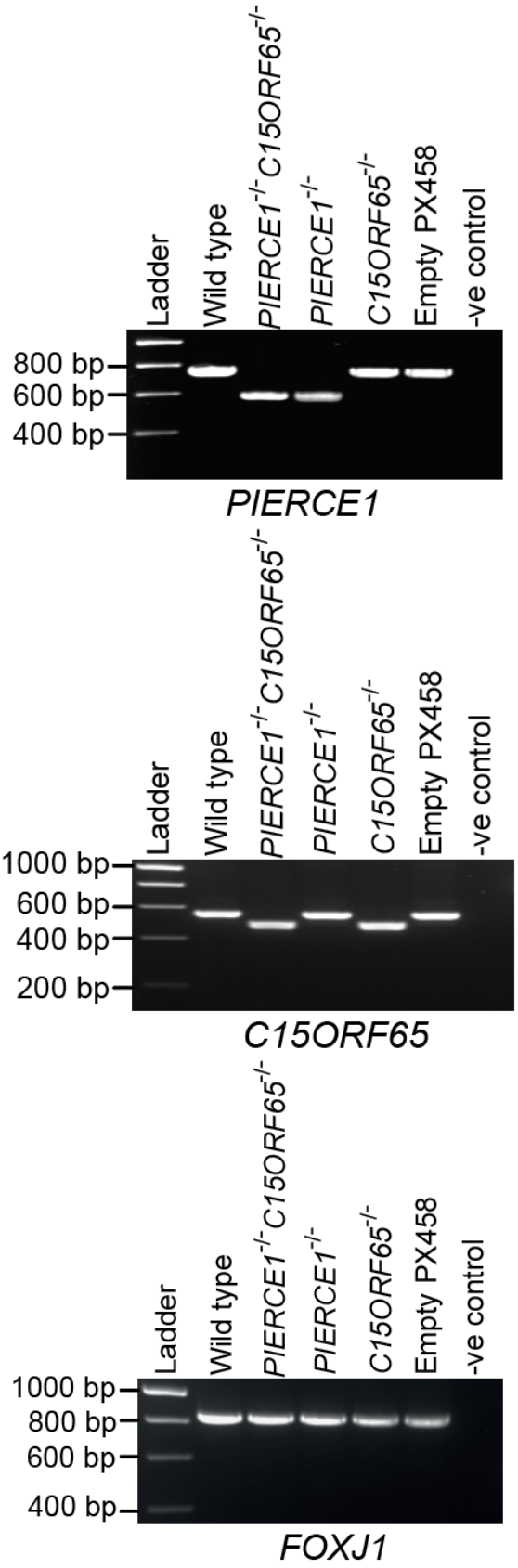

Figure 6.40 Final genotyping of *PIERCE1 C15ORF65* double edited clones. Clone 32-3D21 was re-genotyped for *PIERCE1* and *C15ORF65* along with *FOXJ1*. Empty PX458-transfected HBEC3-KT cells were used as the mock transfection control. Images are representative of n = 3 replicate gels.

6.5 Morphology of the knockout cells

The morphology of wildtype cells and all the knockout cells were observed under a brightfield microscope (Figure 6.41). The morphology of all cells appeared similar with no gross alteration in size or shape. Cobblestone-shaped monolayer cells with dendrite like extensions were observed irrespective of genotype when cells of up to 20 passages were tested.

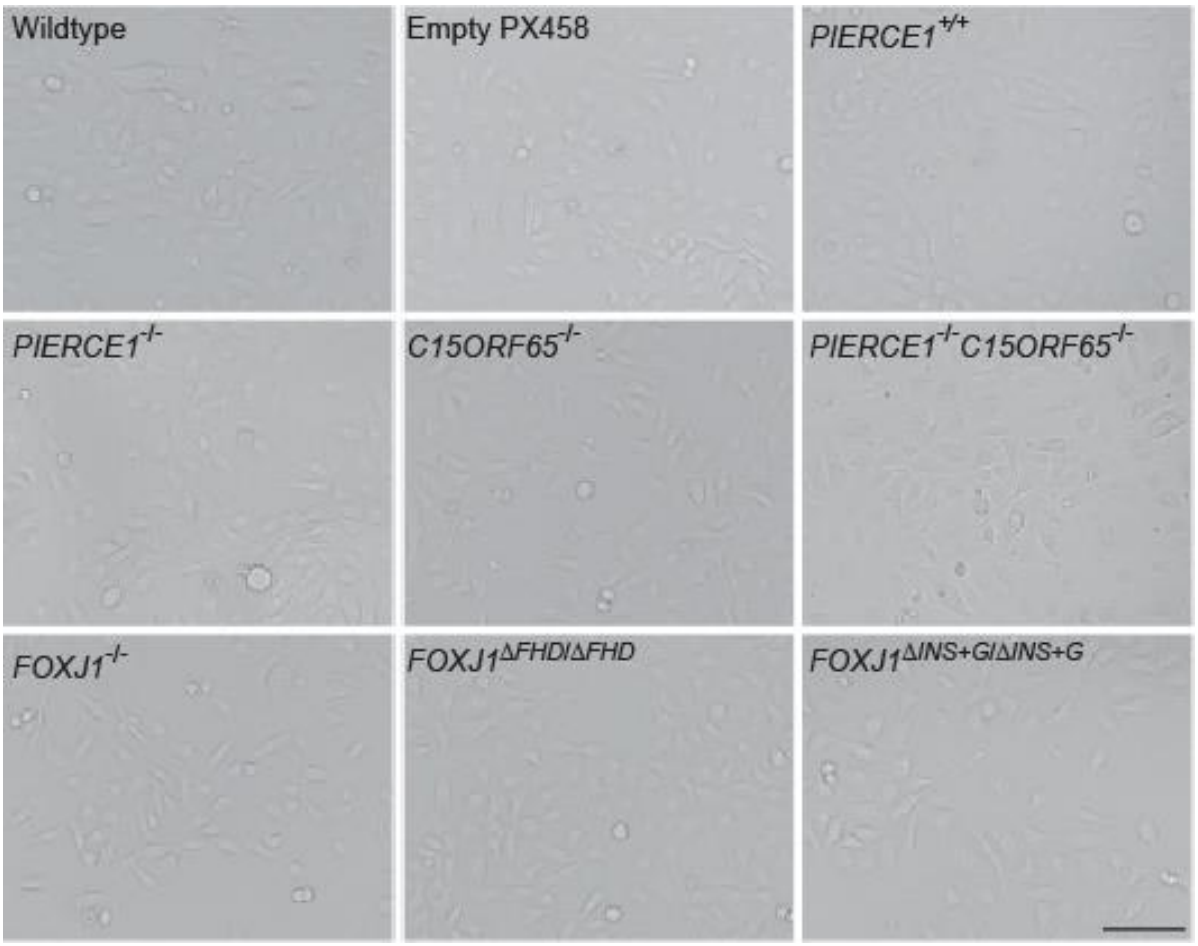

Figure 6.41 Morphology of wildtype and knockout cells. Cells were imaged under brightfield microscope. All images are at the same magnification and the scale bar = 20 μm.

6.6 Chapter discussion

Gene knockout models have been widely used to elucidate the function of many genes (Wassef, Luscan et al. 2017) and plasmid based CRISPR-CAS9 gene editing system are now one of the popular and most utilized method to develop cell lines deficient in a target gene (Giuliano, Lin et al. 2019). Plasmid based CRISPR-CAS9 mediated gene-editing systems require transfection of plasmids containing CAS9 and gRNAs for the target gene. The gene editing plasmid PX458 developed by Zhang lab (Joung, Konermann et al. 2017) that also expresses GFP for use in cell

selection. The transfection efficiency of HBEC3-KT cells used in this study might be compromised as these cells were transfected twice during the development and were grown for many years (Ramirez, Sheridan et al. 2004). Among the methods tested, I found that FuGENE® HD reagent used at a 1:4 (μg plasmid:μl reagent) appeared to be the best method to transfect HBEC3-KT cells.

Though single gRNA delivery alone can be used to knockout a target gene using CRISPR-CAS9 system (Park, Uchida et al. 2022), a dual gRNA-approach is more efficient in generating a defined deletion within a target gene (Spagnuolo and Blenner 2021). In the dual gRNA method, two gRNAs cloned in separate plasmids are co-transfected into a single cell. In such doubly transfected events, each gRNA-CAS9 complex produces a DNA double-strand break. These two DNA double-strand breaks generated this way push the non-homologous end joining-mediated DNA double-strand break repair (NHEJ) pathway. This event results in loss of the genomic region flanked by the generated dual DNA double-strand breaks to produce a defined genomic deletion (Song, Yang et al. 2021). When guide RNAs are cloned in the same plasmid backbone (like PX458), selected cells may contain one or both gRNA-containing plasmids and sometime the efficiency of gRNA-CAS9 complex fails to produce genome editing (Adikusuma, Pfitzner et al. 2017). However, dual guide RNA approach has been shown to reduce possible off-target effects significantly during the gene-editing process (Park, Uchida et al. 2022).

For generation of *FOXJ1*$^{-/-}$ HBEC3-KT cells, the selected cells were transfected only with gRNA F5 containing PX458 and the resulted in a short deletion of 46 bp from the activity of the single gRNA-CAS9 complex. Such events could happen from GFP-positive cells transfected with only one guide RNA containing plasmid and from the different efficiencies of utilized guide RNAs in dual gRNA CRISPR-CAS9 approach (Park, Uchida et al. 2022). For the *FOXJ1*$^{\Delta FHD/\Delta FHD}$, the cells were co-transfected with both gRNA containing plasmids resulting in loss of 300 bp (flanking a major portion of FHD coding region) from CAS9 activity followed by DNA repair. Development of *FOXJ1*$^{\Delta INS+G/\Delta INS+G}$ HBEC3-KT cells confirmed insertional mutagenesis during homologous recombinational dsDNA break repair after the gRNA F5-guided CAS9 cleavage. These show that such approach may yield only small mutations and

confirms the importance of sequence verification of all isolated lines. The predicted mRNAs from *FOXJ1*$^{-/-}$ or *FOXJ1*$^{\Delta INS+G/\Delta INS+G}$ did not encode FOXJ1 and that FOXJ*1*$^{\Delta FHD/\Delta FHD}$ lacked the full FHD domain, thus all of them can be considered as functionally devoid of wildtype FOXJ1 activity and thereby, *FOXJ1*-null.

Interestingly, one clone was found during the development of *PIERCE1*-knockout HBEC3-KT cells, where the cell was transfected with a gRNA-containing PX458, but the CRISPR-CAS9 gene editing failed resulting in a sorted wildtype cell, i.e., *PIERCE1*$^{+/+}$. Similar to the development of *FOXJ1*$^{\Delta FHD/\Delta FHD}$, clones transfected with each of the two gRNA-containing PX458s generated a 180 bp deletion. Such deletion occurs from NHEJ of the dual double-strand DNA breaks facilitated by double gRNA-guided CAS9-mediated DNA cleavage. This 180 bp deletion covers the Kozak sequence of *PIERCE1*. The *PIERCE1* mRNA originated from this *PIERCE1*$^{-/-}$ HBEC3-KT cells should lack sufficient elements required for translation initiation and would be expected to fail to produce functionally active PIERCE1.

Similar observations were found when *C15ORF65*$^{-/-}$ HBEC3-KT cells were developed where 81 bp covering the Kozak sequence was lost from CRISR-CAS9 activity. However, the predicted protein could only be translated from the predicted mRNA that i) lacks an appropriate Kozak sequence (Acevedo, Hoermann et al. 2018, McClements, Butt et al. 2021) (AGAAATG instead of GAAAATG for *C15ORF65*), ii) has start codon far away from 5'-capping, iii) has no known internal ribosomal entry site, and iv) is encoded by a single exon (the exon 2 only in this case). Even though such translation is possible, the translated protein would miss a critical N-terminal region that i) is a part of DUF4490 of C15ORF65, and ii) is required for CFAP53-binding within the microtubule inner protein complex in cilia structure (Figure 6.31B). Thus, the possible protein encoded by *C15ORF65*$^{-/-}$ HBEC3-KT cells could be non-functional in ciliated cells without the structurally important N-terminal domain (Gui, Farley et al. 2021).

Since *PIERCE1*$^{-/-}$ *C15ORF65*$^{-/-}$ HBEC3-KT cells contains the precise deletions observed in *PIERCE1*$^{-/-}$ and *C15ORF65*$^{-/-}$ cells, this double knockout cell line was also considered deficient in wildtype PIERCE1 or C15ORF65.

However, there still exists a possibility that the products encoded by all these edited genes may change the cellular homeostasis to some extent, or other genes might be affected due to the off-target of the gRNAs. Such off-targets can be minimized by carefully designing the guide RNAs in several ways including i) omitting guide RNAs with low specificity scores, ii) omitting guide RNAs with high off-target scores, iii) omitting guide RNAs for those off-targets are already known, and iv) using dual guide RNAs approach (Wienert, Wyman et al. 2019, Park, Uchida et al. 2022). In addition to these, the knockout cells can be tested with PCR-sequencing for potential off-targets regions (Iida, Suzuki et al. 2020). I did not test my knockout cells for off-targets using PCR-sequencing or genome sequencing due to time, funds and resource limitation however the cells were considered off-target free as the designed guide RNAs were highly specific for their targets (on-target score > 95.0), the off-target scores were very low (< 0.5), and the potential off-targets did not cover any exon or gene regulatory region. Nonetheless, the cells grew well, and no morphological alteration was visible indicating that these cells can be used for further studies such as differentiating them at ALI or under submerged condition. All these cells were genotyped in regular intervals by PCR and sequencing of the PCR products to ensure the purity of individual lines and thus was confirmed as gene-knockouts.

In summary, HBEC3-KT cells for six different genotypes covering three genes (*FOXJ1*, *PIERCE1* and *C15ORF65*) were developed and the genotypes of these cells include *FOXJ1*$^{-/-}$, *FOXJ1*$^{\Delta FHD/\Delta FHD}$, *FOXJ1*$^{\Delta INS+G/\Delta INS+G}$, *PIERCE1*$^{-/-}$, *C15ORF65*$^{-/-}$ and *PIERCE1*$^{-/-}$ *C15ORF65*$^{-/-}$. All these cells grew and proliferated well. Thereby, these cells were considered to be useful for further studies related to mucociliary differentiation. In the next chapter, I will describe studies in which these cells will be differentiated at the ALI as well as under submerged conditions along with the wildtype cells (wildtype HBEC3-KT, empty PX458-transfected HBEC3-KT, and *PIERCE1*$^{+/+}$ (sorted wildtype)) to investigate the roles of *FOXJ1*, *PIERCE1* and *C15ORF65* in mucociliogenesis.

Chapter 7: Differentiation of *FOXJ1*, *PIERCE1*, and *C15ORF65* knockout HBEC3-KT cells

7.1 Preface

Research with *FOXJ1*-knockout human cells is very limited and few studies were done using the patient samples harbouring dominant mutations in *FOXJ1* (Wallmeier, Frank et al. 2019, Shapiro, Kaspy et al. 2021). One of the best studies associated with *FOXJ1*-knockdown or CRISPR-CAS9 gene editing claimed maximum 93.4%±1.2% efficiency (Rapiteanu, Karagyozova et al. 2020) for *FOXJ1* deletion in primary human airway cells. Recent study suggested that zebrafish lacking both *pierce1* and *c15orf65* did form cilia, but their Kupffer's vesicle (KV) cilia were immotile although motile cilia were observed in pronephric duct and olfactory pit (Gui, Farley et al. 2021). This study also showed that mice lacking both genes were embryonic lethal but generated nodal cilia with significantly lowered beat frequency (as compared to wildtype mice) when at least one of these genes was missing (Gui, Farley et al. 2021). To complement these studies, I tested the differentiation capacity of all the gene edited HBEC3-KT cells to examine their potential to produce multiciliated cells. For this, I hypothesized that both *PIERCE1* and *C15ORF65* could play important roles in cilia.

7.2 Differentiation at ALI

Gene edited cells were cultured at the ALI for 14 days as described previously followed by brightfield, immunofluorescence microscopy and RT-PCR. Empty PX458, *FOXJ1*$^{-/-}$ and *FOXJ1*$^{\Delta INS+G/\Delta INS+G}$ cells were not included in this experiment due to time and technical limitations (media were out of stock).

7.2.1 Brightfield microscopy studies

Brightfield microscopy suggested typical cobblestone morphology for all of the cells at beginning (day 0) of ALI culture and the cells were tightly packed by day 14 of the ALI culture (Figure 7.1).

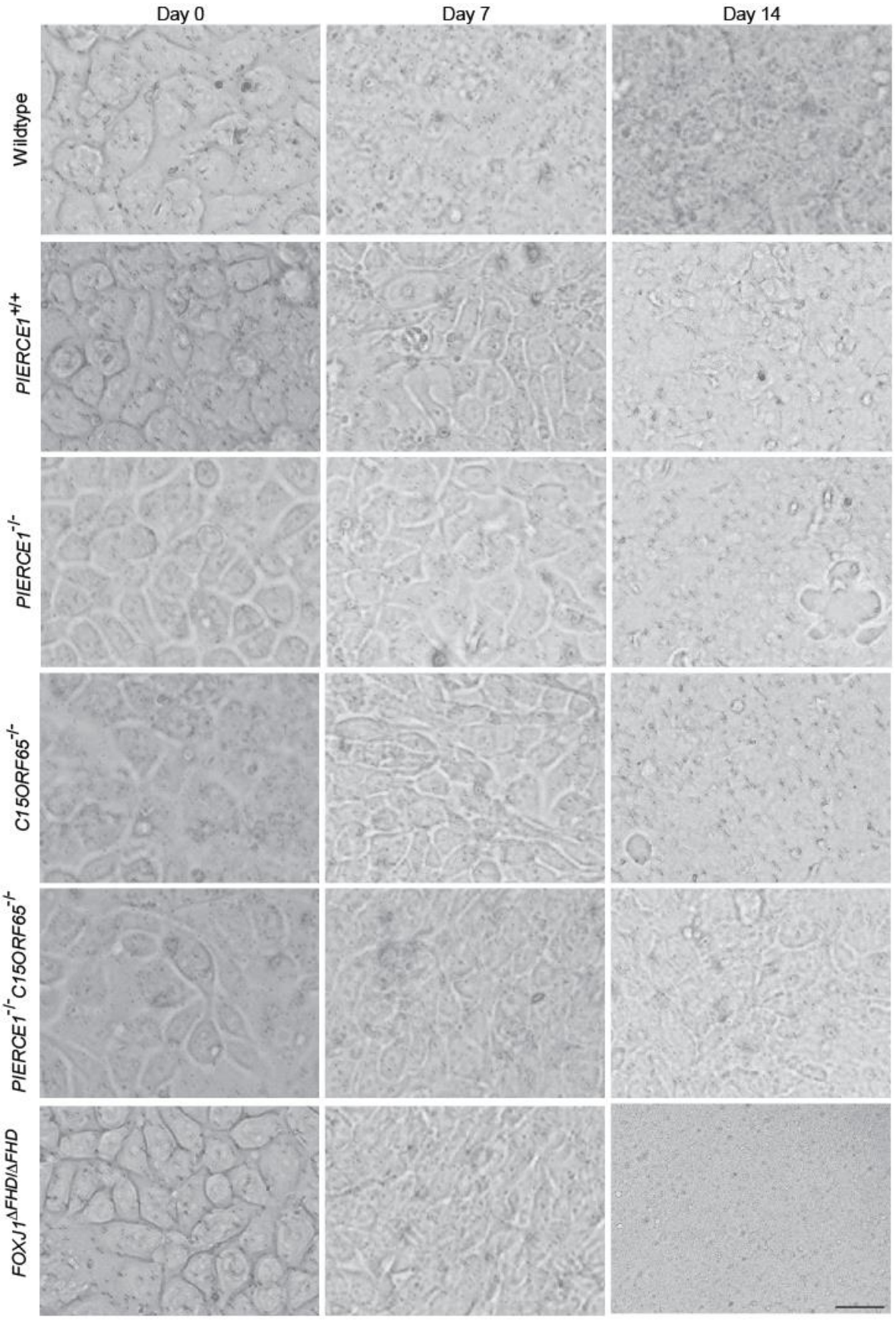

Figure 7.1 Morphology of the knockout cells differentiated at ALI for 14 days. Brightfield images of cells cultured at ALI up to day 0, day 7 and day 14. Scale bar = 20 μm. Images are representative of n = 3 experiments.

7.2.2 Immunofluorescence microscopy studies

Immunofluorescence staining with day 14 samples showed staining of FOXJ1 in acetylated α-TUBULIN-positive cells in wildtype, *PIERCE1*$^{+/+}$, *PIERCE1*$^{-/-}$ and *C15ORF65*$^{-/-}$ HBEC3-KT cells. All *FOXJ1*$^{\Delta FHD/\Delta FHD}$ cells failed to produce any potential progenitors of multiciliated cells as no FOXJ1 or acetylated α-TUBULIN-positive cells were observed (Figure 7.2 and Figure 7.3). *PIERCE1*$^{-/-}$*C15ORF65*$^{-/-}$ cells were also negative for both FOXJ1 and acetylated α-TUBULIN when they were cultured at the ALI (Figure 7.3).

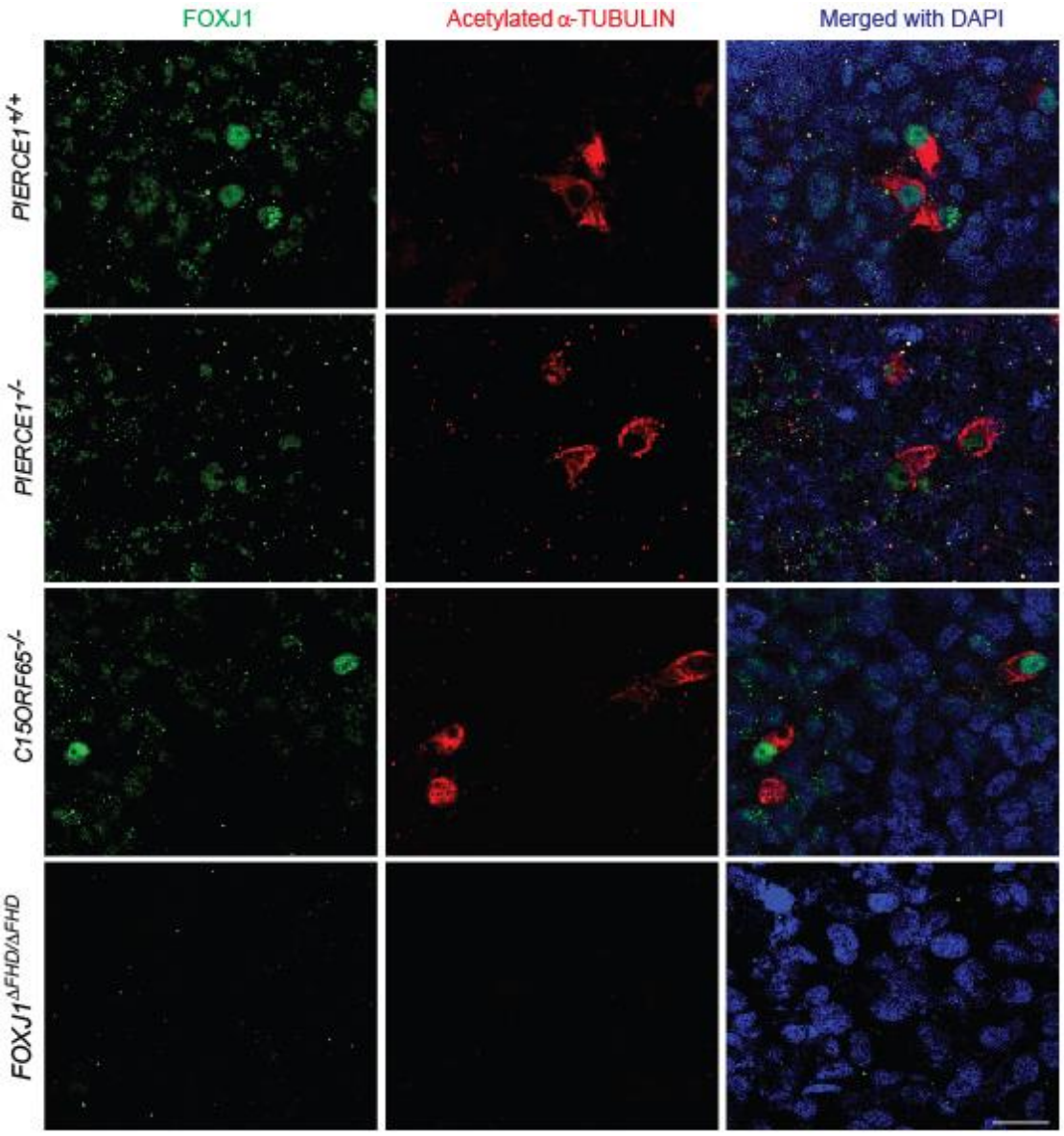

Figure 7.2 Mucociliary differentiation of single knockout cells at the ALI. HBEC3-KT cells of the indicated genotypes were cultured at ALI using PALI media for 14 days followed by immunostaining for FOXJ1 and acetylated α-TUBULIN. Images are representative of n = 3 experiments. Scale bar = 20 μm.

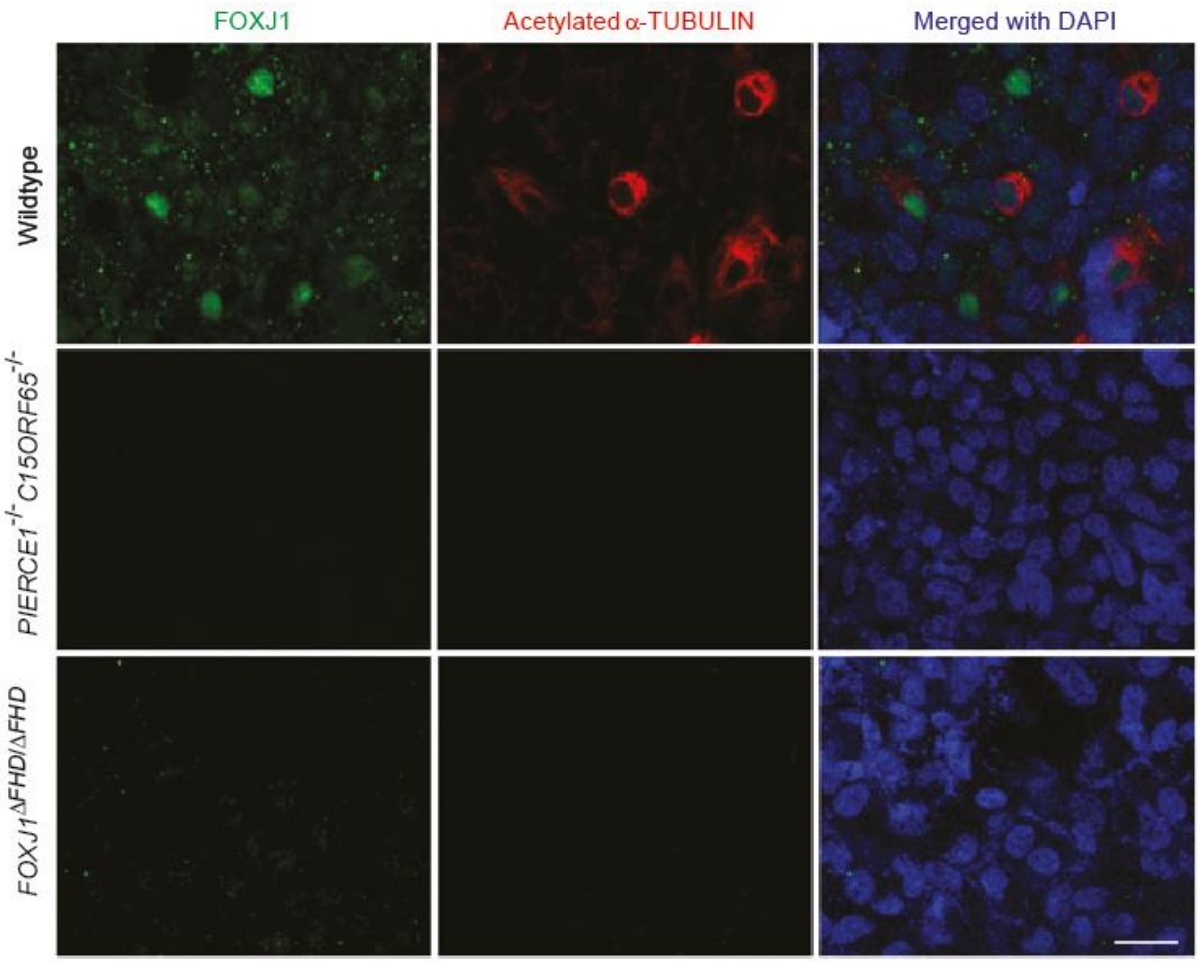

Figure 7.3 Mucociliary differentiation of *PIERCE1*$^{-/-}$*C15ORF65*$^{-/-}$ HBEC3-KT cells at the ALI. ALI-cultured cells of the indicated genotypes were immune-stained with FOXJ1 and acetylated α-TUBULIN antibodies. Images are representative of n = 3 experiments. Wildtype cells were used a positive control. Scale bar = 20 μm.

7.2.3 End-point RT-PCR studies

I next used end-point RT-PCR to study the cellular differentiation in these cultures through the expression of well validated marker genes. All cell types expressed *BPIFA1* after 7 days of ALI culture (Figure 7.4 and Figure 7.5). Wildtype, *PIERCE1*$^{+/+}$ and *PIERCE1*$^{-/-}$ cells expressed *TEKT1* at day 7 of ALI culture but *C15ORF65*$^{-/-}$, *PIERCE1*$^{-/-}$*C15ORF65*$^{-/-}$ and *FOXJ1*$^{\Delta FHD/\Delta FHD}$ cells did not. However, *C15ORF65*$^{-/-}$ cells expressed *TEKT1* at day 14 of ALI culture (Figure 7.4). *FOXJ1*$^{\Delta FHD/\Delta FHD}$ cells expressed *BPIFA1* but not *TEKT1* after day 14 of ALI culture. *PIERCE1*$^{-/-}$*C15ORF65*$^{-/-}$ double knockout cells also expressed *BPIFA1* but not *TEKT1* at day 14 of ALI culture suggesting that these cells differentiated into secretory cells but not into precursors of multiciliated cells (Figure 7.5). It therefore appears that loss of both *PIERCE1* and *C15ORF65* diminishes the capacity of HBEC3-KT cells to differentiate

into potential progenitors of multiciliated cells. Neither *PIERCE1*$^{-/-}$ and *PIERCE1*$^{-/-}$ *C15ORF65*$^{-/-}$ expressed *PIERCE1* confirming they were edited for *PIERCE1*. Similarly, *C15ORF65*$^{-/-}$ and *PIERCE1*$^{-/-}$*C15ORF65*$^{-/-}$ cells did not express *C15ORF65* at any point validating that they were edited for *C15ORF65*. Expression of *C15ORF65* in *PIERCE1*$^{-/-}$ cells, expression of *PIERCE1* in *C15ORF6*$^{-/-}$ cells, and expression of neither gene in *PIERCE1*$^{-/-}$*C15ORF65*$^{-/-}$ cells further confirmed the genotype of these cells (Figure 7.4 and Figure 7.5). The data also suggested that both *PIERCE1* and *C15ORF65* could be expressed when FOXJ1 is absent, suggesting that these genes are not a direct target of FOXJ1.

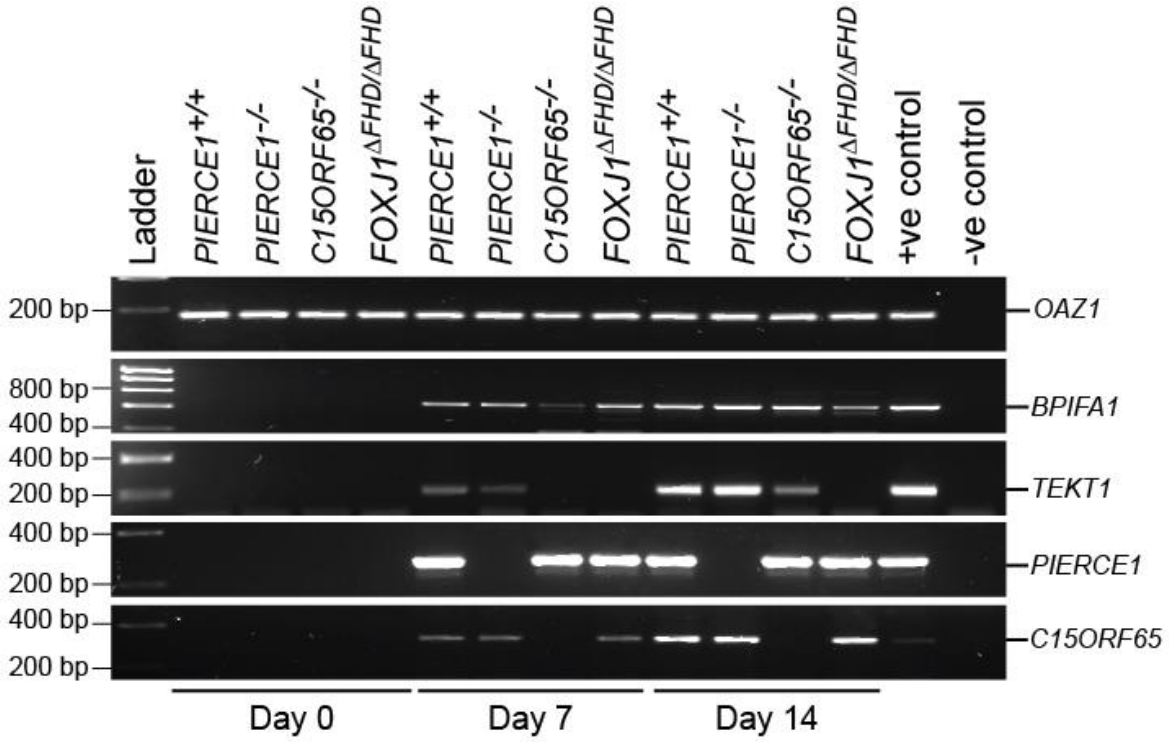

Figure 7.4 Expression of marker genes in single gene knockout HBEC3-KT cells differentiated at ALI. Expression analyses of *BPIFA1*, *TEKT1*, *PIERCE1* and *C15ORF65* were conducted with cDNA samples prepared from ALI-differentiated cells of the indicated genotypes at day 0, day 7 and day 14. The gel is representative of n = 3 experiments.

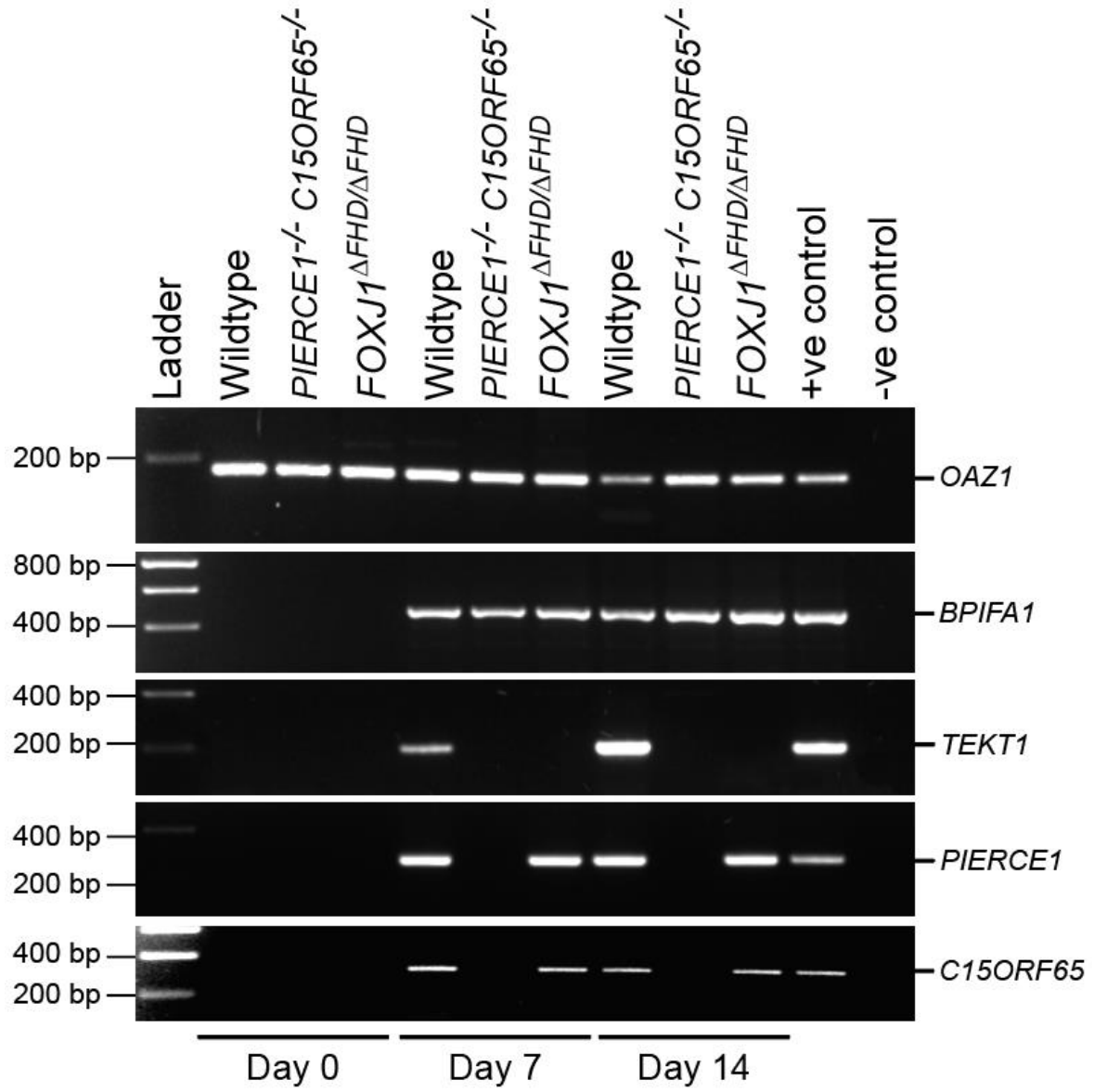

Figure 7.5 Expression of marker genes in *PIERCE1*$^{-/-}$*C15ORF65*$^{-/-}$ HBEC3-KT cells differentiated at ALI. Expression analyses of *BPIFA1*, *TEKT1*, *PIERCE1* and *C15ORF65* were conducted with cDNA samples prepared from ALI-differentiated cells of the indicated genotypes at day 0, day 7 and day 14. The gel is representative of n = 3 experiments.

7.3 Differentiation under submerged condition

To complement the findings observed with ALI-cultured cells, all cell types were differentiated under submerged conditions by culturing them with PALI media for 21 days. Cells cultured with KSFM media under submerged condition for 21 days served as controls. All the cells were fed with fresh media in every two days.

7.3.1 Brightfield microscopy studies

Brightfield microscopy suggested that the cell morphology was altered when cells were cultured with PALI media compared to KSFM providing a visual impression of differentiation. There was no visual difference in morphology between wildtypes (Figure 7.6), *PIERCE1* and *C15ORF65* knockouts (Figure 7.7), and *FOXJ1* knockouts (Figure 7.8) cells.

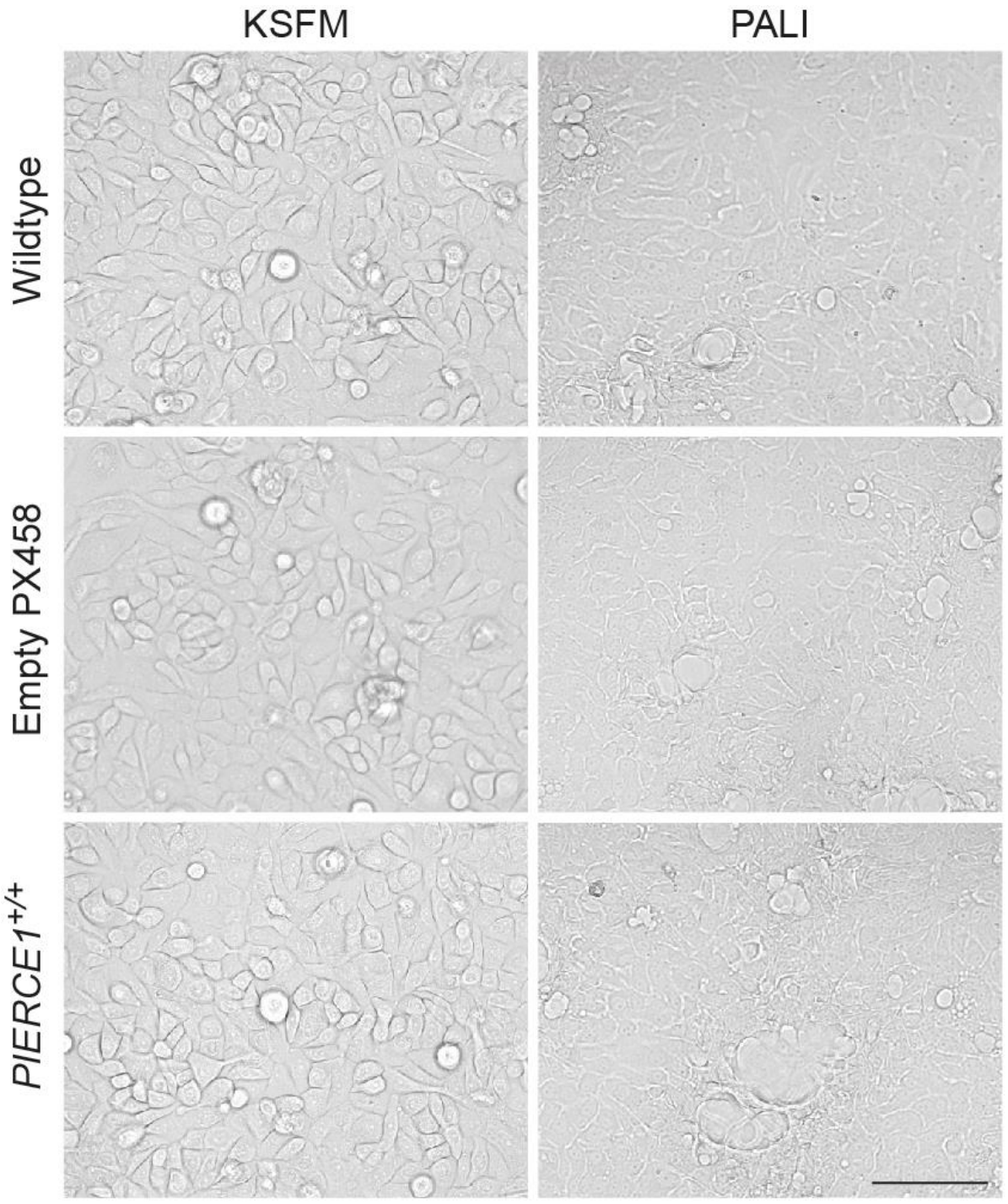

Figure 7.6 Differentiation of wildtype HBEC3-KT cell types under submerged condition. Cells of indicated genotypes were cultured either with KSFM or with PALI media for 21 days under submerged condition followed by acquisition of brightfield images. Images are representative of n = 3 experiments. Scale bar = 100 μm.

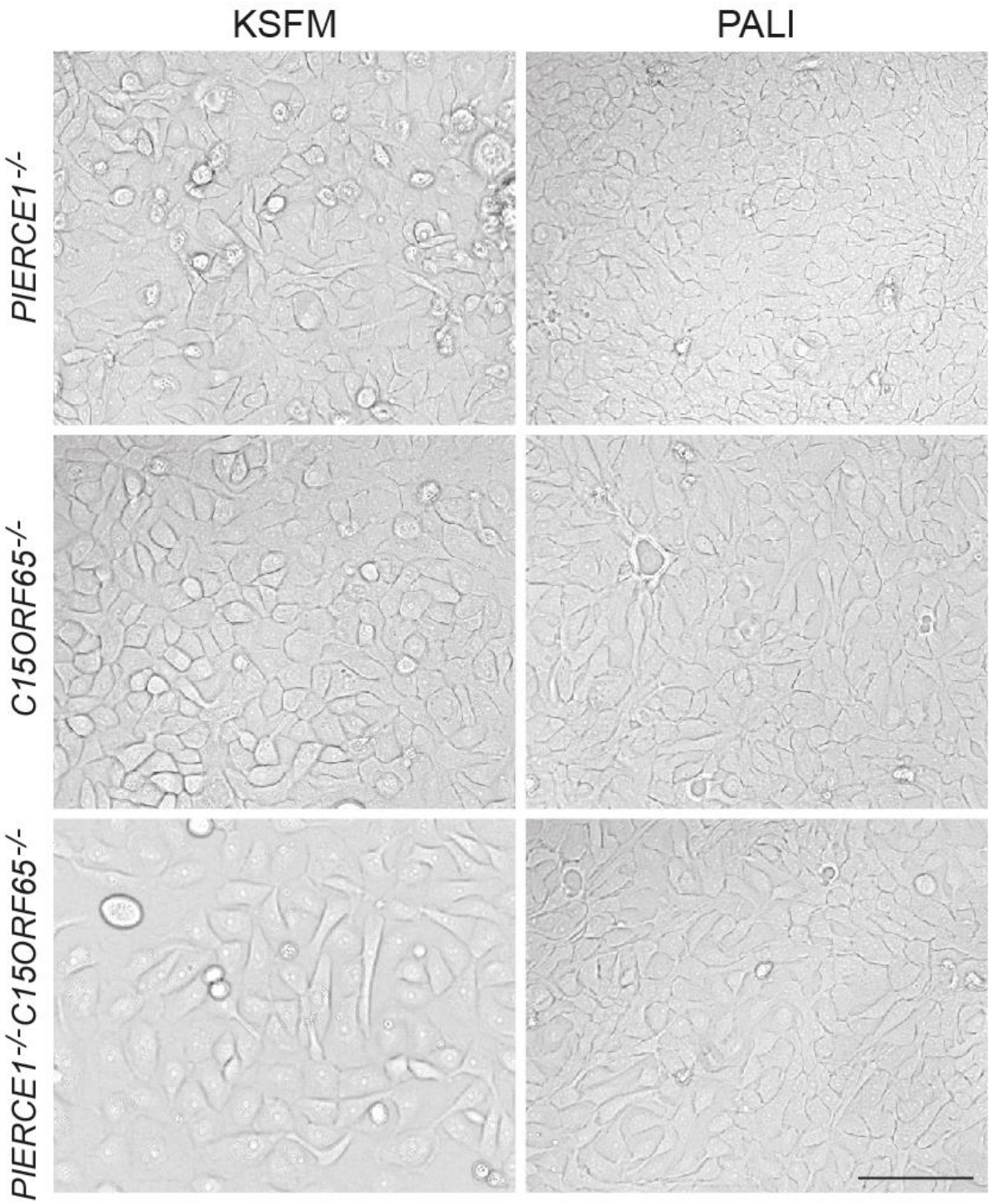

Figure 7.7 Differentiation of *PIERCE1* and *C15ORF65* knockout HBEC3-KT cell types under submerged conditions. Cells of the indicated genotypes were cultured either with KSFM or with PALI media for 21 days under submerged conditions for acquisition of brightfield images. Images are representative of n = 3 experiments. Scale bar = 100 μm.

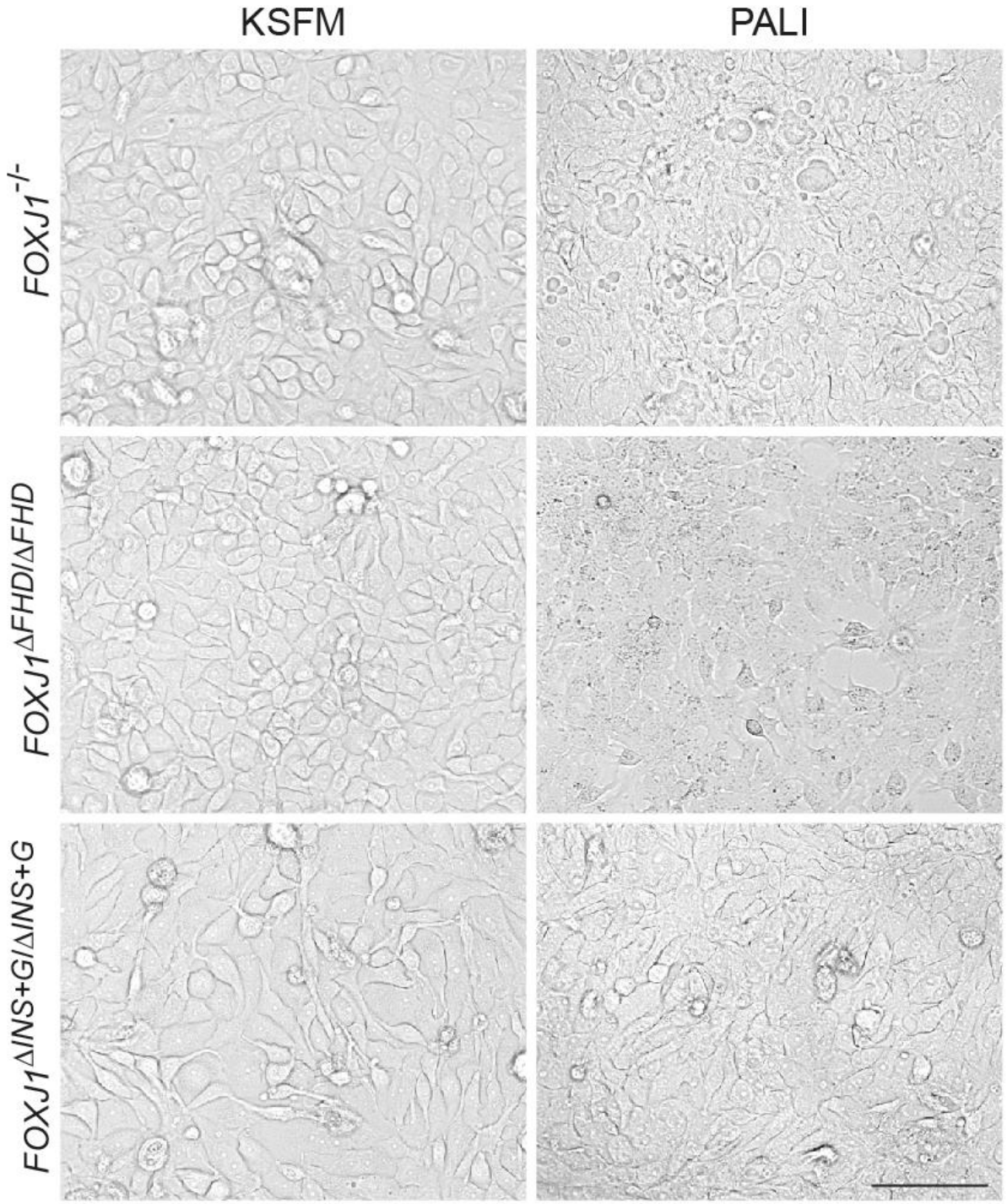

Figure 7.8 Differentiation of *FOXJ1* knockout HBEC3-KT cell types under submerged condition. Cells of the indicated genotypes were cultured either with KSFM or with PALI media for 21 days under submerged conditions and brightfield images were taken. Images are representative of n = 3 experiments. Scale bar = 100 μm.

7.3.2 Immunofluorescence microscopy studies

Immunofluorescence microscopy suggested that wildtype HBEC3-KT, empty PX458-transfected HBEC3-KT and *PIERCE1*$^{+/+}$ HBEC3-KT cells could be differentiated to

produce FOXJ1^{+}/acetylated α-TUBULIN^{+} potential progenitors of multiciliated cells when they were cultured with PALI media under submerged conditions for 21 days (Figure 7.9). FOXJ1 was distinctly localised in the nucleus of the acetylated α-TUBULIN-positive cells. All *FOXJ1*-knockout cells were negative for both FOXJ1 and acetylated α-TUBULIN (Figure 7.10). These observations further validated the phenotype of the *FOXJ1*-knockout HBEC3-KT cells.

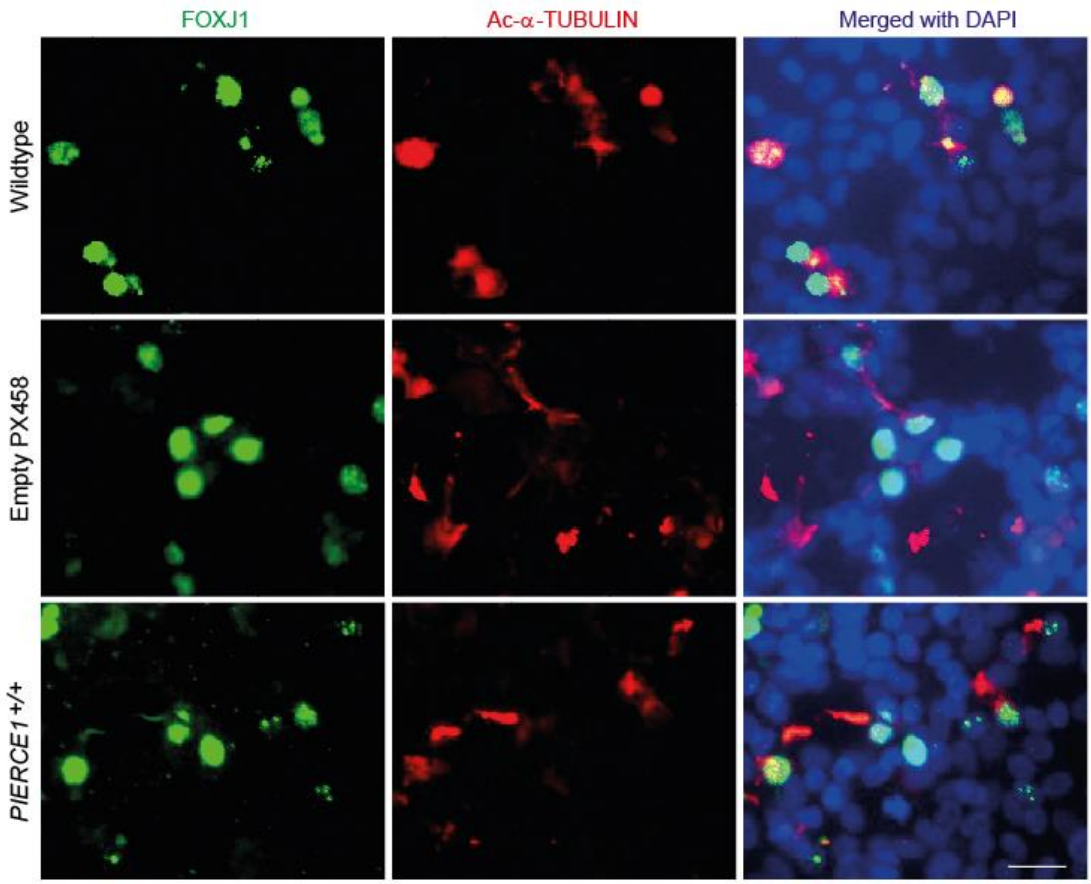

Figure 7.9 Differentiation of different wildtype HBEC3-KT cells under submerged condition. Cells of the indicated genotypes were differentiated with PALI media for 21 days and were stained for FOXJ1 and acetylated α-TUBULIN. Images are representative of n = 3 experiments. Scale bar = 20 μm.

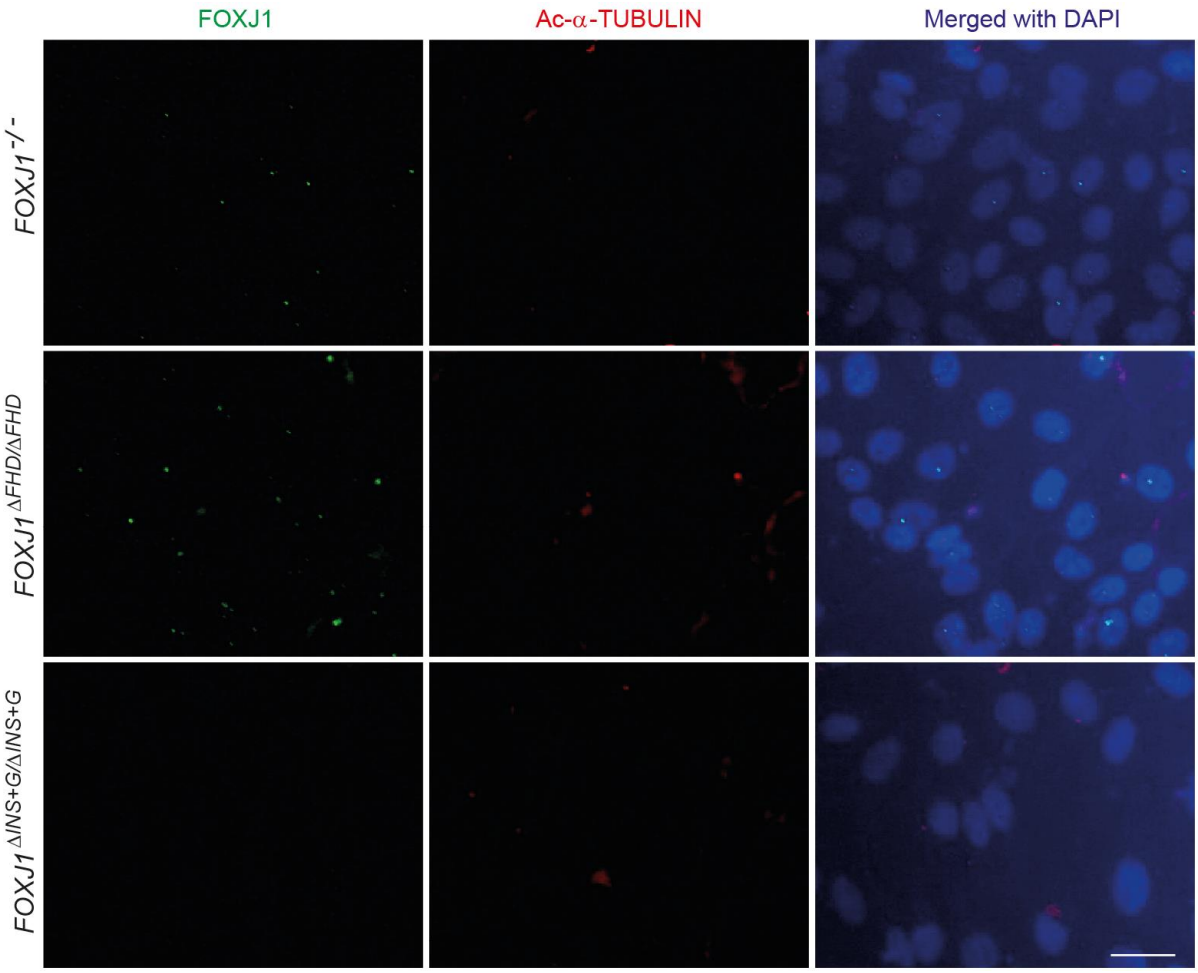

Figure 7.10 Differentiation of different *FOXJ1*-knockout HBEC3-KT cells under submerged condition. Cells of the indicated genotypes were differentiated with PALI media for 21 days and were stained for FOXJ1 and acetylated α-TUBULIN. Images are representative of n = 3 experiments. Scale bar = 20 μm.

When *PIERCE1* and *C15ORF65*-knockout cells were differentiated under submerged conditions for 21 days, these cells could be differentiated to produce FOXJ1^{+}/acetylated α-TUBULIN^{+} potential progenitors of multiciliated cells irrespective of whether they were single knockout or double knockout for these genes (Figure 7.11).

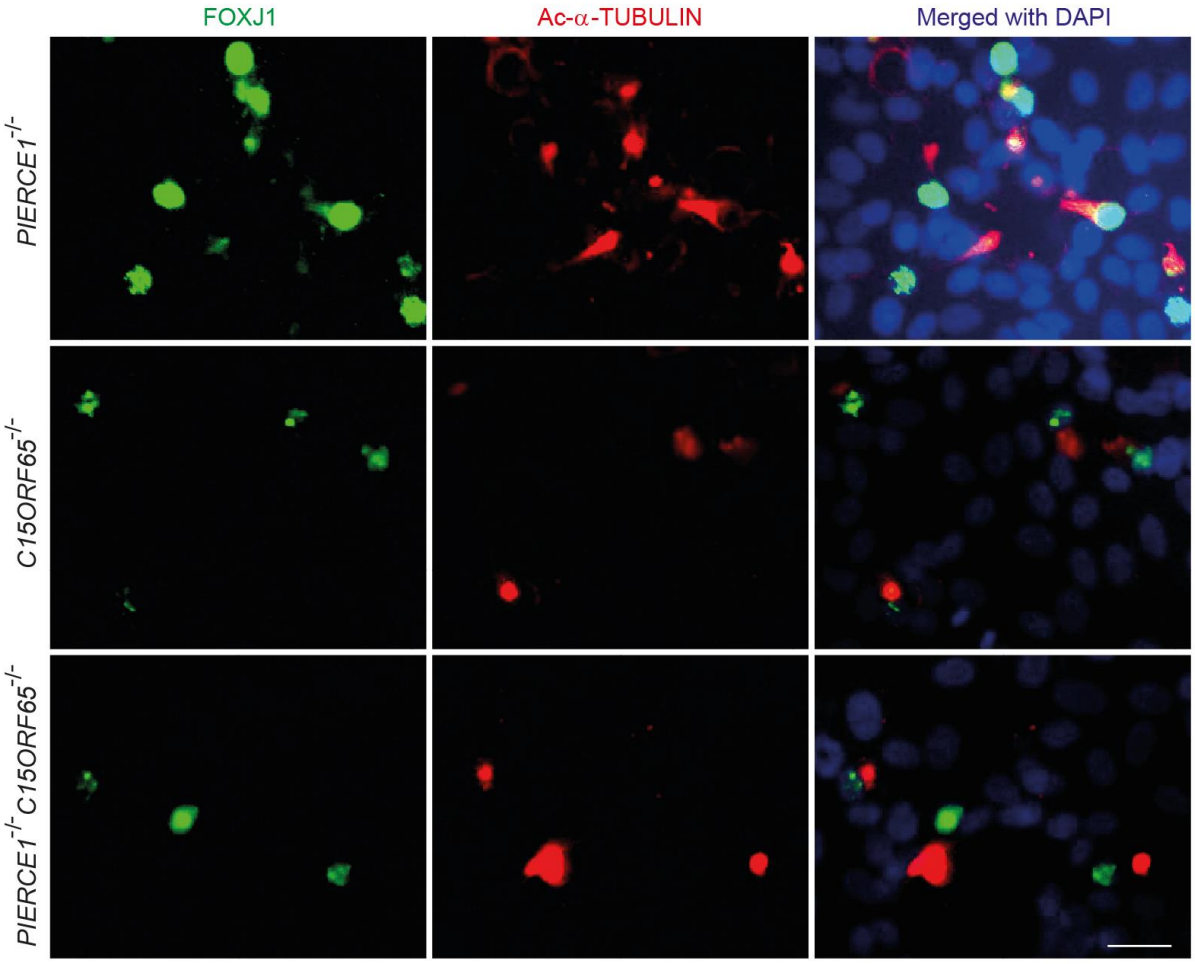

Figure 7.11 Differentiation of *PIERCE1* and *C15ORF65*-knockout HBEC3-KT cells under submerged condition. Cells of the indicated genotypes were differentiated with PALI media for 21 days and were stained for FOXJ1 and acetylated α-TUBULIN. Images are representative of n = 3 experiments. Scale bar = 20 μm.

PIERCE1 expression was not detected in differentiated *PIERCE1*$^{-/-}$ and *PIERCE1*$^{-/-}$ *C15ORF65*$^{-/-}$ cells confirming again that these cells were knocked-out for *PIERCE1* (Figure 7.12). Similarly, expression of C15ORF65 was absent in differentiated *C15ORF65*$^{-/-}$ and *PIERCE1*$^{-/-}$*C15ORF65*$^{-/-}$ HBEC3-KT cells confirming that these cells were also knocked-out for *C15ORF65* (Figure 7.13). Both findings also could validate their corresponding antibodies. Also, acetylated α-TUBULIN was co-localised with both PIERCE1 and C15ORF65 in differentiated wildtype HBEC3-KT cells as observed before (Figure 5.12). PIERCE1 and C15ORF65 staining was detected in the nucleus of wildtype cells as observed before (Figure 5.2), but not in the knockout cells indicating a possible nuclear localisation of both proteins.

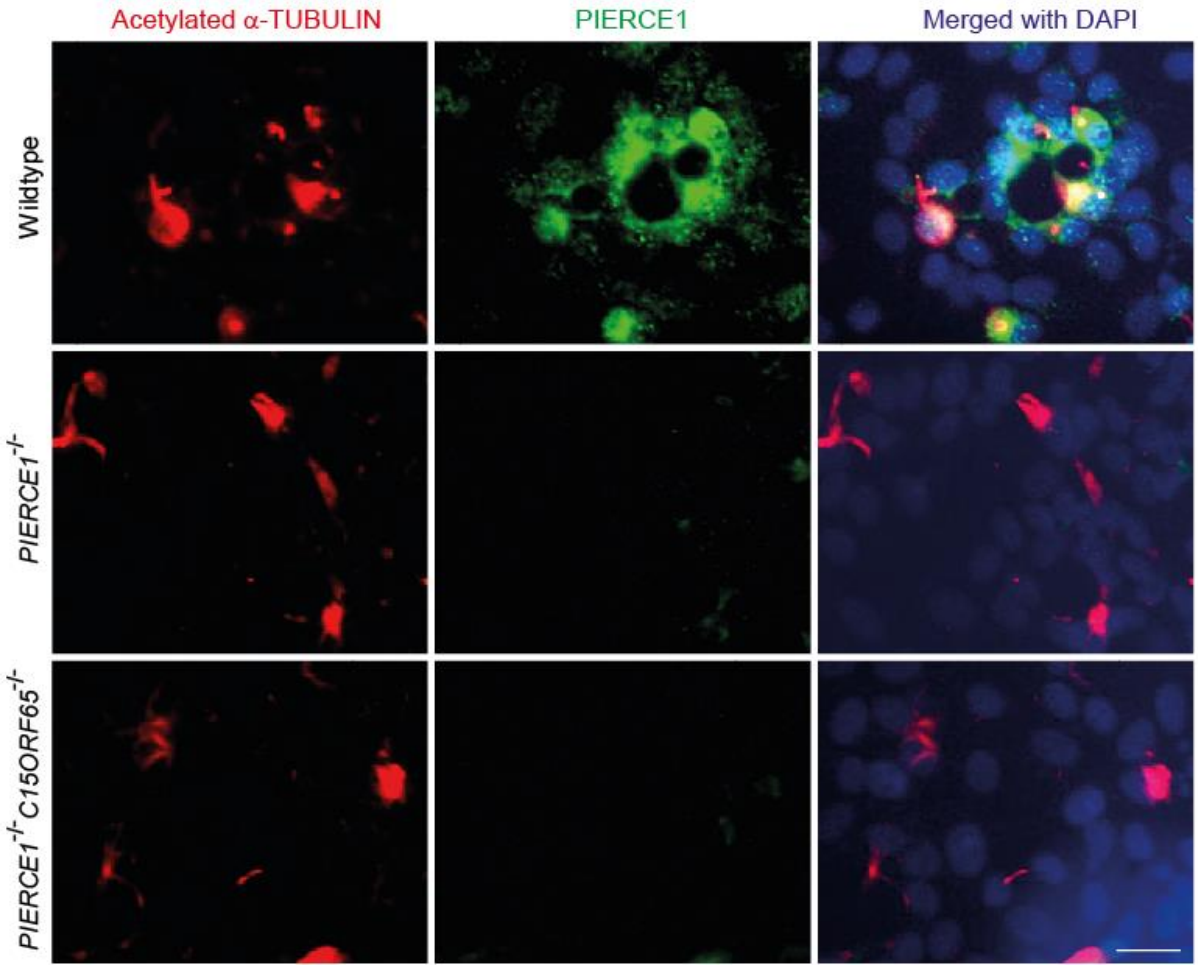

Figure 7.12 Expression of PIERCE1 in *PIERCE1*$^{-/-}$ and double-knockout HBEC3-KT cells differentiated under submerged condition. Cells of the indicated genotypes were differentiated with PALI media for 21 days and were stained for acetylated α-TUBULIN and PIERCE1. Scale bar = 20 μm. Images are representative of n = 3 experiments.

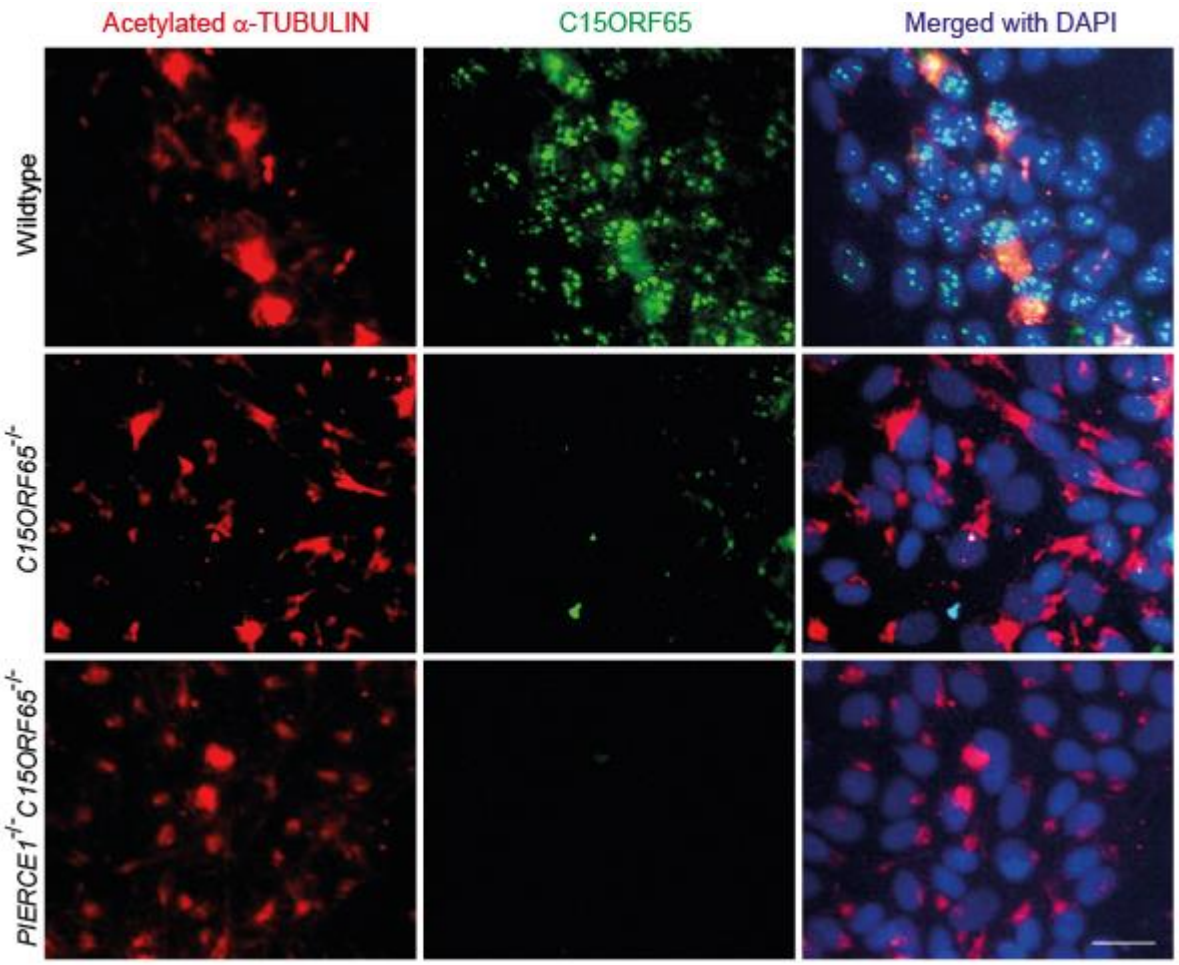

Figure 7.13 Expression of C15ORF65 in *C15ORF65*$^{-/-}$ and double-knockout HBEC3-KT cells differentiated under submerged condition. Cells of the indicated genotypes were differentiated with PALI media for 21 days and were stained for acetylated α-TUBULIN and C15ORF65. Scale bar = 20 μm. Images are representative of n = 3 experiments.

7.3.3 End-point RT-PCR studies

End-point RT-PCR suggested that all *FOXJ1* knockout cells expressed *BPIFA1*, *TEKT1*, *PIERCE1* and *C15ORF65* when they were cultured with PALI media under submerged conditions for 21 days (Figure 7.14).

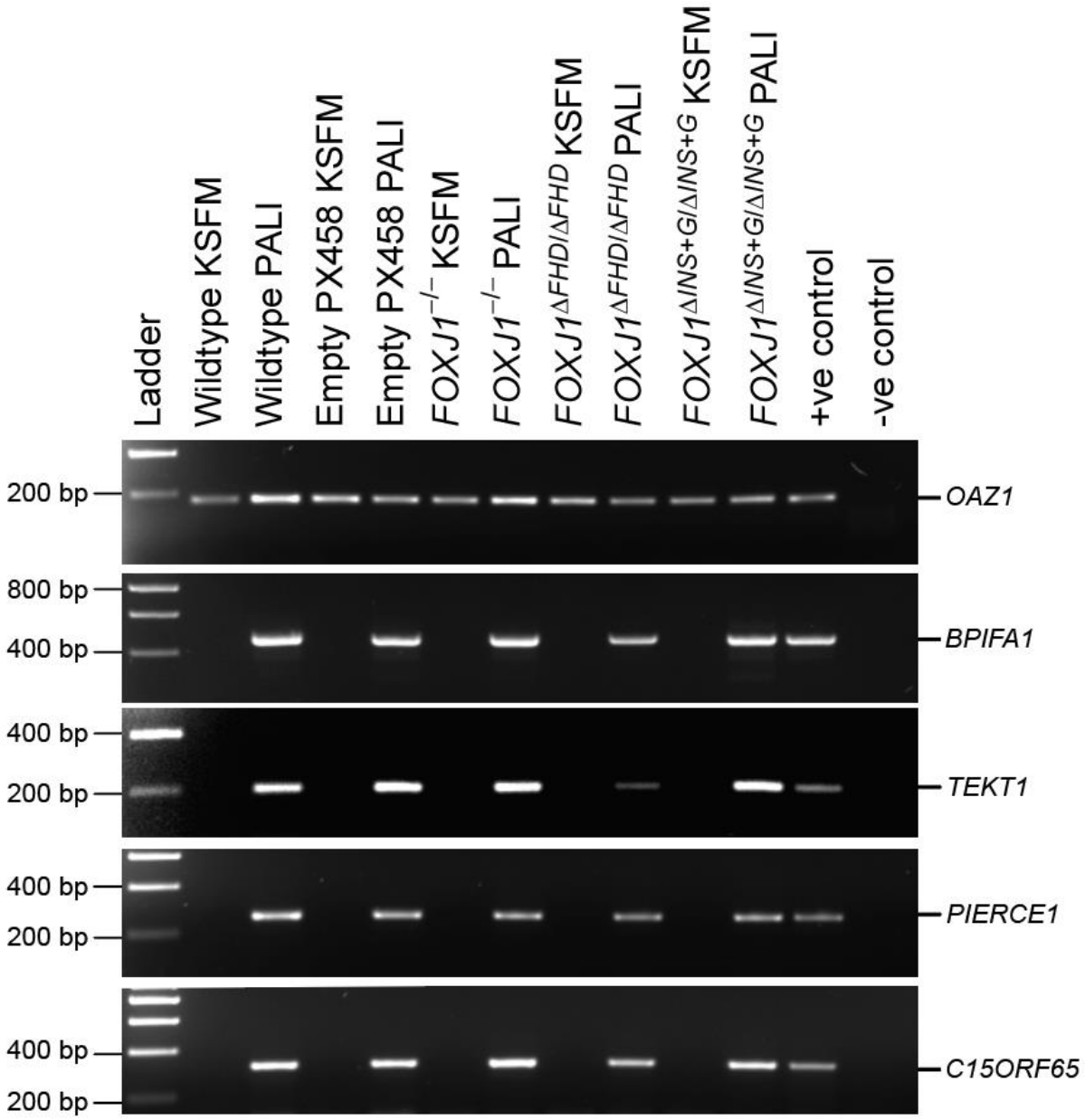

Figure 7.14 Expression of marker genes in submerged differentiated *FOXJ1* knockout HBEC3-KT cells. Cells of the indicated genotypes were grown with either KSFM or PALI media for 21 days and expression of marker genes was assessed with end-point RT-PCR. The gel is representative of n = 3 experiments.

PIERCE1$^{-/-}$ cells expressed *BPIFA1* and *TEKT1* cells as well as *C15ORF65* when they were cultured with PALI media under submerged conditions for 21 days. *PIERCE1* was not detected in these cells further validating their genotype (Figure 7.15).

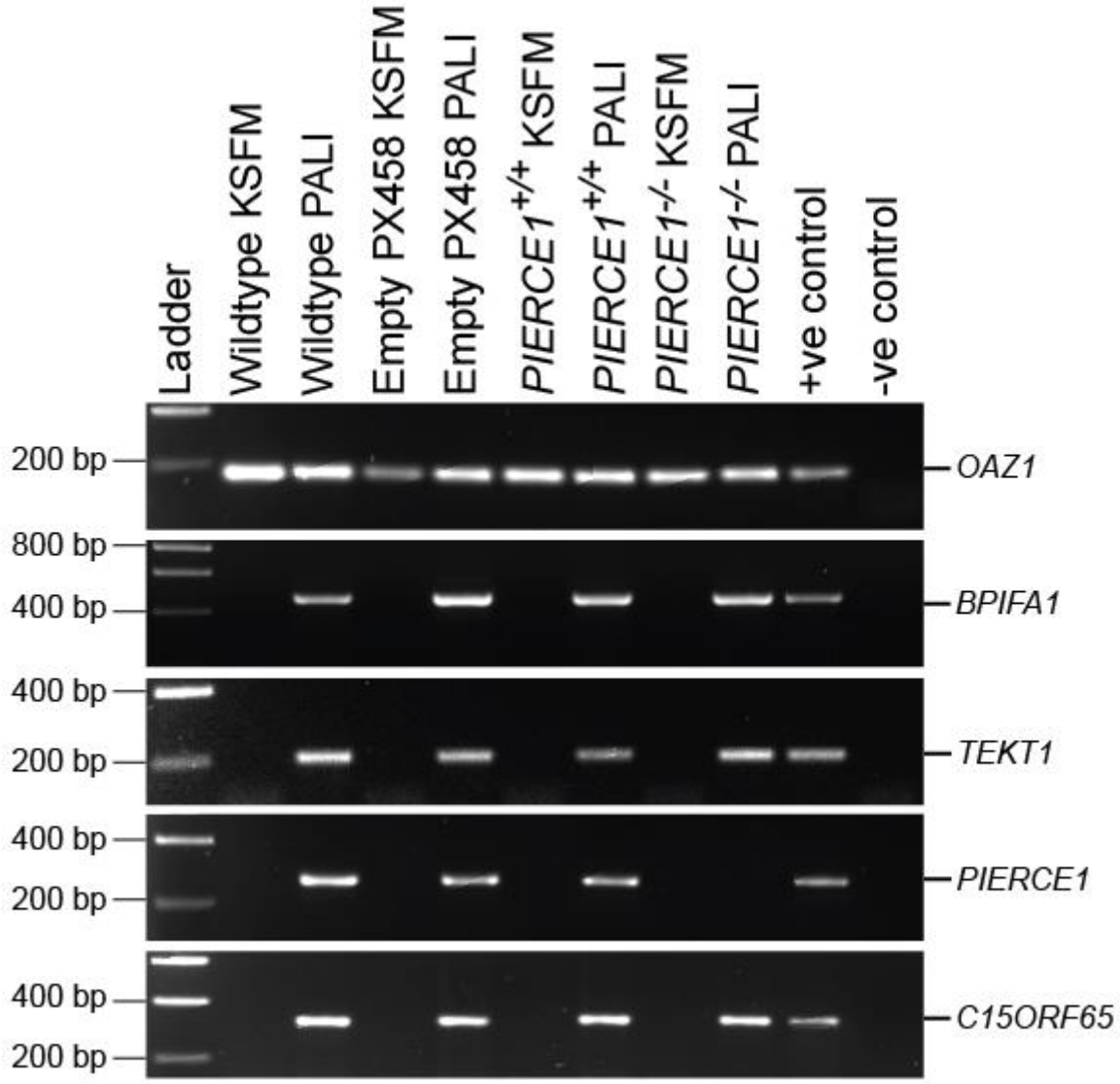

Figure 7.15 Expression of marker genes in submerged differentiated *PIERCE1*$^{-/-}$ HBEC3-KT cells. Cells of the indicated genotypes were grown with either KSFM or PALI media for 21 days and expression of marker genes was assessed with end-point RT-PCR. The gel is representative of n = 3 experiments.

C15ORF65$^{-/-}$ cells also expressed *BPIFA1* and *TEKT1* as well as *PIERCE1* when they were cultured with PALI media under submerged conditions for 21 days. *C15ORF65* was not detected in the *C15ORF65*$^{-/-}$ cells further validating their genotype (Figure 7.16).

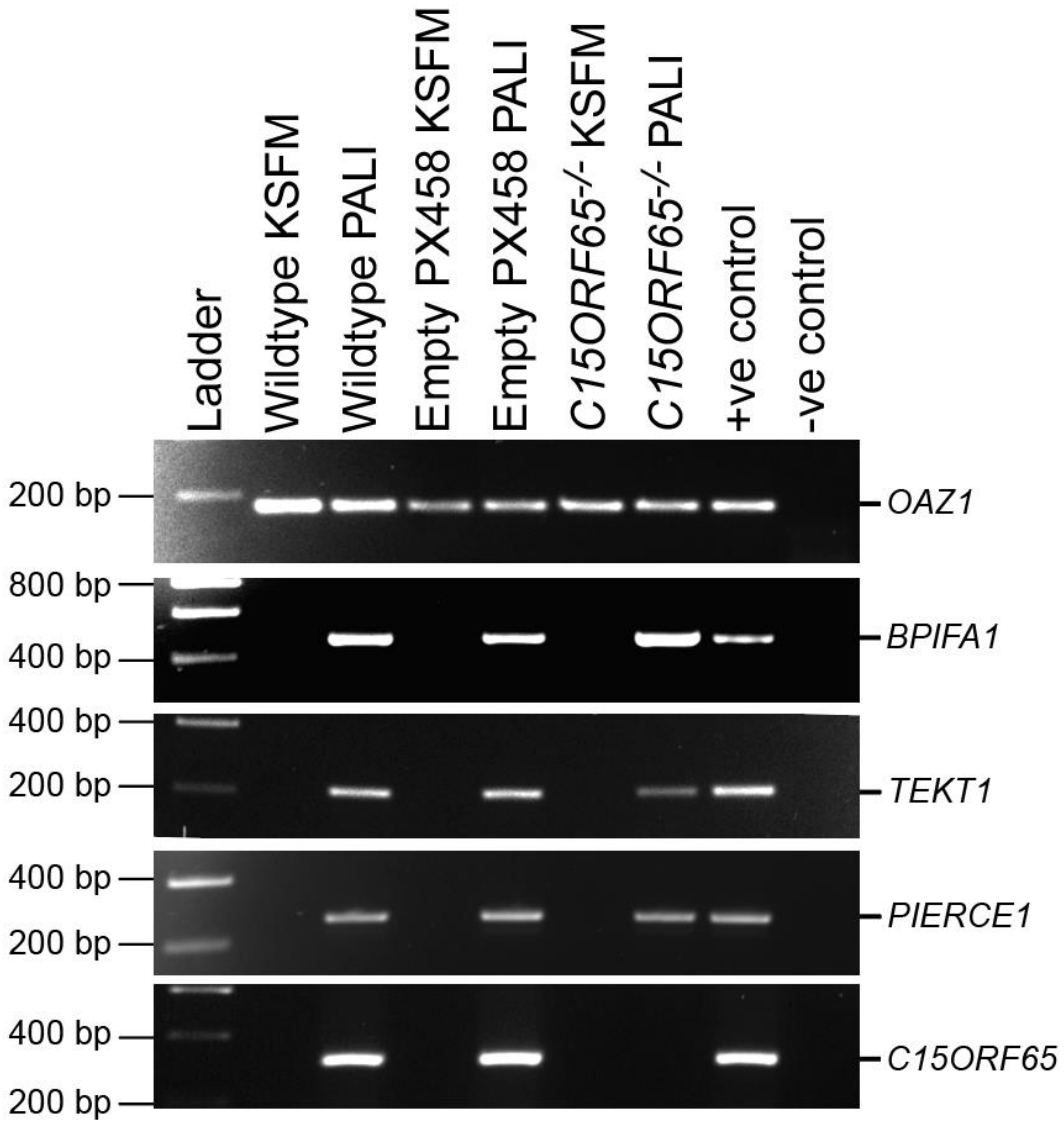

Figure 7.16 Expression of marker genes in *C15ORF65*$^{-/-}$ HBEC3-KT cells differentiated under submerged conditions. Cells of the indicated genotypes were grown with either KSFM or PALI media for 21 days and expression of marker genes was assessed with end-point RT-PCR. The gel is representative of n = 3 experiments.

Expression of *BPIFA1* and *TEKT1* were also detected in *PIERCE1*$^{-/-}$*C15ORF65*$^{-/-}$ when they were cultured with PALI media under submerged conditions for 21 days. This finding was particularly interesting as these cells failed to express *TEKT1* when they were differentiated at ALI (Figure 7.5). However, no mRNA for either *PIERCE1* or *C15ORF65* was detected in these *PIERCE1*$^{-/-}$*C15ORF65*$^{-/-}$ cells further validating their genotype (Figure 7.17).

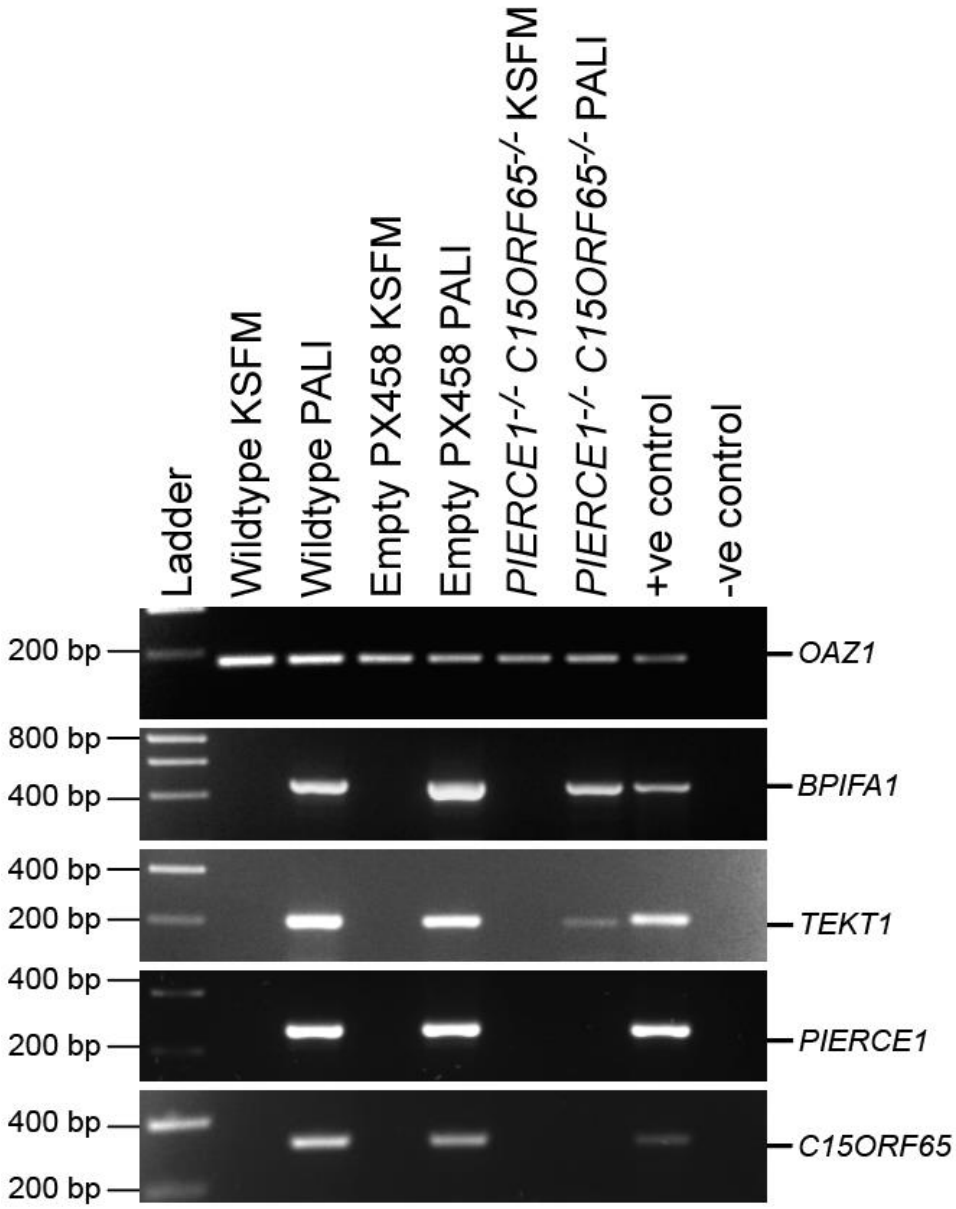

Figure 7.17 Expression of marker genes in *PIERCE1*$^{-/-}$*C15ORF65*$^{-/-}$ HBEC3-KT cells differentiated under submerged conditions. Cells of the indicated genotypes were grown with either KSFM or PALI media for 21 days and expression of marker genes was assessed with end-point RT-PCR. The gel is representative of n = 3 experiments.

7.4 Chapter discussion

A role of PIERCE1 in ciliogenesis was highlighted when *Pierce1*-null mice showed situs abnormality (Sung, Baek et al. 2016), but little was known about the role of PIERCE1 in cilia prior to the outset of my thesis. Data extracted from previously studies showed the upregulation of *PIERCE1* during *in vitro* mucociliary differentiation of human bronchial epithelial cells (Ross, Dailey et al. 2007), a 5.2-fold increase of *pierce1* expression in *foxj1a*-overexpressing zebrafish (Choksi, Babu et al. 2014), and expression and localisation of *PIERCE1* transcript mostly in ciliated cells (Plasschaert, Zilionis et al. 2018). More recently work from a prior student in our group suggested that DAPT could increase *Pierce1* expression in mTECs, PIERCE1 localisation in ciliated cells of the mouse trachea and loss of *PIERCE1* result in defective ciliary movement in Kupffer's vesicle as well as abnormal body situs in zebrafish (Anujan 2018). No information was available this time about the role of C15ORF65, a paralog of PIERCE1. During the courses of my studies, it was shown that FAP182, the PIERCE1 homolog in *Chlamydomonas reinhardtii*, is localised to the flagella (Ma, Stoyanova et al. 2019) and bovine PIERCE1 and C15ORF65 are located in the MIP complex of the ciliary axoneme (Gui, Farley et al. 2021). However, mice or zebrafish lacking either of these proteins can still produce cilia. When both genes were knocked-out, severe ciliopathy was found in zebrafish and embryonic lethality was observed in mice (Gui, Farley et al. 2021). Until now there have been no reports supporting a role of PIERCE1 and C15ORF65 in human cilia. I hypothesized that PIERCE1 and C15ORF65 participate in cilia formation and loss of one or both could cause defective ciliogenesis in the human airway epithelium.

To provide experimental support for this hypothesis, all the wildtype cells and knockout cells were cultured at ALI and/or under submerged conditions to investigate their mucociliary differentiation potential. The cells include the wildtype HBEC3-KT, HBEC3-KT cells transfected with empty PX458 plasmid, the FACS sorted plus clonally selected wildtype *PIERCE1*$^{+/+}$, *FOXJ1*$^{-/-}$, *FOXJ1*$^{\Delta FHD/\Delta FHD}$, *FOXJ1*$^{\Delta INS+G/\Delta INS+G}$, *PIERCE1*$^{-/-}$, *C15ORF65*$^{-/-}$, and *PIERCE1*$^{-/-}$*C15ORF65*$^{-/-}$ HBEC3-KT cells.

Wildtype, *PIERCE1*$^{-/-}$ and *C15ORF65*$^{-/-}$ cells produced potential progenitors of multiciliated cells at ALI, but such scenario was absent in *FOXJ1*$^{\Delta FHD/\Delta FHD}$ and *PIERCE1*$^{-/-}$*C15ORF65*$^{-/-}$ cells. *FOXJ1*$^{\Delta FHD/\Delta FHD}$ cells were differentiated into secretory cells but not into precursors of multiciliated cells. Such an observation was expected as loss of FHD would be expected to negate the function of FOXJ1 resulting in a loss of ciliogenesis. FOXJ1 is a master regulator for motile ciliogenesis (Yu, Ng et al. 2008) and *FOXJ1*$^{\Delta FHD/\Delta FHD}$ cells lack the DNA binding, FHD domain required for FOXJ1 function. The lack of FOXJ1 staining also suggested that any FOXJ1$^{\Delta FHD}$ produced by these cells could not be recognized by the antibody used for staining FOXJ1. In the case of *PIERCE1*$^{-/-}$*C15ORF65*$^{-/-}$ cells, the observation was particularly interesting as the absence of both genes produced immotile cilia in zebrafish whereas it was not possible to detect cilia in double mutant mice due to embryonic lethality (Gui, Farley et al. 2021). It therefore appears that loss of both *PIERCE1* and *C15ORF65* diminishes the capacity of HBEC3-KT cells to differentiate into precursors of multiciliated cells. Two possibilities can be considered for such an observation. Firstly, these cells could show a delay in the formation of the ciliary axoneme and/or secondly, at least one of these two genes are required for ciliogenesis. The latter would indicate a possible regulatory role for the genes in human cell ciliogenesis. Supporting roles for these proteins outside of the cilia axoneme, some nuclear staining for both proteins was detected (Figure 7.12 and Figure 7.13). Absence of *PIERCE1* expression in *PIERCE1*$^{-/-}$ and *PIERCE1*$^{-/-}$ *C15ORF65*$^{-/-}$ cells, and *C15ORF65* expression in *C15ORF65*$^{-/-}$ and *PIERCE1*$^{-/-}$ *C15ORF65*$^{-/-}$ cells after ALI differentiation validate the genotype of these knockout cells tested here. Similarly, expression of *C15ORF65* in *PIERCE1*$^{-/-}$ and *FOXJ1*$^{\Delta FHD/\Delta FHD}$ cells, and expression of *PIERCE1* in *C15ORF65*$^{-/-}$ and *FOXJ1*$^{\Delta FHD/\Delta FHD}$ cells suggested that the expression of these two genes could be independent of each other as well as FOXJ1. Unfortunately, limitation of resources and time restrictions from COVID-19-associated laboratory closure halted further experiments like immunoblotting and immunofluorescence microscopy studies on expression of PIERCE1, C15ORF65 and FOXJ1.

The differentiation potentials of all the cell types were consistent between the two cultured models (ALI vs submerged) except that *PIERCE1*$^{-/-}$*C15ORF65*$^{-/-}$ cells were

differentiated into ciliated cells and all *FOXJ1*-knockout cells expressed *TEKT1* when cultured with PALI. Though observation under brightfield microscope gave an impression of differentiation, all FOXJ1-kockout cell types produced secretory cells but not the precursors of multiciliated cells. This was expected as none of these cells encoded full-length *FOXJ1* required for the cell to undergo ciliogenesis. This is supported by the findings from immunofluorescence staining showing no detectable FOXJ1 in these cells further validating their genotypes. Hence, the process of ciliogenesis was stalled in these cells due to the lack of FOXJ1. Thereby, the partial or truncated FOXJ1 produced by the *FOXJ1*-knockout cells could be unstable and/or non-functional.

PIERCE1$^{-/-}$ and *C15ORF65*$^{-/-}$ cells were consistently differentiated into precursors of multiciliated cells in both ALI and submerged culture systems. Disparity in acetylated-α-TUBULIN expression of *PIERCE1*$^{-/-}$*C15ORF65*$^{-/-}$ cells between ALI and submerged culture could be due to i) difference between the number of days the cells were differentiated (day 14 of ALI vs day 21 of submerged culture), ii) direct exposure of PALI media during submerged culture which could affect the expression of acetylated-α-TUBULIN since the media contains part of human plasma, iii) the submerged condition itself. or iv) a combination of these. No staining of PIERCE1 in *PIERCE1*$^{-/-}$ and *PIERCE1*$^{-/-}$*C15ORF65*$^{-/-}$ cells and absence of C15ORF65 staining in *C15ORF65*$^{-/-}$ and *PIERCE1*$^{-/-}$*C15ORF65*$^{-/-}$ cells validated the antibodies, though noisy signal found in both cases that could be originated from insufficient blocking during immunostaining. However, the nuclear staining observed in the wildtype cells for both proteins could be originated from nuclear localisation of both proteins in cells other than multiciliated cells. Such localisation indicated possible function of these proteins in nucleus, *i.e.,* DNA damage response (Sung, Kim et al. 2010). The expression of *BPIFA1*, *PIERCE1* and *C15ORF65* were consistent between ALI cultured and PALI-cultured cells. The *PIERCE1*$^{-/-}$*C15ORF65*$^{-/-}$ cells seemed to be differentiated when grown under submerged conditions, thus could explain their expression of *TEKT1*. *TEKT1* expression seemed low in *FOXJ1*$^{\Delta FHD/\Delta FHD}$ cells as tested by end-point PCR, but qPCR is required to validate this further, and this is one of the limitations of using end-point PCR. Despite such expression of *TEKT1* in *FOXJ1*$^{\Delta FHD/\Delta FHD}$ cells, expression of *TEKT1* in *FOXJ1*-knockout cells could be

explained by i) *TEKT1* might not be a direct target of FOXJ1 (Jacquet, Salinas-Mondragon et al. 2009), or ii) direct exposure to PALI media might influence the expression of *TEKT1*. Thus, the observation of *TEKT1* expression in these cells suggests that it could be FOXJ1-independent.

In conclusion, *PIERCE1*$^{-/-}$ and *C15ORF65*$^{-/-}$ cells could be differentiated into precursors of multiciliated cells whereas the *FOXJ1*-knockout cells could not. Loss of acetylated-α-TUBULIN and FOXJ1 expression in the *PIERCE1*$^{-/-}$*C15ORF65*$^{-/-}$ cells suggests an important role for these genes in cilia that is only seen in the double knockout cells. Such findings indicate that PIERCE1 and C15ORF65 might supplement each other at least partially and complete loss of both of them could potentially disrupt cilia structure. In future, it would be interesting to evaluate any alteration of ciliary beating in the double knockout cells differentiated under submerged condition as compared to the wildtype. Also, electron micrograph of cross sections could be helpful to find out any structural defect in *PIERCE1*$^{-/-}$ *C15ORF65*$^{-/-}$ cilia.

Chapter 8: Discussion

8.1 Preface

PIERCE1 was discovered as the cell cycle-associated protein *RbEST47*, and its paralogue C15ORF65 was discovered as the fusion partner of major histocompatibility complex class II transactivator *BX648577* in lymphoid cancers (Sung, Kim et al. 2007, Steidl, Shah et al. 2011). Their association with cilia remained undiscovered until the finding that mice lacking *Pierce1* show left-right asymmetry (Sung, Baek et al. 2016) and diminished expression of *C15ORF65* in tetrazoospermia-associated male infertility (Zhang, Wu et al. 2018); as these conditions are often observed in ciliary defects (Ji, Sha et al. 2017, Brennan, Ferkol et al. 2021, Shoemark, Rubbo et al. 2021). A recent study published in late 2021 (towards the end of my studies) suggested the roles of PIERCE1 and C15ORF65 in bovine, mouse, and zebrafish cilia (Gui, Farley et al. 2021), however their function in human cilia remains unknown. Thereby, I hypothesized that PIERCE1 and C15ORF65 alone or in combination may have functional roles in human cilia. To test my hypothesis, I have chosen the RE as a model because ciliated cells are mostly present in the RE, such models can be developed *in vitro* through ALI culture and are used widely for mucociliary studies (Hirst, Rutman et al. 2010, Chen and Schoen 2019). The aim of this study was to rationalize *PIERCE1* and *C15ORF65* as putative cilia genes, validating an immortalized human cell line model for mucociliogenesis studies, and develop and study differentiation of *PIERCE1* and *C15ORF65* knockout cells along with *FOXJ1* as a control. Here, I summarise the significant findings of this study along with the limitations and future directions of this work.

8.2 Bioinformatic analysis to rationalize *PIERCE1* and *C15ORF65* as putative cilia genes

Before the beginning of any laboratory work, I first justified *PIERCE1* and *C15ORF65* as cilia-associated genes. One of the interesting preliminary findings was the conservation of both genes in vertebrates. Despite the fact that PIERCE1 homologs can be found in many lower animals like *Ciona intestinalis* (ascidian chordate), *Drosophila melanogaster* (arthropod) and *Chlamydomonas reinhardtii* (single-cell algae), C15ORF65 homologues were found only in tunicates, lancelets, and

bryozoans in addition to vertebrates. This is possibly due to lack of genome sequence availability or lack of this genes in organisms for which genome sequences are available (*Chlamydomonas reinhardtii* and *Drosophila melanogaster* for example) (Figure 8.1).

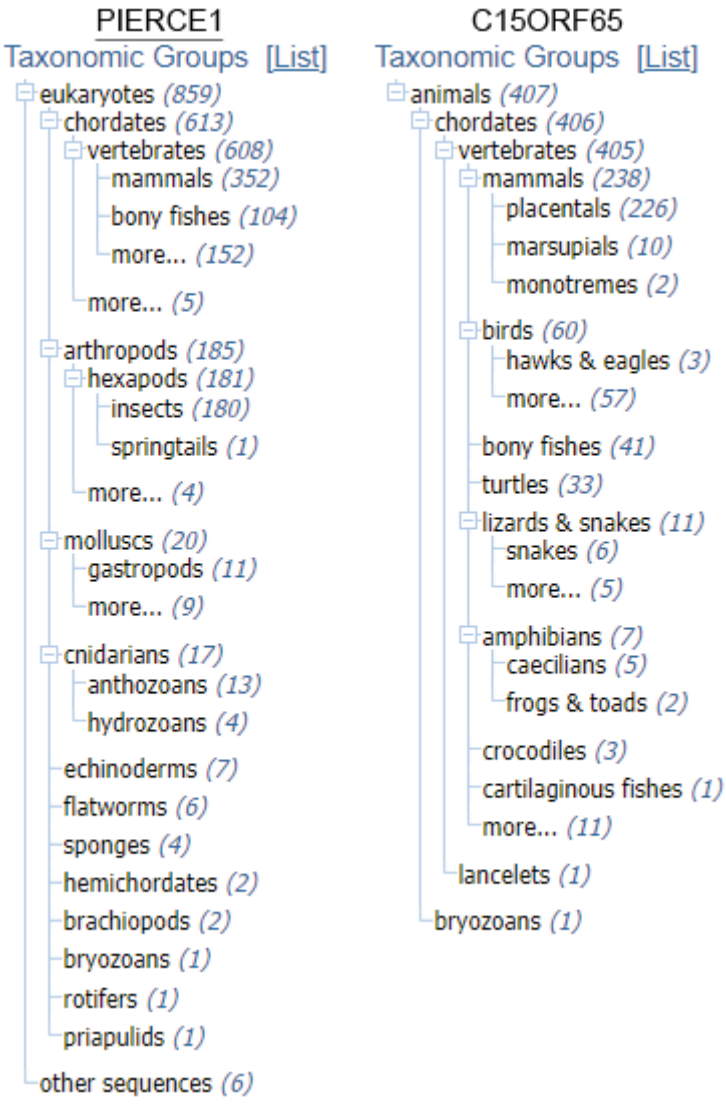

Figure 8.1 List of PIERCE1 and C15ORF65 homologues. The data is retrieved from NCBI. Other sequences include synthetic constructs. Link for PIERCE1: www.ncbi.nlm.nih.gov/protein/?term=c9orf116. Link for C15ORF65: www.ncbi.nlm.nih.gov/protein/?term=c15orf65

Thus, it can be hypothesized that PIERCE1 could be sufficient for supplementing C15ORF65 in lower animals, perhaps even in most of the non-vertebrates. Such hypothesis can explain the lack of any obvious phenotype in *C15orf65*$^{-/-}$ mice though tracheal cilia of these mice showed defective cilia structure, beat pattern, and

reduced beat frequency of nodal cilia (Gui, Farley et al. 2021). Thus, both genes could become more important in primates than in other animals during their course of evolution as suggested by their ML phylogenetic trees. Another important aspect of these proteins is the presence of a domain of unknown function DUF4490, which is considered as an identification mark for these proteins for homology searches. These are the only two proteins considered to possess such DUF4490 (El-Gebali, Mistry et al. 2019). To find an alternative motif to define these proteins and to differentiate them, I have identified two new motifs in PIERCE1 and one new motif in C15ORF65 as conserved domains using MUSCLE alignment. MUSCLE MSA performs more accurately than other aligner like ClustalW, T-COFFEE, Dialign and Kalign etc in shorter period of time (Edgar 2004). So, There is a possibility that these motifs might have functional implication (like supplementing each other) in PIERCE1 and C15ORF65 as the predicted structures of both motifs seemed similar. Most importantly the polyproline motif of PIERCE1 and a possible cysteine-cysteine intramolecular disulphide bond in the newly identified motif of C15ORF65 may affect their structure and thereby their function (Reis and Moraes 2019). In addition to these, the predicted weak glycosylation site 'NNTL' and phosphorylation site 'TA/GPD' could be associated with their function as these are sites for post-translational modification (Wang, Osgood et al. 2022). It is possible that PIERCE1 and C15ORF65 could have multiple functions even though they have no known functional motif. Such a suggestion could be supported by the fact that expression of PIERCE1 and C15ORF65 RNA or protein could be detected in multiple tissue that possess ciliary axonemes (Gui, Farley et al. 2021, Paranjapye, Leir et al. 2022). This study focuses only on the roles of these proteins in precursors of multiciliated cells.

The higher expression of these genes in tissues containing multiciliated epithelia like fallopian tube, testes, and respiratory epithelia, and the current understanding suggested that these transcripts are localised in the ciliated cells. Though immunohistochemical finding at HPA and DeepLoc analysis suggested that both proteins could be localised in the cytoplasm, a potential nuclear function for both proteins cannot be ignored as these proteins were detected in the nucleoplasm of cultured cells (Appendix J). Nonetheless, increased expression of these genes during the mucociliary differentiation of multiple murine multiciliated epithelia and in HBECs (Ross, Dailey et al. 2007), localisation of their transcripts in multiciliated cells

(Travaglini, Nabhan et al. 2020), and detection of these proteins in the bovine ciliary axoneme (Gui, Farley et al. 2021) strongly suggest that both proteins are involved with cilia function. Thereby, *PIERCE1* and *C15ORF65* could be considered as rationale cilia-associate genes. Based on the current literature and the current bioinformatic analysis, it is likely that PIERCE1 and C15ORF65 have functions in cilia. To validate this, I needed a model where I could do experiments to prove this, and I considered that the immortalized bronchial epithelial cell line HBEC3-KT could serve me well for this. Thus, I decided to validate the HBEC3-KT cell line for their mucociliary differentiation potential and their ability to express both *PIERCE1* and *C15ORF65*.

8.3 HBEC3-KT cells as a model to study mucociliogenesis

In vitro studies of RE cell differentiation have answered many fundamental biological questions in the field of respiratory biology, specifically in relation to mucus secretion, cilia function, respiratory infection, and differentiation pathways. Cell line models are very important tools to study the mucociliogenesis *in vitro*. This is because some cell lines can undergo mucociliary differentiation to produce multiple cell types found throughout the RE. Such *in vitro* models can help to validate the effect of different drugs, allow researchers to study the pathogenesis of infectious agents and can broaden the understanding of several biological processes (Chen and Schoen 2019, Michi and Proud 2021). Primary HBECs and human airway epithelial cells are two common cell types used to study mucociliogenesis, but their limited lifespan remains as a major obstacle. Many immortalized cell lines have been evaluated as an alternative to primary cells. HBEC3-KT cells can be considered as a useful immortalized cell line model as this cell line has retained multipotent capacity (Delgado, Kaisani et al. 2011, Stewart, Torr et al. 2012). Here, I have further validated the HBEC3-KT cells as a model for *in vitro* mucociliogenesis.

ALI culture is considered as the ideal *in vitro* condition to study the differentiation of RE cells as well as the biology of secretory and multiciliated cells (Caves, Cook et al. 2018, Jiang, Schaefer et al. 2018, Lee, Petris et al. 2020, Travaglini, Nabhan et al. 2020, Kouthouridis, Goepp et al. 2021). This is particularly because the ALI condition mimics the normal physiology where the cells are exposed to air at the apical surface and the distal surface remains in contact with the body fluid through lamina propria

(Peters-Hall, Coquelin et al. 2018). Two major differences between such ALI culture and the normal physiological condition to mention here are i) a polyester membrane with defined pore size (ideally 0.4 μm) serves as the lamina propria, and ii) undefined or partially defined media is used to provide the cells with nutrients and growth/differentiation factors. Primary HBECs start to differentiate immediately from the start of ALI in transwell permeable supports and the expression of genes associated with ciliogenesis boasts up by day 14, and eventually beating cilia becomes clearly visible (Ross, Dailey et al. 2007). Differentiation may continue after this time (Ross, Dailey et al. 2007). Thereby, I first validate the mucociliary differentiation potentiality of my HBEC3-KT cells at ALI. HBEC3-KT cells differentiated into potentially precursors of ciliated and secretory cells by day 14 at ALI as assessed by end-point PCR and immunostaining.

In parallel to this, I have also evaluated the differentiation capacity of HBEC3-KT cells under submerged conditions since there is a report suggesting that primary HBECs can also be differentiated under such conditions if oxygen remains available to the cells (Kouthouridis, Goepp et al. 2021). This is partly because hypoxia induced from too much submersion can reduce ciliogenesis through NOTCH-dependent manner as the cells only proliferate when cultured under such conditions (Gerovac, Valencia et al. 2014) (Figure 8.2). Since submerged condition does not mimic normal physiology at all and lacks apicobasal polarity, the published literature suggests culturing the cells at the ALI for their differentiation (Gerovac, Valencia et al. 2014, Polke, Seiler et al. 2017, Kouthouridis, Goepp et al. 2021). In my study, HBEC3-KT cells appeared to differentiate by day 14 of submerged culture and expression of FOXJ1 and acetylated α-TUBULIN was observed by immunostaining at day 21 (Figure 5.11). The γ-secretase inhibitor DAPT (*N*-[*N*-(3,5-Difluorophenacetyl)-L-Alanyl]-*S*-Phenylglycine *T*-butyl ester) is known to inhibit NOTCH signalling and promote multiciliated cell differentiation from the basal progenitor cells, and interleukin-13 (IL13) treatment could promote the differentiation of secretory cells from the basal progenitor cells (Gerovac and Fregien 2016, Eenjes, Mertens et al. 2018, Pongjantarasatian, Nowwarote et al. 2022). However, the effects of these agents were not obvious in HBEC3-KT grown under submerged condition. Possibly

the complete PALI media utilized for mucociliary differentiation in my study may already contain these as supplements.

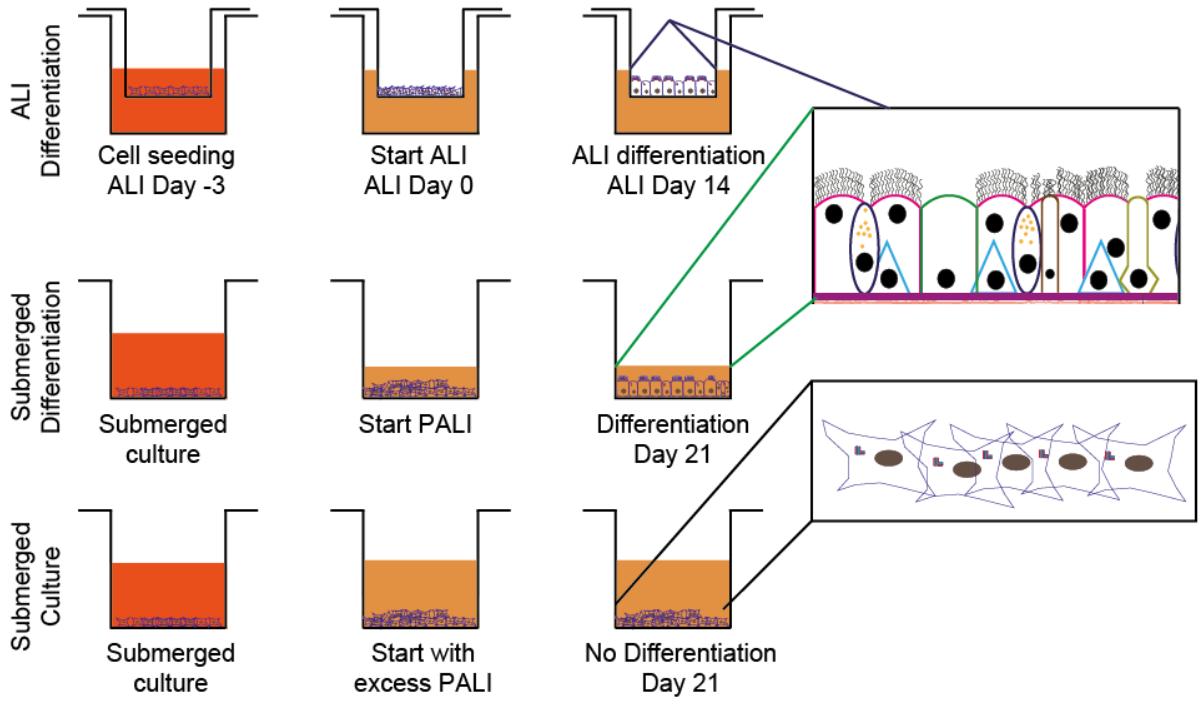

Figure 8.2 Mucociliary differentiation of HBECs at different conditions. HBECs can be differentiated into progenitors of both ciliated and secretory cells when cultured at ALI or with limited submersion by day 14. However, excess submersion can inhibit the process of differentiation.

Uniquely among other immortalized HBEC-KTs, HBEC3-KT cells showed increased expression of cell-cell adhesion-associated genes and such overexpression is particularly important in forming tight junctions required for mucociliary differentiation (Stewart, Torr et al. 2012). Transepithelial/endothelial electrical resistance (TEER) is a measure of electric resistance which could reflect the degree of tight junctions formed during mucociliary differentiation and TEER is increased during such differentiation (Stewart, Torr et al. 2012). Here, TEER was not measured but measuring the TEER in differentiated and undifferentiated HBEC3-KT may have been helpful to further validate their differentiation potentials. Beside TEER, video microscopy showing beating cilia and axonemal staining with cilia markers like ARL13B, RSPH4A, DNAH5 or acetylated α-TUBULIN could undoubtedly confirm the development of cilia in differentiated HBEC3-KT cells. It has been suggested that HBEC3-KT cells poorly produce ciliated cells in ALI culture covering around 5% of

the apical surface (Lodes, Seidensticker et al. 2020). The cilia beat frequency of HBEC3-KT cells was 6.9±0.1 Hz, whereas ciliated cell primary HBEC covered at least 60% of the apical surface with cilia and these had a beat frequency of 11.7±1.2 Hz (Lodes, Seidensticker et al. 2020). This is possibly due to overgrowth and piling of the cells on to each other (as they are not contact inhibited, and the cells were fed with fresh media every two days). Thus, measuring ciliary beat frequency or analysing cilia ultrastructure are difficult with HBEC3-KT cells, especially at day 14.

One important factor for *in vitro* mucociliary differentiation is the media used for cell proliferation and differentiation. Initial proliferation may affect the differentiation capacity of primary HBECs, specifically the mucociliary differentiation potentials increase when proliferated with a specialized media named EpiX (Zhang, Lee et al. 2018). I evaluated the effect of HBE3-KT cell initial expansion with KSFM and PneumaCult™ Ex plus media, and consistently the HBEC3-KT cells started to express secretory cell markers during their proliferation with PneumaCult™ Ex plus media, though they did not express cilia markers (such as *TEKT1*) with such media or KSFM media containing hydrocortisone. Therefore, I concluded that PneumaCult™ Ex plus media could enhance the mucociliary differentiation potentials of HBEC3-KT cells.

Some limitation of this study includes poor immunofluorescence images and lack of quantitative RT-PCR (qRT-PCR) data. End-point RT-PCR is a semi-quantitative process for gene expression evaluation, but less accurate and informative compared to qRT-PCR. Repeating all of the end-point RT-PCR experiments using qRT-PCR should be done in the future to confirm the data presented here. Though I used end-point RT-PCR to validate the gene expression during mucociliary differentiation of HBEC3-KT cells, I also considered two genes only, one for ciliated cells and one for secretory cells. The experiments could have included more genes, and at least two genes for ciliated cell as these cells were in my interest. *FOXJ1* should be considered as a marker gene to follow since it is considered as the master regulator for ciliogenesis (Yu, Ng et al. 2008). I tried to optimize the RT-PCR condition for *FOXJ1*, but these reactions never worked well possibly due to the high GC content of *FOXJ1* mRNA or the count of expressed mRNA in the samples could be too low to be detect. Published literature suggested qRT-PCR for *FOXJ1* expression analysis

(Gerovac, Valencia et al. 2014, Koay, Osterhof et al. 2021). Due to budget and time limitations, *FOXJ1* qRT-PCR was not done but could be completed in the future. Other genes to track ciliogenesis could be *MCIDAS* and *GMNC* as regulatory marker; and *RSPH4A* and *DNAH5* as structural marker.

I was able to show that differentiated HBEC3-KT cells, whether at ALI or under submerged condition, did express *PIERCE1* and *C15ORF65* and both PIERCE1 and C15ORF65 were localised in the potential progenitors of multiciliated cells, enabling these cells as a suitable model to study the roles of these proteins in cilia. Therefore, I used this cell line and hence knockout procedure for these genes was commenced in this cell line.

8.4 Development of gene-knockout HBEC3-KT cells

Gene-knockout cell lines and animals have been used to study the function of a gene and to model many human diseases, mainly based on studying the effect of gene loss-of-function. For a long time, most gene knockout models were developed by exploiting homologous recombination (Wang and Sun 2019). Recently discovered CRISPR-CAS9 technology is a quick, easy, and more efficient method to develop gene knockout models (Gupta, Bhattacharjee et al. 2019). In this technology, a short, engineered guide RNA with sequence complementary to a target region of DNA is introduced to bind the genomic region, and such duplex can be cleaved by CAS9 enzyme at a region named PAM (protospacer adjacent motifs) to produce double-strand DNA break (Yang, Ren et al. 2020). Since such breaks occurs in both homologous chromosomes, NHEJ serves as the DNA repair pathway that erroneously removes a portion of genomic DNA resulting in deletion mutation (Gupta, Bhattacharjee et al. 2019). Since, the binding of guide RNA is specific, the genomic DNA deletion also becomes specific during CRISPR-CAS9 gene editing.

A useful event happens when two guide RNAs separated by few hundred base pairs bind to the genome and become CAS9 targets. In such event, a dual double stand DNA breaks are formed resulting in a definitive NHEJ and thus a region of DNA separated by these guide RNAs are removed (Figure 8.3). Such an approach can effectively and efficiently excise a target gene from the genome without affecting other genes (Spagnuolo and Blenner 2021). Here, I used such dual guide RNA

approach as it can be used to make precise deletions more efficiently than single guide RNA approach and reduces the burden for off-target screening. For FOXJ1, I have used two such guide RNAs to delete a genomic region covering the codons for most part of the FHD.

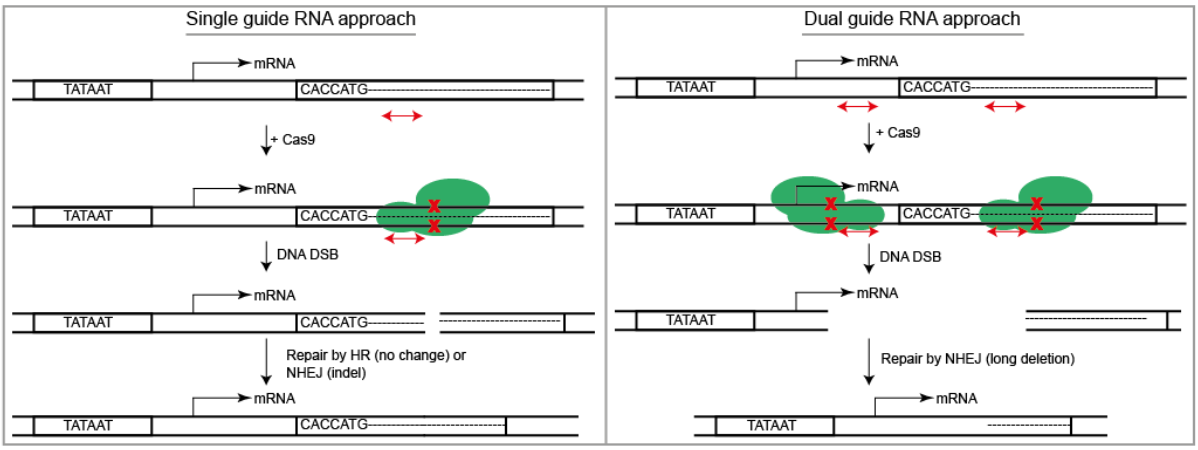

Figure 8.3 CRISPR-CAS9 gene editing using single or dual guide RNA approach. In single guide RNA approach, the gene editing depends on the mode of dsDNA break repair. But, non-homologous end joining serves as the major dsDNA break repair process resulting in a longer deletion.

Guide RNAs to edit these genes could be cloned in two different popular plasmids containing humanized *Streptococcus pyogenes CAS9*, one is PX458 that contains GFP as a marker and another is PX459 that contains Puromycin^{R} as a selection marker as developed by Dr Feng Zhang (Ran, Hsu et al. 2013). However, repeated attempts to undertake Puromycin^{R} selection of HBEC KT cells failed (data not shown) due to previous transgenesis of Puromycin^{R} in these cells during their development (Ramirez, Sheridan et al. 2004). Therefore, only the GFP selection procedure was followed to sort the transfected cells containing guide RNA.

Three different *FOXJ1*-knockout HBEC3-KT cells were developed in this study. Among them, *FOXJ1*$^{\Delta FHD/\Delta FHD}$ was the cell line of interest and the other two, namely *FOXJ1*$^{-/-}$ and *FOXJ1*$^{\Delta INS+G/\Delta INS+G}$, were obtained as by-products during the development of *FOXJ1*$^{\Delta FHD/\Delta FHD}$. This illustrates the fact that gene editing using this system can produce multiple mutations from the same gRNAs. No functional FOXJ1 could be produced from these clones as predicted by bioinformatic analysis based on the sequencing results. My study primarily focused *FOXJ1*$^{\Delta FHD/\Delta FHD}$ HBEC3-KT

cells as these cells contain a precise deletion of FHD allowing the functional studies involving FHD in future. Similarly, *PIERCE1*$^{-/-}$, *C15ORF65*$^{-/-}$, and *PIERCE1*$^{-/-}$ *C15ORF65*$^{-/-}$ HBEC3-KT cells were developed for the functional studies in cilia development. However, the full-length cDNAs produced by all these cells were not sequenced or analysed by PCR as these cells were originated from monoclones which lacked the full-length gene. Hence, a full-length cDNA for the respective genes in the knockout cells would be expected to be absent. Nonetheless the predicted protein structures for the respective clones lacked functional motifs required for their function, or it seems that the mRNA would fail to produce a protein due to lack of Kozak sequence.

Some issues could be considered regarding these monoclones like i) population bottleneck during the selection of monoclones (Hanack, Messerschmidt et al. 2016), ii) spontaneous gain or accumulation of mutations during the process of development of cultures (Kuijk, Jager et al. 2020), ii) possible off-targets by the designed guide RNAs (Grunewald, Zhou et al. 2019), and iv) generation of an altered protein with different function (Cheng, Dong et al. 2019). Since the concept of population bottleneck is an inherent characteristic of monoclonal selection, and sudden gain of mutation is almost unavoidable, these two phenomena should be considered acceptable and whole genome sequencing of the monoclones should be done to find out the genomic similarity of the monoclones with wildtype cells capable of expressing genes associated with mucociliary differentiation. On the other hand, the designed guide RNAs were considered highly specific and use of dual guide RNAs for the development of knockout cells further reduced the possibility of off-target generation during the gene-editing procedure. Bioinformatic analyses suggested no known function for the possible altered proteins in the knockout cells. Thus, it can be considered that the monoclones would exhibit only the loss of function of the target genes (*FOXJ1*, *PIERCE1* or *C15ORF65*) and these monoclonal knockout cells should be suitable for studying their function.

I have tried to detect FOXJ1, PIERCE1 and C15ORF65 by immunoblotting using differentiated HBEC3-KT cell samples, but I could not detect any of them. This is possibly due to i) few precursors of ciliated HBEC3-KT cells in the cultures limiting the detection threshold for FOXJ1 in immunoblot, and ii) the lack of suitable

antibodies for PIERCE1 and C15ORF65 for immunoblotting application. However, the absence of FOXJ1, PIERCE1, and C15ORF65 was validated by immunofluorescence microscopy but such evidence is not considered as conclusive as immunoblotting that also allows to visualize the size of the detected protein. In summary, I generated partially validated three different *FOXJ1*-knockout and *PIERCE1*$^{-/-}$, *C15ORF65*$^{-/-}$, and *PIERCE1*$^{-/-}$*C15ORF65*$^{-/-}$ HBEC3-KT cells. These cells could serve as tools to determine their function in cilia. There, I have differentiated these cells both at ALI and under submerged condition to experiment their role during ciliogenesis in two different conditions.

8.5 Differentiation of the knockout cells

Since differentiated wildtype HBEC3-KT *FOXJ1*, *PIERCE1* and *C15ORF65* were expressed in potential progenitors of ciliated cells, mucociliary differentiation of wildtype and knockout cells could justify the ciliogenic capacity and could evaluate the phenotype of the knockout cells. My finding in chapter 5 suggested that the mucociliary differentiation of HBEC3-KT cells could differ between ALI and submerged culture as the expression of *PIERCE1* and *C15ORF65* was delayed, and acetylated α-TUBULIN staining was visualized a week later under submerged conditions (Figure 5.2, Figure 5.3, Figure 5.10, and Figure 5.11). It is unclear why such delay happens in submerged cultured cells. I decided to differentiate all the knockout cells along with wildtype and controls under both ALI and submerged conditions. As a control, *FOXJ1*$^{\Delta FHD/\Delta FHD}$ cells failed to express markers of ciliated cells at both conditions as expected. This is due to the absolute requirement of FOXJ1 in multiciliogenesis (Yu, Ng et al. 2008). The wildtype and control *PIERCE1*$^{+/+}$ cells differentiated into progenitor multiciliated cells at both ALI and submerged condition. Expression of *PIERCE1*, *C15ORF65* and FOXJ1 in *FOXJ1*$^{\Delta FHD/\Delta FHD}$, *PIERCE1*$^{-/-}$ and *C15ORF65*$^{-/-}$ cells after differentiation at ALI or submerged condition indicated that the expression of these three genes could be independent of each other. Unfortunately, I could not differentiate the *FOXJ1*$^{-/-}$ and *FOXJ1*$^{\Delta INS+G/\Delta INS+G}$ cells at ALI culture due to lack of transwell inserts. However, it can be expected that the phenotypes of ALI-cultured *FOXJ1*$^{\Delta FHD/\Delta FHD}$, *FOXJ1*$^{-/-}$ and *FOXJ1*$^{\Delta INS+G/\Delta INS+G}$ cells would be comparable.

Both *PIERCE1*$^{-/-}$ and *C15ORF65*$^{-/-}$ HBEC3-KT cells could differentiate into acetylated α-TUBULIN-positive cells under both ALI and submerged conditions. *PIERCE1*$^{-/-}$ *C15ORF65*$^{-/-}$ HBEC3-KT cells also expressed FOXJ1 and could differentiate into acetylated α-TUBULIN-positive cells under submerged condition, but they failed to do so when they were differentiated at ALI. It is unclear why these dual knockout cells do so, but such a finding is particularly interesting as *pierce1*$^{-/-}$*c15orf65*$^{-/-}$ zebrafish do form paralysed cilia in the Kupffer's vesicle where these cilia remain under submerged condition, and *Pierce1*$^{-/-}$*C15orfF65*$^{-/-}$ mice do survive up to 20 days (Gui, Farley et al. 2021). Perhaps motile cilia exposed to air (similar to ALI condition) could be more affected than motile cilia under submerged condition due to the loss of both of genes. In addition to these, nuclear or other cytosolic functions of PIERCE1 and C15ORF65 cannot be ignored since both proteins were detected in the nucleus and some staining of the proteins did not co-localise with acetylated α-TUBULIN. It is still unknown how these proteins can be localised to the ciliary axoneme. Updated Interactome3D (Mosca, Ceol et al. 2013, Luck, Kim et al. 2020) data suggested that PIERCE1 could interact with HSPA8 and FHL3, where C15ORF65 could interact with FHL3 through QRICH1 (Luck, Kim et al. 2020). It can be predicted that these proteins could be carried to the ciliary axoneme with the help of these proteins or by unknown factor(s) and additional PIERCE1 and C15ORF65 could localise in the nucleus or remain in the cytoplasm (Figure 8.4).

Though expression of *TEKT1* was reduced as observed by end-point PCR in *PIERCE1*$^{-/-}$*C15ORFF65*$^{-/-}$ and *FOXJ1*$^{\Delta FHD/\Delta FHD}$ HBEC3-KT cells differentiated under submerged condition, this should be further validated by qPCR. Beside such limitations, number of progenitor ciliated cells in submerged differentiated *PIERCE1*$^{-/-}$ *C15ORFF65*$^{-/-}$, *PIERCE1*$^{-/-}$*C15ORFF65*$^{-/-}$, and *PIERCE1*$^{-/-}$*C15ORFF65*$^{-/-}$ cells could be estimated by means of qPCR using cilia-specific markers like *TEKT1*, or by counting the FOXJ1-positive cells under immunofluorescence microscopy. Such data from knockout and wildtype cells could be compared with each other to see whether there is any difference or not. Also, the difference in ciliary axonemal development between wildtype and knockout cells could determine by electron microscopy. Such experiments can clarify whether the loss of PIERCE1 and C15ORF65 alone or in combination could affect the development of ciliary axoneme or not. In addition,

electron microscopy could be carried out to detect any defective outer dynein arm in ciliary axoneme of these cells. Despite the limitations of my data, it can be concluded that loss of both PIERCE1 and C15ORF65 might affect the development of progenitor ciliated cells.

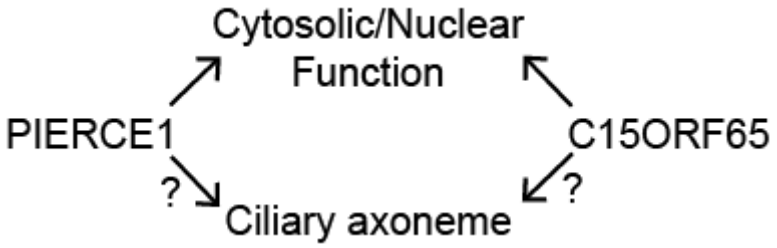

Figure 8.4: Predicting the functions of PIERCE1 and C15ORF65. Both PIERCE1 and C15ORF65 can be localised to the ciliary axoneme, and such localisation could be regulated by unknown factor(s). In addition, these proteins might play roles in the nucleus/cytoplasm.

8.6 Future directions

In the future, qPCR could be conducted to quantitate differences in expression of *TEKT1, FOXJ1, PIERCE1* and *C15ORF65* between HBEC3-KT cells and the knockout cells with undifferentiated, ALI and submerged differentiated samples. Ideally, all of the immunofluorescence microscopic analysis could be repeated with confocal or super-resolution microscopy imaging to obtain better images. Such studies would further strengthen the findings of this study. The phenotypic validation of knockout cells generated in this thesis could be carried out further if a newer antibody is available and by differentiating these cells in relatively large scale (in a 6-well plate insert) to prepare protein samples for western blot. One of the limitations of my study that needs to be addressed is the issue of the length of time that the cells underwent ALI differentiation. Most of my studies were performed using the period of 14-21 days of airlift. This may not be long enough for cells to become fully ciliated. In future, all the cells can be differentiated for longer period (>28 days) with or without using a feeder layer in purpose to observe ciliary beating. If ciliary beating is observed, then the number of cilia, ciliary axonemal length and ciliary beat frequency could be assessed. Then analyses can be carried out to see whether there is a difference in any of these parameters between ALI and submerged cultured cells, for both wildtype and knockout cells. Dissecting the differentially expressed genes

involved with mucociliogenesis or ciliary differentiation by RNA-seq or single-cell RNA-seq in HBEC3-KT cells grown under two different conditions (ALI and submerged) could also reveal novel insights of these process. Furthermore, comparative analysis of ciliome and secretome could be carried out between differentiated HBEC3-KT cells and primary HBECs. Using the *FOXJ1*-knockout cells, FOXJ1 target genes could also be defined in HBEC3-KT cells by comparing genome-wide transcriptome of these knockout cells with wildtype cells. The direct or indirect roles of PIERCE1 and C15ORF65 as transcription factors could be explored also by comparing the transcriptome of individual or dual *PIERCE1* and *C15ORF65* knockout cells with wildtype HBEC3-KT cells.

The roles of PIERCE1 and C15ORF65 in ciliogenesis could be explored further by knocking out these genes in primary HBEC using recently developed CRISPR/CAS9 ribonucleoprotein complex system (Thongsin and Wattanapanitch 2022). In addition to these, association of *PIERCE* and *C15ORF65* with human ciliopathies can be explored further by suggesting genetic tests for these genes in cases whether the causative mutation is unknown or by searching in exome sequencing data to identify mutations. Table 8.1 lists human diseases those could be associated with PIERCE1 and C15ORF65 (Grissa, Junge et al. 2022).

Table 8.1: List of diseases potentially to be associated with *PIERCE1* or *C15ORF65* mutation. ★ signifies the association of disease with the gene, where ★★★★★ is the highest confidence and ★☆☆☆☆ is the lowest (Grissa, Junge et al. 2022).

PIERCE1		**C15ORF65**	
Name	Confidence	Name	Confidence
Situs inversus	★★★☆☆	Hodgkin's lymphoma	★★☆☆☆
Dextrocardia	★★★☆☆	Diffuse large B-cell lymphoma	★★☆☆☆
Cone-rod dystrophy	★★☆☆☆	Dextrocardia	★★☆☆☆
Facial neuralgia	★★☆☆☆	Congenital toxoplasmosis	★★☆☆☆
Ciliopathy	★★☆☆☆	Ciliopathy	★☆☆☆☆

8.7 Concluding remarks

Multiciliogenesis is critically important to maintain the normal respiratory, reproductive, and cerebrospinal fluid movement; and abnormalities of multiciliogenesis can give rise to a number of human diseases (Hyland and Brody 2021). Despite being of such importance, the process of multiciliogenesis still remains to be fully understood. The current study could shed light in understanding the functions of *PIERCE1* and *C15ORF65* in ciliogenesis. This thesis clarified the association of these genes with cilia and showed that loss of both genes could affect the formation of progenitor ciliated cells in HBEC3-KT cells differentiated in ALI culture and may be associated with the process of multiciliation.

Chapter 9: References

Abraham, G., C. Zizzadoro, J. Kacza, C. Ellenberger, V. Abs, J. Franke, H. A. Schoon, J. Seeger, Y. Tesfaigzi and F. R. Ungemach (2011). "Growth and differentiation of primary and passaged equine bronchial epithelial cells under conventional and air-liquid-interface culture conditions." BMC Vet Res **7**: 26.

Acevedo, J. M., B. Hoermann, T. Schlimbach and A. A. Teleman (2018). "Changes in global translation elongation or initiation rates shape the proteome via the Kozak sequence." Sci Rep **8**(1): 4018.

Adikusuma, F., C. Pfitzner and P. Q. Thomas (2017). "Versatile single-step-assembly CRISPR/Cas9 vectors for dual gRNA expression." PLoS One **12**(12): e0187236.

Al Jord, A., N. Spassky and A. Meunier (2019). "Motile ciliogenesis and the mitotic prism." Biol Cell **111**(8): 199-212.

Alford, L. M., D. Stoddard, J. H. Li, E. L. Hunter, D. Tritschler, R. Bower, D. Nicastro, M. E. Porter and W. S. Sale (2016). "The nexin link and B-tubule glutamylation maintain the alignment of outer doublets in the ciliary axoneme." Cytoskeleton (Hoboken) **73**(7): 331-340.

Almagro Armenteros, J. J., C. K. Sonderby, S. K. Sonderby, H. Nielsen and O. Winther (2017). "DeepLoc: prediction of protein subcellular localization using deep learning." Bioinformatics **33**(24): 4049.

Ando, H., M. Kobayashi, S. Toda, F. Kikkawa, T. Masahashi and S. Mizutani (2000). "Establishment of a ciliated epithelial cell line from human Fallopian tube." Hum Reprod **15**(7): 1597-1603.

Antony, D., A. Becker-Heck, M. A. Zariwala, M. Schmidts, A. Onoufriadis, M. Forouhan, R. Wilson, T. Taylor-Cox, A. Dewar, C. Jackson, P. Goggin, N. T. Loges, H. Olbrich, M. Jaspers, M. Jorissen, M. W. Leigh, W. E. Wolf, M. L. Daniels, P. G. Noone, T. W. Ferkol, S. D. Sagel, M. Rosenfeld, A. Rutman, A. Dixit, C. O'Callaghan, J. S. Lucas, C. Hogg, P. J. Scambler, R. D. Emes, Uk10k, E. M. Chung, A. Shoemark, M. R. Knowles, H. Omran and H. M. Mitchison (2013). "Mutations in CCDC39 and CCDC40 are the major cause of primary ciliary dyskinesia with axonemal disorganization and absent inner dynein arms." Hum Mutat **34**(3): 462-472.

Antony, D., H. G. Brunner and M. Schmidts (2021). "Ciliary Dyneins and Dynein Related Ciliopathies." Cells **10**(8).

Anujan, P. (2018). "Functional analysis of novel protein, Pierce1, in motile ciliogenesis." PhD Thesis. University of Sheffield, UK.

Arbi, M., D. E. Pefani, C. Kyrousi, M. E. Lalioti, A. Kalogeropoulou, A. D. Papanastasiou, S. Taraviras and Z. Lygerou (2016). "GemC1 controls multiciliogenesis in the airway epithelium." EMBO Rep **17**(3): 400-413.

Arbi, M., D. E. Pefani, S. Taraviras and Z. Lygerou (2018). "Controlling centriole numbers: Geminin family members as master regulators of centriole amplification and multiciliogenesis." Chromosoma **127**(2): 151-174.

Arquint, C. and E. A. Nigg (2016). "The PLK4-STIL-SAS-6 module at the core of centriole duplication." Biochem Soc Trans **44**(5): 1253-1263.

Arumugam, T. V., S. L. Chan, D. G. Jo, G. Yilmaz, S. C. Tang, A. Cheng, M. Gleichmann, E. Okun, V. D. Dixit, S. Chigurupati, M. R. Mughal, X. Ouyang, L. Miele, T. Magnus, S. Poosala, D. N. Granger and M. P. Mattson (2006). "Gamma secretase-mediated Notch signaling worsens brain damage and functional outcome in ischemic stroke." Nat Med **12**(6): 621-623.

Avasthi, P. and W. F. Marshall (2012). "Stages of ciliogenesis and regulation of ciliary length." Differentiation **83**(2): S30-42.

Baehr, W., C. Hanke-Gogokhia, A. Sharif, M. Reed, T. Dahl, J. M. Frederick and G. Ying (2018). "Insights into photoreceptor ciliogenesis revealed by animal models." Prog Retin Eye Res.

Balestra, F. R. and P. Gonczy (2014). "Multiciliogenesis: multicilin directs transcriptional activation of centriole formation." Curr Biol **24**(16): R746-749.
Barrett, T., S. E. Wilhite, P. Ledoux, C. Evangelista, I. F. Kim, M. Tomashevsky, K. A. Marshall, K. H. Phillippy, P. M. Sherman, M. Holko, A. Yefanov, H. Lee, N. Zhang, C. L. Robertson, N. Serova, S. Davis and A. Soboleva (2013). "NCBI GEO: archive for functional genomics data sets--update." Nucleic Acids Res **41**(Database issue): D991-995.
Barry, P. J. and J. L. Taylor-Cousar (2021). "Triple combination cystic fibrosis transmembrane conductance regulator modulator therapy in the real world - opportunities and challenges." Curr Opin Pulm Med **27**(6): 554-566.
Bastin, B. R. and S. Q. Schneider (2019). "Taxon-specific expansion and loss of tektins inform metazoan ciliary diversity." BMC Evol Biol **19**(1): 40.
Beales, P. and P. K. Jackson (2012). "Cilia - the prodigal organelle." Cilia **1**(1): 1.
Beedle, A. E. M., M. Mora, C. T. Davis, A. P. Snijders, G. Stirnemann and S. Garcia-Manyes (2018). "Forcing the reversibility of a mechanochemical reaction." Nat Commun **9**(1): 3155.
Bergmann, C. (2012). "Educational paper: ciliopathies." Eur J Pediatr **171**(9): 1285-1300.
Billipp, T. E., M. S. Nadjsombati and J. von Moltke (2021). "Tuning tuft cells: new ligands and effector functions reveal tissue-specific function." Curr Opin Immunol **68**: 98-106.
Blackburn, K., X. Bustamante-Marin, W. Yin, M. B. Goshe and L. E. Ostrowski (2017). "Quantitative Proteomic Analysis of Human Airway Cilia Identifies Previously Uncharacterized Proteins of High Abundance." J Proteome Res **16**(4): 1579-1592.
Blouin, J. L., M. Meeks, U. Radhakrishna, A. Sainsbury, C. Gehring, G. D. Sail, L. Bartoloni, V. Dombi, A. O'Rawe, A. Walne, E. Chung, B. A. Afzelius, M. Armengot, M. Jorissen, D. V. Schidlow, L. van Maldergem, H. Walt, R. M. Gardiner, D. Probst, P. A. Guerne, C. D. Delozier-Blanchet and S. E. Antonarakis (2000). "Primary ciliary dyskinesia: a genome-wide linkage analysis reveals extensive locus heterogeneity." Eur J Hum Genet **8**(2): 109-118.
Blue, E., T. L. Louie, J. X. Chong, S. J. Hebbring, K. C. Barnes, N. M. Rafaels, M. R. Knowles, R. L. Gibson, M. J. Bamshad, M. J. Emond, L. U.S. National Heart and P. Blood Institute "Grand Opportunity" Exome Sequencing (2018). "Variation in Cilia Protein Genes and Progression of Lung Disease in Cystic Fibrosis." Ann Am Thorac Soc **15**(4): 440-448.
Bonnelykke, K., P. Sleiman, K. Nielsen, E. Kreiner-Moller, J. M. Mercader, D. Belgrave, H. T. den Dekker, A. Husby, A. Sevelsted, G. Faura-Tellez, L. J. Mortensen, L. Paternoster, R. Flaaten, A. Molgaard, D. E. Smart, P. F. Thomsen, M. A. Rasmussen, S. Bonas-Guarch, C. Holst, E. A. Nohr, R. Yadav, M. E. March, T. Blicher, P. M. Lackie, V. W. Jaddoe, A. Simpson, J. W. Holloway, L. Duijts, A. Custovic, D. E. Davies, D. Torrents, R. Gupta, M. V. Hollegaard, D. M. Hougaard, H. Hakonarson and H. Bisgaard (2014). "A genome-wide association study identifies CDHR3 as a susceptibility locus for early childhood asthma with severe exacerbations." Nat Genet **46**(1): 51-55.
Boon, M., J. Wallmeier, L. Ma, N. T. Loges, M. Jaspers, H. Olbrich, G. W. Dougherty, J. Raidt, C. Werner, I. Amirav, A. Hevroni, R. Abitbul, A. Avital, R. Soferman, M. Wessels, C. O'Callaghan, E. M. Chung, A. Rutman, R. A. Hirst, E. Moya, H. M. Mitchison, S. Van Daele, K. De Boeck, M. Jorissen, C. Kintner, H. Cuppens and H. Omran (2014). "MCIDAS mutations result in a mucociliary clearance disorder with reduced generation of multiple motile cilia." Nat Commun **5**: 4418.
Boudewijns, E. A., G. R. Babu, S. Salvi, A. Sheikh and O. C. van Schayck (2018). "Chronic obstructive pulmonary disease: a disease of old age?" J Glob Health **8**(2): 020306.
Bregeat, P. (1986). "Remarks on the practice of medicine in its specialties." Bull Acad Natl Med **170**(7): 973-975.
Brennan, S. K., T. W. Ferkol and S. D. Davis (2021). "Emerging Genotype-Phenotype Relationships in Primary Ciliary Dyskinesia." Int J Mol Sci **22**(15).
Breslow, D. K. and A. J. Holland (2019). "Mechanism and Regulation of Centriole and Cilium Biogenesis." Annu Rev Biochem **88**: 691-724.
Brooks, E. R. and J. B. Wallingford (2015). "In vivo investigation of cilia structure and function using Xenopus." Methods Cell Biol **127**: 131-159.

Budamagunta, M. S., F. Guo, N. Sun, B. Shibata, P. G. FitzGerald, J. C. Voss and J. F. Hess (2018). "Production of recombinant human tektin 1, 2, and 4 and in vitro assembly of human tektin 1." Cytoskeleton (Hoboken) **75**(1): 3-11.

Bujakowska, K. M., Q. Liu and E. A. Pierce (2017). "Photoreceptor Cilia and Retinal Ciliopathies." Cold Spring Harb Perspect Biol **9**(10).

Bukowy-Bieryllo, Z., P. Daca-Roszak, J. Jurczak, H. Przystalowska-Maciola, R. Jaksik, M. Witt and E. Zietkiewicz (2022). "In vitro differentiation of ciliated cells in ALI-cultured human airway epithelium - The framework for functional studies on airway differentiation in ciliopathies." Eur J Cell Biol **101**(1): 151189.

Bult, C. J., J. A. Blake, C. L. Smith, J. A. Kadin, J. E. Richardson and G. Mouse Genome Database (2019). "Mouse Genome Database (MGD) 2019." Nucleic Acids Res **47**(D1): D801-D806.

Bustamante-Marin, X. M. and L. E. Ostrowski (2017). "Cilia and Mucociliary Clearance." Cold Spring Harb Perspect Biol **9**(4).

Butterfield, R. (2017). "Primary Ciliary Dyskinesia." Pediatr Rev **38**(3): 145-146.

Byers, L. A., L. Diao, J. Wang, P. Saintigny, L. Girard, M. Peyton, L. Shen, Y. Fan, U. Giri, P. K. Tumula, M. B. Nilsson, J. Gudikote, H. Tran, R. J. Cardnell, D. J. Bearss, S. L. Warner, J. M. Foulks, S. B. Kanner, V. Gandhi, N. Krett, S. T. Rosen, E. S. Kim, R. S. Herbst, G. R. Blumenschein, J. J. Lee, S. M. Lippman, K. K. Ang, G. B. Mills, W. K. Hong, J. N. Weinstein, Wistuba, II, K. R. Coombes, J. D. Minna and J. V. Heymach (2013). "An epithelial-mesenchymal transition gene signature predicts resistance to EGFR and PI3K inhibitors and identifies Axl as a therapeutic target for overcoming EGFR inhibitor resistance." Clin Cancer Res **19**(1): 279-290.

Canty, J. T., R. Tan, E. Kusakci, J. Fernandes and A. Yildiz (2021). "Structure and Mechanics of Dynein Motors." Annu Rev Biophys **50**: 549-574.

Carraro, G., J. Langerman, S. Sabri, Z. Lorenzana, A. Purkayastha, G. Zhang, B. Konda, C. J. Aros, B. A. Calvert, A. Szymaniak, E. Wilson, M. Mulligan, P. Bhatt, J. Lu, P. Vijayaraj, C. Yao, D. W. Shia, A. J. Lund, E. Israely, T. M. Rickabaugh, J. Ernst, M. Mense, S. H. Randell, E. K. Vladar, A. L. Ryan, K. Plath, J. E. Mahoney, B. R. Stripp and B. N. Gomperts (2021). "Transcriptional analysis of cystic fibrosis airways at single-cell resolution reveals altered epithelial cell states and composition." Nat Med **27**(5): 806-814.

Carter, A. P., A. G. Diamant and L. Urnavicius (2016). "How dynein and dynactin transport cargos: a structural perspective." Curr Opin Struct Biol **37**: 62-70.

Carvalho-Santos, Z., J. Azimzadeh, J. B. Pereira-Leal and M. Bettencourt-Dias (2011). "Tracing the origins of centrioles, cilia, and flagella." The Journal of Cell Biology **194**(2): 165-175.

Caves, E. A., S. A. Cook, N. Lee, D. Stoltz, S. Watkins and K. H. Y. Shair (2018). "Air-Liquid Interface Method To Study Epstein-Barr Virus Pathogenesis in Nasopharyngeal Epithelial Cells." mSphere **3**(4).

Chalmers, J. D., A. B. Chang, S. H. Chotirmall, R. Dhar and P. J. McShane (2018). "Bronchiectasis." Nat Rev Dis Primers **4**(1): 45.

Chan, D. W., C. Y. Chan, J. W. Yam, Y. P. Ching and I. O. Ng (2006). "Prickle-1 negatively regulates Wnt/beta-catenin pathway by promoting Dishevelled ubiquitination/degradation in liver cancer." Gastroenterology **131**(4): 1218-1227.

Chandrasekaran, A., S. Kouthouridis, W. Lee, N. Lin, Z. Ma, M. J. Turner, J. W. Hanrahan and C. Moraes (2019). "Magnetic microboats for floating, stiffness tunable, air-liquid interface epithelial cultures." Lab Chip.

Chang, E. H., A. L. Willis, H. C. McCrary, G. T. Noutsios, C. H. Le, A. G. Chiu, C. J. Mansfield, D. R. Reed, S. G. Brooks, N. D. Adappa, J. N. Palmer, N. G. Cohen, D. A. Stern, S. Guerra and F. D. Martinez (2017). "Association between the CDHR3 rs6967330 risk allele and chronic rhinosinusitis." J Allergy Clin Immunol **139**(6): 1990-1992 e1992.

Chapelin, C., B. Duriez, F. Magnino, M. Goossens, E. Escudier and S. Amselem (1997). "Isolation of several human axonemal dynein heavy chain genes: genomic structure of the catalytic site, phylogenetic analysis and chromosomal assignment." FEBS Lett **412**(2): 325-330.

Chen, I. C., H. H. Huang, P. F. Chen and H. C. Chiang (2016). "Sirtuin 3 Protects against Urban Particulate Matter-Induced Autophagy in Human Bronchial Epithelial Cells." Toxicol Sci **152**(1): 113-127.
Chen, S. and J. Schoen (2019). "Air-liquid interface cell culture: From airway epithelium to the female reproductive tract." Reprod Domest Anim **54 Suppl 3**: 38-45.
Chen, Y. W., S. X. Huang, A. de Carvalho, S. H. Ho, M. N. Islam, S. Volpi, L. D. Notarangelo, M. Ciancanelli, J. L. Casanova, J. Bhattacharya, A. F. Liang, L. M. Palermo, M. Porotto, A. Moscona and H. W. Snoeck (2017). "A three-dimensional model of human lung development and disease from pluripotent stem cells." Nat Cell Biol **19**(5): 542-549.
Chen, Z. G., Y. Y. Li, Z. N. Wang, M. Li, H. F. Lim, Y. Q. Zhou, L. M. Cai, Y. T. Li, L. F. Yang, T. T. Zhang and D. Y. Wang (2018). "Aberrant epithelial remodeling with impairment of cilia architecture in non-cystic fibrosis bronchiectasis." J Thorac Dis **10**(3): 1753-1764.
Cheng, Q., L. Dong, T. Su, T. Li, Z. Gan, H. Nan, S. Lu, C. Fang, L. Kong, H. Li, Z. Hou, K. Kou, Y. Tang, X. Lin, X. Zhao, L. Chen, B. Liu and F. Kong (2019). "CRISPR/Cas9-mediated targeted mutagenesis of GmLHY genes alters plant height and internode length in soybean." BMC Plant Biol **19**(1): 562.
Cho, K. J., S. H. Noh, S. M. Han, W. I. Choi, H. Y. Kim, S. Yu, J. S. Lee, J. H. Rim, M. G. Lee, F. Hildebrandt and H. Y. Gee (2018). "ZMYND10 stabilizes intermediate chain proteins in the cytoplasmic pre-assembly of dynein arms." PLoS Genet **14**(3): e1007316.
Choksi, S. P., D. Babu, D. Lau, X. Yu and S. Roy (2014). "Systematic discovery of novel ciliary genes through functional genomics in the zebrafish." Development **141**(17): 3410-3419.
Choksi, S. P., G. Lauter, P. Swoboda and S. Roy (2014). "Switching on cilia: transcriptional networks regulating ciliogenesis." Development **141**(7): 1427-1441.
Cokugras, H., N. Akcakaya, Seckin, Y. Camcioglu, N. Sarimurat and F. Aksoy (2001). "Ultrastructural examination of bronchial biopsy specimens from children with moderate asthma." Thorax **56**(1): 25-29.
Colwill, K., G. Renewable Protein Binder Working and S. Graslund (2011). "A roadmap to generate renewable protein binders to the human proteome." Nat Methods **8**(7): 551-558.
Cortellino, S., C. Wang, B. Wang, M. R. Bassi, E. Caretti, D. Champeval, A. Calmont, M. Jarnik, J. Burch, K. S. Zaret, L. Larue and A. Bellacosa (2009). "Defective ciliogenesis, embryonic lethality and severe impairment of the Sonic Hedgehog pathway caused by inactivation of the mouse complex A intraflagellar transport gene Ift122/Wdr10, partially overlapping with the DNA repair gene Med1/Mbd4." Dev Biol **325**(1): 225-237.
Corvol, H., S. M. Blackman, P. Y. Boelle, P. J. Gallins, R. G. Pace, J. R. Stonebraker, F. J. Accurso, A. Clement, J. M. Collaco, H. Dang, A. T. Dang, A. Franca, J. Gong, L. Guillot, K. Keenan, W. Li, F. Lin, M. V. Patrone, K. S. Raraigh, L. Sun, Y. H. Zhou, W. K. O'Neal, M. K. Sontag, H. Levy, P. R. Durie, J. M. Rommens, M. L. Drumm, F. A. Wright, L. J. Strug, G. R. Cutting and M. R. Knowles (2015). "Genome-wide association meta-analysis identifies five modifier loci of lung disease severity in cystic fibrosis." Nat Commun **6**: 8382.
Cozens, A. L., M. J. Yezzi, K. Kunzelmann, T. Ohrui, L. Chin, K. Eng, W. E. Finkbeiner, J. H. Widdicombe and D. C. Gruenert (1994). "CFTR expression and chloride secretion in polarized immortal human bronchial epithelial cells." Am J Respir Cell Mol Biol **10**(1): 38-47.
Cunha-Ferreira, I., I. Bento, A. Pimenta-Marques, S. C. Jana, M. Lince-Faria, P. Duarte, J. Borrego-Pinto, S. Gilberto, T. Amado, D. Brito, A. Rodrigues-Martins, J. Debski, N. Dzhindzhev and M. Bettencourt-Dias (2013). "Regulation of autophosphorylation controls PLK4 self-destruction and centriole number." Curr Biol **23**(22): 2245-2254.
Davis, J. D. and T. P. Wypych (2021). "Cellular and functional heterogeneity of the airway epithelium." Mucosal Immunol **14**(5): 978-990.
De Arcangelis, A., H. Hamade, F. Alpy, S. Normand, E. Bruyere, O. Lefebvre, A. Mechine-Neuville, S. Siebert, V. Pfister, P. Lepage, P. Laquerriere, D. Dembele, A. Delanoye-Crespin, S. Rodius, S. Robine, M. Kedinger, I. Van Seuningen, P. Simon-Assmann, M. Chamaillard, M. Labouesse and E. Georges-Labouesse (2017). "Hemidesmosome integrity protects the colon against colitis and colorectal cancer." Gut **66**(10): 1748-1760.

Deane, J. A., D. G. Cole, E. S. Seeley, D. R. Diener and J. L. Rosenbaum (2001). "Localization of intraflagellar transport protein IFT52 identifies basal body transitional fibers as the docking site for IFT particles." Curr Biol **11**(20): 1586-1590.
Delgado, O., A. A. Kaisani, M. Spinola, X. J. Xie, K. G. Batten, J. D. Minna, W. E. Wright and J. W. Shay (2011). "Multipotent capacity of immortalized human bronchial epithelial cells." PLoS One **6**(7): e22023.
Delgehyr, N., A. Meunier, M. Faucourt, M. Bosch Grau, L. Strehl, C. Janke and N. Spassky (2015). "Ependymal cell differentiation, from monociliated to multiciliated cells." Methods Cell Biol **127**: 19-35.
Dell, K. M. (2015). "The role of cilia in the pathogenesis of cystic kidney disease." Curr Opin Pediatr **27**(2): 212-218.
Didon, L., R. K. Zwick, I. W. Chao, M. S. Walters, R. Wang, N. R. Hackett and R. G. Crystal (2013). "RFX3 modulation of FOXJ1 regulation of cilia genes in the human airway epithelium." Respir Res **14**: 70.
Dummer, A., C. Poelma, M. C. DeRuiter, M.-J. T. H. Goumans and B. P. Hierck (2016). "Measuring the primary cilium length: improved method for unbiased high-throughput analysis." Cilia **5**(1): 7.
Edgar, R. C. (2004). "MUSCLE: a multiple sequence alignment method with reduced time and space complexity." BMC Bioinformatics **5**: 113.
Edgar, R. C. (2004). "MUSCLE: multiple sequence alignment with high accuracy and high throughput." Nucleic Acids Res **32**(5): 1792-1797.
Eenjes, E., T. C. J. Mertens, M. J. Buscop-van Kempen, Y. van Wijck, C. Taube, R. J. Rottier and P. S. Hiemstra (2018). "A novel method for expansion and differentiation of mouse tracheal epithelial cells in culture." Sci Rep **8**(1): 7349.
El-Gebali, S., J. Mistry, A. Bateman, S. R. Eddy, A. Luciani, S. C. Potter, M. Qureshi, L. J. Richardson, G. A. Salazar, A. Smart, E. L. L. Sonnhammer, L. Hirsh, L. Paladin, D. Piovesan, S. C. E. Tosatto and R. D. Finn (2019). "The Pfam protein families database in 2019." Nucleic Acids Res **47**(D1): D427-D432.
Everman, J. L., C. Rios and M. A. Seibold (2018). "Primary Airway Epithelial Cell Gene Editing Using CRISPR-Cas9." Methods Mol Biol **1706**: 267-292.
Everman, J. L., S. Sajuthi, B. Saef, C. Rios, A. M. Stoner, M. Numata, D. Hu, C. Eng, S. Oh, J. Rodriguez-Santana, E. K. Vladar, D. R. Voelker, E. G. Burchard and M. A. Seibold (2019). "Functional genomics of CDHR3 confirms its role in HRV-C infection and childhood asthma exacerbations." J Allergy Clin Immunol.
Fahy, J. V. and B. F. Dickey (2010). "Airway mucus function and dysfunction." N Engl J Med **363**(23): 2233-2247.
Fam, H. K., M. K. Chowdhury, C. Walton, K. Choi, C. F. Boerkoel and G. Hendson (2013). "Expression profile and mitochondrial colocalization of Tdp1 in peripheral human tissues." J Mol Histol **44**(4): 481-494.
Fireman, P. (2003). "Understanding asthma pathophysiology." Allergy Asthma Proc **24**(2): 79-83.
Firth, J. (2019). "Respiratory medicine: bronchiectasis." Clin Med (Lond) **19**(1): 64-67.
Fisch, C. and P. Dupuis-Williams (2011). "The rebirth of the ultrastructure of cilia and flagella." Biol Aujourdhui **205**(4): 245-267.
Fisch, C. and P. Dupuis-Williams (2011). "Ultrastructure of cilia and flagella - back to the future!" Biol Cell **103**(6): 249-270.
Fitzsimons, L. A., V. L. Brewer and K. L. Tucker (2022). "Hedgehog Morphogens Act as Growth Factors Critical to Pre- and Postnatal Cardiac Development and Maturation: How Primary Cilia Mediate Their Signal Transduction." Cells **11**(12).
Flock, A. and A. J. Duvall, 3rd (1965). "The Ultrastructure of the Kinocilium of the Sensory Cells in the Inner Ear and Lateral Line Organs." J Cell Biol **25**: 1-8.
Foil, K. E., A. Powers, K. S. Raraigh, K. Wallis, K. W. Southern and D. Salinas (2018). "The increasing challenge of genetic counseling for cystic fibrosis." J Cyst Fibros.

Fuchs, M., M. Foresti, M. Y. Radeva, D. Kugelmann, R. Keil, M. Hatzfeld, V. Spindler, J. Waschke and F. Vielmuth (2019). "Plakophilin 1 but not plakophilin 3 regulates desmoglein clustering." Cell Mol Life Sci **76**(17): 3465-3476.
Fulcher, M. L., S. E. Gabriel, J. C. Olsen, J. R. Tatreau, M. Gentzsch, E. Livanos, M. T. Saavedra, P. Salmon and S. H. Randell (2009). "Novel human bronchial epithelial cell lines for cystic fibrosis research." Am J Physiol Lung Cell Mol Physiol **296**(1): L82-91.
Gauthier, J., A. T. Vincent, S. J. Charette and N. Derome (2019). "A brief history of bioinformatics." Brief Bioinform **20**(6): 1981-1996.
Gavrilov, Y., S. Dagan and Y. Levy (2015). "Shortening a loop can increase protein native state entropy." Proteins **83**(12): 2137-2146.
Gerbe, F. and P. Jay (2016). "Intestinal tuft cells: epithelial sentinels linking luminal cues to the immune system." Mucosal Immunol **9**(6): 1353-1359.
Gerbe, F., E. Sidot, D. J. Smyth, M. Ohmoto, I. Matsumoto, V. Dardalhon, P. Cesses, L. Garnier, M. Pouzolles, B. Brulin, M. Bruschi, Y. Harcus, V. S. Zimmermann, N. Taylor, R. M. Maizels and P. Jay (2016). "Intestinal epithelial tuft cells initiate type 2 mucosal immunity to helminth parasites." Nature **529**(7585): 226-230.
Gerovac, B. J. and N. L. Fregien (2016). "IL-13 Inhibits Multicilin Expression and Ciliogenesis via Janus Kinase/Signal Transducer and Activator of Transcription Independently of Notch Cleavage." Am J Respir Cell Mol Biol **54**(4): 554-561.
Gerovac, B. J., M. Valencia, N. Baumlin, M. Salathe, G. E. Conner and N. L. Fregien (2014). "Submersion and hypoxia inhibit ciliated cell differentiation in a notch-dependent manner." Am J Respir Cell Mol Biol **51**(4): 516-525.
Ghossoub, R., L. Lindbaek, A. Molla-Herman, A. Schmitt, S. T. Christensen and A. Benmerah (2016). "Morphological and Functional Characterization of the Ciliary Pocket by Electron and Fluorescence Microscopy." Methods Mol Biol **1454**: 35-51.
Giuliano, C. J., A. Lin, V. Girish and J. M. Sheltzer (2019). "Generating Single Cell-Derived Knockout Clones in Mammalian Cells with CRISPR/Cas9." Curr Protoc Mol Biol **128**(1): e100.
Gold, J., P. Hametz, A. I. Sen, P. Maykowski, N. Leone, D. S. Lee, C. Gagliardo, S. Hymes, R. Biller and L. Saiman (2019). "Provider Knowledge, Attitudes, and Practices Regarding Bronchiolitis and Pneumonia Guidelines." Hosp Pediatr.
Goncalves, J. and L. Pelletier (2017). "The Ciliary Transition Zone: Finding the Pieces and Assembling the Gate." Mol Cells **40**(4): 243-253.
Gonczy, P. (2012). "Towards a molecular architecture of centriole assembly." Nat Rev Mol Cell Biol **13**(7): 425-435.
Goodale, B. C., E. J. Rayack and B. A. Stanton (2017). "Arsenic alters transcriptional responses to Pseudomonas aeruginosa infection and decreases antimicrobial defense of human airway epithelial cells." Toxicol Appl Pharmacol **331**: 154-163.
Gough, O. J. (2017). "Expression of PIERCE1 in human cell-lines." MSc Thesis. Uniersity of Sheffield, Sheffield, UK.
Goutaki, M., A. B. Meier, F. S. Halbeisen, J. S. Lucas, S. D. Dell, E. Maurer, C. Casaulta, M. Jurca, B. D. Spycher and C. E. Kuehni (2016). "Clinical manifestations in primary ciliary dyskinesia: systematic review and meta-analysis." Eur Respir J **48**(4): 1081-1095.
Greenan, G. A., R. D. Vale and D. A. Agard (2020). "Electron cryotomography of intact motile cilia defines the basal body to axoneme transition." J Cell Biol **219**(1).
Grimwood, K. and A. B. Chang (2019). "A new dawn: inhaled antibiotics for patients with bronchiectasis." Lancet Respir Med.
Grissa, D., A. Junge, T. I. Oprea and L. J. Jensen (2022). "Diseases 2.0: a weekly updated database of disease-gene associations from text mining and data integration." Database (Oxford) **2022**.
Grunewald, J., R. Zhou, S. P. Garcia, S. Iyer, C. A. Lareau, M. J. Aryee and J. K. Joung (2019). "Transcriptome-wide off-target RNA editing induced by CRISPR-guided DNA base editors." Nature **569**(7756): 433-437.
Gui, M., H. Farley, P. Anujan, J. R. Anderson, D. W. Maxwell, J. B. Whitchurch, J. J. Botsch, T. Qiu, S. Meleppattu, S. K. Singh, Q. Zhang, J. Thompson, J. S. Lucas, C. D. Bingle, D. P.

Norris, S. Roy and A. Brown (2021). "De novo identification of mammalian ciliary motility proteins using cryo-EM." Cell **184**(23): 5791-5806 e5719.
Guo, X., K. Liu, Y. Liu, Y. Situ, X. Tian, K. F. Xu and X. Zhang (2018). "Clinical and genetic characteristics of cystic fibrosis in CHINESE patients: a systemic review of reported cases." Orphanet J Rare Dis **13**(1): 224.
Gupta, D., O. Bhattacharjee, D. Mandal, M. K. Sen, D. Dey, A. Dasgupta, T. A. Kazi, R. Gupta, S. Sinharoy, K. Acharya, D. Chattopadhyay, V. Ravichandiran, S. Roy and D. Ghosh (2019). "CRISPR-Cas9 system: A new-fangled dawn in gene editing." Life Sci **232**: 116636.
Haktanir Abul, M. and W. Phipatanakul (2019). "Severe asthma in children: Evaluation and management." Allergol Int.
Hall, B. G. (2013). "Building phylogenetic trees from molecular data with MEGA." Mol Biol Evol **30**(5): 1229-1235.
Hanack, K., K. Messerschmidt and M. Listek (2016). "Antibodies and Selection of Monoclonal Antibodies." Adv Exp Med Biol **917**: 11-22.
Hasan, N., H. H. Harith, D. A. Israf and C. L. Tham (2020). "The differential effects of commercial specialized media on cell growth and transforming growth factor beta 1-induced epithelial-mesenchymal transition in bronchial epithelial cells." Mol Biol Rep **47**(5): 3511-3519.
Hassan, A. (2018). "Towards modulating cilia in mucociliary airway." MSc Thesis. Uniersity of Sheffield, Sheffield, UK.
Hight, S. K., A. Mootz, R. K. Kollipara, E. McMillan, P. Yenerall, Y. Otaki, L. S. Li, K. Avila, M. Peyton, J. Rodriguez-Canales, B. Mino, P. Villalobos, L. Girard, P. Dospoy, J. Larsen, M. A. White, J. V. Heymach, Wistuba, II, R. Kittler and J. D. Minna (2020). "An in vivo functional genomics screen of nuclear receptors and their co-regulators identifies FOXA1 as an essential gene in lung tumorigenesis." Neoplasia **22**(8): 294-310.
Hill, A. T., A. L. Sullivan, J. D. Chalmers, A. De Soyza, J. S. Elborn, R. A. Floto, L. Grillo, K. Gruffydd-Jones, A. Harvey, C. S. Haworth, E. Hiscocks, J. R. Hurst, C. Johnson, W. P. Kelleher, P. Bedi, K. Payne, H. Saleh, N. J. Screaton, M. Smith, M. Tunney, D. Whitters, R. Wilson and M. R. Loebinger (2018). "British Thoracic Society guideline for bronchiectasis in adults." BMJ Open Respir Res **5**(1): e000348.
Hirsch, S. D., C. L. Elling, T. C. Bootpetch, M. A. Scholes, L. Hafren, S. O. Streubel, H. S. Pine, T. M. Wine, W. Szeremeta, J. D. Prager, E. Einarsdottir, A. Yousaf, E. E. Baschal, S. Rehman, M. J. Bamshad, D. A. Nickerson, S. Riazuddin, S. M. Leal, Z. M. Ahmed, P. J. Yoon, J. Kere, K. H. Chan, P. S. Mattila, N. R. Friedman, T. Chonmaitree, D. N. Frank, A. F. Ryan and R. L. P. Santos-Cortez (2021). "The role of CDHR3 in susceptibility to otitis media." J Mol Med (Berl) **99**(11): 1571-1583.
Hirst, R. A., A. Rutman, G. Williams and C. O'Callaghan (2010). "Ciliated air-liquid cultures as an aid to diagnostic testing of primary ciliary dyskinesia." Chest **138**(6): 1441-1447.
Hjeij, R., A. Onoufriadis, C. M. Watson, C. E. Slagle, N. T. Klena, G. W. Dougherty, M. Kurkowiak, N. T. Loges, C. P. Diggle, N. F. Morante, G. C. Gabriel, K. L. Lemke, Y. Li, P. Pennekamp, T. Menchen, F. Konert, J. K. Marthin, D. A. Mans, S. J. Letteboer, C. Werner, T. Burgoyne, C. Westermann, A. Rutman, I. M. Carr, C. O'Callaghan, E. Moya, E. M. Chung, U. K. Consortium, E. Sheridan, K. G. Nielsen, R. Roepman, K. Bartscherer, R. D. Burdine, C. W. Lo, H. Omran and H. M. Mitchison (2014). "CCDC151 mutations cause primary ciliary dyskinesia by disruption of the outer dynein arm docking complex formation." Am J Hum Genet **95**(3): 257-274.
Ho, L., M. S. Williams and R. A. Spritz (1998). "A gene for autosomal dominant hypohidrotic ectodermal dysplasia (EDA3) maps to chromosome 2q11-q13." Am J Hum Genet **62**(5): 1102-1106.
Hogan, B. L., C. E. Barkauskas, H. A. Chapman, J. A. Epstein, R. Jain, C. C. Hsia, L. Niklason, E. Calle, A. Le, S. H. Randell, J. Rock, M. Snitow, M. Krummel, B. R. Stripp, T. Vu, E. S. White, J. A. Whitsett and E. E. Morrisey (2014). "Repair and regeneration of the respiratory system: complexity, plasticity, and mechanisms of lung stem cell function." Cell Stem Cell **15**(2): 123-138.

Hoque, M., E. N. Kim, D. Chen, F. Q. Li and K. I. Takemaru (2022). "Essential Roles of Efferent Duct Multicilia in Male Fertility." Cells **11**(3).
Horani, A., S. L. Brody, T. W. Ferkol, D. Shoseyov, M. G. Wasserman, A. Ta-shma, K. S. Wilson, P. V. Bayly, I. Amirav, M. Cohen-Cymberknoh, S. K. Dutcher, O. Elpeleg and E. Kerem (2013). "CCDC65 mutation causes primary ciliary dyskinesia with normal ultrastructure and hyperkinetic cilia." PLoS One **8**(8): e72299.
Hornef, N., H. Olbrich, J. Horvath, M. A. Zariwala, M. Fliegauf, N. T. Loges, J. Wildhaber, P. G. Noone, M. Kennedy, S. E. Antonarakis, J. L. Blouin, L. Bartoloni, T. Nusslein, P. Ahrens, M. Griese, H. Kuhl, R. Sudbrak, M. R. Knowles, R. Reinhardt and H. Omran (2006). "DNAH5 mutations are a common cause of primary ciliary dyskinesia with outer dynein arm defects." Am J Respir Crit Care Med **174**(2): 120-126.
Hosokawa, T., T. Betsuyaku, M. Nishimura, A. Furuyama, K. Katagiri and K. Mochitate (2007). "Differentiation of tracheal basal cells to ciliated cells and tissue reconstruction on the synthesized basement membrane substratum in vitro." Connect Tissue Res **48**(1): 9-18.
Huang, N., Y. Xia, D. Zhang, S. Wang, Y. Bao, R. He, J. Teng and J. Chen (2017). "Hierarchical assembly of centriole subdistal appendages via centrosome binding proteins CCDC120 and CCDC68." Nat Commun **8**: 15057.
Huter, P., S. Arenz, L. V. Bock, M. Graf, J. O. Frister, A. Heuer, L. Peil, A. L. Starosta, I. Wohlgemuth, F. Peske, J. Novacek, O. Berninghausen, H. Grubmuller, T. Tenson, R. Beckmann, M. V. Rodnina, A. C. Vaiana and D. N. Wilson (2017). "Structural Basis for Polyproline-Mediated Ribosome Stalling and Rescue by the Translation Elongation Factor EF-P." Mol Cell **68**(3): 515-527 e516.
Hyland, R. M. and S. L. Brody (2021). "Impact of Motile Ciliopathies on Human Development and Clinical Consequences in the Newborn." Cells **11**(1).
Iida, M., M. Suzuki, Y. Sakane, H. Nishide, I. Uchiyama, T. Yamamoto, K. T. Suzuki and S. Fujii (2020). "A simple and practical workflow for genotyping of CRISPR-Cas9-based knockout phenotypes using multiplexed amplicon sequencing." Genes Cells **25**(7): 498-509.
Ishikawa, H. and W. F. Marshall (2011). "Ciliogenesis: building the cell's antenna." Nat Rev Mol Cell Biol **12**(4): 222-234.
Ishikawa, T. (2017). "Axoneme Structure from Motile Cilia." Cold Spring Harb Perspect Biol **9**(1).
Jackson, A. D. and C. H. Goss (2018). "Epidemiology of CF: How registries can be used to advance our understanding of the CF population." J Cyst Fibros **17**(3): 297-305.
Jackson, P. K. and L. D. Attardi (2016). "p73 and FoxJ1: Programming Multiciliated Epithelia." Trends Cell Biol **26**(4): 239-240.
Jacquet, B. V., R. Salinas-Mondragon, H. Liang, B. Therit, J. D. Buie, M. Dykstra, K. Campbell, L. E. Ostrowski, S. L. Brody and H. T. Ghashghaei (2009). "FoxJ1-dependent gene expression is required for differentiation of radial glia into ependymal cells and a subset of astrocytes in the postnatal brain." Development **136**(23): 4021-4031.
Ji, Z. Y., Y. W. Sha, L. Ding and P. Li (2017). "Genetic factors contributing to human primary ciliary dyskinesia and male infertility." Asian J Androl **19**(5): 515-520.
Jiang, D., N. Schaefer and H. W. Chu (2018). "Air-Liquid Interface Culture of Human and Mouse Airway Epithelial Cells." Methods Mol Biol **1809**: 91-109.
Jiang, Y. Y., W. Maier, R. Baumeister, G. Minevich, E. Joachimiak, D. Wloga, Z. Ruan, N. Kannan, S. Bocarro, A. Bahraini, K. K. Vasudevan, K. Lechtreck, E. Orias and J. Gaertig (2019). "LF4/MOK and a CDK-related kinase regulate the number and length of cilia in Tetrahymena." PLoS Genet **15**(7): e1008099.
Jiao, J., P. Hu, M. Zhuang, Y. Li, C. Cai, X. Wang and L. Zhang (2022). "Transcriptome sequencing reveals altered ciliogenesis under hypoxia in nasal epithelial cells from chronic rhinosinusitis with nasal polyps." Clin Transl Allergy **12**(6): e12168.
Joachimiak, E., D. Wloga, A. Filipek and H. Fabczak (2018). "Ciliopaties - diseases caused by abnormal cilia functioning." Postepy Biochem **64**(4): 338-350.

Joung, J., S. Konermann, J. S. Gootenberg, O. O. Abudayyeh, R. J. Platt, M. D. Brigham, N. E. Sanjana and F. Zhang (2017). "Genome-scale CRISPR-Cas9 knockout and transcriptional activation screening." Nat Protoc **12**(4): 828-863.
Kapsimali, M. (2017). "Epithelial cell behaviours during neurosensory organ formation." Development **144**(11): 1926-1936.
Karlsson, M., C. Zhang, L. Mear, W. Zhong, A. Digre, B. Katona, E. Sjostedt, L. Butler, J. Odeberg, P. Dusart, F. Edfors, P. Oksvold, K. von Feilitzen, M. Zwahlen, M. Arif, O. Altay, X. Li, M. Ozcan, A. Mardinoglu, L. Fagerberg, J. Mulder, Y. Luo, F. Ponten, M. Uhlen and C. Lindskog (2021). "A single-cell type transcriptomics map of human tissues." Sci Adv **7**(31).
Kempeneers, C. and M. A. Chilvers (2018). "To beat, or not to beat, that is question! The spectrum of ciliopathies." Pediatr Pulmonol **53**(8): 1122-1129.
Kent, K. D. and J. A. Bomser (2003). "Bovine pituitary extract provides remarkable protection against oxidative stress in human prostate epithelial cells." In Vitro Cell Dev Biol Anim **39**(8-9): 388-394.
Kesimer, M., S. Kirkham, R. J. Pickles, A. G. Henderson, N. E. Alexis, G. Demaria, D. Knight, D. J. Thornton and J. K. Sheehan (2009). "Tracheobronchial air-liquid interface cell culture: a model for innate mucosal defense of the upper airways?" Am J Physiol Lung Cell Mol Physiol **296**(1): L92-L100.
Khalil, S. M., I. Bernstein, H. Kulaga, N. Gour, N. Rowan, S. Lajoie and A. P. Lane (2020). "Interleukin 13 (IL-13) alters hypoxia-associated genes and upregulates CD73." Int Forum Allergy Rhinol **10**(9): 1096-1102.
Khan, N. A., N. Willemarck, A. Talebi, A. Marchand, M. M. Binda, J. Dehairs, N. Rueda-Rincon, V. W. Daniels, M. Bagadi, D. B. Thimiri Govinda Raj, F. Vanderhoydonc, S. Munck, P. Chaltin and J. V. Swinnen (2016). "Identification of drugs that restore primary cilium expression in cancer cells." Oncotarget **7**(9): 9975-9992.
Khatri, S. B. and S. C. Erzurum (2019). "Asthma." Clin Chest Med **40**(1): xiii-xiv.
Kim, H. J., S. E. Lee, H. Na, J. S. Roe, J. I. Roh and H. W. Lee (2020). "Divergence of the PIERCE1 expression between mice and humans as a p53 target gene." PLoS One **15**(8): e0236881.
Kim, K. W. and C. Ober (2019). "Lessons Learned From GWAS of Asthma." Allergy Asthma Immunol Res **11**(2): 170-187.
Kim, S., K. Lee, J. H. Choi, N. Ringstad and B. D. Dynlacht (2015). "Nek2 activation of Kif24 ensures cilium disassembly during the cell cycle." Nat Commun **6**: 8087.
King, S. M. (2016). "Axonemal Dynein Arms." Cold Spring Harb Perspect Biol **8**(11).
King, S. M. (2018). Composition and assembly of axonemal dyneins∗∗This chapter has been updated and modified from the first edition. Dyneins: Structure, Biology and Disease (Second Edition). S. M. King, Academic Press**:** 162-201.
Knowles, M. R., M. Zariwala and M. Leigh (2016). "Primary Ciliary Dyskinesia." Clin Chest Med **37**(3): 449-461.
Koay, T. W., C. Osterhof, I. M. C. Orlando, A. Keppner, D. Andre, S. Yousefian, M. Suarez Alonso, M. Correia, R. Markworth, J. Schodel, T. Hankeln and D. Hoogewijs (2021). "Androglobin gene expression patterns and FOXJ1-dependent regulation indicate its functional association with ciliogenesis." J Biol Chem **296**: 100291.
Kouthouridis, S., J. Goepp, C. Martini, E. Matthes, J. W. Hanrahan and C. Moraes (2021). "Oxygenation as a driving factor in epithelial differentiation at the air-liquid interface." Integr Biol (Camb) **13**(3): 61-72.
Kuijk, E., M. Jager, B. van der Roest, M. D. Locati, A. Van Hoeck, J. Korzelius, R. Janssen, N. Besselink, S. Boymans, R. van Boxtel and E. Cuppen (2020). "The mutational impact of culturing human pluripotent and adult stem cells." Nat Commun **11**(1): 2493.
Kuo, C. S. and M. A. Krasnow (2015). "Formation of a Neurosensory Organ by Epithelial Cell Slithering." Cell **163**(2): 394-405.
Kusak, B., E. Grzesik, K. Konarska-Gabrys, Z. Pacek, B. Piwowarczyk and G. Lis (2018). "Bronchiolitis in children - do we choose wisely?" Dev Period Med **22**(4): 323-328.

Lai, C. K., N. Gupta, X. Wen, L. Rangell, B. Chih, A. S. Peterson, J. F. Bazan, L. Li and S. J. Scales (2011). "Functional characterization of putative cilia genes by high-content analysis." Mol Biol Cell **22**(7): 1104-1119.
Laoukili, J., E. Perret, T. Willems, A. Minty, E. Parthoens, O. Houcine, A. Coste, M. Jorissen, F. Marano, D. Caput and F. Tournier (2001). "IL-13 alters mucociliary differentiation and ciliary beating of human respiratory epithelial cells." J Clin Invest **108**(12): 1817-1824.
Lattao, R., L. Kovacs and D. M. Glover (2017). "The Centrioles, Centrosomes, Basal Bodies, and Cilia of Drosophila melanogaster." Genetics **206**(1): 33-53.
Lee, D. D. H., A. Petris, R. E. Hynds and C. O'Callaghan (2020). "Ciliated Epithelial Cell Differentiation at Air-Liquid Interface Using Commercially Available Culture Media." Methods Mol Biol **2109**: 275-291.
Legendre, M., L.-E. Zaragosi and H. M. Mitchison (2021). "Motile cilia and airway disease." Seminars in Cell & Developmental Biology **110**: 19-33.
Lemeille, S., M. Paschaki, D. Baas, L. Morle, J. L. Duteyrat, A. Ait-Lounis, E. Barras, F. Soulavie, J. Jerber, J. Thomas, Y. Zhang, M. J. Holtzman, W. S. Kistler, W. Reith and B. Durand (2020). "Interplay of RFX transcription factors 1, 2 and 3 in motile ciliogenesis." Nucleic Acids Res **48**(16): 9019-9036.
Lens, S. M., E. E. Voest and R. H. Medema (2010). "Shared and separate functions of polo-like kinases and aurora kinases in cancer." Nat Rev Cancer **10**(12): 825-841.
Leung, C., S. J. Wadsworth, S. J. Yang and D. R. Dorscheid (2020). "Structural and functional variations in human bronchial epithelial cells cultured in air-liquid interface using different growth media." Am J Physiol Lung Cell Mol Physiol **318**(5): L1063-L1073.
Leventea, E., K. Hazime, C. Zhao and J. Malicki (2016). "Analysis of cilia structure and function in zebrafish." Methods Cell Biol **133**: 179-227.
Levine, M. and A. Holland (2017). "Cell cycle proteins moonlight in multiciliogenesis." Science **358**(6364): 716-718.
Li, C. and P. W. Tucker (1993). "DNA-binding properties and secondary structural model of the hepatocyte nuclear factor 3/fork head domain." Proc Natl Acad Sci U S A **90**(24): 11583-11587.
Li, K., Y. B. Ma, Z. Zhang, Y. H. Tian, X. L. Xu, Y. Q. He, L. Xu, Y. Gao, W. T. Pan, W. J. Song, X. He and L. Wei (2018). "Upregulated IQUB promotes cell proliferation and migration via activating Akt/GSK3beta/beta-catenin signaling pathway in breast cancer." Cancer Med **7**(8): 3875-3888.
Li, P., Y. He, G. Cai, F. Xiao, J. Yang, Q. Li and X. Chen (2019). "CCDC114 is mutated in patient with a complex phenotype combining primary ciliary dyskinesia, sensorineural deafness, and renal disease." J Hum Genet **64**(1): 39-48.
Li, X., S. Yang, V. Deepak, Z. Chinipardaz and S. Yang (2021). "Identification of Cilia in Different Mouse Tissues." Cells **10**(7).
Lin, Y. C., M. Boone, L. Meuris, I. Lemmens, N. Van Roy, A. Soete, J. Reumers, M. Moisse, S. Plaisance, R. Drmanac, J. Chen, F. Speleman, D. Lambrechts, Y. Van de Peer, J. Tavernier and N. Callewaert (2014). "Genome dynamics of the human embryonic kidney 293 lineage in response to cell biology manipulations." Nat Commun **5**: 4767.
Liu, L., P. Zhang, Y. Shao, F. Quan and H. Li (2019). "Knockdown of FOXJ1 inhibits the proliferation, migration, invasion, and glycolysis in laryngeal squamous cell carcinoma cells." J Cell Biochem **120**(9): 15874-15882.
Liu, Y., L. Zhang, W. Li, Q. Huang, S. Yuan, Y. Li, J. Liu, S. Zhang, G. Pin, S. Song, P. F. Ray, C. Arnoult, C. Cho, B. Garcia-Reyes, U. Knippschild, J. F. Strauss and Z. Zhang (2019). "The sperm-associated antigen 6 interactome and its role in spermatogenesis." Reproduction **158**(2): 181-197.
Lo, C. H., I. H. Lin, T. T. Yang, Y. C. Huang, B. E. Tanos, P. C. Chou, C. W. Chang, Y. G. Tsay, J. C. Liao and W. J. Wang (2019). "Phosphorylation of CEP83 by TTBK2 is necessary for cilia initiation." J Cell Biol **218**(10): 3489-3505.
Lobo, L. J., M. A. Zariwala and P. G. Noone (2014). "Primary ciliary dyskinesia." QJM **107**(9): 691-699.

Lodes, N., K. Seidensticker, A. Perniss, S. Nietzer, H. Oberwinkler, T. May, T. Walles, H. Hebestreit, S. Hackenberg and M. Steinke (2020). "Investigation on Ciliary Functionality of Different Airway Epithelial Cell Lines in Three-Dimensional Cell Culture." Tissue Eng Part A **26**(7-8): 432-440.

Lodh, S., J. Yano, M. S. Valentine and J. L. Van Houten (2016). "Voltage-gated calcium channels of Paramecium cilia." J Exp Biol **219**(Pt 19): 3028-3038.

Lu, H., P. Anujan, F. Zhou, Y. Zhang, Y. L. Chong, C. D. Bingle and S. Roy (2019). "Mcidas mutant mice reveal a two-step process for the specification and differentiation of multiciliated cells in mammals." Development **146**(6).

Lu, Z. and T. Hunter (2010). "Ubiquitylation and proteasomal degradation of the p21(Cip1), p27(Kip1) and p57(Kip2) CDK inhibitors." Cell Cycle **9**(12): 2342-2352.

Luck, K., D. K. Kim, L. Lambourne, K. Spirohn, B. E. Begg, W. Bian, R. Brignall, T. Cafarelli, F. J. Campos-Laborie, B. Charloteaux, D. Choi, A. G. Cote, M. Daley, S. Deimling, A. Desbuleux, A. Dricot, M. Gebbia, M. F. Hardy, N. Kishore, J. J. Knapp, I. A. Kovacs, I. Lemmens, M. W. Mee, J. C. Mellor, C. Pollis, C. Pons, A. D. Richardson, S. Schlabach, B. Teeking, A. Yadav, M. Babor, D. Balcha, O. Basha, C. Bowman-Colin, S. F. Chin, S. G. Choi, C. Colabella, G. Coppin, C. D'Amata, D. De Ridder, S. De Rouck, M. Duran-Frigola, H. Ennajdaoui, F. Goebels, L. Goehring, A. Gopal, G. Haddad, E. Hatchi, M. Helmy, Y. Jacob, Y. Kassa, S. Landini, R. Li, N. van Lieshout, A. MacWilliams, D. Markey, J. N. Paulson, S. Rangarajan, J. Rasla, A. Rayhan, T. Rolland, A. San-Miguel, Y. Shen, D. Sheykhkarimli, G. M. Sheynkman, E. Simonovsky, M. Tasan, A. Tejeda, V. Tropepe, J. C. Twizere, Y. Wang, R. J. Weatheritt, J. Weile, Y. Xia, X. Yang, E. Yeger-Lotem, Q. Zhong, P. Aloy, G. D. Bader, J. De Las Rivas, S. Gaudet, T. Hao, J. Rak, J. Tavernier, D. E. Hill, M. Vidal, F. P. Roth and M. A. Calderwood (2020). "A reference map of the human binary protein interactome." Nature **580**(7803): 402-408.

Lund, P., L. Pilgaard, M. Duroux, T. Fink and V. Zachar (2009). "Effect of growth media and serum replacements on the proliferation and differentiation of adipose-derived stem cells." Cytotherapy **11**(2): 189-197.

Luo, L., X. Yang, Y. Takihara, H. Knoetgen and M. Kessel (2004). "The cell-cycle regulator geminin inhibits Hox function through direct and polycomb-mediated interactions." Nature **427**(6976): 749-753.

Luo, M., M. Cao, Y. Kan, G. Li, W. Snell and J. Pan (2011). "The phosphorylation state of an aurora-like kinase marks the length of growing flagella in Chlamydomonas." Curr Biol **21**(7): 586-591.

Ma, C., H. Wu, D. Zhu, Y. Wang, Q. Shen, H. Cheng, J. Zhang, H. Geng, Y. Liu, X. He, F. Tao, Y. Cao and X. Xu (2021). "Bi-allelic mutations in MCIDAS and CCNO cause human infertility associated with abnormal gamete transport." Clin Genet **100**(6): 731-742.

Ma, M., M. Stoyanova, G. Rademacher, S. K. Dutcher, A. Brown and R. Zhang (2019). "Structure of the Decorated Ciliary Doublet Microtubule." Cell **179**(4): 909-922 e912.

Mahjoub, M. R., R. Nanjundappa and M. N. Harvey (2022). "Development of a multiciliated cell." Curr Opin Cell Biol **77**: 102105.

Maiti, A. K., L. Bartoloni, H. M. Mitchison, M. Meeks, E. Chung, S. Spiden, C. Gehrig, C. Rossier, C. D. DeLozier-Blanchet, J. Blouin, R. M. Gardiner and S. E. Antonarakis (2000). "No deleterious mutations in the FOXJ1 (alias HFH-4) gene in patients with primary ciliary dyskinesia (PCD)." Cytogenet Cell Genet **90**(1-2): 119-122.

Manojlovic, Z., R. Earwood, A. Kato, B. Stefanovic and Y. Kato (2014). "RFX7 is required for the formation of cilia in the neural tube." Mech Dev **132**: 28-37.

Margulis, L. (1980). "Undulipodia, flagella and cilia." Biosystems **12**(1-2): 105-108.

Marshall, C. B., D. J. Mays, J. S. Beeler, J. M. Rosenbluth, K. L. Boyd, G. L. Santos Guasch, T. M. Shaver, L. J. Tang, Q. Liu, Y. Shyr, B. J. Venters, M. A. Magnuson and J. A. Pietenpol (2016). "p73 Is Required for Multiciliogenesis and Regulates the Foxj1-Associated Gene Network." Cell Rep **14**(10): 2289-2300.

Marshall, W. F. (2008). "Basal bodies platforms for building cilia." Curr Top Dev Biol **85**: 1-22.

Mather, M. W., B. Verdon, R. A. Botting, J. Engelbert, L. Delpiano, X. Xu, C. Hatton, T. Davey, S. Lisgo, P. Yates, N. Dawe, C. D. Bingle, M. Haniffa, J. Powell and C. Ward (2021). "Development of a physiological model of human middle ear epithelium." Laryngoscope Investig Otolaryngol **6**(5): 1167-1174.
May-Simera, H., K. Nagel-Wolfrum and U. Wolfrum (2017). "Cilia - The sensory antennae in the eye." Prog Retin Eye Res **60**: 144-180.
Mayer, A. K., H. Bartz, F. Fey, L. M. Schmidt and A. H. Dalpke (2008). "Airway epithelial cells modify immune responses by inducing an anti-inflammatory microenvironment." Eur J Immunol **38**(6): 1689-1699.
Mayer, O., R. Campbell, P. Cahill and G. Redding (2016). "Thoracic Insufficiency Syndrome." Curr Probl Pediatr Adolesc Health Care **46**(3): 72-97.
McClements, M. E., A. Butt, E. Piotter, C. F. Peddle and R. E. MacLaren (2021). "An analysis of the Kozak consensus in retinal genes and its relevance to gene therapy." Mol Vis **27**: 233-242.
Meneguello, L., N. M. Barbosa, K. D. Pereira, A. R. G. Proenca, L. Tamborlin, F. M. Simabuco, L. K. Iwai, C. F. Zanelli, S. R. Valentini and A. D. Luchessi (2019). "The polyproline-motif of S6K2: eIF5A translational dependence and importance for protein-protein interactions." J Cell Biochem **120**(4): 6015-6025.
Miao, R., D. Leng, Y. Wang, J. F. Li, J. N. Gong, Y. Liang and Y. H. Yang (2017). "Differentially expressed genes analysis in expression profile data of pulmonary fibrosis with pulmonary hypertension." Zhonghua Yi Xue Za Zhi **97**(16): 1240-1243.
Michi, A. N. and D. Proud (2021). "A toolbox for studying respiratory viral infections using air-liquid interface cultures of human airway epithelial cells." Am J Physiol Lung Cell Mol Physiol **321**(1): L263-L280.
Miller, A. J., B. R. Dye, D. Ferrer-Torres, D. R. Hill, A. W. Overeem, L. D. Shea and J. R. Spence (2019). "Generation of lung organoids from human pluripotent stem cells in vitro." Nat Protoc.
Miller, J. A., V. Menon, J. Goldy, A. Kaykas, C. K. Lee, K. A. Smith, E. H. Shen, J. W. Phillips, E. S. Lein and M. J. Hawrylycz (2014). "Improving reliability and absolute quantification of human brain microarray data by filtering and scaling probes using RNA-Seq." BMC Genomics **15**: 154.
Mirza, S., R. D. Clay, M. A. Koslow and P. D. Scanlon (2018). "COPD Guidelines: A Review of the 2018 GOLD Report." Mayo Clin Proc **93**(10): 1488-1502.
Mizuno, N., M. Taschner, B. D. Engel and E. Lorentzen (2012). "Structural studies of ciliary components." J Mol Biol **422**(2): 163-180.
Modarage, K., S. A. Malik and P. Goggolidou (2022). "Molecular Diagnostics of Ciliopathies and Insights Into Novel Developments in Diagnosing Rare Diseases." Br J Biomed Sci **79**: 10221.
Molla-Herman, A., R. Ghossoub, T. Blisnick, A. Meunier, C. Serres, F. Silbermann, C. Emmerson, K. Romeo, P. Bourdoncle, A. Schmitt, S. Saunier, N. Spassky, P. Bastin and A. Benmerah (2010). "The ciliary pocket: an endocytic membrane domain at the base of primary and motile cilia." J Cell Sci **123**(Pt 10): 1785-1795.
Monti, C., M. Zilocchi, I. Colugnat and T. Alberio (2019). "Proteomics turns functional." J Proteomics **198**: 36-44.
Montoro, D. T., A. L. Haber, M. Biton, V. Vinarsky, B. Lin, S. E. Birket, F. Yuan, S. Chen, H. M. Leung, J. Villoria, N. Rogel, G. Burgin, A. M. Tsankov, A. Waghray, M. Slyper, J. Waldman, L. Nguyen, D. Dionne, O. Rozenblatt-Rosen, P. R. Tata, H. Mou, M. Shivaraju, H. Bihler, M. Mense, G. J. Tearney, S. M. Rowe, J. F. Engelhardt, A. Regev and J. Rajagopal (2018). "A revised airway epithelial hierarchy includes CFTR-expressing ionocytes." Nature **560**(7718): 319-324.
Mosca, R., A. Ceol and P. Aloy (2013). "Interactome3D: adding structural details to protein networks." Nat Methods **10**(1): 47-53.
Moyer, T. C. and A. J. Holland (2019). "PLK4 promotes centriole duplication by phosphorylating STIL to link the procentriole cartwheel to the microtubule wall." Elife **8**.

Muhlhans, J., J. H. Brandstatter and A. Giessl (2011). "The centrosomal protein pericentrin identified at the basal body complex of the connecting cilium in mouse photoreceptors." PLoS One **6**(10): e26496.
Mulay, A., K. Akram, L. Bingle and C. D. Bingle (2019). "Isolation and Culture of Primary Mouse Middle Ear Epithelial Cells." Methods Mol Biol **1940**: 157-168.
Mulay, A., K. M. Akram, D. Williams, H. Armes, C. Russell, D. Hood, S. Armstrong, J. P. Stewart, S. D. Brown, L. Bingle and C. D. Bingle (2016). "An in vitro model of murine middle ear epithelium." Dis Model Mech **9**(11): 1405-1417.
Munye, M. M., A. Shoemark, R. A. Hirst, J. M. Delhove, T. V. Sharp, T. R. McKay, C. O'Callaghan, D. L. Baines, S. J. Howe and S. L. Hart (2017). "BMI-1 extends proliferative potential of human bronchial epithelial cells while retaining their mucociliary differentiation capacity." Am J Physiol Lung Cell Mol Physiol **312**(2): L258-L267.
Nakauchi, M., N. Nagata, I. Takayama, S. Saito, H. Kubo, A. Kaida, K. Oba, T. Odagiri and T. Kageyama (2019). "Propagation of Rhinovirus C in Differentiated Immortalized Human Airway HBEC3-KT Epithelial Cells." Viruses **11**(3).
Narita, K. and S. Takeda (2021). "Ultrastructural evidence for an unusual mode of ciliogenesis in mouse multiciliated epithelia." Microscopy (Oxf) **70**(3): 308-315.
Nemajerova, A., I. Amelio, J. Gebel, V. Dotsch, G. Melino and U. M. Moll (2018). "Non-oncogenic roles of TAp73: from multiciliogenesis to metabolism." Cell Death Differ **25**(1): 144-153.
Nemajerova, A., D. Kramer, S. S. Siller, C. Herr, O. Shomroni, T. Pena, C. Gallinas Suazo, K. Glaser, M. Wildung, H. Steffen, A. Sriraman, F. Oberle, M. Wienken, M. Hennion, R. Vidal, B. Royen, M. Alevra, D. Schild, R. Bals, J. Donitz, D. Riedel, S. Bonn, K. Takemaru, U. M. Moll and M. Lize (2016). "TAp73 is a central transcriptional regulator of airway multiciliogenesis." Genes Dev **30**(11): 1300-1312.
Nigg, E. A. and A. J. Holland (2018). "Once and only once: mechanisms of centriole duplication and their deregulation in disease." Nat Rev Mol Cell Biol **19**(5): 297-312.
Niziolek, M., M. Bicka, A. Osinka, Z. Samsel, J. Sekretarska, M. Poprzeczko, R. Bazan, H. Fabczak, E. Joachimiak and D. Wloga (2022). "PCD Genes-From Patients to Model Organisms and Back to Humans." Int J Mol Sci **23**(3).
Nonaka, S., Y. Tanaka, Y. Okada, S. Takeda, A. Harada, Y. Kanai, M. Kido and N. Hirokawa (1998). "Randomization of left-right asymmetry due to loss of nodal cilia generating leftward flow of extraembryonic fluid in mice lacking KIF3B motor protein." Cell **95**(6): 829-837.
O'Donnell, A. E. (2018). "Medical management of bronchiectasis." J Thorac Dis **10**(Suppl 28): S3428-S3435.
Oba, Y., E. Keeney, N. Ghatehorde and S. Dias (2018). "Dual combination therapy versus long-acting bronchodilators alone for chronic obstructive pulmonary disease (COPD): a systematic review and network meta-analysis." Cochrane Database Syst Rev **12**: CD012620.
Okoye-Okafor, U. C., B. Bartholdy, B. Woolcock, M. Kawahara, T. I. Todorova, R. D. Gascoyne, C. Steidl and U. Steidl (2012). "Identification of a Novel Protein-Coding Gene (TIHL) and Its Functional Relevance in Myeloid Cells." Blood **120**(21): 2333.
Ong, T., S. G. Marshall, B. A. Karczeski, D. L. Sternen, E. Cheng and G. R. Cutting (1993). Cystic Fibrosis and Congenital Absence of the Vas Deferens. GeneReviews((R)). M. P. Adam, H. H. Ardinger, R. A. Pagon et al. Seattle (WA).
Orr, J. C. and R. E. Hynds (2021). "Stem Cell-derived Respiratory Epithelial Cell Cultures as Human Disease Models." Am J Respir Cell Mol Biol **64**(6): 657-668.
Palmenberg, A. C. (2017). "Rhinovirus C, Asthma, and Cell Surface Expression of Virus Receptor CDHR3." J Virol **91**(7).
Panizzi, J. R., A. Becker-Heck, V. H. Castleman, D. A. Al-Mutairi, Y. Liu, N. T. Loges, N. Pathak, C. Austin-Tse, E. Sheridan, M. Schmidts, H. Olbrich, C. Werner, K. Haffner, N. Hellman, R. Chodhari, A. Gupta, A. Kramer-Zucker, F. Olale, R. D. Burdine, A. F. Schier, C. O'Callaghan, E. M. Chung, R. Reinhardt, H. M. Mitchison, S. M. King, H. Omran and I. A. Drummond (2012). "CCDC103 mutations cause primary ciliary dyskinesia by disrupting assembly of ciliary dynein arms." Nat Genet **44**(6): 714-719.

Papon, J. F., A. Coste, F. Roudot-Thoraval, M. Boucherat, G. Roger, A. Tamalet, A. M. Vojtek, S. Amselem and E. Escudier (2010). "A 20-year experience of electron microscopy in the diagnosis of primary ciliary dyskinesia." Eur Respir J **35**(5): 1057-1063.
Paranjapye, A., S. H. Leir, F. Huang, J. L. Kerschner and A. Harris (2022). "Cell function and identity revealed by comparative scRNA-seq analysis in human nasal, bronchial and epididymis epithelia." Eur J Cell Biol **101**(3): 151231.
Park, B. M., H. J. Kim, J. H. Oh, J. I. Roh and H. W. Lee (2020). "Effect of PIERCE1 on colorectal cancer." Exp Anim **69**(4): 414-422.
Park, S. B., T. Uchida, S. Tilson, Z. Hu, C. D. Ma, M. Leek, M. Eichner, S. G. Hong and T. J. Liang (2022). "A dual conditional CRISPR-Cas9 system to activate gene editing and reduce off-target effects in human stem cells." Mol Ther Nucleic Acids **28**: 656-669.
Patir, A., A. M. Fraser, M. W. Barnett, L. McTeir, J. Rainger, M. G. Davey and T. C. Freeman (2020). "The transcriptional signature associated with human motile cilia." Sci Rep **10**(1): 10814.
Patrucco, F., L. Venezia, F. Gavelli, R. Pellicano and P. Solidoro (2018). "Alpha1-antitrypsin deficiency: what's new after European Respiratory Society Statement." Panminerva Med **60**(3): 101-108.
Peabody, J. E., R. J. Shei, B. M. Bermingham, S. E. Phillips, B. Turner, S. M. Rowe and G. M. Solomon (2018). "Seeing cilia: imaging modalities for ciliary motion and clinical connections." Am J Physiol Lung Cell Mol Physiol **314**(6): L909-L921.
Pennarun, G., E. Escudier, C. Chapelin, A. M. Bridoux, V. Cacheux, G. Roger, A. Clement, M. Goossens, S. Amselem and B. Duriez (1999). "Loss-of-function mutations in a human gene related to Chlamydomonas reinhardtii dynein IC78 result in primary ciliary dyskinesia." Am J Hum Genet **65**(6): 1508-1519.
Peters-Hall, J. R., M. L. Coquelin, M. J. Torres, R. LaRanger, B. R. Alabi, S. Sho, J. F. Calva-Moreno, P. J. Thomas and J. W. Shay (2018). "Long-term culture and cloning of primary human bronchial basal cells that maintain multipotent differentiation capacity and CFTR channel function." Am J Physiol Lung Cell Mol Physiol **315**(2): L313-L327.
Pezzulo, A. A., T. D. Starner, T. E. Scheetz, G. L. Traver, A. E. Tilley, B. G. Harvey, R. G. Crystal, P. B. McCray, Jr. and J. Zabner (2011). "The air-liquid interface and use of primary cell cultures are important to recapitulate the transcriptional profile of in vivo airway epithelia." Am J Physiol Lung Cell Mol Physiol **300**(1): L25-31.
Plasschaert, L. W., R. Zilionis, R. Choo-Wing, V. Savova, J. Knehr, G. Roma, A. M. Klein and A. B. Jaffe (2018). "A single-cell atlas of the airway epithelium reveals the CFTR-rich pulmonary ionocyte." Nature **560**(7718): 377-381.
Polke, M., F. Seiler, P. M. Lepper, A. Kamyschnikow, F. Langer, D. Monz, C. Herr, R. Bals and C. Beisswenger (2017). "Hypoxia and the hypoxia-regulated transcription factor HIF-1alpha suppress the host defence of airway epithelial cells." Innate Immun **23**(4): 373-380.
Pongjantarasatian, S., N. Nowwarote, V. Rotchanakitamnuai, W. Srirodjanakul, R. Saehun, K. Janebodin, J. Manokawinchoke, B. P. J. Fournier and T. Osathanon (2022). "A gamma-Secretase Inhibitor Attenuates Cell Cycle Progression and Invasion in Human Oral Squamous Cell Carcinoma: An In Vitro Study." Int J Mol Sci **23**(16).
Priyanka, P. P. and S. Yenugu (2021). "Coiled-Coil Domain-Containing (CCDC) Proteins: Functional Roles in General and Male Reproductive Physiology." Reprod Sci **28**(10): 2725-2734.
Qi, F., M. Motz, K. Jung, J. Lassak and D. Frishman (2018). "Evolutionary analysis of polyproline motifs in Escherichia coli reveals their regulatory role in translation." PLoS Comput Biol **14**(2): e1005987.
Qin, Q., Q. Wu, Y. Wang, R. Xiong, L. Guo, X. Fu, H. Rosenfeldt, M. Bryant and X. Cao (2019). "Effects of cellular differentiation in human primary bronchial epithelial cells: Metabolism of 4-(methylnitrosamine)-1-(3-pyridyl)-1-butanone." Toxicol In Vitro **55**: 185-194.
Qiu, Q., Y. Peng, Z. Zhu, Z. Chen, C. Zhang, H. H. Ong, K. S. Tan, H. Hong, Y. Yan, H. Huang, J. Liu, X. Li, H. N. Nam, N. T. N. Dung, L. Shi, Q. Yang, C. D. Bingle and D. Y.

Wang (2018). "Absence or mislocalization of DNAH5 is a characteristic marker for motile ciliary abnormality in nasal polyps." Laryngoscope **128**(3): E97-E104.
Quarmby, L. M. (2004). "Cellular deflagellation." Int Rev Cytol **233**: 47-91.
Quigley, I. K. and C. Kintner (2017). "Rfx2 Stabilizes Foxj1 Binding at Chromatin Loops to Enable Multiciliated Cell Gene Expression." PLoS Genet **13**(1): e1006538.
Rai, K. K., P. Adab, J. G. Ayres and R. E. Jordan (2018). "Systematic review: chronic obstructive pulmonary disease and work-related outcomes." Occup Med (Lond) **68**(2): 99-108.
Raidt, J., C. Werner, T. Menchen, G. W. Dougherty, H. Olbrich, N. T. Loges, R. Schmitz, P. Pennekamp and H. Omran (2015). "Ciliary function and motor protein composition of human fallopian tubes." Hum Reprod **30**(12): 2871-2880.
Rambhatla, L., C. P. Chiu, R. D. Glickman and C. Rowe-Rendleman (2002). "In vitro differentiation capacity of telomerase immortalized human RPE cells." Invest Ophthalmol Vis Sci **43**(5): 1622-1630.
Ramirez, R. D., S. Sheridan, L. Girard, M. Sato, Y. Kim, J. Pollack, M. Peyton, Y. Zou, J. M. Kurie, J. M. Dimaio, S. Milchgrub, A. L. Smith, R. F. Souza, L. Gilbey, X. Zhang, K. Gandia, M. B. Vaughan, W. E. Wright, A. F. Gazdar, J. W. Shay and J. D. Minna (2004). "Immortalization of human bronchial epithelial cells in the absence of viral oncoproteins." Cancer Res **64**(24): 9027-9034.
Ran, F. A., P. D. Hsu, J. Wright, V. Agarwala, D. A. Scott and F. Zhang (2013). "Genome engineering using the CRISPR-Cas9 system." Nat Protoc **8**(11): 2281-2308.
Rapiteanu, R., T. Karagyozova, N. Zimmermann, K. Singh, G. Wayne, M. Martufi, N. N. Belyaev, E. M. Hessel, D. Michalovich, R. Macarron, W. C. Rowan, W. J. Cairns, J. Roger, J. Betts, S. Beinke and K. Maratou (2020). "Highly efficient genome editing in primary human bronchial epithelial cells differentiated at air-liquid interface." Eur Respir J **55**(5).
Raslan, A. A. and J. K. Yoon (2020). "WNT Signaling in Lung Repair and Regeneration." Mol Cells **43**(9): 774-783.
Rawlins, E. L. and B. L. Hogan (2008). "Ciliated epithelial cell lifespan in the mouse trachea and lung." Am J Physiol Lung Cell Mol Physiol **295**(1): L231-234.
Rayko, M., A. Komissarov, J. C. Kwan, G. Lim-Fong, A. C. Rhodes, S. Kliver, P. Kuchur, S. J. O'Brien and J. V. Lopez (2020). "Draft genome of Bugula neritina, a colonial animal packing powerful symbionts and potential medicines." Sci Data **7**(1): 356.
Reddel, R. R., Y. Ke, B. I. Gerwin, M. G. McMenamin, J. F. Lechner, R. T. Su, D. E. Brash, J. B. Park, J. S. Rhim and C. C. Harris (1988). "Transformation of human bronchial epithelial cells by infection with SV40 or adenovirus-12 SV40 hybrid virus, or transfection via strontium phosphate coprecipitation with a plasmid containing SV40 early region genes." Cancer Res **48**(7): 1904-1909.
Reid, L., B. Meyrick, V. B. Antony, L. Y. Chang, J. D. Crapo and H. Y. Reynolds (2005). "The mysterious pulmonary brush cell: a cell in search of a function." Am J Respir Crit Care Med **172**(1): 136-139.
Reis, R. and I. Moraes (2019). "Structural biology and structure-function relationships of membrane proteins." Biochem Soc Trans **47**(1): 47-61.
Reiter, J. F., O. E. Blacque and M. R. Leroux (2012). "The base of the cilium: roles for transition fibres and the transition zone in ciliary formation, maintenance and compartmentalization." EMBO Rep **13**(7): 608-618.
Ritchie, M. E., B. Phipson, D. Wu, Y. Hu, C. W. Law, W. Shi and G. K. Smyth (2015). "limma powers differential expression analyses for RNA-sequencing and microarray studies." Nucleic Acids Res **43**(7): e47.
Robinot, R., M. Hubert, G. D. de Melo, F. Lazarini, T. Bruel, N. Smith, S. Levallois, F. Larrous, J. Fernandes, S. Gellenoncourt, S. Rigaud, O. Gorgette, C. Thouvenot, C. Trebeau, A. Mallet, G. Dumenil, S. Gobaa, R. Etournay, P. M. Lledo, M. Lecuit, H. Bourhy, D. Duffy, V. Michel, O. Schwartz and L. A. Chakrabarti (2021). "SARS-CoV-2 infection induces the dedifferentiation of multiciliated cells and impairs mucociliary clearance." Nat Commun **12**(1): 4354.

Rodrigues, R., C. S. Gabetta, K. P. Pedro, F. Valdetaro, M. I. Fernandes, P. K. Magalhaes, J. N. Januario and L. M. Maciel (2008). "Cystic fibrosis and neonatal screening." Cad Saude Publica **24 Suppl 4**: s475-484.

Roh, J. I., J. Lee, Y. H. Sung, J. Oh, D. Y. Hyeon, Y. Kim, S. Lee, S. Devkota, H. J. Kim, B. Park, T. Nam, Y. Song, Y. Kim, D. Hwang and H. W. Lee (2020). "Impaired AKT signaling and lung tumorigenesis by PIERCE1 ablation in KRAS-mutant non-small cell lung cancer." Oncogene **39**(36): 5876-5887.

Roman-Gomez, J., J. A. Castillejo, A. Jimenez, F. Cervantes, C. Boque, L. Hermosin, A. Leon, A. Granena, D. Colomer, A. Heiniger and A. Torres (2003). "Cadherin-13, a mediator of calcium-dependent cell-cell adhesion, is silenced by methylation in chronic myeloid leukemia and correlates with pretreatment risk profile and cytogenetic response to interferon alfa." J Clin Oncol **21**(8): 1472-1479.

Ross, A. J., L. A. Dailey, L. E. Brighton and R. B. Devlin (2007). "Transcriptional profiling of mucociliary differentiation in human airway epithelial cells." Am J Respir Cell Mol Biol **37**(2): 169-185.

Rossi, G. A., P. Morelli, L. J. Galietta and A. A. Colin (2019). "Airway microenvironment alterations and pathogen growth in cystic fibrosis." Pediatr Pulmonol.

Roy, M. G., A. Livraghi-Butrico, A. A. Fletcher, M. M. McElwee, S. E. Evans, R. M. Boerner, S. N. Alexander, L. K. Bellinghausen, A. S. Song, Y. M. Petrova, M. J. Tuvim, R. Adachi, I. Romo, A. S. Bordt, M. G. Bowden, J. H. Sisson, P. G. Woodruff, D. J. Thornton, K. Rousseau, M. M. De la Garza, S. J. Moghaddam, H. Karmouty-Quintana, M. R. Blackburn, S. M. Drouin, C. W. Davis, K. A. Terrell, B. R. Grubb, W. K. O'Neal, S. C. Flores, A. Cota-Gomez, C. A. Lozupone, J. M. Donnelly, A. M. Watson, C. E. Hennessy, R. C. Keith, I. V. Yang, L. Barthel, P. M. Henson, W. J. Janssen, D. A. Schwartz, R. C. Boucher, B. F. Dickey and C. M. Evans (2014). "Muc5b is required for airway defence." Nature **505**(7483): 412-416.

Rubbo, B. and J. S. Lucas (2017). "Clinical care for primary ciliary dyskinesia: current challenges and future directions." Eur Respir Rev **26**(145).

Ruiz Garcia, S., M. Deprez, K. Lebrigand, A. Cavard, A. Paquet, M. J. Arguel, V. Magnone, M. Truchi, I. Caballero, S. Leroy, C. H. Marquette, B. Marcet, P. Barbry and L. E. Zaragosi (2019). "Novel dynamics of human mucociliary differentiation revealed by single-cell RNA sequencing of nasal epithelial cultures." Development **146**(20).

Rumman, N., C. Jackson, S. Collins, P. Goggin, J. Coles and J. S. Lucas (2017). "Diagnosis of primary ciliary dyskinesia: potential options for resource-limited countries." Eur Respir Rev **26**(143).

Sahabandu, N., D. Kong, V. Magidson, R. Nanjundappa, C. Sullenberger, M. R. Mahjoub and J. Loncarek (2019). "Expansion microscopy for the analysis of centrioles and cilia." J Microsc **276**(3): 145-159.

Saint-Criq, V., L. Delpiano, J. Casement, J. C. Onuora, J. Lin and M. A. Gray (2020). "Choice of Differentiation Media Significantly Impacts Cell Lineage and Response to CFTR Modulators in Fully Differentiated Primary Cultures of Cystic Fibrosis Human Airway Epithelial Cells." Cells **9**(9).

Sarkar, M., R. Bhardwaz, I. Madabhavi and M. Modi (2019). "Physical signs in patients with chronic obstructive pulmonary disease." Lung India **36**(1): 38-47.

Satir, P. and S. T. Christensen (2007). "Overview of structure and function of mammalian cilia." Annu Rev Physiol **69**: 377-400.

Satir, P. and S. T. Christensen (2008). "Structure and function of mammalian cilia." Histochem Cell Biol **129**(6): 687-693.

Satir, P., L. B. Pedersen and S. T. Christensen (2010). "The primary cilium at a glance." J Cell Sci **123**(Pt 4): 499-503.

Savant, A. P. and S. A. McColley (2018). "Cystic fibrosis year in review 2017." Pediatr Pulmonol **53**(9): 1307-1317.

Schamberger, A. C., C. A. Staab-Weijnitz, N. Mise-Racek and O. Eickelberg (2015). "Cigarette smoke alters primary human bronchial epithelial cell differentiation at the air-liquid interface." Sci Rep **5**: 8163.

Schilling, A. L., A. R. Carcella, J. Moore, M. Zahid, C. Lo, E. W. Wang, S. E. Lee and S. R. Little (2021). "Compatibility of a Thermoresponsive and Controlled Release System for Promoting Sinonasal Cilia Regeneration." Macromol Biosci **21**(11): e2100277.
Schmid, A., J. Sailland, L. Novak, N. Baumlin, N. Fregien and M. Salathe (2017). "Modulation of Wnt signaling is essential for the differentiation of ciliated epithelial cells in human airways." FEBS Lett **591**(21): 3493-3506.
Seidl, C., F. Da Silva, K. Zhang, K. Wohlgemuth, H. Omran and C. Niehrs (2023). "Mucociliary Wnt signaling promotes cilia biogenesis and beating." Nat Commun **14**(1): 1259.
Sha, Y., X. Yang, L. Mei, Z. Ji, X. Wang, L. Ding, P. Li and S. Yang (2017). "DNAH1 gene mutations and their potential association with dysplasia of the sperm fibrous sheath and infertility in the Han Chinese population." Fertil Steril **107**(6): 1312-1318 e1312.
Shah, A. S., Y. Ben-Shahar, T. O. Moninger, J. N. Kline and M. J. Welsh (2009). "Motile cilia of human airway epithelia are chemosensory." Science **325**(5944): 1131-1134.
Shahid, U. and P. Singh (2018). "Emerging Picture of Deuterosome-Dependent Centriole Amplification in MCCs." Cells **7**(10).
Shamseldin, H. E., M. Tulbah, W. Kurdi, M. Nemer, N. Alsahan, E. Al Mardawi, O. Khalifa, A. Hashem, A. Kurdi, Z. Babay, D. K. Bubshait, N. Ibrahim, F. Abdulwahab, Z. Rahbeeni, M. Hashem and F. S. Alkuraya (2015). "Identification of embryonic lethal genes in humans by autozygosity mapping and exome sequencing in consanguineous families." Genome Biol **16**: 116.
Shapiro, A. J., S. D. Davis, D. Polineni, M. Manion, M. Rosenfeld, S. D. Dell, M. A. Chilvers, T. W. Ferkol, M. A. Zariwala, S. D. Sagel, M. Josephson, L. Morgan, O. Yilmaz, K. N. Olivier, C. Milla, J. E. Pittman, M. L. A. Daniels, M. H. Jones, I. A. Janahi, S. M. Ware, S. J. Daniel, M. L. Cooper, L. M. Nogee, B. Anton, T. Eastvold, L. Ehrne, E. Guadagno, M. R. Knowles, M. W. Leigh, V. Lavergne and P. American Thoracic Society Assembly on (2018). "Diagnosis of Primary Ciliary Dyskinesia. An Official American Thoracic Society Clinical Practice Guideline." Am J Respir Crit Care Med **197**(12): e24-e39.
Shapiro, A. J., K. Kaspy, M. L. A. Daniels, J. R. Stonebraker, V. H. Nguyen, L. Joyal, M. R. Knowles and M. A. Zariwala (2021). "Autosomal dominant variants in FOXJ1 causing primary ciliary dyskinesia in two patients with obstructive hydrocephalus." Mol Genet Genomic Med **9**(7): e1726.
Sharma, S., A. Hanukoglu and I. Hanukoglu (2018). "Localization of epithelial sodium channel (ENaC) and CFTR in the germinal epithelium of the testis, Sertoli cells, and spermatozoa." J Mol Histol **49**(2): 195-208.
Shoemark, A., M. Boon, C. Brochhausen, Z. Bukowy-Bieryllo, M. M. De Santi, P. Goggin, P. Griffin, R. G. Hegele, R. A. Hirst, M. W. Leigh, A. Lupton, K. MacKenney, H. Omran, J. C. Pache, A. Pinto, F. P. Reinholt, J. Schroeder, P. Yiallouros, E. Escudier and B.-P. C. D. N. G. D. G. representing the (2020). "International consensus guideline for reporting transmission electron microscopy results in the diagnosis of primary ciliary dyskinesia (BEAT PCD TEM Criteria)." Eur Respir J **55**(4).
Shoemark, A., B. Rubbo, M. Legendre, M. R. Fassad, E. G. Haarman, S. Best, I. C. M. Bon, J. Brandsma, P. R. Burgel, G. Carlsson, S. B. Carr, M. Carroll, M. Edwards, E. Escudier, I. Honore, D. Hunt, G. Jouvion, M. R. Loebinger, B. Maitre, D. Morris-Rosendahl, J. F. Papon, C. M. Parsons, M. P. Patel, N. S. Thomas, G. Thouvenin, W. T. Walker, R. Wilson, C. Hogg, H. M. Mitchison and J. S. Lucas (2021). "Topological data analysis reveals genotype-phenotype relationships in primary ciliary dyskinesia." Eur Respir J **58**(2).
Shpak, M., M. M. Goldberg and M. C. Cowperthwaite (2014). "Cilia gene expression patterns in cancer." Cancer Genomics Proteomics **11**(1): 13-24.
Siebel, C. and U. Lendahl (2017). "Notch Signaling in Development, Tissue Homeostasis, and Disease." Physiol Rev **97**(4): 1235-1294.
Sievers, F. and D. G. Higgins (2018). "Clustal Omega for making accurate alignments of many protein sequences." Protein Sci **27**(1): 135-145.
Sigg, M. A., T. Menchen, C. Lee, J. Johnson, M. K. Jungnickel, S. P. Choksi, G. Garcia, 3rd, H. Busengdal, G. W. Dougherty, P. Pennekamp, C. Werner, F. Rentzsch, H. M. Florman,

N. Krogan, J. B. Wallingford, H. Omran and J. F. Reiter (2017). "Evolutionary Proteomics Uncovers Ancient Associations of Cilia with Signaling Pathways." Dev Cell **43**(6): 744-762 e711.
Siller, S. S., H. Sharma, S. Li, J. Yang, Y. Zhang, M. J. Holtzman, W. Winuthayanon, H. Colognato, B. C. Holdener, F. Q. Li and K. I. Takemaru (2017). "Conditional knockout mice for the distal appendage protein CEP164 reveal its essential roles in airway multiciliated cell differentiation." PLoS Genet **13**(12): e1007128.
Smith, C. E. L., A. V. R. Lake and C. A. Johnson (2020). "Primary Cilia, Ciliogenesis and the Actin Cytoskeleton: A Little Less Resorption, A Little More Actin Please." Front Cell Dev Biol **8**: 622822.
Soares, H., B. Carmona, S. Nolasco, L. Viseu Melo and J. Goncalves (2019). "Cilia Distal Domain: Diversity in Evolutionarily Conserved Structures." Cells **8**(2).
Song, B., S. Yang, G. H. Hwang, J. Yu and S. Bae (2021). "Analysis of NHEJ-Based DNA Repair after CRISPR-Mediated DNA Cleavage." Int J Mol Sci **22**(12).
Spagnuolo, M. and M. Blenner (2021). "Gene Excision by Dual-Guide CRISPR-Cas9." Methods Mol Biol **2307**: 85-94.
Spassky, N. and A. Meunier (2017). "The development and functions of multiciliated epithelia." Nat Rev Mol Cell Biol **18**(7): 423-436.
Stanke, F. (2015). "The Contribution of the Airway Epithelial Cell to Host Defense." Mediators Inflamm **2015**: 463016.
Stauber, M., M. Weidemann, O. Dittrich-Breiholz, K. Lobschat, L. Alten, M. Mai, A. Beckers, M. Kracht and A. Gossler (2017). "Identification of FOXJ1 effectors during ciliogenesis in the foetal respiratory epithelium and embryonic left-right organiser of the mouse." Dev Biol **423**(2): 170-188.
Steffen, W. and R. W. Linck (1988). "Evidence for tektins in centrioles and axonemal microtubules." Proc Natl Acad Sci U S A **85**(8): 2643-2647.
Steidl, C., S. P. Shah, B. W. Woolcock, L. Rui, M. Kawahara, P. Farinha, N. A. Johnson, Y. Zhao, A. Telenius, S. B. Neriah, A. McPherson, B. Meissner, U. C. Okoye, A. Diepstra, A. van den Berg, M. Sun, G. Leung, S. J. Jones, J. M. Connors, D. G. Huntsman, K. J. Savage, L. M. Rimsza, D. E. Horsman, L. M. Staudt, U. Steidl, M. A. Marra and R. D. Gascoyne (2011). "MHC class II transactivator CIITA is a recurrent gene fusion partner in lymphoid cancers." Nature **471**(7338): 377-381.
Stein, W. D. (2019). "The ages of the cancer-associated genes." Semin Oncol **46**(1): 10-18.
Stewart, C. E., E. E. Torr, N. H. Mohd Jamili, C. Bosquillon and I. Sayers (2012). "Evaluation of differentiated human bronchial epithelial cell culture systems for asthma research." J Allergy (Cairo) **2012**: 943982.
Sugiaman-Trapman, D., M. Vitezic, E. M. Jouhilahti, A. Mathelier, G. Lauter, S. Misra, C. O. Daub, J. Kere and P. Swoboda (2018). "Characterization of the human RFX transcription factor family by regulatory and target gene analysis." BMC Genomics **19**(1): 181.
Sun, X., A. K. Perl, R. Li, S. M. Bell, E. Sajti, V. V. Kalinichenko, T. V. Kalin, R. S. Misra, H. Deshmukh, G. Clair, J. Kyle, L. E. Crotty Alexander, J. A. Masso-Silva, J. A. Kitzmiller, K. A. Wikenheiser-Brokamp, G. Deutsch, M. Guo, Y. Du, M. P. Morley, M. J. Valdez, H. V. Yu, K. Jin, E. E. Bardes, J. A. Zepp, T. Neithamer, M. C. Basil, W. J. Zacharias, J. Verheyden, R. Young, G. Bandyopadhyay, S. Lin, C. Ansong, J. Adkins, N. Salomonis, B. J. Aronow, Y. Xu, G. Pryhuber, J. Whitsett, E. E. Morrisey and N. L. Consortium (2022). "A census of the lung: CellCards from LungMAP." Dev Cell **57**(1): 112-145 e112.
Sung, Y. H., I. J. Baek, Y. H. Kim, Y. S. Gho, S. P. Oh, Y. J. Lee and H. W. Lee (2016). "PIERCE1 is critical for specification of left-right asymmetry in mice." Sci Rep **6**: 27932.
Sung, Y. H., H. J. Kim, S. Devkota, J. Roh, J. Lee, K. Rhee, Y. Y. Bahk and H. W. Lee (2010). "Pierce1, a novel p53 target gene contributing to the ultraviolet-induced DNA damage response." Cancer Res **70**(24): 10454-10463.
Sung, Y. H., H. J. Kim and H. W. Lee (2007). "Identification of a novel Rb-regulated gene associated with the cell cycle." Mol Cells **24**(3): 409-415.

Tadokoro, T., Y. Wang, L. S. Barak, Y. Bai, S. H. Randell and B. L. Hogan (2014). "IL-6/STAT3 promotes regeneration of airway ciliated cells from basal stem cells." Proc Natl Acad Sci U S A **111**(35): E3641-3649.
Taschner, M. and E. Lorentzen (2016). "The Intraflagellar Transport Machinery." Cold Spring Harb Perspect Biol **8**(10).
Terre, B., M. Lewis, G. Gil-Gomez, Z. Han, H. Lu, M. Aguilera, N. Prats, S. Roy, H. Zhao and T. H. Stracker (2019). "Defects in efferent duct multiciliogenesis underlie male infertility in GEMC1-, MCIDAS- or CCNO-deficient mice." Development **146**(8).
Teves, M. E., P. R. Sears, W. Li, Z. Zhang, W. Tang, L. van Reesema, R. M. Costanzo, C. W. Davis, M. R. Knowles, J. F. Strauss, 3rd and Z. Zhang (2014). "Sperm-associated antigen 6 (SPAG6) deficiency and defects in ciliogenesis and cilia function: polarity, density, and beat." PLoS One **9**(10): e107271.
Thomas, B., M. S. Koh, C. O'Callaghan, J. C. Allen, Jr., A. Rutman, R. A. Hirst, J. Connolly, S. Y. Low, O. Thun How, L. Chian Min, W. T. Lim, L. Lin Ean Oon, Q. He, O. H. Teoh and T. S. Lapperre (2021). "Dysfunctional Bronchial Cilia Are a Feature of Chronic Obstructive Pulmonary Disease (COPD)." COPD **18**(6): 657-663.
Thomas, B., A. Rutman, R. A. Hirst, P. Haldar, A. J. Wardlaw, J. Bankart, C. E. Brightling and C. O'Callaghan (2010). "Ciliary dysfunction and ultrastructural abnormalities are features of severe asthma." J Allergy Clin Immunol **126**(4): 722-729 e722.
Thongsin, N. and M. Wattanapanitch (2022). "CRISPR/Cas9 Ribonucleoprotein Complex-Mediated Efficient B2M Knockout in Human Induced Pluripotent Stem Cells (iPSCs)." Methods Mol Biol **2454**: 607-624.
Tilley, A. E., M. S. Walters, R. Shaykhiev and R. G. Crystal (2015). "Cilia dysfunction in lung disease." Annu Rev Physiol **77**: 379-406.
Travaglini, K. J., A. N. Nabhan, L. Penland, R. Sinha, A. Gillich, R. V. Sit, S. Chang, S. D. Conley, Y. Mori, J. Seita, G. J. Berry, J. B. Shrager, R. J. Metzger, C. S. Kuo, N. Neff, I. L. Weissman, S. R. Quake and M. A. Krasnow (2020). "A molecular cell atlas of the human lung from single-cell RNA sequencing." Nature **587**(7835): 619-625.
Truszkowski, J. and N. Goldman (2016). "Maximum Likelihood Phylogenetic Inference is Consistent on Multiple Sequence Alignments, with or without Gaps." Syst Biol **65**(2): 328-333.
Tunyasuvunakool, K., J. Adler, Z. Wu, T. Green, M. Zielinski, A. Zidek, A. Bridgland, A. Cowie, C. Meyer, A. Laydon, S. Velankar, G. J. Kleywegt, A. Bateman, R. Evans, A. Pritzel, M. Figurnov, O. Ronneberger, R. Bates, S. A. A. Kohl, A. Potapenko, A. J. Ballard, B. Romera-Paredes, S. Nikolov, R. Jain, E. Clancy, D. Reiman, S. Petersen, A. W. Senior, K. Kavukcuoglu, E. Birney, P. Kohli, J. Jumper and D. Hassabis (2021). "Highly accurate protein structure prediction for the human proteome." Nature **596**(7873): 590-596.
Uhlen, M., L. Fagerberg, B. M. Hallstrom, C. Lindskog, P. Oksvold, A. Mardinoglu, A. Sivertsson, C. Kampf, E. Sjostedt, A. Asplund, I. Olsson, K. Edlund, E. Lundberg, S. Navani, C. A. Szigyarto, J. Odeberg, D. Djureinovic, J. O. Takanen, S. Hober, T. Alm, P. H. Edqvist, H. Berling, H. Tegel, J. Mulder, J. Rockberg, P. Nilsson, J. M. Schwenk, M. Hamsten, K. von Feilitzen, M. Forsberg, L. Persson, F. Johansson, M. Zwahlen, G. von Heijne, J. Nielsen and F. Ponten (2015). "Proteomics. Tissue-based map of the human proteome." Science **347**(6220): 1260419.
van Dorp, D. B., A. F. Wright, A. D. Carothers and E. M. Bleeker-Wagemakers (1992). "A family with RP3 type of X-linked retinitis pigmentosa: an association with ciliary abnormalities." Hum Genet **88**(3): 331-334.
Varadarajan, R. and N. M. Rusan (2018). "Bridging centrioles and PCM in proper space and time." Essays Biochem **62**(6): 793-801.
Venkatesh, D. (2017). "Primary cilia." J Oral Maxillofac Pathol **21**(1): 8-10.
Villanueva, G., G. Marceniuk, M. S. Murphy, M. Walshaw, R. Cosulich and C. Guideline (2017). "Diagnosis and management of cystic fibrosis: summary of NICE guidance." BMJ **359**: j4574.

Volz, A. C., B. Huber, A. M. Schwandt and P. J. Kluger (2017). "EGF and hydrocortisone as critical factors for the co-culture of adipogenic differentiated ASCs and endothelial cells." Differentiation **95**: 21-30.
Vos, T., A. A. Abajobir, C. Abbafati, K. M. Abbas, K. H. Abate, F. Abd-Allah, A. M. Abdulle and e. al. (2017). "Global, regional, and national incidence, prevalence, and years lived with disability for 328 diseases and injuries for 195 countries, 1990-2016: a systematic analysis for the Global Burden of Disease Study 2016." Lancet **390**(10100): 1211-1259.
Walentek, P. and I. K. Quigley (2017). "What we can learn from a tadpole about ciliopathies and airway diseases: Using systems biology in Xenopus to study cilia and mucociliary epithelia." Genesis **55**(1-2).
Walko, G., M. J. Castanon and G. Wiche (2015). "Molecular architecture and function of the hemidesmosome." Cell Tissue Res **360**(3): 529-544.
Wallmeier, J., D. Frank, A. Shoemark, T. Nothe-Menchen, S. Cindric, H. Olbrich, N. T. Loges, I. Aprea, G. W. Dougherty, P. Pennekamp, T. Kaiser, H. M. Mitchison, C. Hogg, S. B. Carr, M. A. Zariwala, T. Ferkol, M. W. Leigh, S. D. Davis, J. Atkinson, S. K. Dutcher, M. R. Knowles, H. Thiele, J. Altmuller, H. Krenz, M. Woste, A. Brentrup, F. Ahrens, C. Vogelberg, D. J. Morris-Rosendahl and H. Omran (2019). "De Novo Mutations in FOXJ1 Result in a Motile Ciliopathy with Hydrocephalus and Randomization of Left/Right Body Asymmetry." Am J Hum Genet **105**(5): 1030-1039.
Wallmeier, J., K. G. Nielsen, C. E. Kuehni, J. S. Lucas, M. W. Leigh, M. A. Zariwala and H. Omran (2020). "Motile ciliopathies." Nat Rev Dis Primers **6**(1): 77.
Walters, M. S., K. Gomi, B. Ashbridge, M. A. Moore, V. Arbelaez, J. Heldrich, B. S. Ding, S. Rafii, M. R. Staudt and R. G. Crystal (2013). "Generation of a human airway epithelium derived basal cell line with multipotent differentiation capacity." Respir Res **14**: 135.
Wan, H., H. L. Winton, C. Soeller, G. A. Stewart, P. J. Thompson, D. C. Gruenert, M. B. Cannell, D. R. Garrod and C. Robinson (2000). "Tight junction properties of the immortalized human bronchial epithelial cell lines Calu-3 and 16HBE14o." Eur Respir J **15**(6): 1058-1068.
Wang, C. and H. Sun (2019). "Progress in gene knockout mice." Sheng Wu Gong Cheng Xue Bao **35**(5): 784-794.
Wang, F., S. Chen, H. B. Liu, C. A. Parent and P. A. Coulombe (2018). "Keratin 6 regulates collective keratinocyte migration by altering cell-cell and cell-matrix adhesion." J Cell Biol **217**(12): 4314-4330.
Wang, K., X. Chen, C. Y. Guo, F. Q. Liu, J. R. Wang and L. F. Sun (2018). "Cilia ultrastructural and gene variation of primary ciliary dyskinesia: report of three cases and literatures review." Zhonghua Er Ke Za Zhi **56**(2): 134-137.
Wang, S., A. O. Osgood and A. Chatterjee (2022). "Uncovering post-translational modification-associated protein-protein interactions." Curr Opin Struct Biol **74**: 102352.
Wassef, M., A. Luscan, A. Battistella, S. Le Corre, H. Li, M. R. Wallace, M. Vidaud and R. Margueron (2017). "Versatile and precise gene-targeting strategies for functional studies in mammalian cell lines." Methods **121-122**: 45-54.
Webb, S., A. G. Mukhopadhyay and A. J. Roberts (2020). "Intraflagellar transport trains and motors: Insights from structure." Semin Cell Dev Biol **107**: 82-90.
Wesolowska-Andersen, A., J. L. Everman, R. Davidson, C. Rios, R. Herrin, C. Eng, W. J. Janssen, A. H. Liu, S. S. Oh, R. Kumar, T. E. Fingerlin, J. Rodriguez-Santana, E. G. Burchard and M. A. Seibold (2017). "Dual RNA-seq reveals viral infections in asthmatic children without respiratory illness which are associated with changes in the airway transcriptome." Genome Biol **18**(1): 12.
Whitsett, J. A. (2018). "Airway Epithelial Differentiation and Mucociliary Clearance." Ann Am Thorac Soc **15**(Supplement_3): S143-S148.
Whitsett, J. A. and T. Alenghat (2015). "Respiratory epithelial cells orchestrate pulmonary innate immunity." Nat Immunol **16**(1): 27-35.
Whitsett, J. A., T. V. Kalin, Y. Xu and V. V. Kalinichenko (2019). "Building and Regenerating the Lung Cell by Cell." Physiol Rev **99**(1): 513-554.

Wienert, B., S. K. Wyman, C. D. Richardson, C. D. Yeh, P. Akcakaya, M. J. Porritt, M. Morlock, J. T. Vu, K. R. Kazane, H. L. Watry, L. M. Judge, B. R. Conklin, M. Maresca and J. E. Corn (2019). "Unbiased detection of CRISPR off-targets in vivo using DISCOVER-Seq." Science **364**(6437): 286-289.
Wong, J. Y., A. Rutman and C. O'Callaghan (2005). "Recovery of the ciliated epithelium following acute bronchiolitis in infancy." Thorax **60**(7): 582-587.
Wu, C., X. Jin, G. Tsueng, C. Afrasiabi and A. I. Su (2016). "BioGPS: building your own mash-up of gene annotations and expression profiles." Nucleic Acids Res **44**(D1): D313-316.
Xian, S., D. Shang, G. Kong and Y. Tian (2018). "FOXJ1 promotes bladder cancer cell growth and regulates Warburg effect." Biochem Biophys Res Commun **495**(1): 988-994.
Xu, Z. Z., Z. J. Li, L. X. Du, J. Li and L. Y. Wang (2013). "Using bovine pituitary extract to increase proliferation of keratocytes and maintain their phenotype in vitro." Int J Ophthalmol **6**(6): 758-765.
Yamamoto, Y. and N. Mizushima (2021). "Autophagy and Ciliogenesis." JMA J **4**(3): 207-215.
Yamaya, M., W. E. Finkbeiner, S. Y. Chun and J. H. Widdicombe (1992). "Differentiated structure and function of cultures from human tracheal epithelium." Am J Physiol **262**(6 Pt 1): L713-724.
Yang, H., S. Ren, S. Yu, H. Pan, T. Li, S. Ge, J. Zhang and N. Xia (2020). "Methods Favoring Homology-Directed Repair Choice in Response to CRISPR/Cas9 Induced-Double Strand Breaks." Int J Mol Sci **21**(18).
Yang, J., R. Yan, A. Roy, D. Xu, J. Poisson and Y. Zhang (2015). "The I-TASSER Suite: protein structure and function prediction." Nat Methods **12**(1): 7-8.
Yankaskas, J. R., J. E. Haizlip, M. Conrad, D. Koval, E. Lazarowski, A. M. Paradiso, C. A. Rinehart, Jr., B. Sarkadi, R. Schlegel and R. C. Boucher (1993). "Papilloma virus immortalized tracheal epithelial cells retain a well-differentiated phenotype." Am J Physiol **264**(5 Pt 1): C1219-1230.
Ye, J., G. Coulouris, I. Zaretskaya, I. Cutcutache, S. Rozen and T. L. Madden (2012). "Primer-BLAST: a tool to design target-specific primers for polymerase chain reaction." BMC Bioinformatics **13**: 134.
Youn, Y. H. and Y. G. Han (2018). "Primary Cilia in Brain Development and Diseases." Am J Pathol **188**(1): 11-22.
Yu, X., C. P. Ng, H. Habacher and S. Roy (2008). "Foxj1 transcription factors are master regulators of the motile ciliogenic program." Nat Genet **40**(12): 1445-1453.
Yulis, M., D. H. M. Kusters and A. Nusrat (2018). "Cadherins: cellular adhesive molecules serving as signalling mediators." J Physiol **596**(17): 3883-3898.
Zahid, M., T. N. Feinstein, A. Oro, M. Schwartz, A. D. Lee and C. W. Lo (2020). "Rapid Ex-Vivo Ciliogenesis and Dose-Dependent Effect of Notch Inhibition on Ciliogenesis of Respiratory Epithelia." Biomolecules **10**(8).
Zaidman, N. A., A. Panoskaltsis-Mortari and S. M. O'Grady (2016). "Differentiation of human bronchial epithelial cells: role of hydrocortisone in development of ion transport pathways involved in mucociliary clearance." Am J Physiol Cell Physiol **311**(2): C225-236.
Zaiss, D. M. W. and P. J. Coffer (2018). "Forkhead box transcription factors as context-dependent regulators of lymphocyte homeostasis." Nat Rev Immunol **18**(11): 703-715.
Zaragosi, L. E., M. Deprez and P. Barbry (2020). "Using single-cell RNA sequencing to unravel cell lineage relationships in the respiratory tract." Biochem Soc Trans **48**(1): 327-336.
Zhang, C., H. J. Lee, A. Shrivastava, R. Wang, T. J. McQuiston, S. S. Challberg, B. A. Pollok and T. Wang (2018). "Long-Term In Vitro Expansion of Epithelial Stem Cells Enabled by Pharmacological Inhibition of PAK1-ROCK-Myosin II and TGF-beta Signaling." Cell Rep **25**(3): 598-610 e595.
Zhang, K., Y. Harada, X. Wei, D. Shukla, A. Rajendran, K. Tawansy, M. Bedell, S. Lim, P. X. Shaw, X. He and Z. Yang (2011). "An essential role of the cysteine-rich domain of FZD4 in

Norrin/Wnt signaling and familial exudative vitreoretinopathy." J Biol Chem **286**(12): 10210-10215.
Zhang, L., A. Bukreyev, C. I. Thompson, B. Watson, M. E. Peeples, P. L. Collins and R. J. Pickles (2005). "Infection of ciliated cells by human parainfluenza virus type 3 in an in vitro model of human airway epithelium." J Virol **79**(2): 1113-1124.
Zhang, S. H., J. H. Zhang, X. P. Ding, S. Zhang, H. H. Chen and Y. L. Jing (2016). "Association of polymorphisms in tektin-t gene with idiopathic asthenozoospermia in Sichuan, China." J Assist Reprod Genet **33**(2): 181-187.
Zhang, T., J. Wu, C. Liao, Z. Ni, J. Zheng and F. Yu (2018). "System analysis of teratozoospermia mRNA profile based on integrated bioinformatics tools." Mol Med Rep **18**(2): 1297-1304.
Zhang, Y., G. Huang, L. P. Shornick, W. T. Roswit, J. M. Shipley, S. L. Brody and M. J. Holtzman (2007). "A transgenic FOXJ1-Cre system for gene inactivation in ciliated epithelial cells." Am J Respir Cell Mol Biol **36**(5): 515-519.
Zheng, H., D. M. Pritchard, X. Yang, E. Bennett, G. Liu, C. Liu and W. Ai (2009). "KLF4 gene expression is inhibited by the notch signaling pathway that controls goblet cell differentiation in mouse gastrointestinal tract." Am J Physiol Gastrointest Liver Physiol **296**(3): G490-498.
Zheng, W., C. Zhang, Y. Li, R. Pearce, E. W. Bell and Y. Zhang (2021). "Folding non-homologous proteins by coupling deep-learning contact maps with I-TASSER assembly simulations." Cell Rep Methods **1**(3).
Zhu, M., T. Iwano and S. Takeda (2019). "Estrogen and EGFR Pathways Regulate Notch Signaling in Opposing Directions for Multi-Ciliogenesis in the Fallopian Tube." Cells **8**(8).
Ziegler, C. G. K., S. J. Allon, S. K. Nyquist, I. M. Mbano, V. N. Miao, C. N. Tzouanas, Y. Cao, A. S. Yousif, J. Bals, B. M. Hauser, J. Feldman, C. Muus, M. H. Wadsworth, 2nd, S. W. Kazer, T. K. Hughes, B. Doran, G. J. Gatter, M. Vukovic, F. Taliaferro, B. E. Mead, Z. Guo, J. P. Wang, D. Gras, M. Plaisant, M. Ansari, I. Angelidis, H. Adler, J. M. S. Sucre, C. J. Taylor, B. Lin, A. Waghray, V. Mitsialis, D. F. Dwyer, K. M. Buchheit, J. A. Boyce, N. A. Barrett, T. M. Laidlaw, S. L. Carroll, L. Colonna, V. Tkachev, C. W. Peterson, A. Yu, H. B. Zheng, H. P. Gideon, C. G. Winchell, P. L. Lin, C. D. Bingle, S. B. Snapper, J. A. Kropski, F. J. Theis, H. B. Schiller, L. E. Zaragosi, P. Barbry, A. Leslie, H. P. Kiem, J. L. Flynn, S. M. Fortune, B. Berger, R. W. Finberg, L. S. Kean, M. Garber, A. G. Schmidt, D. Lingwood, A. K. Shalek, J. Ordovas-Montanes, H. C. A. L. B. N. E. a. lung-network@humancellatlas.org and H. C. A. L. B. Network (2020). "SARS-CoV-2 Receptor ACE2 Is an Interferon-Stimulated Gene in Human Airway Epithelial Cells and Is Detected in Specific Cell Subsets across Tissues." Cell **181**(5): 1016-1035 e1019.

Appendices

Appendix A: Expression of *PIERCE1* transcript variants in different cell lines and ALI-cultured primary HBEC.

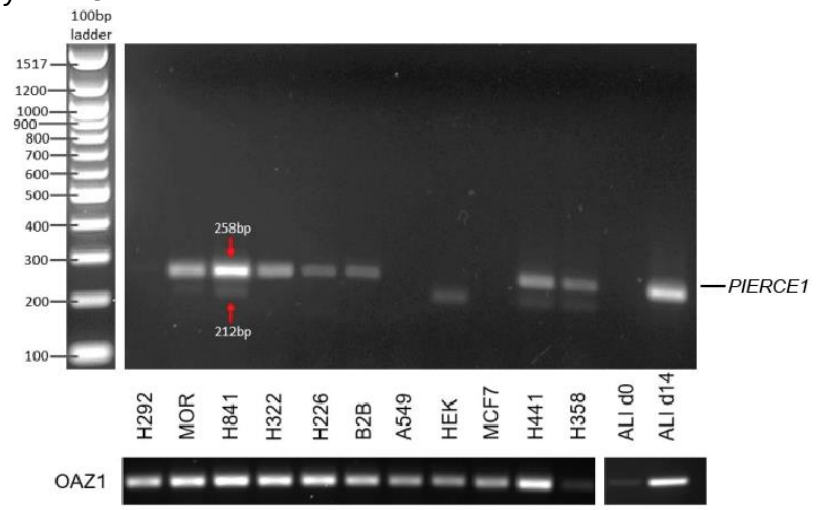

Figure: Detection of *PIERCE1* alternate transcripts. RT-PCR showing two transcript variants of PIERCE1 in different cancer cell lines as well as in ALI cultured primary HBECs. The amplicon size for major transcript is 258 bp and the same for minor transcript is 218 bp as indicated by red arrows. This work was done previously by Oliver Gough (Gough 2017).

Appendix B: Detailed phylogenetic tree of PIERCE1.

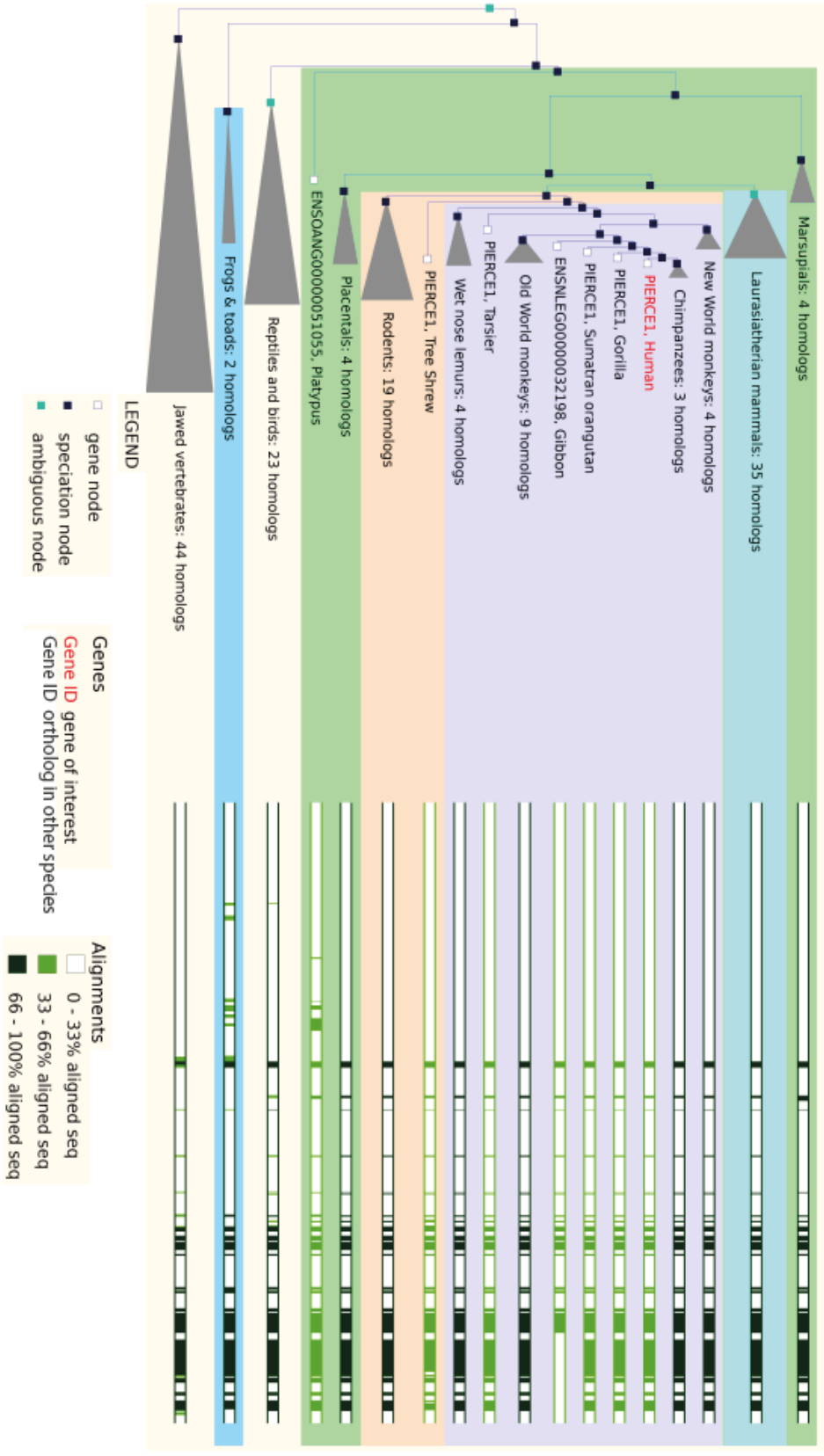

Figure: PIERCE1 phylogenetic tree made by TreeBeST fetched from Ensembl (www.ensembl.org). Sequence alignments showing conserved regions are given below the tree.

Appendix C: Detailed phylogenetic tree of C15ORF65 (PIERCE2).

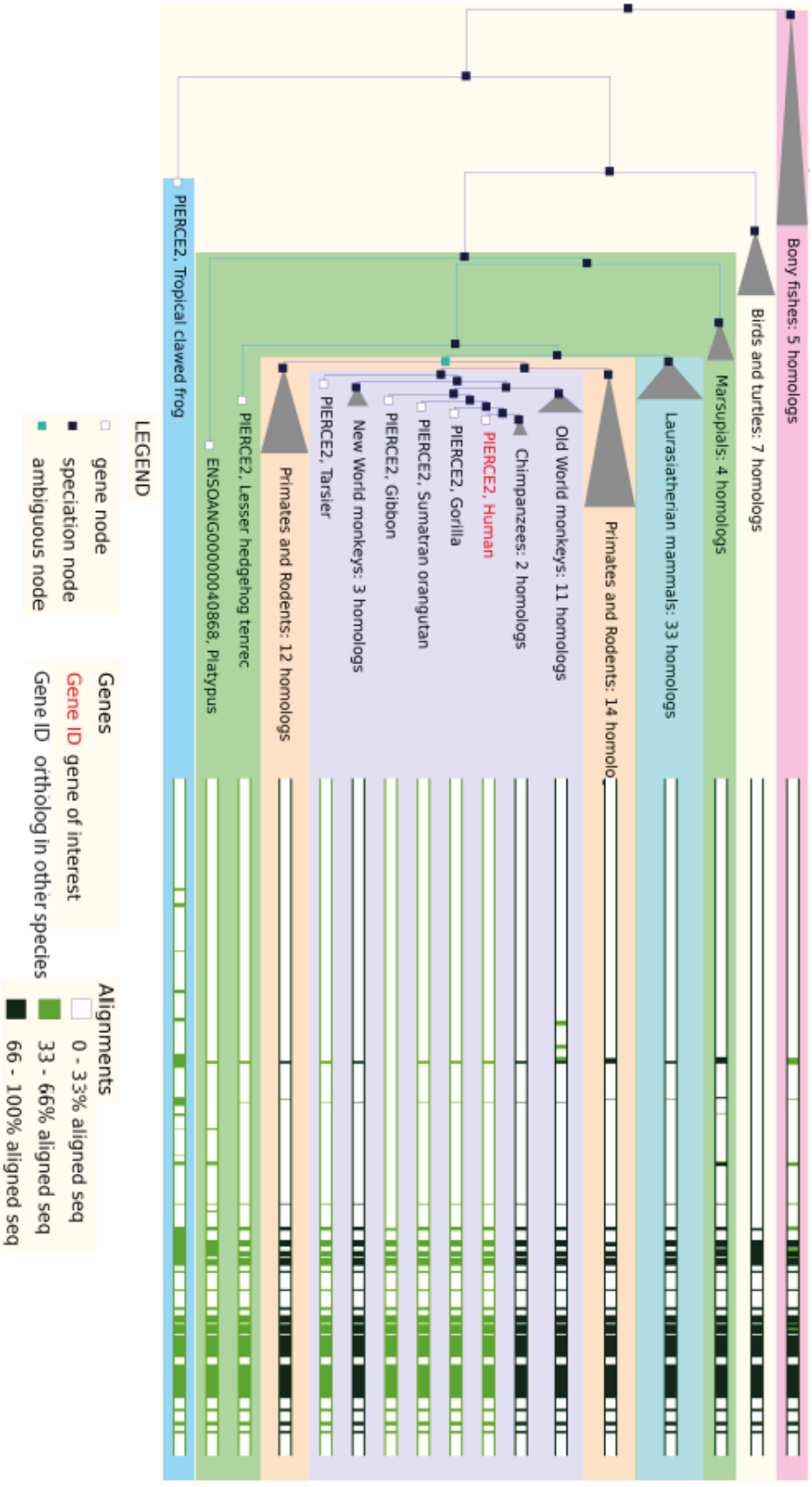

Figure: C15ORF65 (or Pierce2) phylogenetic tree made by TreeBeST fetched from Ensembl (www.ensembl.org). Sequence alignments showing the conserved regions are given below the tree.

Appendix D: BioGPS data on *PIERCE1* and *C15ORF65* expression in human tissues.

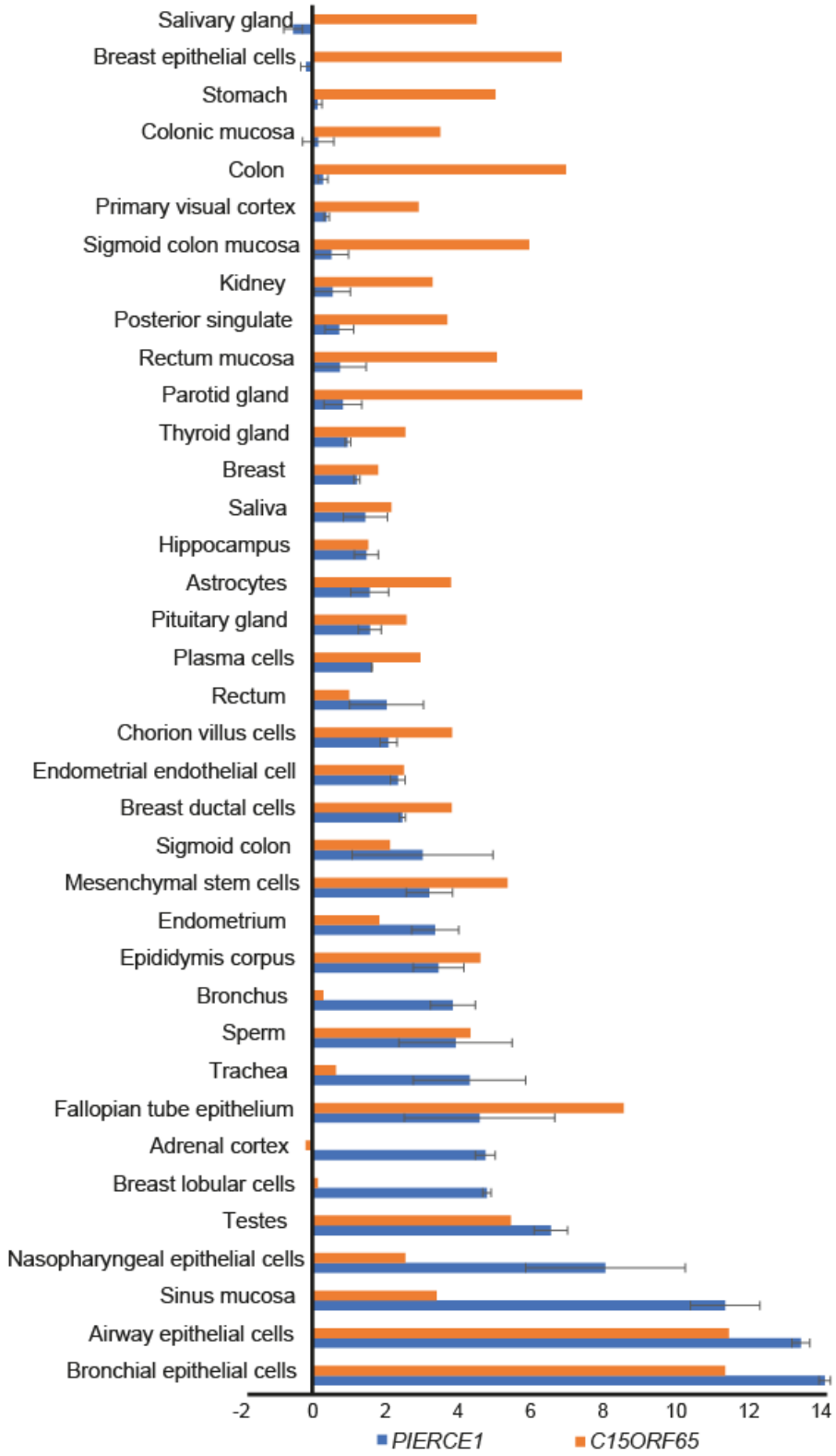

Figure: Expression of *PIERCE1* and *C15ORF65* across different human tissues and cells as obtained from BioGPS (www.biogps.org). BDS_00001 (human) dataset was used to generate this graph after normalization with frozen robust multi-array analysis (FRMA). Values on X-axis indicates the comparative normalized z-score where z > 5 indicates the expression of a gene in a given tissue.

Appendix E: BioGPS data on *Pierce1* and *C15orf65* expression in mouse tissues.

Figure: Expression of *Pierce1* and *C15orf65* across different mouse tissues and cells as obtained from BioGPS (www.biogps.org). GeneAtlas MOE430 (GSE10246, mouse) dataset was used to generate this graph after normalization with guanine cytosine robust multi-array analysis (GCRMA). Values on X-axis indicates the comparative normalized score (per-gene normalisation to the median).

Appendix F: Nuclear localisation signal sequence in PIERCE1 and C15ORF65.

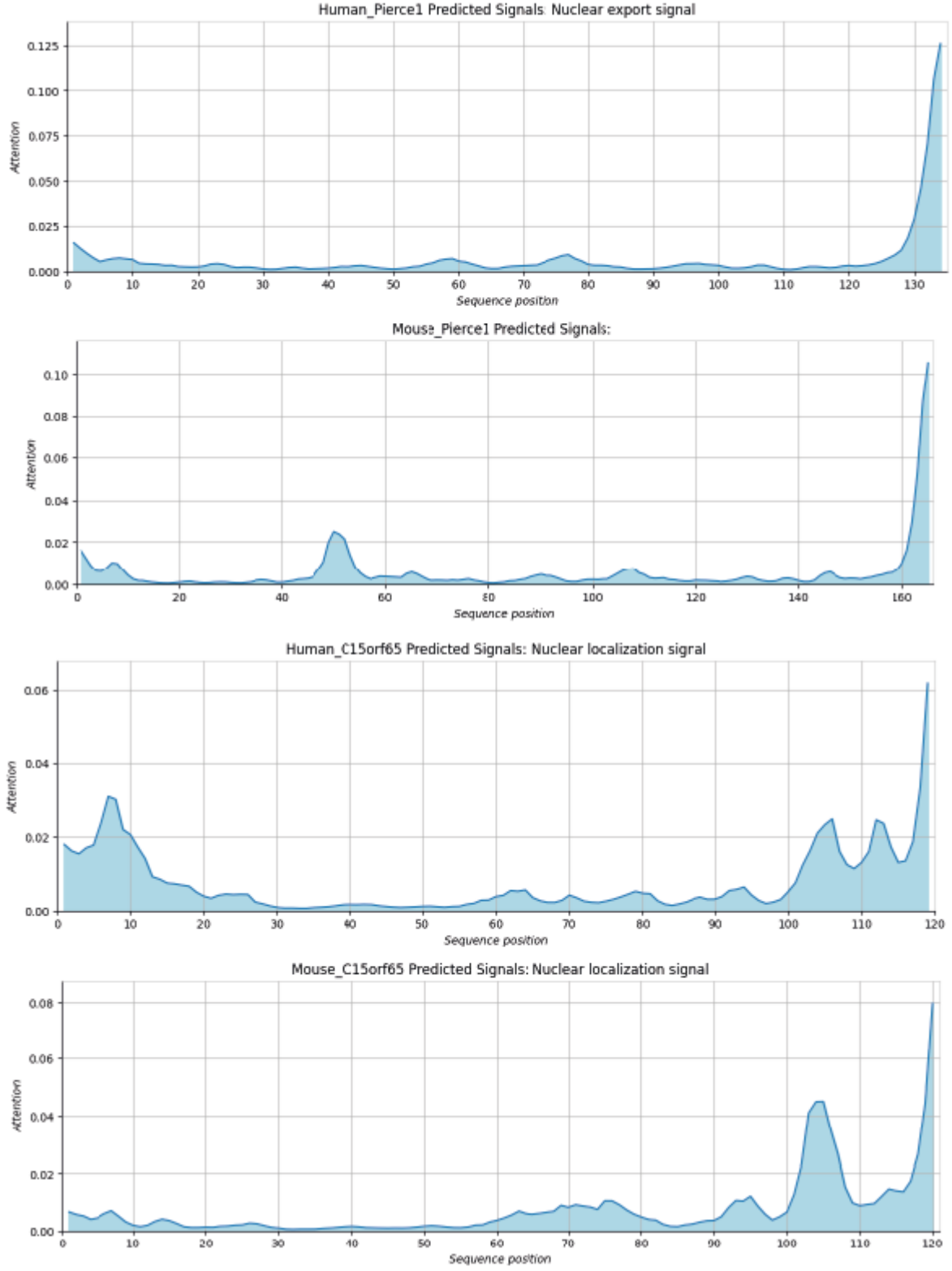

Figure: Nuclear export or nuclear localisation signal sequence was detected in human and mouse PIERCE1 and C15ORF65 using DeepLoc version 2.0. Estimated nuclear localisation probability of PIERCE1 was 0.41 for human and 0.34 for mouse, and the same for C15ORF65 was 0.47 for human and 0.43 for mouse.

Appendix G: Localisation of Pierce1 in ALI-differentiated murine nasal cavity and tracheal epithelial cells.

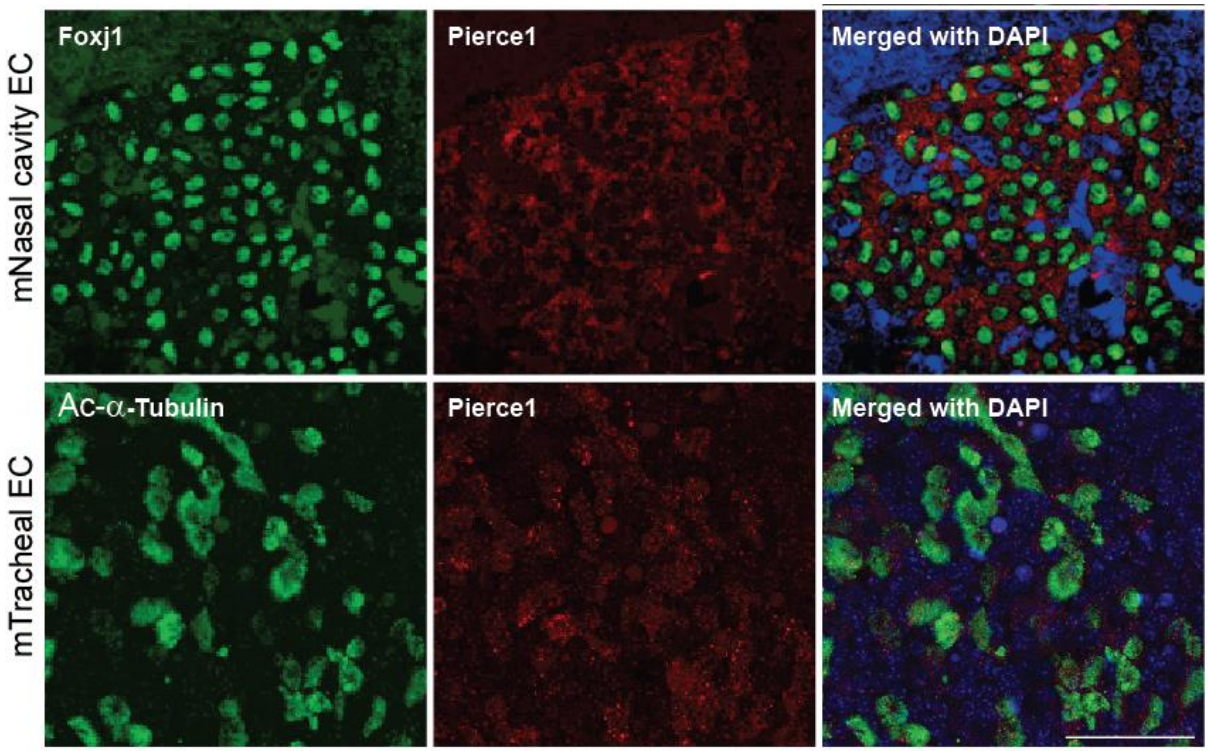

Figure: Murine epithelial cells collected from nasal cavity and trachea were differentiated at ALI for two weeks and were stained for ciliated cell markers like Foxj1 or acetylated α-Tubulin and Pierce1. Nucleus was counterstained with DAPI. Scale bar = 100 μm. This work was previously done by Dr Priyanka Anujan (Anujan 2018).

Appendix H: Predicted structures of human PIERCE1.

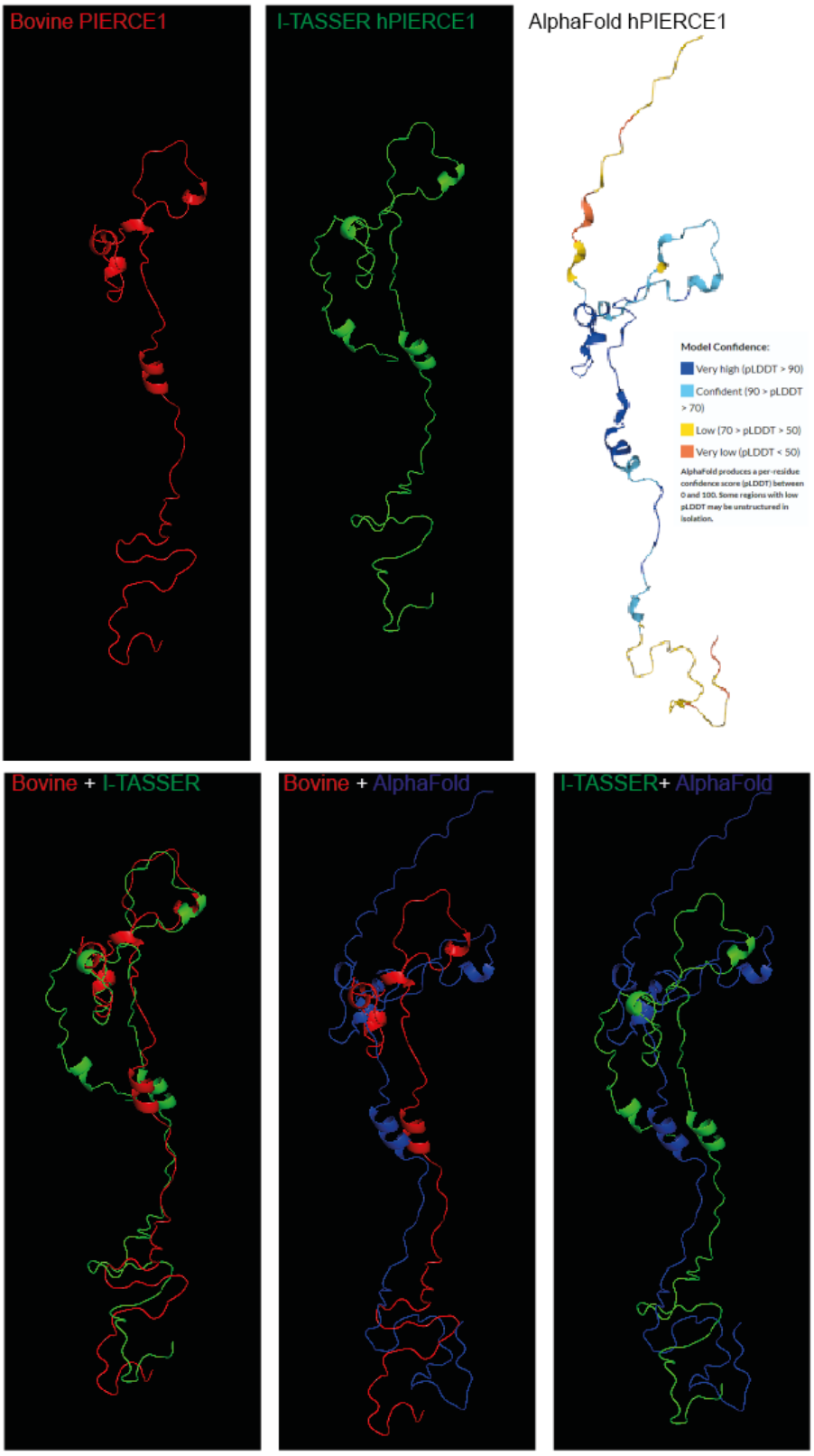

Figure: Crystal structure of bovine PIERCE1 was fetched from PDBID: 7RRO (Gui, Farley et al. 2021) and used as a template to predict human PIERCE1 using I-TASSER. AlphaFold structure (ID: Q5BN46) was collected from AlphaFoldDB (www.alphafold.ebi.ac.uk) (Top). All these structures were compared with each other by aligning them pair-wise using PyMOL (Bottom).

Appendix I: Predicted structures of human C15ORF65.

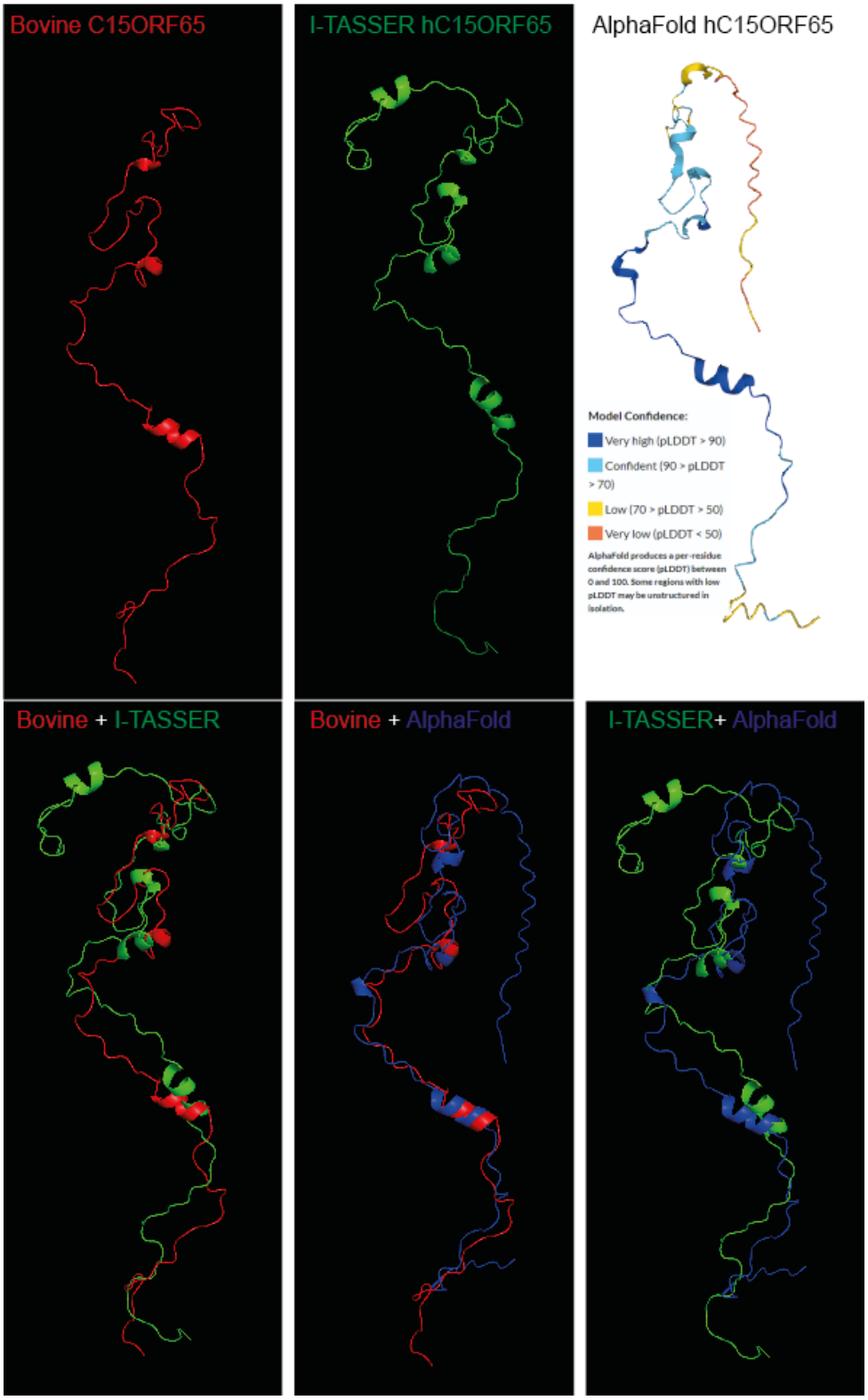

Figure: Crystal structure of bovine C15ORF65 was fetched from PDBID: 7RRO (Gui, Farley et al. 2021) and used as a template to predict human C15ORF65 using I-TASSER. AlphaFold structure (ID: H3BRN8) was collected from AlphaFoldDB (www.alphafold.ebi.ac.uk) (Top). All these structures were compared with each other by aligning them pair-wise using PyMOL (Bottom).

Appendix J: Localisation of PIERCE1 and C15ORF65 in cultured cells.

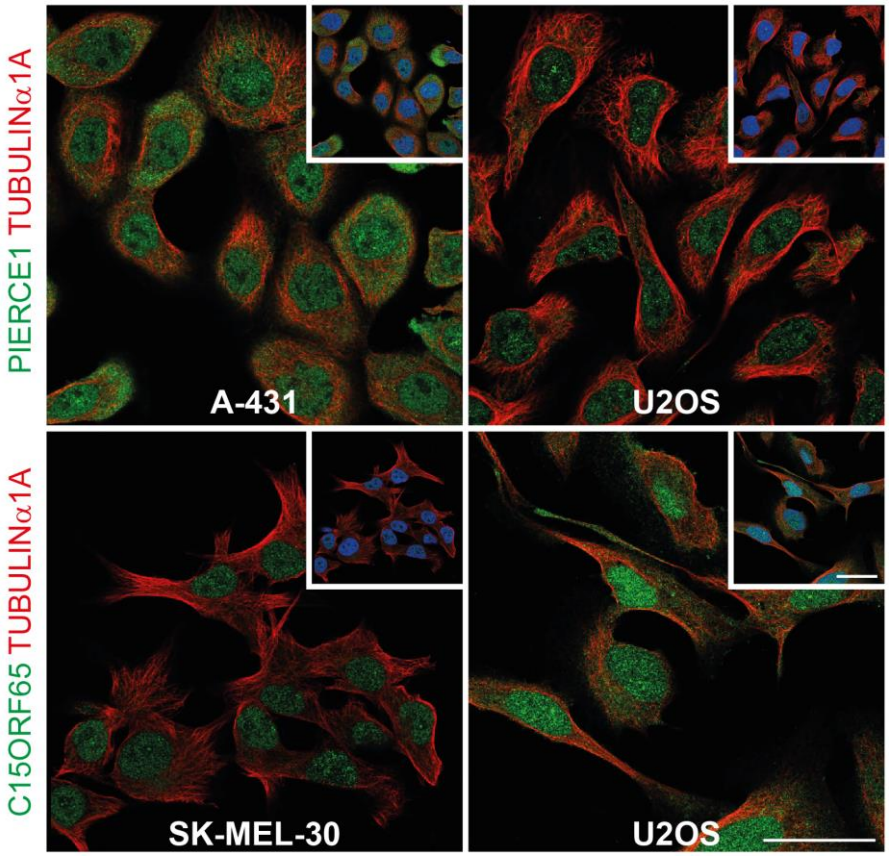

Figure: Localisation of PIERCE1 and C15ORF65 in the nucleus and cytoplasm of cultured human cell lines. All the images were collected from the Human Protein Atlas (www.proteinatlas.org). Inset shows the image merged with DAPI (stains nucleus). Scale bar = 40 μm.